Aquaporin-5 expression, trafficking, and interacting partners in the bovine lens

By

Romell Bernard Gletten

Dissertation

Submitted to the Faculty of the

Graduate School of Vanderbilt University

in partial fulfillment of the requirements

for the degree of

DOCTOR OF PHILOSOPHY

in

Biochemistry

December 17, 2022

Nashville, Tennessee

Approved:

Charles R. Sanders, Ph.D.

Kevin L. Schey, Ph.D.

Richard M. Caprioli, Ph.D.

Matthew Tyska, Ph.D.

Jeffrey M. Spraggins, Ph.D.

ACKNOWLEDGEMENTS

This thesis is dedicated to all of many that made it possible for me to achieve a Ph.D. at Vanderbilt University. Those not listed are by no means forgotten, and I will always remember each of you and your sacrifices for me to be here. I want to personally thank my boss, Dr. Kevin L. Schey, for all of the time and energy that he has sacrificed for me to succeed. I have by no means been an easy graduate student to deal with at times, but he has relentlessly stuck with me every single step of the way. He has served as an admirable example of a consummate scientist, professional, and overall kindhearted leader for me to emulate. I greatly appreciate all that you have done for me, and I hope that I have made you proud.

I also thank Dr. Zhen Wang for her unwavering support over the years. She has been a consummate example of unwavering hard work, and dedication to science and productivity. I also learned many life lessons from her and respect her greatly. I hope that I have made you proud as well, Zhen. I thank my committee members and my committee chair, Dr. Chuck Sanders for their guidance, support, and patience during the times where experimental results were slow (e.g. viable LC3B antibodies). They have absolutely been in my corner during this process, and I am very appreciative. I thank Dr. Nicole Weekes, Dr. Hughes Suffren, Dr. Habibeh Khoshbouei, Dr. Maureen Hahn, Dr. Randy Blakely, Dr. Linda Sealy, Dr. Roger Chalkley, and Dr. Alyssa Hasty. They have all been indispensable in the completion of my Ph.D., and their support has been unwavering for me since day one. Each of them gave me support when during periods of my life when I needed it, and for this I am grateful. I also thank my labmates Jessica Paredes, Lee Cantrell, Carla O'Neale, Minh Tran, Ankita Kotnala, Sarah Zelle, the Mass Spectrometry Resource Center, the Vanderbilt Biochemistry Department, Vanderbilt IMSD, Dr. Manny Ascano, and all of those involved in my development professionally. I am very grateful for your support (and tolerance) through this process.

I would like to thank my friends for their unwavering support during this process. Hussain Jinnah, David Wharton, Raaj Gowrishankar, Apara Shekar, David Anderson, Jenny and Brad Nelson, Michael Wooten and the Wooten family, Leo Khmelniker and the Khmelniker family, Murphy Jordan Goodman and the Goodman family, Maria Williams and the Williams family, Demario Dayton, Michael and Judy Lawson (my California mom), Stanley Onyebueke, Myles Durkee, Gaben and Sarah Crawford, Matt Walters and the Walters family, Alan "Shoulders" Schulman, David Matson, the Church of Messiah, and all that have all supported me through this process. To my friends Baron Fann, Randall "Moogie" Osborne, Chris Middleton, Charles "Chuck" Karlosky thank you so much for your support and encouragement.

Lastly, I want to thank my family. I thank my father Bernard Gletten, my mother Deborah Gletten, and my brother Rashad Kelley for the sacrifices that they have made for me to get to this point. I love you very much. I thank and love my nieces Anaeya and Cierra Kelley, aunt Julia Gletten, uncle Allen Robinson, late uncle Charles Gletten, aunt Earnestine Rollins, aunt Doris Gray, cousins Naomi Hayes, Reuben Hayes, Reuben Hayes, Jr., Reggie Hayes, Maurice Hayes, Charles "Chuck" Gletten, Sharon "Nerl" Martin, Varneal Smith, Roxanne Smith, John Echols, Jr., Aprel Robinson, Omari Gletten, Jerome Martin, Jeremy Martin, Briana Jackson, Chandra Monae Jackson, Fred Gletten, Jr., Jason Gletten, Sidney Smith, Billy Smith, Sanel Deviservic and the Deviservic family, and my many other family members for your support and unconditional love over the years. To my late grandfathers Homer Gletten and Otis Dotson, I love you and I hope that I have upheld your honor and made you proud. To my late grandmother Clora Dotson, I love you and thank you for showing me the meaning of truly genuine kindness. To my grandmother Mary L. Smith, I love you and thank you for the wisdom that you have instilled within me. To my late uncle Fred Gletten, M.D., I love you and wish you lived to see this day. I hope to see you again when my time in this realm is complete and thank you again for life lessons and the love that you showed me.

TABLE OF CONTENTS

LIST OF TABLES

LIST OF FIGURES

LIST OF ABBREVIATIONS

ACN	acetonitrile
AQP	aquaporin
AQP5	aquaporin-5
AQP0	aquaporin-0
DMP	dimethyl pimelimidate
DTT	dithiothreitol
ESI	electrospray ionization
FDR	false discovery rate
GRIN	gradient refractive index
HPLC	high performance liquid chromatography
IDP	immunodepleted fraction
LC	liquid chromatography
LC-MS/MS	liquid chromatography-tandem mass spectrometry
MCS	lens microcirculation system
m/z	mass-to-charge ratio
MS	mass spectrometry
NKCC1	Na-K-Cl cotransporter 1
OC	outer cortex
OCT	optimum cutting temperature medium
PBS	phosphate-buffered saline
P_{H2O}	transmembrane water permeability
PKA	protein kinase A
PKC	protein kinase C
Q	quadrupole
TEM	transmission electron microscopy
WGA	wheat germ agglutinin

CHAPTER I. Introduction

The ocular lens is a transparent, biconvex tissue in the eye that adjustably refracts visible light onto the retina enabling sharp vision over a wide range of distances[1–3]. The unique structural properties and molecular composition of the lens enable it to function as a biological optic lens.

The lens is comprised of a monolayer of epithelial cells that overlay and metabolically sustain lens fiber cells, which comprise the bulk of lens cellular mass. Lens fiber cells continuously differentiate from lens epithelial cells resulting in concentric fiber cell layers with younger fiber cells atop older fiber cells. Fiber cells differentiation is gradual and is characterized by spatiotemporal protein expression and organelle degradation resulting in an optically transparent tissue with a high index of refraction that is able to accommodate as necessary to focus light from different distances.

Aquaporins (AQPs) represent a group of spatiotemporally expressed lens proteins which mediate lens transparency. AQPs facilitate osmotic water diffusion across the plasma membrane at a cellular level and are theorized to be integral to the lens microcirculation system (MCS) which convects nutrients to and wastes from the deeper cellular layers of the lens by means of circulating sodium currents and concomitant water flow. AQP5 is the most recently discovered lens AQP and the second most abundant AQP in lens fiber cells after aquaporin-0 (AQP0). Deletion studies suggest that lenticular AQP5 compensates for perturbations to lens osmotic balance and may prevent diabetic cataract. Functional studies suggest that plasma membrane insertion of cytoplasmic AQP5 increases lens fiber cell water permeability. AQP5 inherently affects differentiation in various cell types though a role for AQP5 in fiber cell differentiation has not been investigated.

A major goal of my work was to better understand lenticular AQP5 regulation broadly using the bovine lens as a model system. In this project, we investigate bovine lenses to define AQP5 spatial expression patterns, subcellular localization, trafficking mechanisms, and interacting proteins. We speculate on cellular processes which AQP5 might regulate in bovine lenses via protein-protein interactions. Our work is critical to determining how AQP5 might be regulated and thereby understanding its role of AQP5 normal lens physiology.

1.1 Anatomy of the Ocular Lens

1.1.1 Eye Anatomy & Function

The eyes are a complex optical unit within the visual system which function to sense and transmit incoming visible light from the environment to the brain via the retina. The retina contains the photoreceptor cell layer of the eye and is responsible for the initial processing of electromagnetic radiation in the visible light wavelength spectrum. In metazoans, light from the environment enters the eye via the cornea which functions as fixed, convex optical lens. The cornea is responsible for two-thirds of the refractive power of the eye, or about 40 diopters in humans. Refracted light then traverses the aqueous humor, a transparent ionic solution similar in chemical composition to blood with low protein concentrations, through the pupil, which functions as a biological aperture similar to that of a camera. Thereafter, light reaches the ocular lens. The ocular lens is responsible for about one-third of the refractive power of the eye, or about 20 diopters in humans. The refractive power of the lens is a consequence of its exceptionally high lens crystallin protein concentration, which forms a gradient which corrects for spherical aberration of the cornea. The curvature of the lens is reflexively changed in

humans through the process of accommodation. Accommodation changes the refractive power of the lens up to 15 diopters enabling focus on objects at variable distances.

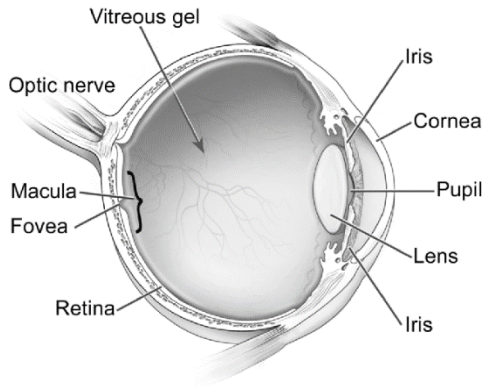

Figure 1.1. Diagram of the human eye.
Light passes through the cornea, pupil, and lens before focusing onto the retina.
Adapted from the National Eye Institute; https://medialibrary.nei.nih.gov/[4]

Light then passes through the vitreous humor, a gel-like substance comprised of primarily of water with collagen, proteins, salts and sugars. The vitreous fills the space between the lens and retina and is responsible for assisting the eye in maintaining its overall shape. Light then reaches the retina where photons are converted into action potentials in the ganglia of the optic nerve in the process of visual phototransduction. The conversion occurs when light is absorbed by and excites 11-cis-retinal, a derivative of vitamin A. 11-cis-retinal is covalently bound to cone opsins and rod opsins (i.e. rhodopsins) and photoisomerizes to all-trans retinal upon photon absorption inducing conformational changes in opsins. This conformational change initiates a signaling cascade which is transmitted to the optic nerve downstream and further processed in the visual cortex of the brain. The final product is a visual image of the outside world which is clear and enables metazoans to respond actively to the world around them.

1.1.2 Ocular Lens Anatomy & Development

During embryogenesis, the surface ectoderm forms the cornea and the lens[5]. The surface ectoderm thickens to form the lens placode. Lens placode cells, which are lens precursor cells, invaginate, enclose, and separate from the surface ectoderm by enclosing to form the lens vesicle. The surface ectoderm then differentiates to form corneal epithelial cells. The optic vesicle, which lies posterior to lens placode cells, involutes around the posterior portion of the lens vesicle without enclosing to form a “cup” like structure termed the optic cup. The posterior cells of the lens placode undergo terminal differentiation and elongate across the lumen of the lens vesicle to form primary lens fiber cells. The anterior cells of the lens vesicle differentiate into lens epithelial cells.

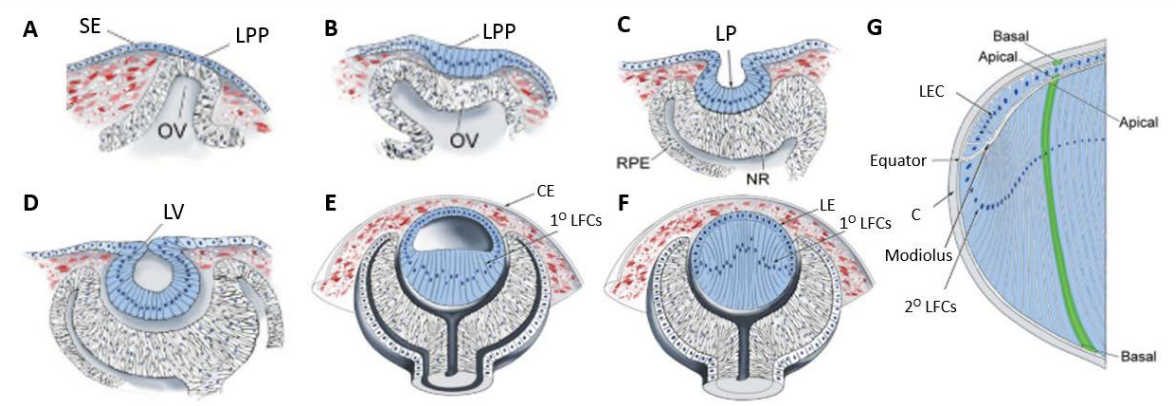

Figure 1.2. Ocular lens induction and morphogenesis
Adapted with permission from Figure 3 in Cvekl and Ashery-Padan 2014 in *Development*[5].
DOI: 10.1242/dev.107953
(**A**) Lens placode precursor (LPP) cells originate from the surface ectoderm (SE). The optic vesicle underlies the surface ectoderm. (**B**) LPP cells undergo morphogenesis. (**C**) The lens placode (LP) begins to invaginate while the OV involutes around LP. The OV eventually forms retina. The retina is comprised of the retinal pigmented epithelium (RPE) and the neuroretina (NR) or the retinal cell layers comprised of neurons. (**D**)The lens placode eventually encloses and separates from the surface ectoderm cells, which (**E**) eventually form the corneal epithelium (CE). The anterior cells of the lens placode form the lens epithelial cells (LEC). The posterior cells of the lens placode differentiate into primary lens fiber cells (1^{O} LFCs) which elongate and migrate until their apical plasma membranes abut with the apical plasma membranes of the LECs. (**F**) Thereafter, a complete lens is formed, (**G**) and secondary lens fiber cells (2^{O} LFCs) differentiate from LECs at the lens equator forming the lens modiolus. The basal plasma membranes of LECs and LFCs abut with the lens capsule a collagenous basement membrane (C).

1.1.3. Ocular Lens Cellular Structure

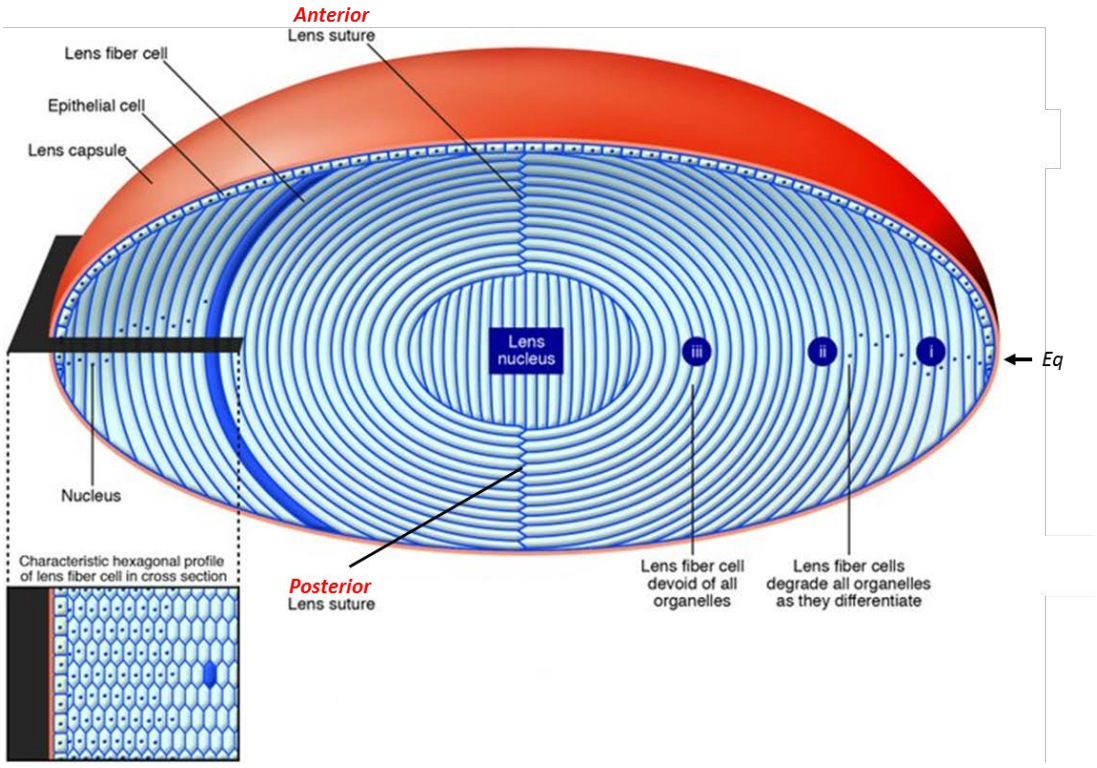

Figure 1.3. **The cellular structure of the ocular lens.**
Adapted with permission from Figure 1 in Song et al 2009 in *J Clin Invest*[6].
DOI: 10.1172/JCI38277
The ocular lens is comprised of an anterior layer of epithelial cells which undergo cellular differentiation at the lens equator (*Eq*) into elongated, hexagonal lens fiber cells. The anterior and posterior fiber cell tips of differentiating lens fiber cells migrate towards the lens center forming the anterior and posterior lens sutures. Differentiating lens fiber cells also undergo organelle degradation in which subcellular organelles are eliminated to avert light scatter during lens light refraction. Lens fiber cell differentiation is complete following organelle degradation and apposition of contralateral lens fiber cell tips at lens sutures.

The ocular lens is a specialized epithelial tissue structure comprised of two cell types (**Figure 1.2** and **Figure 1.3**). The first type is lens epithelial cells which form a one-cell thick layer covering the anterior surface of the lens. The second type is lens fiber cells. Lens fiber cells are highly elongated, post-mitotic cells which differentiate stochastically from lens epithelial cells near the lens equator[7]. Lens fiber cells comprise approximately 99% of the lens cellular mass[8].

1.1.3.1. Lens Epithelial Cells

The lens epithelial cells are metabolically active simple cuboidal epithelial cells[9]. These cells remain mitotic and proliferative throughout the life of the organism[10,11].

1.1.3.2. Lens Fiber Cell Differentiation

Fiber cell differentiation is defined by gradual (i.e. over many concentric cell layers) (1) cellular elongation, (2) expression of fiber cell-specific proteins (e.g. AQP0, filensin, phakinin, etc.), (3) the extremely high expression and short order packing[12] of α-crystallins to establish the refractive properties of the lens, and the (4) programmed loss of nuclei and subcellular organelles[13–16]. The gradual nature of lens fiber cell differentiation and concentric fiber cell layers based on age results in spatiotemporal expression of proteins across the lens.

The tips of lens fiber cells are comprised of apical and basal plasma membranes which migrate towards the optical axis along the lens epithelial cell basal plasma membranes and the lens capsule, respectively. Fiber cell differentiation is complete once cellular elongation ceases, lens fiber cell tips separate from epithelial cell membranes and the capsule and abut with fiber cell antipodal fiber cell tips from the contralateral side of the lens, and fiber cell nuclei and large subcellular organelles are abruptly degraded to prevent light scatter[13,17,18]. Lens fiber cells can be regionally divided into three cellular anatomical regions – the outer cortex, the inner cortex, and the nucleus[13,19,20]. The outer cortex is composed of differentiating fiber cells, the inner cortex is composed of differentiating fiber cells and mature fiber cells, and the nucleus is composed of mature lens fiber cells. The nucleus is further subdivided into four regions[13,19,20]. From the periphery of the nucleus to the center of the lens, these are the adult nucleus, juvenile nucleus, fetal nucleus, and embryonic nucleus.

1.2. Ocular Lens Function

The physiological function of the ocular lens is to adjustably focus light traversing the cornea onto the retina for phototransduction. The lens also corrects corneal Seidel aberrations such as negative spherical aberration (~80% correction in humans) and positive coma (~50% correction in humans)[21]. In addition to its primary physiological function, the lens actively maintains its transparency and a microcirculation system for metabolic exchange as an avascular structure. Spatiotemporal protein expression and a specialized cellular structure form the basis of these lens physiological functions.

1.2.1. Lens Crystallins

Lens crystallins represent one such group of spatiotemporally expressed proteins in the ocular lens. Lens crystallins are water-soluble structural proteins expressed in the lens and several other tissues including the cornea, heart, spleen, liver, and brain[22,23]. Three classes – α ,β ,γ – and fourteen major crystallins – αA-, αB-, βA1-, βA3-, βA4-, βB1-, βB2-, βB3-, γA-, γB-, γC-, γD-, γE, and γS-crystallins – are expressed in mammalian lenses[24]. Lens crystallins are evolutionarily classified into two major protein superfamilies termed the α-crystallins and the βγ-crystallins. The polydispersity of crystallins in mammals in general is important to maintain lens transparency by preventing lens crystallin protein phase separation, crystallization, or precipitation in the lens[25–27].

αA-crystallin and αB-crystallin are expressed in lens epithelial cells and their expression increases dramatically upon fiber cell differentiation[28]. αA-crystallin and αB-crystallin are evolutionarily related to the Hsp20 family of small heat shock proteins (sHsp)[29] forming high molecular weight protein oligomers in the lens (i.e. 300 – 1,200 kDa; avg. ~ 700 kDa)[30,31]. αA-crystallin and αB-crystallin function as molecular chaperones by binding denatured lens proteins and preventing their aggregation[32]. Additionally, αA-crystallin: αB-crystallin multimers catalyzed the refolding of denatured γ-crystallin[32]. βA1-, βA3-, βA4-, βB1-, βB2-, βB3-, γC-, γD-, and γS-

crystallin are βγ-crystallins are evolutionarily related and comprised of two intercalating "Greek-key" motifs connected by a linker peptide[33]. β-crystallins form high molecular weight oligomers that are primarily dimers of βA1-crystallin – βA4-crystallin and βB1-crystallin – βB3-crystallin, while γ-crystallins exist as monomers. βγ-crystallins primarily function as structural proteins.

Fiber cells are distinguished from lens epithelial cells by the initiation of high crystallin gene expression during the process of fiber cell differentiation. The gradual nature of fiber cell maturation and fiber cell compaction results an increasing gradient of cytoplasmic crystallin concentration of 250 mg/mL to greater than 400 mg/mL[31,34] from the lens periphery to the lens center. The lenticular crystallin gradient, which is termed the gradient index of refraction (GRIN), is necessary to increase the refractive optical properties of the lens[35].

1.2.2. Lens Aquaporins

AQPs are conserved, transmembrane channels which allow diffusion of water across cell membranes down osmotic gradients[36]. Aquaporins maintain cellular homeostasis by regulating osmotic balance across the plasma membrane via their water channel function. Thirteen aquaporins, AQP0-AQP12, are differentially expressed within mammalian tissues collectively maintaining proper tissue water balance necessary for complex organ system function. AQP0[37–40], AQP1[40–42], AQP5[40,43–46], AQP7[47], and AQP8[48,49] are expressed in mammalian lenses. AQP1, AQP5, AQP7, and AQP8 are expressed in the lens epithelial cells, while AQP0 and AQP5 are expressed in the lens fiber cells.

1.2.2.1. Aquaporins – Function, Types, and Tissue Distribution

Aquaporins are differentially expressed throughout the body to regulate overall organ and cellular water content (**Table 1.1**). Mammalian AQPs can be divided into classic AQPs (AQP0, AQP1, AQP2, AQP4, AQP5, AQP6, and AQP8), aquaglyceroporins allow facilitated diffusion of glycerol as well (AQP3, AQP7, AQP9, and AQP10), and superaquaporins whose function is less well understood (AQP11-AQP12)[50–55]. AQPs also transport urea, carbon dioxide, and hydrogen peroxide in certain instances. AQPs with significant contributions to global organ function in major organ systems will be outlined succinctly in this section.

Type	Permeability	Tissue Expression	Associated Role	Phenotypes: AQP-null mice	Phenotypes: Mutant AQP in humans	References
AQP0	H_2O , H_2O_2	**ocular lens (*fiber cells*)**, retina (*ganglion cell layer* , *inner nuclear layer*)	**lenticular biomechanics, lenticular transparency, lenticular osmotic homeostasis, lenticular fiber cell structure, lenticular microcirculation system (MCS)**	**Cataract**	**Cataract**	**Fitzgerald et al 1983; Shiels et al 2001; Takata, Matsuzaki, and Tajika 2004; Verkman, Anderson, and Papadopoulos 2014; Schey et al 2014; Verkerk, Lodder, and Wilders 2019; Varadaraj and Kumari 2020**
AQP1	H_2O , H_2O_2, CO_2	**ocular lens (*epithelium*)**, cornea (*endothelium* ; *stromal keratocytes*), the ciliary body (*epithelium* , *trabecular meshwork*), retina (*inner plexiform layer* , *outer plexiform layer* , *retinal pigment epithelium*), red blood cells, vasculature (*excluding the brain*), skeletal muscle, nervous system (*afferent sensory nerve fibers* ; *choroid plexus*), kidneys (*proximal tubule* ; *descending limb of Henle epithelia* ; *vasa recta endothelia*)	**lenticular transparency, lenticular osmotic homeostasis, lenticular microcirculation system (MCS)**, corneal transparency, aqueous humor production*, angiogenesis (*increases vascularity and hemoglobin content*), cerebrospinal fluid production*, urine concentration, water reabsorption	**cataract, increased lens water content,** diuresis, reduced tumor angiogenesis, reduced intraocular pressure, reduced CSF secretion, reduced nociception	nephrogenic diabetes insipidus	Ernst, Palacios, and Siegel 1986; Fushimi et al 1993; Nielsen et al 1993; Stamer et al 1994; Funaki et al 1998; Hamann et al 1998; Ma et al 1998; Wu et al 1998; Li et al 1999; Yoshimichi et al 2001; Solenov et al 2002; Thiagarajah and Verkman 2002; Macnamara et al 2004; Takata, Matsuzaki, and Tajika 2004; Saadoun et al 2005; Au et al 2008; Verkman, Ruiz-Ederra, and Levin 2008; Verkman, Anderson, and Papadopoulos 2014; Verkerk, Lodder, and Wilders 2019
AQP2	H_2O	**kidney cortical collecting duct, testis (*vas deferens principal cells*), ear (*Organ of Corti*)**	**urine concentration, water reabsorption, systemic hydration**	**nephrogenic diabetes insipidus**	**nephrogenic diabetes insipidus**	**Sasaki et al 1994; Yang et al 2001; Takata, Matsuzaki, and Tajika 2004; Verkman, Anderson, and Papadopoulos 2014; Ikeda and Matsuzaki 2015; Jung and Kwon 2016; Verkerk, Lodder, and Wilders 2019**
AQP3	H_2O, urea, glycerol, NH_3 , arsenite	conjunctiva, cornea (*epithelium*), epidermis, kidney cortical collecting duct, T-cells, intestine (*epithelium*), red blood cells	epidermis hydration, T-cell migration	diuresis, dry skin, reduced skin tumor growth, impaired skin wound healing, impaired colonic epithelium regeneration, impaired leukocyte function	Unclear	Ishibashi et al 1997; Ma et al 2000; Takata, Matsuzaki, and Tajika 2004; Nakahigashi et al 2011; Hara-Chikuma et al 2012; Verkman, Anderson, and Papadopoulos 2014; Verkerk, Lodder, and Wilders 2019
AQP4	H_2O	**lung (*alveolar cells*), skeletal muscle tissue, kidney (*collecting duct cells*), central nervous system (*astrocytes* , *retinal Muller cells*), lacrimal gland, salivary duct, inner ear, olfactory epithelium, gastric parietal cells, airways, placenta, intestine (*epithelium*)**	**osmotic regulation in the central nervous (brain edema and ischemic stroke), protection against muscle dystrophy diseases such as Duchenne muscle dystrophy (DMD)* and limb-girdle muscular dystrophy type 2B (LGMD2B)***	**Reduced cytotoxic edema, increased vasogenic CNS edema, accelerated obstructive hydrocephalus, increased seizure threshold and duration, deafness, anosmia**	**None identified**	**Dermietzel 1973; Rash and Ellisman 1974; Shibuya and Wakayama 1988; Hasegawa et al 1994; Frigeri et al 1995; Manley et al 2000; Solenov et al 2002; Wakayama et al 2002; Takata, Matsuzaki, and Tajika 2004; Au et al 2008; Yang, Zador, and Verkman 2008; Wolburg et al 2011; Verkman, Anderson, and Papadopoulos 2014; Verkerk, Lodder, and Wilders 2019**
AQP5	H_2O, H_2O_2	**ocular lens (*epithelium* , *fiber cells*)**, cornea (*epithelium*), lacrimal glands, salivary glands, airway submucosal glands, lung (*Type I alveolar cells*), sweat glands, epidermis, digestive system	**lenticular osmotic homeostasis, lenticular transparency, lenticular microcirculation system (MCS)**, maintenance of corneal thickness; maintenance of intraocular pressure, corneal biomechanics, macular integrity, saliva production, tear production, sweat production	**increased lens water content, cataract**, reduced corneal thickness, reduced tear volume, reduced saliva secretion, reduced airway submucosal secretion	**cataract**, palmoplantar keratoderma	Raina et al 1995; Funaki et al 1998; Nejsum et al 2002; Thiagarajah and Verkman 2002; Matsuzaki et al 2003; Ehlers and Hjortdal 2004; Takata, Matsuzaki, and Tajika 2004; Weng, Han, and Schey 2008; Bassnett, Wilmarth, and David 2009; Sindhu Kumari and Varadaraj 2013; Verkman, Anderson, and Papadopoulos 2014; Petrova et al. 2018; Verkerk, Lodder, and Wilders 2019; Varadaraj and Kumari 2020
AQP6	H_2O, NH_3 , anions	**kidney (intracellular vesicles in *duct acid-secreting α-intercalated cells*)**	**glomerular filtration*, tubular endocytosis*, and acid-base metabolism***	**Not reported**	**Not identified**	**Yasui et al. 1999; Takata, Matsuzaki, and Tajika 2004; Verkman, Anderson, and Papadopoulos 2014; Verkerk, Lodder, and Wilders 2019**
AQP7	H_2O, urea, glycerol, NH_3 , arsenite	**ocular lens (*epithelium*)**, adipocytes, kidney (proximal tubule), heart muscle (*cardiomyocytes*), skeletal muscle, testis	glycerol metabolism	obesity, insulin resistance, hyperglyceroluria	hyperglyceroluria	Takata, Matsuzaki, and Tajika 2004; Skowronski et al 2007; Verkman, Anderson, and Papadopoulos 2014; Verkerk, Lodder, and Wilders 2019
AQP8	H_2O, H_2O_2, urea, NH3	**ocular lens (*epithelium*)**, brain (*mitochondria*), kidney (*mitochondria*), lung (myoepithelial cell), liver (*hepatocytes*), testis (*spermatogenic cells* , *Sertoli cells*), colon, rectum, pancreas (*glandular cell*)	H_2O_2 transport across mitochondrial membranes	**No major abnormalities**	**None identified**	**Elkjer et al 2001; Takata, Matsuzaki, and Tajika 2004; Calamita et al 2005; Verkman, Anderson, and Papadopoulos 2014; Zhu, Ran, and Yang 2017; Verkerk, Lodder, and Wilders 2019**
AQP9	H_2O, H_2O_2, urea, glycerol, NH_3 , arsenite	liver (*hepatocytes*), red blood cells, testis (*Leydig cells* , *epididymal principal cells*), brain (*mitochondria* , *astrocytes* , *tanycytes* , *ependymal cells*), leukocytes, ovary (*oocytes*), intestine (*epithelium*), ear	glycerol metabolism, H_2O_2 transport across mitochondrial membranes	hyperglycerolaemia, reduced red cell glycerol permeability, H_2O_2 transport across mitochondrial membranes	None identified	Elkjar et al 2000; Takata, Matsuzaki, and Tajika 2004; Verkman, Anderson, and Papadopoulos 2014; Verkerk, Lodder, and Wilders 2019
AQP10	H_2O, urea, glycerol	**adipocytes, intestine (*epithelial cells* , *enterochromaffin cells*)**	**glycerol and water permeability in adipocytes**	**AQP10 is a pseudogene in mice**	**None identified**	**Hatakeyama et al 2001; Ishibashi et al 2002; Morinaga et al 2002; Takata, Matsuzaki, and Tajika 2004; Laforenza, Scaffino, and Gastaldi 2013a; Laforenza, Scaffino, and Gastaldi 2013b; Verkman, Anderson, and Papadopoulos 2014; Verkerk, Lodder, and Wilders 2019**
AQP11	H_2O, H_2O_2, glycerol	Liver, testis, kidney (proximal tubule), brain	regulation of proximal tubule endosomal acidification	polycystic kidneys, hepatocyte vacuolization, premature death	None identified	Takata, Matsuzaki, and Tajika 2004;Morishita et al 2005; Verkman, Anderson, and Papadopoulos 2014; Verkerk, Lodder, and Wilders 2019
AQP12	H_2O	**pancreas (*acinar cells*)**	**regulation of pancreatic beta-cell inflammatory phenotype**	**No major abnormalities**	**None identified**	**Takata, Matsuzaki, and Tajika 2004; Itoh et al 2005; Verkman, Anderson, and Papadopoulos 2014; Verkerk, Lodder, and Wilders 2019; da Silva et al 2020**

Table 1.1. Aquaporin permeability, tissue expression, roles, and associated pathologies in mice and humans.

AQP0

AQP0 is expressed in the ocular lens fiber cells and in the retina[38,39,56]. As the major AQP in lens fiber cells and most abundant lens transmembrane protein, AQP0 expression is indispensable to normal lens homeostasis. AQP0 functions as a water channel[57,58], a junctional protein[38,39,59–61], and a cell-cell adhesion protein[62,63] in the lens. AQP0 sets the baseline water permeability and water content in the ocular lens[58]. Genetic deletion of AQP0 increases *baseline* water content by almost 10%[58]. AQP0 is also required for proper lens cellular structure and gross morphology[58,64,65]. AQP0$^{-/-}$ mouse lenses exhibit abnormally wide extracellular spaces, large cytoplasmic vacuoles, abnormal suture formation, severe inner cortical and nuclear fiber cell disintegration, and abnormal gross lens morphology. These abnormalities are not rescued by transgenic expression of AQP1 in lens fiber cells despite increased AQP1 P_{H2O} in transgenic mice[64,65]. Importantly, AQP0 is required for lenticular transparency. AQP0-deficiency or mutation results in diminished lens optical quality (i.e. proper back focal length) and cataract[58,66–69]. AQP0 also regulates ocular lens biomechanics[70] and exhibits peroxiporin function (transmembrane, facilitated diffusion of H_2O_2) .

AQP1

AQP1 is significantly expressed in the vasculature[71], skeletal muscle[72], nervous system[73], and kidneys[50,74]. In the vasculature, AQP1 has a role in angiogenesis by increasing vascularity and hemoglobin content[75]. In the nervous system, AQP1 is strongly expressed in afferent sensory nerve fibers and in the choroid plexus[71,76,77]. AQP1 is theorized to play a role in cerebrospinal fluid production. In the kidneys, AQP1 is strongly expressed in the proximal tubule, descending limb of Henle epithelia, and vasa recta endothelia. AQP1 is important in concentrating urine and proper proximal tubular fluid reabsorption[78]. In the eye, AQP1 is expressed in the corneal endothelium and stromal keratocytes[79–85], the lens[74], and the ciliary body epithelium[71]. AQP1 expression maintains corneal and lenticular transparency during osmotic perturbation[86]. In the ciliary epithelium, AQP1 plays a putative role in aqueous humor production.

AQP2

AQP2 is expressed in the kidney cortical collecting duct, testes, and the Organ of Corti of the ear[87–89]. AQP2 regulates kidney water reabsorption, urine concentration, and systemic dehydration by undergoing stimulated secretion from AQP2-containing vesicles to cortical collecting duct plasma membranes in response to vasopressin, also known as the anti-diuretic hormone (ADH)[90,91]. AQP2-deficiency is associated with nephrogenic diabetes insipidus (NDI)[92].

AQP3

AQP3 is expressed in the skin, in the kidney cortical and medullary collecting duct, T-cells, red blood cells, and the digestive system[93–95]. In the skin, AQP3 is the most abundant skin aquaglyceroporin and important to skin epidermis hydration in mammals. In addition to being an aquaglyceroporin, AQP3 also functions as peroxiporin whose expression is important to T-cell migration[95]. AQP3 knockout mice also develop nephrogenic diabetes insipidus[96]. In the eye, AQP3 is also expressed in the conjunctiva and cornea.

AQP4

AQP4 is expressed in lung alveolar cells, skeletal muscle tissue, digestive system, highly expressed in the central nervous system (CNS) in astrocytes, salivary gland, lacrimal gland, ear, olfactory cells, and in kidney collecting duct cells[88,89,97–101]. In the CNS, AQP4 is important to osmotic regulation in the central nervous and implicated in brain edema and ischemic stroke[73,102,103]. Brain water content correlates linearly with brain AQP4 protein expression which implies it is the rate-limiting for brain water accumulation[103].In muscle cells, evidence suggests

that AQP4 expression is protective against muscle dystrophy diseases such as Duchenne muscle dystrophy (DMD) and limb-girdle muscular dystrophy type 2B (LGMD2B)[72,104,105].

AQP5

AQP5 is expressed primarily expressed in exocrine glands including the salivary glands[80,106], lacrimal glands[80,106], sweat glands[107], lungs[80,106], digestive system[108], and the ocular lens[43,45,46]. AQP5 is important for proper water content in saliva, tears, and sweat. In the eye, AQP5 is significantly expressed in the cornea where it maintains corneal thickness which is important to the maintenance of intraocular pressure, corneal biomechanics, and macular integrity[86,109]. AQP5 is also expressed throughout the ocular lens where it is essential for lenticular osmotic homeostasis[110,111] and lenticular transparency[110,112]. AQP5 is also an integral component of the lens microcirculation system[113–116] (**Section 1.3.5.**). These functions are discussed in dedicated sections later in this Introduction.

AQP6

AQP6 is expressed in cytoplasmic vesicles with H^+-ATPase in kidney duct acid-secreting α-intercalated cells[117]. In the kidney, AQP6 is predicted to play a role in glomerular filtration, tubular endocytosis, and acid-base metabolism[117].

AQP7

AQP7 is expressed in adipose tissue, heart muscle, skeletal muscle, and testes[88,118]. AQP7 regulates glycerol metabolism. AQP7 is also expressed in the ocular lens though the function of lenticular AQP7 remains unclear.

AQP8

AQP8 is primarily expressed in the lung, liver hepatocytes, testes, pancreas glandular cells, mitochondria of the kidney and brain, and the digestive system[88,119,120]. AQP8 is also expressed in the ocular lens where it exhibits peroxiporin function[49].

AQP9

AQP9 is expressed in liver hepatocytes, the testes, the brain (mitochondria, astrocytes, hypothalamus, and ventricles), oocytes, the ear, red blood cells, and the digestive system[88,89,121]. AQP9 functions in glycerol metabolism and exhibits peroxiporin function.

AQP10

AQP10 is expressed in the human gastrointestinal tract duodenum and the absorptive epithelial cells of the jejunum[54,122]. AQP10 is also expressed in white adipocytes in both the plasma membrane in cytoplasmic vesicles[123]. AQP10 is important to glycerol and water permeability in adipocytes[88,89,124,125]. Its expression is not conserved across mammalians as it is a pseudogene in mice[126] and cattle[127].

Superaquaporins – AQP11 and AQP12

Aquaporins are classified based on structure and function. AQP11 and AQP12, the superaquaporins or unorthodox aquaporins, have low homology in comparison to the classical aquaporins and the aquaglyceroporins[128]. Their NPA motifs deviate from the other mammalian AQPs and superaquaporins have less than 20% homology with other aquaporins. AQP11 has an NPC motif in the first NPA motif and normal second NPA motif. AQP12 has an NPT motif in the first NPA motif and normal second NPA motif.

AQP11

AQP11 is expressed in the liver, testes, kidney proximal tubule, and the brain[88,89]. The water transport of AQP11 is comparable to that of AQP1 in reconstituted liposomes[129]. AQP11 is expressed cytoplasmically in the proximal tubule in the kidneys where it is thought to regulate endosomal acidification and prevent hepatocyte vacuolization[88,89,130].

AQP12

AQP12 is expressed in pancreatic acinar cells where it regulates pancreatic beta-cell inflammatory phenotype[88,89,131]

1.2.2.2. Aquaporin Structure

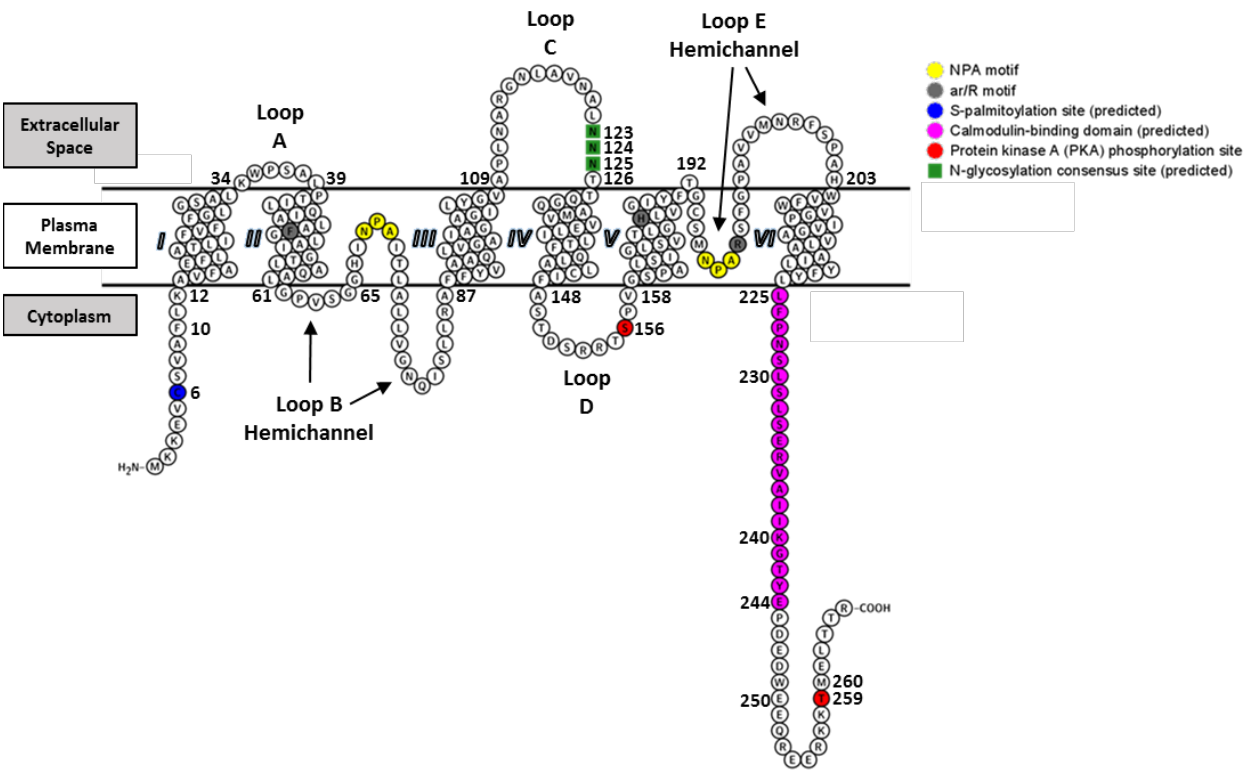

Figure 1.4. Membrane topology of human aquaporin-5 (AQP5).
Created with Protter[132].
Topology of human AQP5 (Uniprot accession number: P55064). AQP5 is an integral membrane protein with cytoplasmic N-and C-termini, six transmembrane helices (**I** – **VI**), and five loop regions (**Loop A** – **Loop E**). Two NPA motifs (yellow residues) are present within two half-helices which fold into the plasma membrane and in conjunction with the aromatic/arginine (ar/R) motif form a water-selective pore. Serine-156 and threonine-259 (red residues) are experimentally confirmed phosphorylation sites within protein kinase A (PKA) consensus sites. Asparagine-123, aspargine-124, and asparagine-125 residues represent N-glycosylation consensus sites (green residues). Residues 225-244 represent a putative calmodulin-binding domain (purple residues) and residue cysteine-6 represents an S-palmitoylation site (blue residue) based on homology to AQP0 and bovine AQP5, respectively. Aquaporin water transport function is due to intrinsic aquaporin protein structure and isoform-specific, cell-specific regulation of aquaporin expression, channel gating, and subcellular localization.

AQPs share structural homology comprised of two homologous halves with a conserved asparagine-proline-alanine (NPA) motif and an aromatic/arginine (ar/R) motif comprised of three amino acids[129,133] (**Figure 1.4**). Aquaporins contain six transmembrane domains, cytoplasmic N-terminus and C-terminus, two extracellular loops referred to as Loop A and Loop C, one cytoplasmic loop termed Loop D, and two hemichannel loops termed Loop B and Loop E which partially traverse the plasma membrane forming a seventh pseudotransmembrane domain and with each one containing an NPA motif[134,135]. Four AQP monomers associate *in vivo* to form a homotetramer and thereby form a narrow pore in the center of the oligomer that is hydrophobic

and thought to allow gas permeation of gases like CO_2[136]. The ar/R and NPA motifs constitute two separate selectivity filters (i.e. restriction sites) in the 20 angstrom AQP pore with the ar/R motif functioning as an outer pore selectivity filter[137,138] and the NPA motif functioning as a central pore selectivity filter[137]. The C-terminus of AQPs is variable amongst AQPs but often the site of regulatory posttranslational modifications and protein-protein interactions[135].

The NPA motif functions as a selectivity filter for cation exclusion (e.g. K^+, Rb^+, Na^+, Cs^+, Li^+). The asparagine residue of NPA motifs is of particular importance to cation exclusion and forms a constriction site within the channel pore[137]. Evidence suggests that mutation of this residue can affect water permeability, glycerol permeability, and/or cation exclusion[139]. Evidence also suggests that the NPA motif may be important for plasma membrane trafficking. NPA motifs are important to normal AQP plasma membrane trafficking as mutagenic deviation from NPA motifs can result in endoplasmic reticulum retention of AQP4[140] and AQP5[141]. Superaquaporins AQP11 and AQP12 have deviant Loop B NPA motifs comprised of NPC and NPT, respectively, and both AQP are localized cytoplasmically[142].

The ar/R motif functions as a second selectivity filter for solute selectivity and proton exclusion[143]. The ar/R motif is localized at the extracellular AQP pore mouth and functions as a selectivity filter in the narrowest point of the channel excluding molecules larger in size than H_2O in classic AQPs[137,138]. The extracellular AQP pore mouth in aquaglyceroporins is slightly larger, by approximately 1 angstrom, than that of classic AQPs enabling transport of glycerol and other small solutes like urea and ammonia[137,138]. Functional studies have shown that the positive charges in the ar/R motif form an electrostatic barrier to protons and mutation of these residues to uncharged amino acid residues allows proton passage into channel[138]. The ar/R motif selectivity filter region also contains four water binding sites that are important for the prevention of hydroxide ion (OH^-) passage through AQPs[144].

The C-terminus of AQPs is broadly important for regulatory posttranslational modifications and protein-protein interactions. Current structural data suggests that mammalian AQP C-termini contain a short, flexible α-helix whose local conformation may affected by phosphorylation[137,145–148]. The C-terminus of AQPs is the primary AQP interacting protein binding site[149], and AQPs are commonly phosphorylated in this region. In AQP0 and AQP2, protein-protein interactions are regulated by C-terminal phosphorylation. AQP0 contains a calmodulin-binding domain (CBD) and C-terminal phosphorylation reduces its interaction with calmodulin (CaM)[150,151]. Likewise, AQP2 C-terminal phosphorylation reduces its interaction with lysosomal trafficking regulator (LYST)-interacting protein 5 (LIP5)[152], G-actin[153], annexin-2[153], protein phosphatase 1C[153], clathrin heavy chain[153], dynamin[153], heat shock cognate 71 kDa protein (Hsc70)[153], and heat shock protein 70 (Hsp70)[153]. The regulatory relationship between AQP5 C-terminal phosphorylation and AQP5 protein-protein interactions remains to be broadly investigated as the AQP5 C-terminus is the binding site of several interacting proteins[154]. Furthermore, AQP5 has a putative CBD based on homology to AQP0[155] and can be phosphorylated at threonine-259 presumably by protein kinase A (PKA)[156]. This is particularly true for AQP5 as the effects of AQP5 C-terminal phosphorylation at threonine-259 upon its protein-protein interactions and subsequent function are unknown. AQP5 also is phosphorylated at serine-156 in cancer cells[157] and whether this phosphorylation affects protein-protein interactions also should be investigated.

AQPs also contain commonly contain N-linked glycosylation consensus sites in their extracellular loops[158]. AQP1[159–161], AQP2[92,162–164], AQP3[165], and AQP8[166]. AQP5 is presumed to be expressed with varying levels of glycosylation in the salivary glands, lung, cornea, and ocular lens[46,80]. These sites are often inefficiently recognized by oligosaccharyltransferase during protein synthesis which generates a mixture of glycosylated and unglycosylated species. Current evidence suggests that N-glycosylation is not believed to be important in the transport function of aquaporins[158], but may increase its cell surface expression in the case of AQP2[163]. AQP5 has a three asparagine amino acid residue motif at aspargine-123, asparagine-124, and

asparagine-125. Further research is needed to address the regulation of AQP5 glycosylation and AQP glycosylation in general to better understand the role of this posttranslational modification particularly in the ocular lens.

1.2.2.3. Lens Aquaporin Expression

The subcellular localization of AQPs in lens epithelial cells is non-uniform. AQP1 is expressed in apical and basolateral plasma membranes of lens epithelial cells[40–42]. AQP5 is expressed cytoplasmically in lens epithelial cells[40,45,46,111] but is observed with plasma membrane subcellular localization in these cells in lenses with age-related nuclear cataract[167]. AQP7 is expressed cytoplasmically and in apical plasma membranes in lens epithelial cells[47]. AQP8 is the most recently discovered lens AQP at the protein level being detected in human lens epithelial cells via Western blot[49] and immunofluorescence[48]. AQP8 is expressed cytoplasmically in lens epithelial cells.

As with AQPs in lens epithelial cells, the subcellular localization of AQP0 and AQP5 is distinctive across lens fiber cells. In lens fiber cells, AQP0 localizes to the plasma membrane. Alternatively, AQP5 is expressed cytoplasmically in the nascent outer cortical fiber cells[45,46,111,168]. From there, AQP5 is spatiotemporally expressed along a gradient of decreasing cytoplasmic localization and increasing plasma membrane localization with fiber cell differentiation. Cytoplasmic localization of AQP5 becomes undetectable by the inner cortical fiber cells. Thenceforth, AQP5 expression is restricted to the plasma membrane in nuclear fiber cells[45,46,168]. Cytoplasmic AQP5 in the outer cortex also dynamically trafficks between cytoplasmic compartments and the plasma membrane in response to changes in lens zonular tension[111,116].

1.2.2.4. Aquaporin Regulation

AQPs are regulated broadly via control of their expression, gating, and changes in subcellular localization via trafficking. This section will outline mechanisms of AQP regulation in mammals and additional mechanisms that have been observed such as mechanosensitive regulation of AQP1.

1.2.2.4.1. Regulation of Aquaporin Expression

Regulation of AQP expression is complex and varies by AQP type (e.g. AQP1 compared to AQP5) and often in cell-specific manner. Generally, AQP expression is regulated by hormones and small, non-hormonal signaling molecules as well as cellular microenvironmental signals such as changes in osmolarity. The expression of cellular context-specific proteins such as hypoxia inducible factor (HIF-1a) also is reported to regulate AQP expression. Thus, the regulation of AQP expression is broad, but there are some common patterns of regulation between certain classic AQPs and the aquaglyceroporins as outlined below.

Hormonal & Non-hormonal Signaling Molecule Regulation of AQP Expression

Hormones and small, non-hormonal signaling molecules represent common regulators of AQP expression. Upstream signaling hormones can trigger signal transduction cascades and thereby alter AQP expression.

Vasopressin, which triggers the vasopressin-cAMP-PKA pathway in the kidney, represents an example of one such hormone. Vasopressin (i.e. anti-diuretic hormone; ADH) is a peptide hormone secreted by the hypothalamus which binds the vasopressin V2 receptor (V2R) triggering increased cAMP production and thereby PKA activity[91]. Long-term cAMP increases AQP2 expression in the kidney in a manner dependent upon PKA activity[90,169]. V2R stimulation

can also be induced by other stimulants such as psychotropic drugs like haloperidol, sertraline, and carbamazepine[170].

AQP5 expression is also regulated via PKA activity in a cell-specific manner. Short-term treatment of AQP5-expressing cells with cAMP (or cAMP analogues) typically causes AQP5 internalization and degradation whereas prolonged treatment typically increases total AQP5 protein expression. Such is the case in uterine explants[171] and lung epithelial cells[172]. However, alterations to AQP5 expression is not observed in salivary gland cells despite them being responsive to PKA activity resulting in phosphorylation of AQP5[156].

Additionally, metabolism-related hormones and non-hormonal signaling molecules can alter AQP expression. AQP2 expression is reduced by adenosine triphosphate (ATP), uridine triphosphate (UTP), and dopamine via internalization and lysosomal degradation[173]. Aquaglyceroporin AQP9 expression is positively regulated by insulin[174].

Cytokines and steroids associated with inflammation are another common regulator of AQP expression. Tumor necrosis factor-α, a pro-inflammatory cytokine, reduces AQP5 expression in cultured mouse lung epithelial cells via agonism of tumor necrosis factor receptor superfamily member 1A (TNFR1)[175]. Progesterone and estradiol increase AQP1 and AQP5 expression in porcine uterine explants[171], and estradiol increases AQP5 expression in endometrial cells[176]. AQP1 expression increases in newborn rat lungs after treatment with the corticosteroid betamethasone[177]. Short-term cortisone stimulation increases AQP7 mRNA in white and brown differentiated adipocytes up to 6 fold[178]. In contrast, long-term cortisone stimulation decreases AQP7 mRNA expression[178]. AQP9 also has a glucocorticosteroid receptor being site in its promoter[179] and is also downregulated by estradiol treatment in the epididymis[180].

Cellular Microenvironmental Regulation of AQP Expression

AQP expression is regulated by alterations to the cellular microenvironment such as changes in tonicity and hypoxia. Hypertonicity increases AQP1 expression in the kidney[181–184]. Hypertonicity induces extracellular signal-regulated kinase (ERK)-dependent increase in AQP5 expression in mouse lung epithelial cells [185].

Hypotonicity also affects the expression of multiple AQPs. Hypotonicity induces TRPV4 activation-dependent decrease in AQP5 expression in mouse lens epithelial cells[186]. Hypotonicity downregulates AQP8 protein expression in amnion epithelial cells[187]. AQP1 expression in the choroid plexus is decreased in response to hypotonic challenge with hyponatremia[188].

Hypoxia affects the expression of both AQP2 and AQP5 via hypoxia inducible factor (HIF-1α) expression. AQP2 protein expression is positively correlated with HIF-1a expression[189], while hypoxia and hypoxia-mimetics as cobalt induce HIF-1α-dependent reduction in AQP5 expression in lung cells[190].

1.2.2.4.2. Regulation of Aquaporin Gating – Posttranslational Modifications

Gating is defined as the transition process between open and closed channels states, which controls permeation of substrates such as water and glycerol for aquaglyceroporins, through an AQP channel[191]. Of the thirteen mammalian AQPs, most are constitutively open without strong evidence of gating regulation. However, gating regulation has been demonstrated for AQP0, AQP3, AQP4, and AQP6. AQP posttranslational modification via phosphorylation, truncation, or pH is the primary mechanism of AQP gating regulation though evidence suggests AQP1 gating via mechanosensation.

AQP0

AQP0 gating is regulated by pH, Ca^{2+}-mediated calmodulin (CaM) binding, C-terminal phosphorylation[150,151], C-terminal truncation[192,193], and the lipid microenvironment[194]. Electron crystallographic data indicate that C-terminal truncation lowers AQP0 permeability[146]. Lower pH increases AQP0 water permeability. In transfected oocytes, a pH shift from 7.5 to 6.5 increases bovine AQP0 water permeability by a factor of 1.8[195]. CaM binds to the AQP0 C-terminus decreasing AQP0 water permeability by allosterically closing the cytoplasmic gate of AQP0[155,195,196]. AQP0 C-terminal phosphorylation at serine-235 (S235) represents the major phosphorylation site followed by serine-231 (S231) and serine-229 (S229)[192,197]. AQP0 C-terminal phosphorylation reduces CaM binding 20-50 fold[150,151]. AQP0 water permeability is also reduced with increased sphingomyelin and cholesterol lipid bilayer content[194].

In the ocular lens, pH decreases significantly from the lens surface to the lens core[198–200]. In contrast, cytoplasmic Ca^{2+} increases significantly towards the lens core[201–203] which increases the CaM-AQP0 C-terminal interaction and reduces AQP0 P_{H2O}. Collectively, lens pH and Ca^{2+} will exert opposing gating effects on AQP0 and respectively increase and decrease P_{H2O} from the lens periphery towards the lens core. AQP0 C-terminal S229 and S235 phosphorylation also varies spatiotemporally with age decreasing from the lens periphery to the lens core in older human subjects particularly after the lens barrier region[192,197].

Lenticular AQP0 also undergoes significant deamidation at aspargine-243, asparagine-246, and asparagine-259 and sequential C-terminal truncation (i.e. cleavage) via nonenzymatic peptide backbone cleavage[192,193]. Deamidation kinetics vary based on several factors including pH, temperature, time, protein structure (i.e. 1^O and 2^O), and organism age[204]. AQP0 C-terminal truncation is associated with the cell junctional form of AQP0 and potential restriction of gating[59,146,205].

Lastly, AQP0 gating may be regulated by localization within plasma membrane in lens fiber cells. AQP0 also undergoes protein lipidation via palmitoylation and oleoylation on amino acid residues methionine-1 (M1) and lysine-238 (K238) residues[206]. AQP0 lipidation is thought to regulate AQP0 by targeting AQP0 to lipid raft domains, and lipidated AQP0 is highly enriched in lipid raft domains[207,208], which contain higher sphingomyelin and cholesterol content relative to non-lipid raft domains[209]. Additionally, sphingomyelin and cholesterol content increase spatiotemporally from lens periphery to the lens core[210] and with fiber cell age[211,212]. Thus, AQP0 lipidation and plasma membrane domain localization are increasingly expected to reduce AQP0 P_{H2O} spatiotemporally towards the lens core with age.

AQP3

AQP3 gating is pH-dependent. Exogenously expressed rat AQP3 (rAQP3) P_{H2O} and glycerol permeability (P_{Gl}) are abolished below pH 5.5 and pH 5.6[213], respectively. AQP3 pH-sensitivity varies slightly across mammals with human AQP3 (hAQP3) gating is abolished below approximately pH 5.0[214].

AQP4

AQP4 gating is regulated by phosphorylation at S111 and S180 in its cytoplasmic loop domains and by pH. S111 phosphorylation increases AQP4 P_{H2O}[215,216] while S180 phosphorylation decreases AQP4 P_{H2O}[217,218]. AQP4 S180 phosphorylation is protein kinase C (PKC)-dependent[217,218]. In contrast to AQP3 and AQP6, alkaline pH increases AQP4 P_{H2O}. A pH shift from 7.5 to 8.5 increases exogenously transfected AQP4 water permeability by1.9 fold[195].

AQP6

AQP6 gating is pH-dependent but differs in pH-sensitivity range to other AQPs[219]. AQP6 P_{H2O} is abolished above pH 5.5, but increases rapidly below pH 5.5. AQP6 is also permeable to anions such as chloride (Cl^-) below pH 5.5[219].

1.2.2.4.3. Regulation of Aquaporin Subcellular Localization

Regulation of AQP subcellular localization is an additional mechanism of cellular water content and osmotic control. Most AQPs are constitutively trafficked to the plasma membrane, but AQP2 and AQP5 undergo regulated trafficking to the plasma membrane. AQPs are also observed to undergo internalization via endocytosis. Posttranslational modification and protein-protein interactions are common mechanisms by which AQP subcellular localization is regulated.

Regulation of AQP2 Subcellular Localization

V2R activity regulates AQP2 subcellular localization in the kidney. Short-term V2R activation induces trafficking of cytoplasmic AQP2 to cortical collecting duct plasma membranes via C-terminal phosphorylation at serine-256 (S256), serine-S264 (S264), and serine-S269 (S269)[90,91,220,221]. In turn, AQP2 S269 phosphorylation regulates AQP2 endocytosis[153,222]. AQP2 also undergoes PKA-independent S269 phosphorylation-dependent plasma membrane trafficking in response to Src kinase inhibition[223]. Src inhibition induces AQP2 S269 phosphorylation which inhibits clathrin-mediated endocytosis[223].

AQP2 C-terminal modification regulates trafficking-related AQP2 protein-protein interactions. AQP2 S256 and S269 phosphorylation reduce AQP2 interaction with proteins which positively regulate endocytosis including Hsp70, Hsc70, dynamin, and clathrin heavy chain[153]. AQP2 C-terminal S256, S261, and S264 phosphorylation all reduce the interaction of AQP2 with lysosomal-trafficking regulator (LYST)-interacting protein 5 (LIP5)[152], which targets AQP2 for degradation[224]. In contrast, AQP2 lysine-270 ubiquitination triggering endocytosis for plasma membrane recycling or lysosomal degradation[225].

Regulation of AQP4 Subcellular Localization

Vasopressin and histamine were shown to induce AQP4 endocytosis in oocytes[226] and in human gastric cells[227], respectively.

Regulation of AQP6 Subcellular Localization

Subcellular targeting sequences can be encoded into the amino acid sequences of AQPs. AQP6 contains an N-terminal cytoplasmic retention sequence[228]. AQP1 and AQP6 chimera proteins, in which their N-terminal sequences are swapped, exhibit swapped subcellular localization with the AQP1 chimera and AQP6 chimera exhibiting cytoplasmic and plasma membrane subcellular localization, respectively[228]. Calmodulin binds AQP6 at its N-terminus (Ca^{2+}-dependent)[229]. Whether calmodulin binding affects AQP6 subcellular localization is unclear.

1.2.3. Lens Gradient Index of Refraction (GRIN)

As mentioned above, crystallin synthesis is greatly upregulated as lens fiber cells undergo differentiation. Following fiber cell maturation protein turnover ceases due to organelle degradation, yet lens crystallin concentration increases as a gradient radially inward towards the lens center past the organelle-free zone giving the lens a parabolic GRIN across its equatorial diameter[230]. That is, crystallin concentration increases without protein synthesis in the lens organelle-free zone (OFZ) which is attributable to lens fiber compaction as lens fiber cells age. Lens fiber cell volume reduction via cellular compaction is presumed to be attributable to water loss from the cytosol and extracellular spaces[70,230].

The lens GRIN performs multiple functions. Lens GRIN directly renders negative spherical aberration in the ocular lens relative to a homogenous refractive index[231]. Lens negative spherical aberration counteracts corneal positive aberration, which in turn minimizes total eye spherical aberration. Additionally, the lens GRIN reduces the protein synthesis burden required to achieve the equivalent refractive index, the equivalent refractive index for a lens of uniform composition with the same physical dimensions. The protein concentration required to achieve equivalent refractive index is significantly larger than measured lens protein concentrations and would alter lens viscoelastic properties and thereby likely alter lens accommodation kinetics[230].

Lens GRIN is also actively maintained by positive and negative feedback systems of lens ion transporters and channels that establish the lens microcirculation system such as the Na^+/K^+ ATPase and lens aquaporins. Vaghefi et al demonstrated that inhibition of bovine lens Na^+/K^+ ATPases pharmacologically with the inhibitor ouabain or electrochemically by reversal of cellular ionic gradients with artificially high extracellular K^+ concentration disrupts lens GRIN by inhibiting the lens microcirculation system and increasing lens free water content [232]. Consequently, lens aquaporins are functionally relevant to the cellular process of fiber cell compaction. Aquaporin-0 (AQP0) deficiency significantly decreases lens fiber cell compaction and increases extracellular space[70]. AQP0 C-terminal truncation alone even with proper protein expression levels is theorized to disrupt lens GRIN[233–235]. Lens optical quality was also perturbed in these experiments resulting in lens power, spherical aberration, or visual distortion abnormalities. AQP5-deficient mouse lenses also exhibit visual distortion under osmotic perturbation attributable to fiber cell swelling and cataract[110] which suggests a direct relationship to the lens GRIN. The direct effects of lenticular AQP5 expression on fiber cell compaction and lens GRIN remain to be tested experimentally.

1.3. Ocular Lens Physiology

1.3.1. Lens Sodium and Potassium Channels and Transporters

Ionic homeostasis is intrinsically connected to proper lens function. That is, dysregulation of lens ionic balance alters lens water content which in turn affects lens optical quality and transparency. Thus, in addition to several AQPs such as AQP5, the lens expresses several sodium and potassium channels and transporters to maintain homeostasis and therefore osmotic balance. These include but are not limited to Na^+/K^+ ATPase, Na-K-Cl cotransporter 1 (NKCC1), Na^+-Cl^- cotransporter (NCC), K^+Cl^- cotransporter (KCC), transient receptor potential cation channel subfamily V member 1 (TRPV1), and transient receptor potential cation channel subfamily V member 4 (TRPV4). TRPV1 and TRPV4 are mechanosensitive, nonselective cation channels and will be discussed in **Section 1.3.2.**. Many of these are integral proteins of the lens microcirculation system (MCS). Their roles in the MCS will be discussed in detail in **Section 1.3.5.**.

Na+/K+ ATPase in the Lens

Na^+/K^+ ATPase is a ubiquitous active transporter in animal cells that regulates cellular ionic homeostasis, resting membrane potential, and cellular volume[236]. Na^+/K^+ ATPase transports three sodium ions (Na^+) from the cytoplasm to the extracellular space and two potassium ions (K^+) from the extracellular space into the cytoplasm.

Na^+/K^+ ATPase is essential to the establishment of the lens MCS and in part a function of spatiotemporally stratified Na^+/K^+ ATPase activity in the lens[8,237–239]. In human lenses, the epithelium, cortex, and nucleus are responsible for approximately 38%, 48%, and 14% of total

lens Na^+/K^+ ATPase activity[240]. Relative Na^+/K^+ ATPase activity is highest in equatorial lens epithelial and cortical fiber cells[240]. Fiber cell Na^+/K^+ ATPase activity is largely confined to differentiating fiber cells and decreases with fiber cell age[239]. Global lenticular Na^+/K^+ ATPase activity generates circulating Na^+ currents which osmotically drive concomitant, circulating water flow. AQPs are proposed to transport this Na^+-driven water flow in conjunction with lens gap junctions[20,238,241,242]. This fluid flow forms the basis of the lens MCS as discussed in **Section 1.3.5.**.

Na-K-Cl cotransporter 1 (NKCC1) in the Lens

Na-K-Cl cotransporter 1 (NKCC1) also regulates the lens MCS by cotransporting one sodium, one potassium, and two chloride ions from the extracellular space to the cellular cytoplasm. The lens expresses NKCC1 in epithelial and equatorial cortical fiber cells[243–245]. In rat lenses, NKCC1 is expressed cytoplasmically in the cortex and outermost nuclear fiber cells[244]. As lens fiber cell age increases, NKCC1 expression transitions to the plasma membrane and is detectable immunohistochemically throughout the remainder of the lens nucleus aside from the fetal and embryonic nucleus[244].

Functionally, NKCC1 in conjunction with lens AQPs regulates peripheral fiber cell volume and extracellular space volume in the lens. NKCC1 is activated by both cell shrinkage and decreased cytoplasmic Cl^- concentration[246]. Pharmacological NKCC1 inhibition with bumetanide induces peripheral cortical fiber cell shrinkage, inner cortical extracellular space swelling, and cortical cataract[244].

Na^+-Cl^- cotransporter (NCC) in the Lens

Na^+-Cl^- cotransporter (NCC) is an additional Na^+ transporter implicated in lens MCS function through the cotransport of one sodium and one chloride ion from the extracellular space to the cytoplasm. In the rat lens, NCC is expressed cytoplasmically and in the plasma membrane in the lens cortex and nucleus, respectively[244]. Hypotonic osmotic perturbation induces internalization of plasma membrane localized NCC[244].

K^+Cl^- cotransporter (KCC) in the Lens

K^+Cl^- cotransporter (KCC) is a K^+ transporter implicated in lens MCS function through cotransport of one potassium ion and one chloride ion from the cytoplasm to the extracellular space. Mouse and rabbit lenses express all KCC four isoforms – KCC1, KCC2, KCC3, and KCC4[245,247]. KCC1 and -3 are expressed in the lens cortex while KCC2 and KCC4 are expressed throughout the lens cortex and nucleus. Cortical fiber cell KCC expression is primarily cytoplasmic while nuclear fiber cell KCC expression is primarily localized to the plasma membrane. KCC regulates peripheral fiber cell volume and extracellular space volume in the lens. Inhibition of KCC channels with [(dihydronindenyl)oxy] alkanoic acid (DIOA) induced cortical fiber cell swelling and cataract[247] while activation of KCC channels with N-ethylmaleimide (NEM) induced peripheral cortical fiber cell shrinkage and cell swelling in older lens fiber cells.

1.3.2. Lens Transient Receptor Potential (TRP) Channels

Transient receptor potential (TRP) channels are transmembrane ion channels in animal cells that function in sensory signal transduction including vision, thermosensation, olfaction, hearing, and mechanosensation[248]. TRP channels in animal cells are classified into seven subfamilies – TRPC, TRPV, TRPM, TRPN, TRPA, TRPP, and TRPML, which respectively stand for the canonical (-C), vanilloid (-V), melastatin (-M), no mechanoreceptor potential C (-N), ankyrin (-A), polycystic (-P), and mucolipin (-ML) subfamilies[248,249].

TRP channels are nonselective cation channels permeable to sodium, potassium, calcium and magnesium[250,251].. TRP channels are typically closed at resting state but open after activation in response to diverse endogenous and exogenous stimuli. The focus of this section will be TRPV1 and TRPV4, the primary TRP channels expressed in mammalian lenses. The role of TRP channels in the lens microcirculation system (MCS) will discussed in detail in **Section 1.3.5.**.

TRPV1 and TRPV4 Activation and Permeability

TRPV1 canonically regulates bodily responses to ambient temperature and is widely expressed in nociceptors, neurons responsible for pain response. TRPV1 is activated by capsaicin, thermally nociceptive stimuli (temperatures > 43ºC), hypoxia, hypertonicity, extracellular acidic pH and is modulated by phosphorylation and lipids[251–253]. TRPV1 was demonstrated to be a nonselective cation channel following electrophysiological analysis of exogenously TRPV1-transfected HEK293 cells[251]. TRPV1 is permeable to monovalent cations and calcium[254].

TRPV1 activity is negatively regulated via interaction with calmodulin in a Ca^{2+}-dependent manner[255]. Cytoplasmic and extracellular Ca^{2+} concentrations regulate TRPV1 desensitization with cytoplasmic Ca^{2+} increases inducing acute desensitization[256] and extracellular calcium depletion inducing slow desensitization[257].

TRPV4 also regulates bodily response to temperature and is activated by moderate thermal stimulus (24ºC - 27ºC), hypotonicity, and endocannabinoids, an endogenous class of lipids[258]. Mammalian TRPV4 is both mechanosensitive and osmosensitive and thus can be activated by osmotic cell swelling and mechanical stimuli[259]. Like TRPV1, TRPV4 is also a nonselective cation channel that is permeable to monovalent cations, calcium ions, and magnesium ions[260].

TRPV1 and TRPV4 Expression in the Lens

TRPV1 spatial expression in the mammalian lens varies by species. In humans and rabbits, TRPV1 appears to be cytoplasmically expressed in lens epithelial cells[261] while in mice TRPV1 is expressed in lens epithelial and fiber cells[262]. Mouse TRPV1 is cytoplasmic in differentiating lens fiber cells and is localized to the plasma membrane in mature lens fiber cells.

TRPV4 spatial expression has only been defined in the mouse lens although TRPV4 expression is detected by Western blot in the porcine lens epithelial and cortical lens fibers[263]. TRPV4 is expressed in mouse lens epithelial and fiber cells with very similar spatial localization to TRPV1[262]. TRPV4 spatial expression is regulated by tension across lens zonular fibers (i.e. zonules of Zinn) with loss of tension inducing a shift from cytoplasmic expression to plasma membrane expression in the lens cortex[262].

TRPV1 and TRPV4 Function in the Lens

TRPV1 and TRPV4 activity maintains lens volume, ionic and osmotic homeostasis, and downstream signal transduction related to their activation (e.g. Ca^{2+} signaling). General TRPV1 and TRPV4 function in the lens will be discussed in this section. Lenticular TRPV1 and TRPV4 are critical components of the MCS which will be discussed further in **Section 1.3.5.**.

TRPV1 regulates ionic and osmotic balance in the lens by activating NKCC1 and AQP5 cytoplasmic and plasma membrane subcellular localization upon hypertonic challenge in the ocular lens[115,116,262,264]. Pharmacological TRPV1 inhibition via antagonist A-889425 treatment blocks NKCC1 activation-associated current (i.e. cotransport) and phosphorylation. TRPV4 also maintains lenticular ionic and osmotic balance upon hypoosmotic challenge via direct regulation of Na^+/K^+ ATPase[265]. TRPV4 activation via hypotonic challenge increases Na^+/K^+ ATPase activity in porcine lenses[265]. TRPV1-mediated Na^+/K^+ ATPase activation requires hemichannel-dependent, Ca^{2+}-mediated ATP release and is coupled with Src kinase activation (i.e. phosphorylation), which is required for lenticular Na^+/K^+ ATPase activation[263]. Additionally,

although TRPV4 spatial expression is limited to the lens epithelium, TRPV4-mediated Na^+/K^+ ATPase is sensitive to changes in significantly distant lens fiber cell perturbations[263].

1.3.3. Lens Gap Junctions

Connexins are transmembrane proteins which oligomerize into hexameric channels termed connexons, or gap junction channels. Connexons are permeable to small solutes $\leq$ ~1 kDa enabling bidirectional diffusion of small molecules across their pores[266,267]. Mammalian lenses spatiotemporally express connexin-43 (Cx43), connexin-46 (Cx46), and connexin-50 (Cx50) with Cx43 and Cx50 being expressed in lens epithelial cells, while Cx46 and Cx50 are expressed in lens fiber cells[268–275]. In the lens, gap junction channels allow passage of metabolites (e.g. glucose, ascorbate), ions, and water to maintain lenticular homeostasis[276]. Cx46 and Cx50 expression are essential for lens transparency with Cx46-deficiency and Cx50-deficiency in mice resulting in nuclear cataracts[272,277–280].

Gap Junction Channel Coupling in the Lens

Gap junction channels are concentrated within the broad sides of lens fiber cell plasma membranes[281] and can associate in the hundreds to form gap junction plaques[276]. Diffusion across gap junction plaques is dependent upon gap junction coupling, which in turn is affected by posttranslational modifications, local pH, local calcium concentration, and protein-protein interactions[282–285]. Collectively, lenticular spatiotemporal differences in these factors result in regional differences in gap junction coupling in the ocular lens[286], and these regional differences in coupling along with lens AQP expression serve to direct fluid flow of the lens MCS into lens sutures, across fiber cell membranes in the lens core, and ultimately back to the lens equatorial surface via an intercellular pathway[242].

1.3.4. Lens Extracellular Diffusion Barrier

Maintenance of fiber cell packing and extracellular space is critical for proper light refraction and lens transparency. Fiber cell swelling or extracellular space dilation increases lenticular light scattering[287,288]. Extracellular space between lens fiber cells decreases spatiotemporally with increasing fiber cell age. Paterson 1970 conducted radiolabel uptake analysis and determined rabbit lens extracellular space to be approximately 4.5% and 3.4% of total cortical and nuclear volume, respectively[289]. Thus, extracellular space varies regionally within the lens. Maintenance of fiber cell packing and extracellular space is critical for proper light refraction and lens transparency. Fiber cell swelling or extracellular space dilation or increases lenticular light scattering[287,288].

Comprehensive analysis of spatiotemporal changes in extracellular space revealed an extracellular space diffusion barrier that restricts small molecule diffusion via the extracellular space between the cortex to the nucleus[290–293]. Vaghefi et al 2012 measured extracellular space diffusion and morphology by analyzing gadolinium (Gd) reagent (Gd^{3+} and Gd-diethylenetriamine pentaacetic acid [Gd-DTPA]) penetration via inversion recovery-spin echo (IR-SE) magnetic resonance imaging (MRI) and histochemical analysis. Surprisingly, extracellular space is virtually undetectable in the inner cortex with Gd reagents indicating profound extracellular space constriction and the formation of a diffusion barrier between peripheral and core lens fiber cells. Gd reagent penetration to the extracellular space between lens core fiber cells appears to occur via lens sutures. The spatial localization of this extracellular bovine lens “diffusion barrier” is broad in width with the normalized distance of its outer boundary and inner boundaries equal to ~ *r/a* 0.7 and 0.4, respectively, through recent

estimates demonstrate that outer boundary could extend as far as *r/a* 0.9 based on the size and type of reagent used. Extracellular diffusion barrier is observed in in rats and humans though its boundaries vary in a species-specific manner.

The extracellular diffusion barrier was recently determined to coincide spatially with broad proteomics changes in bovine lenses. In particular, AQP0, gap junction proteins, several cell junctional proteins, the AQP0- and AQP5-interacting cytoskeletal protein ezrin, and the related AQP0-interacting cytoskeletal protein radixin all increase in expression concomitantly with the development of the extracellular diffusion barier[291]. AQP0 phosphorylation at serine-229 and serine-235 also decreases substantially with age after the extracellular diffusion barrier[294]. The decrease in AQP0 C-terminal phosphorylation, which is shown to reduce calmodulin binding affinity[150,151], may contribute to extracellular diffusion barrier formation by restricting water permeability in this region. Cell junctional protein changes are also associated with the paracellular barrier formation and changes in extracellular space[295].

AQP5 directly interacts with and regulates multiple cell junctional proteins at the plasma membrane reducing their expression as outlined in **Section 1.6.3.2.** Thus, both lens AQP0 and AQP5 are implicated in lens extracellular diffusion barrier formation. Nevertheless, the role of AQP5 water transport and cell junction protein expression regulation in lens barrier formation remains unclear. Understanding the relationship between AQP5 subcellular localization, protein-protein interactions, C-terminal phosphorylation, and this putative role would be of particular importance as AQP5 water transport and cell junction function are regulated by the former two. Ultimately, AQP5 water transport function and cell junction function are essential to understand to determine the specific roles of AQP5 in the lens MCS.

1.3.5. Lens Microcirculation System (MCS)

The lens is the largest avascular organ in the body[238]. The kinetics of diffusion within lens tissue are insufficient for proper cellular nutrient supply and waste removal in the stead of a blood supply[8]. The lens microcirculation system (MCS) is a system of circulating ion fluxes and concomitant water flow driven by lens ion transporters, ion channels, and lens aquaporins that fulfills this role by convecting nutrients to and waste from deeper fiber cell layers[8,238,296,297]. The MCS maintains lens ionic and osmotic homeostasis and thereby maintains lens transparency and optical properties[8,238,298].

The MCS is generated by a circulating Na^+ current which is primarily driven by Na^+/K^+ ATPase activity, which is concentrated at the lens equator region. Na^+ enters the lens sutures via the lens poles (i.e. influx region) into the extracellular space similar to Gd reagents and traverses fiber cell membranes via hypothesized Na^+ leak channels and in part by Cx46 hemichannels[20,241,242,299]. The electrochemical gradient of Na^+ results in a driving force for Na^+ to enter lens fiber cells, and the lens extracellular barrier is proposed to restrict passage of extracellular Na^+ from the lens core towards the lens periphery[290,291]. Once Na^+ enters lens fiber cells, Na^+ is driven out the lens at the lens equator (i.e. efflux region) by Na^+/K^+ ATPase activity through an intercellular outflow pathway via gap junction channels[242]. Water flows in parallel with Na^+ currents generating fluid flow with water also entering the lens via the lens poles and exiting at the lens equator[297]. This fluid flow convects nutrients and antioxidants such as glutathione and ascorbic acid to deeper fiber cell layers where transmembrane transporters enable their import into these cells[300]. These transmembrane transporters include three glucose transporters – GLUT1, GLUT3, and SGLUT2, six glutamate transporters – EAAT1-EAAT5 and ASCT2, two glycine transporters – GLYT1 and GLYT2, the cystine/glutamate antiporter xCT, and the ascorbic acid transporter SVCT2[300]. The extracellular diffusion barrier is proposed to preferentially direct the flow of water and associated nutrients and antioxidants to the sutures

and extracellular spaces (i.e. similar to Gd reagents) by restricting radial extracellular space diffusion in the inner cortex[20,241,242,290].

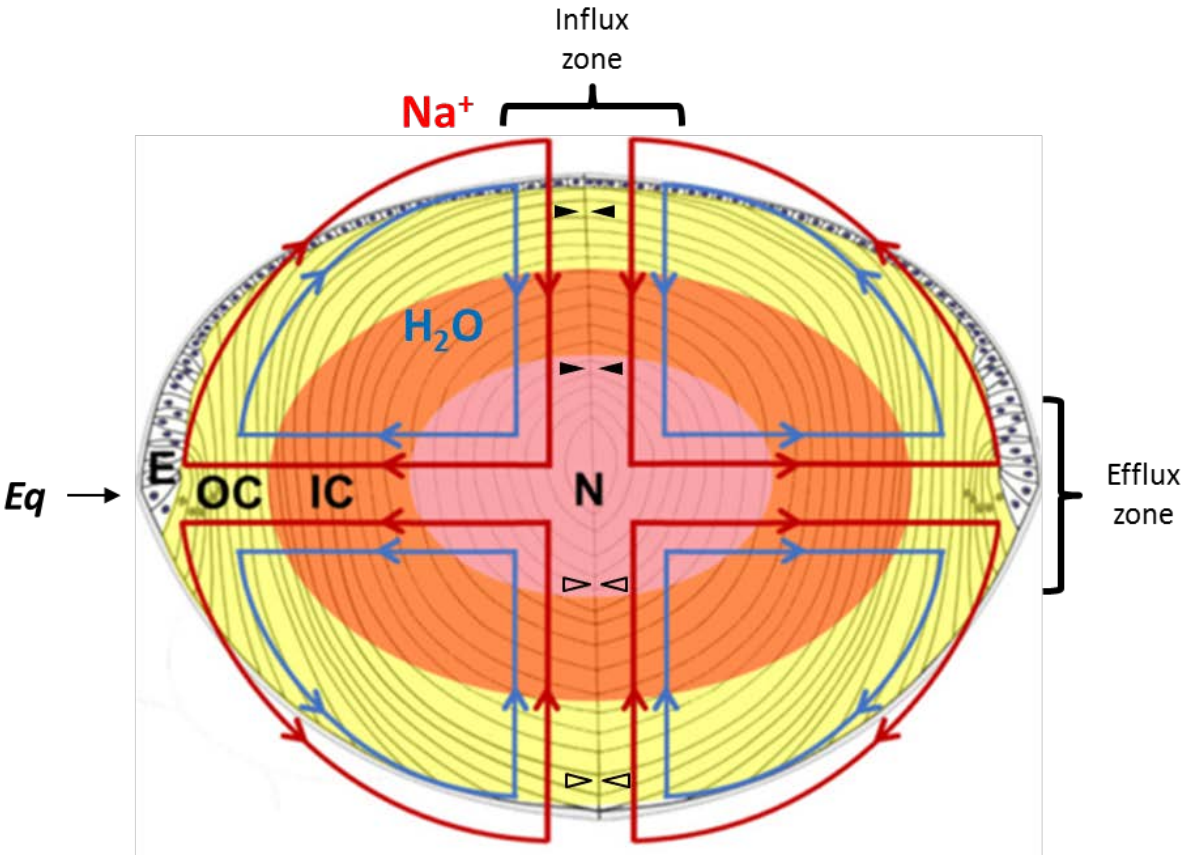

Figure 1.5. The lens microcirculation system (MCS).
Adapted with permission from Figure 1B in Schey et al 2017 in *Int J Mol Sci*[20].
DOI: 10.3390/ijms18122693
The anterior surface of the ocular lens consists of a monolayer of epithelial cells (**E**) which differentiate at the lens equator (***Eq***) into elongated fiber cells. Fiber cells, which comprise the bulk of lens cellular mass, become organized into symmetrical growth shells in which the older, centermost cells comprise the lens nucleus (**N**) while newly differentiating fiber cells are found in the surrounding outer cortex (**OC**) and inner cortex (**IC**) lens regions. Fluid flow comprised of circulating Na^+ currents (red arrows) generated by the Na^+/K^+ ATPase and concomitant water flow (H_2O; blue arrows) enters the lens at the anterior and posterior sutures (closed arrowheads and open arrowheads, respectively) then exits at the lens equator. These circulating fluid flows and the lens ion transporters, ion channels, and aquaporins that generate them represent the lens microcirculation system (MCS). The lens MCS convects cellular nutrients to and cellular waste products from the avascular lens faster than would be achieved solely by passive diffusion. The suture regions and the lens equator regions are termed the MCS *influx zone* and *efflux zone*.

Circulating Na^+ currents also generate intracellular hydrostatic pressure which also drives water to the lens surface via the intracellular outflow pathway[301,302]. Inhibition of circulating Na^+

currents pharmacologically with the Na^+/K^+ ATPase inhibitor ouabain or via substitution of normal extracellular Na^+ and K^+ concentrations respectively reduce or eliminate the lenticular hydrostatic pressure gradient[301]. Gao et al 2013 demonstrated that this pressure is approximately 335 mmHg at the lens surface and 0 mmHg in the lens center in all species examined[302]. Gap junction expression and coupling are both critical to establishment of proper intracellular lens hydrostatic pressure gradient with intracellular lens hydrostatic pressure at the center of the lens varying inversely to gap junction channel quantity[301].

Hydrostatic pressure at the lens surface is maintained at 0 mmHg via a complex feedback regulation loop regulated by TRPV1 and TRPV4 upstream of Na^+/K^+ ATPase activity. Gao et al 2015 details this signaling pathway[113] which was later updated by Shahidullah et al 2020[115]. Briefly, negative hydrostatic pressure changes activate TRPV4 inducing ATP release and activating purinergic receptor P2Y, which positively regulates Src kinase activation. Src kinase activation activates Na^+/K^+ ATPase which reduces intracellular osmolarity and raises surface hydrostatic pressure to counteract negative hydrostatic pressure. In contrast, positive hydrostatic pressure changes activate TRPV1 inducing ERK1/2 activation which activates phosphoinositide 3-kinase (PI3K). PI3K positively regulates Akt kinase which activates NKCC1. NKCC1 activation increases intracellular osmolarity decreasing surface hydrostatic pressure to counteract positive hydrostatic pressure. Chen et al. 2019 demonstrated that TRPV channels are in turn regulated upstream by the ciliary muscle, which controls tension across lens zonular fibers[114]. Ciliary muscle contraction increases lens intracellular pressure via TRPV1 activation while ciliary muscle relaxation decreases lens intracellular pressure via TRPV4 activation.

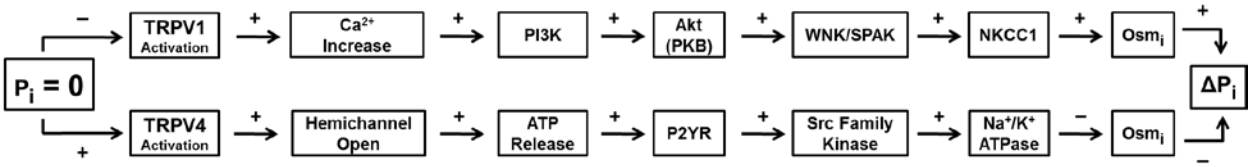

Figure 1.6. Lens hydrostatic pressure feedback regulation.
A schematic depicting short-term a dual feedback loop by which lens surface cells regulate intracellular hydrostatic pressure. One arm of responds to hypertonicity via TRPV1 activation while the second arm responds to hypotonicity via TRPV4 activation. The original lens hydrostatic pressure feedback loop was summarized in Gao et al 2015[113] and subsequently updated in Shahidullah et al 2020[115].

Lenticular aquaporin (AQP) expression is integral to the establishment of the MCS. AQPs enable the transmembrane diffusion of water down osmotic gradients. Fluid flow that follows circulating Na^+ current patterns was confirmed in an isolated bovine lens[290,297,303], and lens AQPs and gap junctions formed by lens connexins mediate this fluid flow. Genetic ablation of AQP0 reduced fiber cell membrane water permeability in AQP0-null ($AQP0^{-/-}$) mice[304]. AQP5 also contributes significantly to fiber cell membrane water permeability. AQP5-null mouse lenses exhibit osmotic swelling and increased lens water weight[110]. Additionally, AQP5 is dynamically trafficked between cytoplasmic vesicles and the plasma membrane as a function of TRPV4 activity[111,116]. TRPV4 activation induces AQP5 internalization from fiber cell plasma membranes in the lens efflux and influx regions which directly implicates AQP5 water transport function in lens MCS function via reduction of lenticular intracellular osmolarity and regulation of negative hydrostatic pressure at the lens surface. Fluid flow in lenses remains to be examined in AQP-null mice to determine the direct effects of AQP genetic ablation on the lens MCS.

Nevertheless, it is likely that fluid flow, and thereby the lens MCS, will be altered significantly in the absence of lenticular AQPs such as AQP5.

1.4. Autophagy

Autophagy (Greek for 'eating of self') is a cellular process characterized by bulk degradation of proteins and organelles[305]. Autophagy is a mechanism for degradation of soluble proteins, aggregated proteins, organelles, macromolecular complexes, and foreign bodies[305]. Autophagy is canonically upregulated through cellular starvation and represents a cellular mechanism of catabolism that “recycles” amino acids, fatty acids, nucleosides, nucleotides, and saccharides that can be reused to synthesize new macromolecules or regenerate metabolic precursors[306]. Autophagy is a constitutive process in the ocular lens[307] and significant evidence implicates autophagic degradation in lenticular organelle degradation via phosphoinositide-3-kinase – Akt – mammalian target of rapamycin (PI3K-Akt-mTOR) pathway activity [308–311]. AQP5 is routed to autophagosomes and lysosomes for degradation via PI3K activity in salivary glands[312,313] which suggests a potential relationship between PI3K-Akt-mTOR pathway activity and regulation of AQP5 function in the ocular lens. Mechanistic details of AQP5 regulation via PI3K-Akt-mTOR pathway activity remain to be established.

1.4.1. Phosphoinositide-3-kinase – Akt – Mammalian Target of Rapamycin Pathway in Autophagic Induction

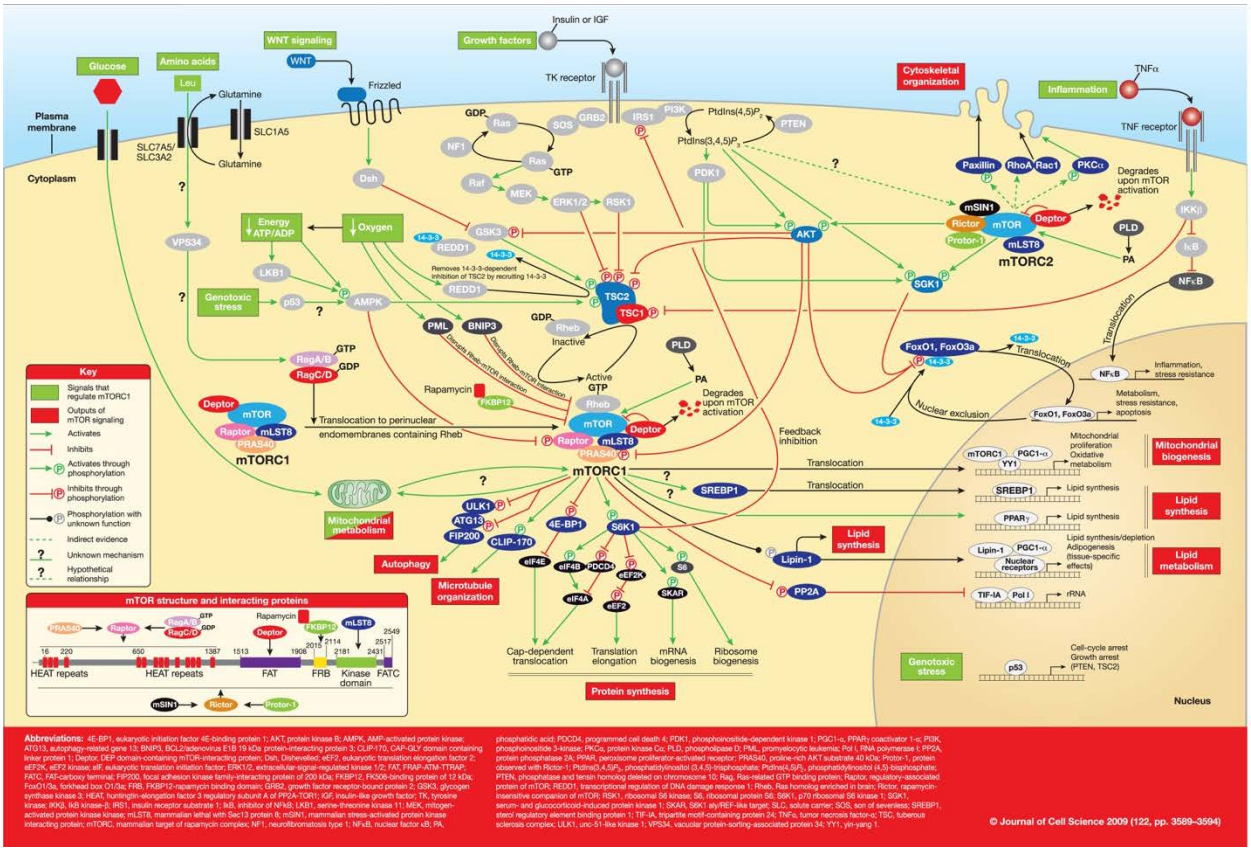

Figure 1.7. Phosphoinositide-3-kinase – Akt – mammalian target of rapamycin cell signal transduction pathway

Adapted with permission from Sabatini and Laplante 2009 in *J Cell Sci*[314].
DOI: 10.1242/jcs.051011

The PI3K-Akt-mTOR pathway is a central cell signaling pathway which broadly regulates many cellular processes such as cellular survival, proliferation and growth[315]. The PI3K-Akt-mTOR pathway is also a central regulator of cellular metabolism including anabolic processes such as macromolecule synthesis and catabolic processes such as autophagic degradation[315]. As such, the PI3K-Akt-mTOR pathway integrates numerous signaling molecules, their target proteins (i.e. receptors, transporters, and channels), effector proteins, and second messengers molecules with Class I PI3K (PI3K), Akt, and mTOR representing the canonical central effector proteins within the pathway. PI3K is a serine/threonine kinase activated by receptor tyrosine kinases (RTKs) upon the binding of specific growth factors such as insulin growth factor[314]. Akt, also known as protein kinase B, is a serine/threonine kinase with over 100 substrates[316]. mTOR is also a serine/threonine kinase and forms the catalytic core of two distinct multi-protein complexes with unique regulation and substrates termed mTOR complex 1 (mTORC1) and mTOR complex 2 (mTORC2).

Activated PI3K phosphorylates the plasma membrane lipid phosphatidylinositol 4,5-bis phosphate (PIP_2 (4,5)) to generate phosphatidylinositol 3,4,5-triphosphate (PIP_3 (3,4,5))[317,318].

PI3K activity is regulated indirectly via the phosphatase PTEN which dephosphorylates 3′ phosphate from PIP_3 (3,4,5) to yield PIP_2 (4,5) again[319,320]. PIP_3 (3,4,5) serves as a docking site for 3-phosphoinositide-dependent protein kinase 1 (PDK1) and mTOR complex 2 (mTORC2), which activate Akt via phosphorylation at amino acid residues threonine-308[321,322] and serine-473[323], respectively. Akt activates mTORC1 via inhibitory phosphorylation of proline-rich AKT1 substrate 1 (PRAS40) and the tuberous sclerosis complex (TSC), which both negatively regulate mTORC1 activity[314].

mTOR specifically functions as a central regulator of cellular metabolism by upregulating protein synthesis, lipid synthesis, and mitochondrial metabolism, mitochondrial biogenesis, and inhibition of autophagy[314]. Active mTORC1 phosphorylates and thereby activates 70 ribosomal S6 kinase 1 (S6K1)[324–326], which increases mRNA transcription and translation[324–326]. mTORC1 inhibits autophagy via inhibitory phosphorylation of Unc-51-like kinase 1 (ULK1 / ATG1) [327–329] and autophagy-related (ATG) protein 13[327–329], which comprise part of a multi-protein complex that initiates autophagy[330,331] (**Section 1.4.2.1.**). Low ATP:ADP ratios activate 5'-AMP-activated protein kinase (AMPK) which suppresses mTORC1 activation via inhibitory phosphorylation of regulatory-associated protein of mTOR (Raptor), a scaffolding and regulatory protein within mTORC1, and stimulatory phosphorylation of the TSC[332]. Low amino acid concentration inactivates mTORC1 stimulating autophagic induction[333]. AMPK directly phosphorylates ULK1 and Unc-51-like kinase 2 (ULK2) stimulating its activity and thereby autophagic induction[334,335]. Lysosomal degradation of protein increases amino acid levels in the cell resulting in reactivation of mTORC1[333]. Ultimately, inhibition of PI3K-Akt-mTOR pathway activity via inhibition of PI3K, Akt, or mTOR induces autophagy, and inhibition of this pathway results in AQP5 incorporation into autophagosomes and ultimately lysosomes[313].

1.4.2. Mechanisms and Regulation of Autophagy

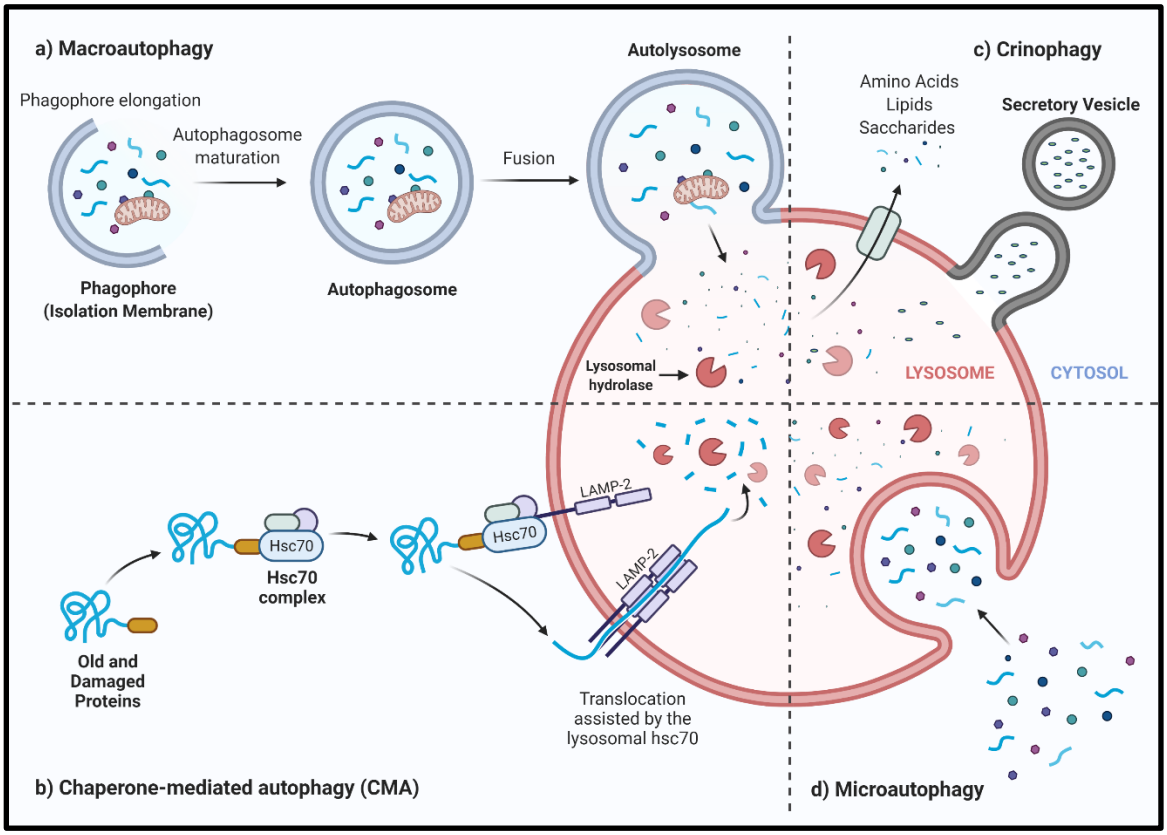

Figure 1.8. Four known types of autophagy.
Created with BioRender.com.
Macroautophagy (**a**), **chaperone-mediated autophagy** (**CMA**) (**b**), **crinophagy** (**c**), and **microautophagy** (**d**) are the four known types of autophagy and are distinguished by their target cargo and mechanisms of cargo delivery into the lysosome.

There are four known types of autophagy - macroautophagy, chaperone-mediated autophagy, crinophagy, and microautophagy (**Figure 1.8**). Macroautophagy is defined as autophagic degradation mediated by the formation of *de novo* double-membraned transport vesicles termed autophagosomes that engulf target proteins or organelles and merge with lysosomes[305,336]. Thereafter, autophagosomal contents are degraded via lysosomal hydrolases[305,336]. In chaperone-mediated autophagy, heat shock cognate 71 kDa protein (Hsc70) binds target proteins that are old or damaged and transports them into the lysosome via lysosome-associated membrane glycoprotein 2 (LAMP2), a lysosomal transmembrane protein[337]. LAMP2 and associated proteins form a channel for translocation of these proteins from the cytoplasm into the lysosomal lumen for degradation[337]. Crinophagy is defined as fusion of unreleased secretory vesicles with late endosomes for targeting to lysosomes or lysosomes directly[338,339]. Crinophagy results in the degradation of excess or obsolete secretory material[339]. Microautophagy is the direct engulfment of surrounding cytoplasmic material in bulk or following HSC70 binding into the lysosome by invagination of the lysosomal membrane. During

microautophagy, small intraluminal vesicles containing the cytoplasmic material are then degraded via lysosomal hydrolases as in macroautophagy[340].

Autophagy is defined as either nonselective or selective[336]. In nonselective autophagy, a random portion of the cytoplasm is engulfed via an autophagosomes during nutrient deprivation (i.e. starvation) and targeted to a lysosome[336,341]. In selective autophagy, a specific protein, organelle cargo, or invading microbe is engulfed into autophagosomes then targeted to a lysosome[336,341]. Specific types of selective autophagy have been designated in terms of the target cargo. For example, selective autophagy of mitochondria is termed "mitophagy"[341]. Likewise, selective autophagy of peroxisomes, ribosomes, endoplasmic reticular compartments, lysosomes, foreign substances, and components of the nucleus such as lamins are referred to as pexophagy, ribophagy, reticulophagy, lysophagy, xenophagy, and nucleophagy, respectively[341,342].

Macroautophagy is the best characterized form of autophagy and will henceforth be referred to simply as "autophagy". Autophagy-related (ATG) proteins were often originally discovered in yeast genetic screens with their mammalian ortholog identified thereafter based on sequence homology[343–345]. Autophagy is either dependent or independent of traditional autophagy proteins such as ATG5, ATG7, and LC3[346]. The former is the canonical type of autophagy while the latter is often referred to as "alternative autophagy".

1.4.2.1. Mechanisms of Canonical Autophagy

Canonical autophagy occurs through autophagosome initiation, phagophore elongation, maturation, lysosomal fusion, and degradation of autophagosomal contents. As mentioned above, autophagic initiation is triggered by activation of ULK1. ULK1 associates in a protein complex comprised of ULK1, RB1-inducible coiled-coil protein 1 (RB1CC1), ATG13, and ATG101[330,331], and activated ULK1 complex activates the Beclin-1–VPS34 complex by phosphorylating Beclin-1[347,348]. VPS34 then phosphorylates phosphatidylinositol (PI) generating phosphatidylinositol 3-phosphate (PI3P) spawning generation and elongation of a phagophore (i.e. autophagosome "isolation membrane")[347,349,350]. The pro-protein microtubule-associated protein light chain 3 (LC3) is C-terminally cleaved by ATG4 protease to form LC3-I which is conjugated by the ATG12-ATG5-ATG16L1 complex to phosphatidylethanolamine (PE) generating LC3-II[351,352], which also contributes to phagophore and is commonly used as a marker of autophagic induction[353].

Cargo is incorporated into autophagosomes during the process of phagophore elongation. During "non-selective" autophagy, cytoplasmic components coincidentally localized at sites of autophagosome nucleation sites are incorporated into autophagosomes[352]. During selective autophagy, cargo is recruited to autophagosomes by cargo receptor proteins. These cargo receptors are known to bind to ubiquitinated proteins or a variety of other specific ligands such as mitochondria[352,354] (**Table 1.2**). Sequestosome-1 (SQSTM1), also known as ubiquitin-binding protein p62, localizes to autophagosomes is the most commonly known selective autophagy cargo receptor in mammalian cells across different forms of selective autophagy including pexophagy, mitophagy, lysophagy, and xenophagy[355] . SQSTM1 binds to ubiquitinated proteins destined for degradation and LC3-II via an LC3-interacting region (LIR) sequestering cargo (i.e. protein or organelle) into the autophagosome.

Process	Ligand	Receptor
Pexophagy	Peroxisomes (Ub)	SQSTM1/p62, NBR1
Mitophagy		SQSTM1/p62, BNIP3L/Nix, OPTN, FUNDC1, PHB2
Reticulophagy	Endoplasmic reticulum	RETREG1/FAM134B
Lysophagy	Lysosomes (Ub)	SQSTM1/p62
Xenophagy	Bacteria (Ub), viruses	SQSTM1/p62, CALCOCO2/NDP52, OPTN
Lipophagy	Lipid droplets	-
Ferritinophagy	Ferritin	NCOA4
Glycophagy	Glycogen	STBD1

Ub, ubiquitinated.

Table 1.2. Selective autophagy types, ligands, and cargo receptors in mammalian cells. Adapted with permission from Gatica, Lahiri, and Klionsky 2018 in *Nat Cell Biol*[355]. DOI: 10.1038/s41556-018-0037-z

Following phagophore expansion and autophagosome closure, autophagosomes then fuse with lysosomes for degradation of their contents. Prerequisites to this process include acquisition of autophagosomal fusion SNARE syntaxin-17, tethering of autophagosomes and lysosomes, and finally autophagosome-lysosome fusion. Syntaxin-17, the autophagosomal SNARE protein required for autophagosome-lysosome fusion, is inserted into the autophagosomal membrane[356]. The HOPS (homotypic fusion and vacuole protein sorting) complex functions as the tethering protein complex by binding both an autophagosome and lysosome to facilitate fusion. The HOPS complex binds autophagosomal and lysosomal associated proteins including Rab7 adaptor protein Plekhm1, Rab7 adaptor protein RILP, the lysosomal small GTPase ADP-ribosylation factor-like protein (ARL8), the Mon1-Ccz1 complex (i.e. an Arl8 GEF), PI3P, and syntaxin-17[357]. Sytnaxin-17 forms a SNARE complex with lysosomal SNARE proteins VAMP7 and VAMP8 and cytosolic SNARE protein synaptosomal-associated protein 29 (SNAP-29)[357]. HOPS also facilitates autophagosome-lysosome SNARE complex assembly, zippering, and prevents disassembly[357,358]. Thereafter, the outer membrane of autophagosomes fuses with lysosomes, the inner autophagosomal membrane and its contents are degraded. Lysosomal compartments are restored through the process of autophagic lysosome reformation[359].

1.4.3. Autophagy in the Lens

Autophagy is constitutively active process in most tissues including the lens. In contrast to most other tissues, autophagy in the lens is not upregulated in response to starvation[360]. Nevertheless, autophagy is constitutively active in both lens epithelial and fiber cells[308,309,360–364]. There is strong evidence for autophagy as mechanism by which lens fiber cells degrade their organelles during terminal differentiation[308–310,365,366] though there is some debate regarding the necessity of autophagy to accomplish this cellular process as organelle degradation proceeds in the absence of autophagy-associated genes ATG5 and VPS34, also known as phosphoinositide-3-kinase class 3 (PIK3C3), due to genetic ablation[361,363].

Evidence in support of autophagy as a mechanism of organelle degradation in lens fiber cells includes the observation that cellular organelles such as mitochondria are widely incorporated into autophagosomes and autolysosomes throughout the lens fiber cells as determined through immunofluorescence and electron microscopy[308–310,363,364]. Additionally, inhibition of mTORC1, which canonically upregulates autophagy, through upstream inhibition of the MAP kinase c-Jun N-terminal kinase (JNK) upregulates autophagic induction and induces premature organelle degradation in embryonic chick lenses primary fibers[309]. The necessity of autophagy for organelle degradation was subsequently investigated in mice with genetic ablation of BCL2/adenovirus E1B 19 kDa protein-interacting protein 3-like (BNIP3L/NIX)[310]. BNIP3L is a mitophagy cargo receptor comprised of a LIR-motif (i.e. LC3-interacting region)[367,368] and its dimerization results in recruitment of autophagosomes and mitochondria[369]. BNIP3L expression is required for mitochondrial clearance in erythrocytes[370–372], which also undergo organelle degradation during cellular maturation[373,374]. BNIP3L expression in the embryonic chick lens peaks in the cortical region where organelle degradation occurs[375]. Most importantly, BNIP3L-null ($BNIP3L^{-/-}$) mice fail to undergo organelle degradation retaining their mitochondria, Golgi, and ER[310].

1.5. Unconventional Plasma Membrane Protein Secretion via Autophagosome & Lysosome Secretion

1.5.1. Conventional and Unconventional Protein Secretion

Secretory proteins are trafficked following synthesis to the plasma membrane through either the conventional secretory pathway or through unconventional protein secretion. In conventional protein secretion, proteins are synthesized at the endoplasmic reticulum (ER), trafficked via coat protein complex II (COPII)-coated vesicles to the Golgi apparatus for additional posttranslational modification, and finally trafficked to the plasma membrane[376]. Proteins that undergo conventional protein secretion contain a cleavable signal peptide comprised of a positively charged N-terminus, a hydrophobic central region, and a cleavable C-terminus, which enables removal of the signal peptide in the ER[377]. Signal peptides are also referred to as signal sequences or leader sequences[378].

Unconventional protein secretion includes secretion of proteins without a signal peptide, referred to as leaderless proteins, and proteins that bypass the Golgi apparatus to the plasma membrane[378]. There are four types of unconventional protein secretion. Type I, Type II, and Type III unconventional protein secretion are defined as leaderless proteins that are inserted into the plasma membrane via direction translocation, an ATP-binding cassette (ABC) transporter, or a membranous organelle, respectively. Type IV unconventional protein secretion, also known as the Golgi bypass, occurs when proteins with a signal peptide bypass the Golgi apparatus during secretion to the plasma membrane[379]. Type III unconventional secretion includes plasma membrane trafficking of secretory autophagosomes[380] and secretory lysosomes[381], and integral membrane proteins are targeted to the plasma membrane via Type III and Type IV unconventional protein secretion[378]. Unconventional protein secretion can be induced in many cell types as a function of cellular stress including inflammation, starvation, and ER stress[379,382,383].

Protein secretion is also defined as either constitutive or regulated. Constitutive secretion occurs continuously and proteins are trafficked to the plasma membrane in the absence of an external signaling molecule[376]. Proteins that undergo regulated secretion, such as AQP2 and AQP5, are stored in secretory granules or vesicles and their trafficking to the plasma membrane is triggered by an external signaling molecule[376].

1.5.2. Autophagosome Secretion

Autophagy-dependent secretion, or secretory autophagy, is a form of Type III unconventional protein secretion that is dependent upon autophagic machinery and in which autophagosomes are secreted to the plasma membrane rather than trafficked to the lysosome for degradation of their cargo[377]. Aside from protein, secretory autophagosome cargo can include mitochondria as well as pathogens[370,384].

The mechanisms that underpin autophagosome secretion are poorly understood. The mechanisms that are known in mammalian cells were primarily discerned from investigation of plasma membrane secretion of interleukin-1β (IL1β), an anti-inflammatory cytokine, via secretory autophagy. Secretory autophagy is upregulated under conditions in which degradative autophagy is upregulated. Mature IL1β is sequestered into secretory autophagosomes via binding to the ubiquitin E3 ligase TRIM16[385,386], which functions simultaneously as a scaffold protein and interacting protein with sequestosome-1 (SQSTM1), ATG16L1, and LC3B (i.e. LC3)[387]. TRIM16 is necessary for incorporation of IL1β into secretory autophagosomes[388].

The IL1β-TRIM16 complex interacts with vesicle-trafficking protein SEC22b (Sec22β), a SNARE protein involved in targeting and fusion of vesicles trafficking between the endoplasmic reticulum (ER) and Golgi apparatus, rather than syntaxin-17 which is associated with autophagosomes targeted to the lysosome for cargo degradation[356,389]. Syntaxin-17 mediates autophagosome-lysosome fusion[356]. Secretory autophagosomes also contain Golgi reassembly-stacking protein 1 (GRASP65), which is necessary for IL1β secretion[390,391]. Thus, secretory autophagosomes canonically should contain LC3-II, SEC22β, GRASP65, and TRIM16 on their cytoplasmic membrane while “degradative autophagosomes” should contain LC3-II and syntaxin-17[388]. Secretory autophagosomal Sec22β interacts with SNARE proteins syntaxin-3, syntaxin-4, synaptosome-associated protein 23 (SNAP23), and synaptosome-associated protein 29 (SNAP29) forming a SNARE complex to mediate secretory autophagosome fusion with the plasma membrane[377,392]. While IL1β represents canonical secretory autophagy, several other proteins have been demonstrated to be secreted via secretory autophagosomes including interleukin-6 (IL6), interleukin-8 (CXCL8), interleukin-18 (IL18), high mobility group protein B1 (HMGB1), transforming growth factor beta-1 (TGFβ1), insulin-degrading enzyme (IDE), α-synuclein (SNCA), acyl-CoA-binding protein (Acb1; in yeast), and mutant cystic fibrosis transmembrane conductance regulator (CFTRΔF508)[377,393].

1.5.3. Lysosome Secretion

Mammalian cells are known to secrete lysosomes in response to specific stimuli including but not limited to plasma membrane repair and remodeling, pathogenic immune response, antigen presentation, and ATP release[381,391,394].

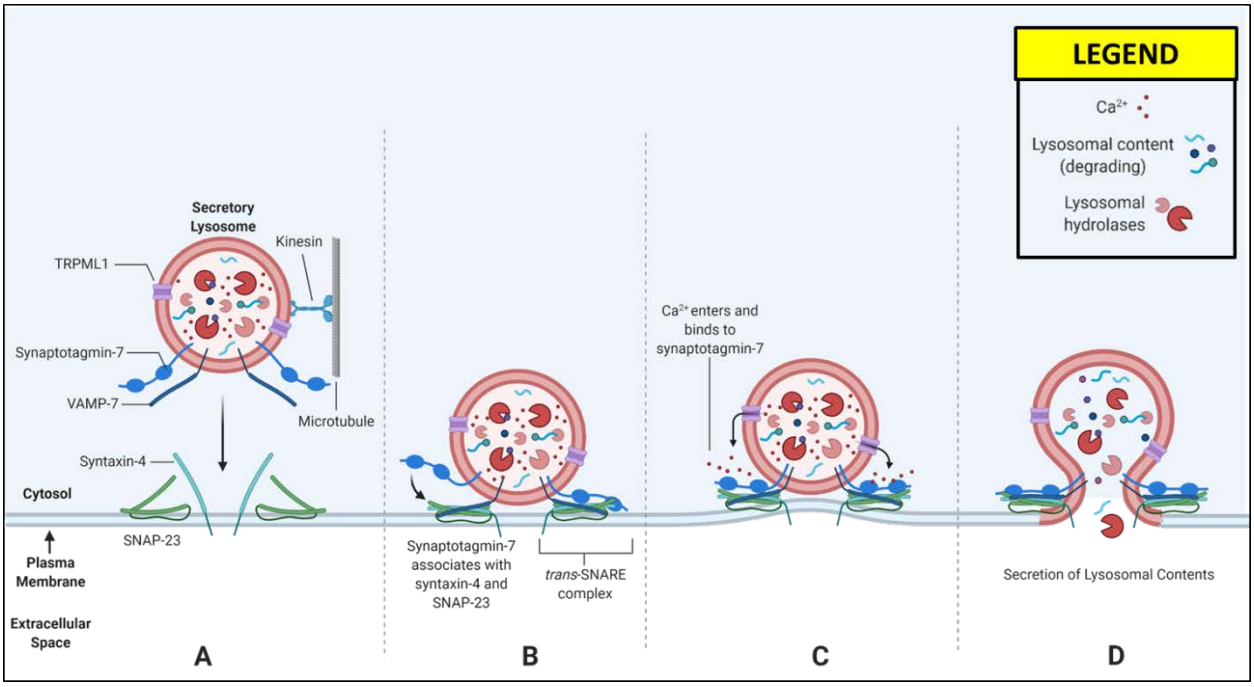

Figure 1.9. Lysosome secretion in mammalian cells.
Created with BioRender.com.
Canonical lysosome secretion in mammalian cells is a cellular process which occurs in four major steps: secretory lysosomes travel to the cell periphery via kinesin motor proteins along microtubules. (**B**) Once at the cell periphery, a trans-SNARE complex forms at the plasma membrane between lysosomal SNARE protein vesicle-associated membrane protein 7 (VAMP7) and plasma membrane SNARE proteins syntaxin-4 and synaptosomal-associated protein 23 (SNAP-23). The calcium sensor synaptotagmin-7 associates with the trans-SNARE complex. (**C**) Calcium (Ca^{2+}) then enters the cytoplasm via the lysosomal transient receptor potential channel mucolipin 1 (TRPML1) from the lysosomal lumen or via another mechanism (e.g. plasma membrane rupture) resulting in increased local cytoplasmic calcium concentration. Ca^{2+} binds synaptotagmin-7 triggering the initiation of lysosome-plasma membrane fusion. (**D**) During lysosome-plasma membrane fusion, intralumenal lysosome contents are secreted and lysosome membrane proteins are incorporated into the plasma membrane.

Lysosome secretion is a Ca^{2+}-dependent process of trafficking to the plasma membrane which occurs under low micromolar Ca^{2+} concentration[381] (**Figure 1.9**). Secretory lysosomes associate with the motor protein kinesin and translocate from the perinuclear region to the plasma membrane upon initiation of lysosome secretion[395,396]. Lysosomes contain the lysosomal SNARE protein vesicle-associated membrane protein 7 (VAMP7), which forms a trans-SNARE complex with plasma membrane SNARE proteins syntaxin-4 and SNAP23[397]. The calcium sensor protein synaptotagmin-7 then interacts with the preformed SNARE complex and plasma

membrane phospholipids triggering fusion of peripherally positioned lysosomes upon increased local calcium concentration[398]. The TRP channel transient receptor potential mucolipin 1 (TRPML1) is required for lysosome secretion and triggers local cytoplasmic calcium influx from the lysosomal lumen upon activation[391,399,400].

As with autophagosome secretion, the mechanisms which underlie lysosome secretion are only loosely understood. The thrombopoietin receptor protein Mpl represents a mammalian transmembrane plasma membrane protein which appears to traffick to the plasma membrane via both conventional and autolysosome-mediated unconventional protein secretion[401]. Mpl association with Jak2 shifts Mpl trafficking towards conventional protein secretion to the plasma membrane, while the absence of Jak2 shifts Mpl subcellular localization towards autophagosomes and autolysosomes and *apparent* unconventional protein secretion to the plasma membrane.

1.6. Aquaporin-5 (AQP5)

Aquaporin-5 (AQP5) is a 265 amino acid AQP primarily expressed in exocrine gland cells. Dysregulation of AQP5 trafficking is characterized by loss of this regulation and implicated in bronchitis, cystic fibrosis, cancer, and Sjögren's syndrome[402].

1.6.1. The Roles and Regulation of Aquaporin-5 in the Secretory Cells

1.6.1.1. Aquaporin-5 in the Salivary Glands

There are three major bilateral pairs of salivary glands – parotid, submandibular, and sublingual – and 800-1000 smaller minor salivary glands[403]. Saliva is comprised of 99% water, electrolytes, urea, ammonia, proteins such as amylase, immunoglobulins, mucins, agglutinins, cystatins, lysozymes, and extraparotid glycoproteins[404].

Saliva secretion (~1-1.5 liters per day in humans) occurs via both stimulated and unstimulated mechanisms. AQP5 expression in salivary glands is essential for proper salivary water content and consequently total saliva volume, tonicity, and viscosity in salivary secretions[405]. The generation of saliva is a two-step process in which salivary gland acinar cells first secrete an isotonic, serum-like fluid which is modified thereafter primarily by NaCl resorption by ductal cells[406–408]. AQP5 expression is critical to the first step, the secretion of isotonic "primary" saliva. Specifically, multiple plasma membrane ion transporters including the Na^+/K^+ ATPase, NKCC1, Na^+/H^+ exchanger, and Cl^-/HCO_3^- exchanger drive transcellular Cl^- current from the salivary acinar interstitium to the lumen[408,409]. The transepithelial cell osmotic gradient generated by this Cl^- current drives transepithelial cell water flow via AQP5 thereby adding water content to "primary" saliva.

The importance of AQP5 expression to salivary water content can be observed in AQP5-null mice. Pilocarpine-stimulated saliva production in AQP5-null mice was reduced by approximately 60% in mice[405,410]. Additionally, saliva from AQP5-null mice increased in osmolality from being hypotonic to hypertonic. Hypertonic saliva from AQP5-null mice is characterized by higher Na^+, K^+, and Cl^- ionic concentrations, which reflects the coupled regulation of water and ionic homeostasis by AQP5 and AQPs in general. Improper AQP5 expression and subcellular localization in salivary glands is associated with dry mouth and Sjögren's syndrome[411–414].

1.6.1.2. Aquaporin-5 in the Lacrimal Glands

There are two bilateral lacrimal glands that, in conjunction with Meibomian glands, generate the ocular tear film, a thin, tripartite fluid layer atop the external cornea and conjunctiva[415]. The tear film serves multiple functions include light refraction, eye lubrication and dehydration retardation, nutrient supply to the cornea, removal of exogenous substances from the eye, and antimicrobial defense. Tear composition is similar to saliva composition and AQP5 expression in lacrimal glands is also essential to proper tear formation[415–417].

The mechanism of tear secretion is similar to the mechanism of salivary secretion. That is, a transepithelial Cl^- current drives concomitant transepithelial water flow facilitated by AQP5 producing "primary" tear secretion whose composition is modified thereafter by ductal cells[417–419]. As in the salivary glands, AQP5-null mice exhibit drastic reduction in tear production compared to wild-type controls as well as dry eye symptoms[416,417]. Improper AQP5 expression and subcellular localization in lacrimal glands is associated with dry eye and Sjögren's syndrome in humans[412,420–422].

1.6.1.3. Regulation of Aquaporin-5 Trafficking in the Salivary and Lacrimal Glands

AQP5 subcellular localization is regulated through multiple mechanisms outside the lens. In salivary gland cells, M_3-muscaric acetylcholinergic receptor (M_3 mAChR) agonism, α_{1A}-adrenergic receptor agonism, TRPV4-mediated hypotonicity, and TRPV1 activation induce cytoplasmic AQP5 trafficking to the plasma membrane[423–431]. AQP5 trafficking in these cells is dependent upon nitric oxide/Ca^{2+}-mediated protein kinase G (PKG; also known as cGMP-dependent protein kinase) activation, calmodulin II kinase activity, and myosin light chain kinase activity[423]. Interestingly, AQP5 is also trafficked to the nuclear membrane in response to M_3 mAChR agonism[426]. Increased local calcium concentration is a common downstream signal that induces cytoplasmic AQP5 trafficking to the plasma membrane via different upstream cell signaling pathways in salivary glands and in other exocrine gland tissues such as mouse lung epithelial cells which express AQP5[432].

AQP5 subcellular localization in salivary glands is also regulated through protein-protein interactions. Recently, Chivasso et al 2021 demonstrated that AQP5 interacts with ezrin, a member of the ezrin-radixin-moesin (ERM) family of cytoskeletal linker proteins which links actin filaments to the plasma membrane[432–435]. In Sjögren's syndrome patients, salivary gland AQP5-ezrin interactions are absent or mislocalized from the apical plasma membrane where AQP5 is normally expressed[435]. AQP5 also interacts via its C-terminus with prolactin-inducible protein (PIP), whose expression correlates with AQP5 plasma membrane subcellular localization[422,436]. In mouse salivary glands, this correlation is female-specific, and decreased PIP expression increases the probability of mislocalized or lost AQP5 plasma membrane expression[436]. In human minor salivary glands, normal PIP expression and apical and basolateral AQP5 plasma membrane expression were frequently partially or totally lost in patients with Sjögren's syndrome. In the mouse lacrimal gland, AQP5 plasma membrane subcellular localization is absent in PIP-null mice. AQP5 interacts via its C-terminus with murine urinary protein 4 (Mup4) in NOD mice, a mouse model of Sjögren's syndrome, rather than PIP, and AQP5 plasma membrane localization is undetectable[422].

AQP5 is also modified by C-terminal phosphorylation at amino acid residue threonine-259 (AQP5 pT259) in human and mouse submandibular and parotid glands in response to PKA and PKC activation[156]. *In vivo* treatment with the β-adrenergic agonist isoproterenol increased AQP5 pT259 expression levels and resulted in AQP5 pT259-positive, vacuole-like plasma membrane formations[156,437]. Current evidence suggests that AQP5 T259 phosphorylation affects AQP5 plasma membrane diffusion in a complex manner. In exogenously transfected Madin-Darby canine kidney (MDCK) cells, forskolin-mediated cAMP elevation and H-89-mediated PKA

inhibition decrease lateral plasma membrane AQP5 diffusion[438]. In turn, AQP5 T259 mutation to alanine (T259A) decreases baseline lateral AQP5 plasma membrane diffusion which was rescued by cAMP elevation[438]. Slower plasma membrane protein diffusion coefficients are associated with lipid raft microdomains[439], and cytoplasmic AQP5 undergoes stimulated trafficking to lipid raft domains in apical plasma membranes then rapidly shifts to primarily non-lipid raft domains in salivary gland cells[424,440]. Evidence suggests that AQP C-terminal phosphorylation is inhibitory towards AQP protein-protein interactions[150–153,196], so it is probable that AQP5 T259 phosphorylation generally regulates AQP5 protein-protein interactions.

Lastly, the molecular composition of cytoplasmic vesicles provides mechanistic data which underpins regulation of AQP5 subcellular localization. Rab4 and Rab5 are molecular marker proteins of early endosomes and clathrin-coated vesicles, while Rab5 is a molecular marker protein for recycling endosomes[441]. AQP5 is expressed in Rab4-positive, Rab5-positive, α-adaptin-positive cytoplasmic vesicles in rat parotid glands cells, which suggests that AQP5 is internalized via endocytosis from the plasma membrane to early endosomes and possibly recycles between endosomal compartments and the plasma membrane[441–443]. In turn, LC3B is a molecular marker protein of autophagosomes, amphisomes, and autolysosomes, while LAMP-2 is an autolysosomal and lysosomal membrane marker protein[306,444,445]. AQP5 is partially expressed in both LC3B-positive and LAMP-2 vesicular compartments at a low level in rat submandibular gland cells which increases drastically following chorda tympani parasympathetic denervation[312]. This increase is in agreement with *in vitro* data which demonstrate increased AQP5 degradation in SMG extracts. AQP5 also colocalizes more strongly with LC3B in the submandibular glands of diabetic model mice and patients which corresponds with its increased degradation[313].

In summary, AQP5 trafficking to the plasma membrane is broadly regulated by multiple cell signaling pathways which converge downstream with local calcium concentration increase, by AQP5 C-terminal protein-protein interactions, and putatively by C-terminal phosphorylation at threonine-259 through regulation of AQP5 C-terminal protein-protein interactions. Furthermore, molecular marker analysis of AQP5-containing cytoplasmic vesicles provides mechanistic data about the regulation of AQP5 subcellular localization.

1.6.2. Roles of Aquaporin-5 in the Lens

AQP5 is distinct amongst lenticular AQPs (i.e. AQP0, AQP1, and AQP8) in several ways that engender a unique contribution for AQP5 in lenticular ionic homeostasis, osmotic homeostasis, and thereby transparency. For example, AQP5 water transport kinetics are distinct. AQP0, AQP1, and AQP5 have respective single-channel water permeabilities (x 10^{-14} cm^{-3}/s) of 0.25, 6.0, and 5.0, respectively[57]. The water permeability of AQP7 is approximately half that of AQP1[446], and the water permeability of AQP8 is approximately the same as that of AQP1[447]. Thus, AQP5 water permeability (P_{H2O}) is approximately 20 times higher than that of AQP0, 0.8 times that of AQP1 and AQP8, and about twice as high as AQP7[57].

AQP5 is also distinct amongst lenticular AQPs in spatiotemporal expression (discussed in **Section 1.2.2.3.**). As stated previously, AQP5 is the second and only other known AQP in mammalian lens fiber cells except AQP0. Grey et al. 2013 estimated total lenticular AQP5 protein expression to be roughly 5% of, or 20 times less than, AQP0[46]. Basal water content of $AQP5^{-/-}$ mouse lenses is not significantly different than wild-type lenses, but the water content and volume of $AQP5^{-/-}$ mouse lenses osmotically challenged via *ex vivo* culture in hyperglycemic media for 60 hours increased by ~22% and 12%, respectively, relative to WT lenses[110].

As outlined in previous sections, lenticular ionic homeostasis, osmotic homeostasis, and transparency are directly interconnected. Thus, lenticular AQP5 expression is preventative

against cataract[167]. Clear AQP5$^{-/-}$ mouse lenses subjected to *ex vivo* culture in hyperglycemic medium develop cataract within 60 hours whereas wild-type lenses remain transparent[110]. AQP5$^{-/-}$ mice develop cataracts at 6 months of age at a significantly elevated rate relative to wild-type mice[112]. In humans, AQP5 subcellular localization switches from the cytoplasm to the plasma membrane in the epithelial cells of lenses with nuclear cataract[167] further suggesting an association with AQP5 function and lenticular transparency.

AQP5 also regulates lenticular transparency outside of direct water transport function by regulating the expression of the cytoskeletal protein vimentin in the lens. AQP5 regulates vimentin expression by regulating expression of the micro-RNA miR-124–3p.1[112]. AQP5 expression positively regulates miR-124–3p.1 expression which, in turn, negatively regulates vimentin expression. An AQP5 missense mutation at residue 51 from leucine to proline (AQP5 L51P) upregulates vimentin expression in humans and mice and is associated with autosomal dominant congenital cataract in humans[112].

1.6.3. Regulation of Aquaporin-5 in the Lens

While detailed mechanisms by which extralenticular AQP5 is regulated in tissues such as salivary glands are demonstrated in the published literature, mechanistic details underpinning regulation of lenticular AQP5 are less well characterized. Nevertheless, it is reasonable to expect lenticular AQP5 to share broad similarities in regulation with extralenticular AQP5 as several proteins involved in AQP5 regulation in the salivary gland, for example, are expressed in the lens such as mAChR receptors[448] and TRPV4. Thus, it is feasible that downstream mechanisms which involve local calcium influx, AQP5 protein-protein interactions, and AQP5 posttranslational modifications such as C-terminal phosphorylation to regulate lenticular AQP5 function through alteration of its subcellular localization. The PI3K-Akt-mTOR cell signaling pathway is also active in the lens as discussed in **Section 1.4.1.**. Thus, this pathway potentially regulates AQP5 function in the lens via control of its expression and its subcellular localization. AQP5 subcellular localization, protein-protein interactions, and posttranslational modification in the lens are addressed by the work in this thesis.

1.6.3.1. Regulation of Aquaporin-5 Subcellular Localization in the Lens

AQP5 is expressed in cytoplasmic vesicles in peripheral outer cortical and nuclear fiber cell plasma membranes of adult mammalian ocular lenses[46,111,116,168]. AQP5-containing cytoplasmic vesicles in the lens cortex gradually traffick to fiber cell plasma membranes prior to the completion of cellular differentiation[46,111,116,168]. Recently, AQP5 subcellular localization in the peripheral outer cortex was shown to be dynamic and shuttle between cytoplasmic compartments and the plasma membrane in the lens microcirculation efflux and anterior influx zone in adult mouse lenses[111,116,168]. Thus, AQP5 secretion to the plasma membrane in mammalian lenses represents a form of regulated trafficking. The mechanisms that underpin AQP5 trafficking in the lens are an active area of research in our group.

Petrova et al. produced correlative data that suggest possible regulatory mechanisms that underpin initial AQP5 trafficking to fiber cell plasma membranes in the lens core early in development[168]. AQP5 expression in mice is entirely cytoplasmic throughout lens embryonic development and that AQP5-containing cytoplasmic vesicles in the lens core traffick to fiber cell plasma membranes thereafter postnatally[168]. In mouse lenses, AQP5 fiber cell plasma membrane insertion in the lens core coincides temporally with apoptotic disintegration of the hyaloid vascular system, the blood vessel system which nourishes the developing lens with direct blood supply, and spatially with AQP0 C-terminal truncation[168,449]. The lens MCS is theorized to functionally replace the hyaloid vascular system to fulfill the role of lens cellular

nutrient supply and waste removal and AQPs are integral to the lens MCS[20]. Thus, the temporal coincidence of AQP5 plasma membrane insertion in the fiber cells of the lens core and hyaloid vascular system disintegration suggests that AQP5 trafficking in these cells is important to the initial establishment of the lens MCS.

The temporal coincidence of AQP0 truncation in the lens core further supports the importance of AQP5 plasma membrane insertion in establishment of the lens MCS. As stated above, electron crystallographic data indicate that AQP0 C-terminal truncation abrogates AQP0 water gating and renders AQP0 into a cell-cell adhesion protein in the lens[59,146,205]. Thus, AQP5 may rectify osmotic perturbation to the lens as a result of abrogated AQP0 water permeability due to C-terminal truncation. Petrova et al. demonstrated that AQP5 fiber cell plasma membrane insertion increases fiber cell water permeability[111]. Functional studies are required to determine the relationship between AQP5 fiber cell plasma membrane insertion in the lens core, lens MCS establishment, and AQP0 C-terminal truncation.

Functional studies have provided insight into the regulation of dynamic AQP5 trafficking in the lens MCS efflux and anterior influx zones. Lenticular zonular fiber tension is controlled by relaxation and contraction of the ciliary muscle, which increase and decrease zonular tension, respectively[114]. Tropicamide, a nonselective muscarinic acetylcholinergic receptor (mAChR) antagonist, and pilocarpine, a broad mAChR agonist, respectively induce relaxation and contraction of the ciliary muscle[114]. Tropicamide application to lens with intact zonules results in a TRPV4-dependent decrease in lens hydrostatic pressure, while pilocarpine application results in a TRPV1-dependent increase in lens hydrostatic pressure[114]. Lenticular TRPV1 activation triggers NKCC1 activation and is inhibitory towards Na^+/K^+ ATPase activity[113,264]. Furthermore, TRPV1-dependent increase in lens hydrostatic pressure requires lenticular PI3K expression as lens intracellular hydrostatic pressure is not increased in p110a PI3K-null mice with intact zonules despite contraction of ciliary muscles[114].

Pilocarpine treatment and the associated reduction in lens zonular tension also regulates AQP5 subcellular localization within the lens. In the MCS efflux zones and anterior influx zones (i.e. anterior sutures) of mouse lenses, AQP5 expression is primarily localized to the plasma membrane[116]. Reduction of lens zonular tension via severance or pharmacologically with pilocarpine application induces significant AQP5 internalization in these regions, while increased zonular fiber tension has no effect on AQP5 subcellular localization[111,116]. Interestingly, AQP5 plasma membrane subcellular localization is rescued in the lens efflux zone following zonular severance-mediated internalization after approximately two hours. Thereafter, AQP5 expression is primarily localized to the plasma membrane again in this region[111,116].

These results clearly implicate ciliary muscle activity, zonular tension, and TRPV1 in the regulation of AQP5 in the lens and lenticular AQP5 trafficking in lens MCS function via regulation of TRPV1-dependent increase in lens hydrostatic pressure. Furthermore, these results implicate PI3K expression and activity in the regulation of AQP5 subcellular localization in the ocular lens. The data from these studies raise several questions including how PI3K-Akt-mTOR pathway activity directly affects AQP5 subcellular localization in the ocular lens, how metabolic pathways which are controlled via PI3K-Akt-mTOR pathway activity such as autophagy regulate AQP5 subcellular localization and function in the ocular lens, and how the factors which regulate extralenticular AQP5 subcellular localization and function (i.e. calcium-dependent AQP5 trafficking mechanisms, AQP5 protein-protein interactions, and C-terminal phosphorylation) are related to these cell signaling pathways.

1.6.3.2. Aquaporin-5 Protein-Protein Interactions in the Lens

Extralenticular AQP5 interacting proteins in the salivary glands and lacrimal glands regulate AQP5 subcellular localization and proper trafficking to the plasma membrane[422,432,435,436] as outlined in **Section 1.6.1.3.**. AQP5 also interacts *in vitro* via its C-terminus at the plasma

membrane with cell junctional proteins tight junction protein ZO-1, plakoglobin, β-catenin, and desmoglein-2 in exogenously transfected Madin Darby canine kidney (MDCK) cells[154]. In MDCK cells, AQP5 interaction with cell junctional proteins reduces their expression which attributes a novel role to AQP5 as a structural protein to AQP5 and a specific role in cell junction formation. Thus, AQP5 subcellular localization is regulated via protein interactions with its C-terminus and AQP5 regulates cellular processes outside direct water transport function via protein interactions with its C-terminus.

Aside from Mup4, expression of all extralenticular AQP5 interacting proteins have been confirmed in ocular lens fiber cells[43,44,291,450,451] with Cantrell et al. 2021 most recently identifying PIP expression in human lens fiber cells via data-independent acquisition mass spectrometry[451]. Ezrin in particular interacts with the C-terminus of AQP0 in the ocular which raises the possibility of ezrin interacting with AQP5 in lens fiber cells. Furthermore, lenticular AQP5 regulation of vimentin expression demonstrates an indirect structural role for AQP5 in the ocular lens, and, in turn, raises the possibility that AQP5 directly functions as a structural protein in the lens via C-terminal protein-protein interactions with ZO-1, plakoglobin, β-catenin, and desmoglein-2. In MDCK cells, AQP5 interacts with additional proteins such as CDGSH iron-sulfur domain-containing protein 2 (CISD2), which regulates autophagic induction at the ER, and voltage-dependent calcium channel subunit alpha-2/delta-1 (CACNA2D1), which regulates local calcium concentrations[154].

These results indicate the importance of defining lenticular AQP5 interacting proteins to better understand the regulation of AQP5 subcellular in the ocular lens. AQP5 C-terminal phosphorylation (i.e. AQP5 phospho-T259) should be defined in detail in the ocular lens as AQP C-terminal phosphorylation canonically regulates AQP protein-protein interactions. Additionally, these results suggest the importance of identifying AQP5 C-terminal interactions to define potentially novel, direct roles associated with AQP5 expression in the ocular lens. AQP5 interaction with the autophagy regulator CISD2 is of particular interest with respect to the relationship between PI3K-Akt-mTOR pathway activity and AQP5 subcellular localization in the lens. In this thesis, putative AQP5 interacting proteins are defined to further investigate this relationship (**Chapter 4**).

1.6.3.3. Aquaporin-5 Posttranslational Modifications in the Lens

AQP5 Palmitoylation in the Lens

S-palmitoylation is a reversible form of protein lipidation in which a 16-carbon palmitic acid moiety is covalently attached via thioester linkage to a cysteine residue[452]. Protein *S*-palmitoylation is associated with several cellular process including functioning as a hydrophobic tether to anchor proteins to lipid membranes[453], protein quality control[454–456], protein oligomerization[457,458], and protein trafficking and subcellular localization targeting[459] including lipid raft targeting, specifically[460–462]. Wang et al. discovered AQP5 *S*-palmitoylation on amino acid residue cysteine-6 (AQP5 C6) in the lens[463]. AQP5 C6 palmitoylation was observed in a narrow region of lens inner cortical fiber cells and absent in lens epithelial cells, the remainder of the lens cortex, and the lens nucleus[463]. AQP5 represents the third known AQP to be posttranslationally modified via *S*-palmitoylation along with AQP0[206] and AQP4[464].

The role of AQP5 C6 palmitoylation in the lens is unclear, but there are a few conceivable possibilities based on previous experimental evidence. The association of AQP5 with lipid raft domains suggests a possible role for palmitoylation in targeting AQP5 to lipid raft domains in the lens as appears to be the case with AQP0[208]. Another potential role for AQP5 palmitoylation is cytoplasmic AQP5 trafficking to the lens fiber cell plasma membrane. AQP5 has been shown to dynamically traffick to the plasma membrane in response to changes in zonular tension[111,116]. AQP5 trafficking outside the lens is regulated by several stimuli and this is likely to be true in the lens. Furthermore, molecular mechanisms that underlie AQP5 trafficking

in the lens, so AQP5 C6 palmitoylation certainly may play a role in AQP5 plasma membrane insertion particularly since it is a reversible lipid modification. The AQP5 C6 palmitoylation in lens fiber cells coincides spatially with plasma membrane insertion of cytoplasmic AQP5 supports this possibility.

AQP5 Phosphorylation in the Lens

AQP5 was shown to be modified in the lens by phosphorylation at amino acid residue threonine 259 (AQP5 pT259) during a lens membrane proteomics screen by Wang et al 2013[450]. In this study, fiber cell membranes were isolated and AQP5 T259 phosphorylation was detected via a proteomics screen. Lenticular AQP5 pT259 expression levels and spatial expression are unclear. Nevertheless, AQP5 pT259 may regulate AQP5 localization within lipid raft and non-lipid raft regions of the plasma membrane in conjunction with AQP5 C6 S-palmitoylation. It is also reasonably possible that AQP5 pT259 regulates AQP5 protein-protein interactions in the ocular lens. Chapter 4 of this thesis serves as a preliminary investigation of these possibilities through defining relative lenticular AQP5 pT259 expression levels (i.e. relative to unphosphorylated AQP5) and AQP5 pT259 spatial expression. Future studies should build upon this work and investigate the relationship between these findings and the role of AQP5 within the lens microcirculation system and normal lens physiology.

1.7. Conclusions

As outlined above, regulation of AQP5 subcellular localization is critical to overall AQP5-specific function in several tissues including the ocular lens. This is particularly true in cortical lens fiber cells where AQP5 exhibits dynamic subcellular localization between cytoplasmic vesicles and the plasma membrane. AQP5 water transport function is essential to lens transparency and proper functioning of the lens microcirculation system, which nourishes the avascular lens in the absence of vasculature.

Currently, there are gaps in lenticular AQP5 understanding regarding mechanistic details that underpin regulation of lenticular AQP5 subcellular localization and trafficking to the plasma membrane including relevant cell signaling pathways, protein-protein interactions, and posttranslational modifications such as C-terminal phosphorylation. Furthermore, there are no details in the literature regarding the molecular identity of the cytoplasmic, vesicular compartments that express AQP5 in the ocular lens, which will identify general trafficking pathways of lenticular AQP5 (e.g. endosome-plasma membrane recycling). There are also no roles attributed to lenticular AQP5 specifically outside water transport and peroxiporin function in the ocular lens. I suspect that lenticular AQP5-containing cytoplasmic vesicles traffick to the plasma membrane via a calcium-based trafficking mechanism as appears to be a general mechanism of corresponding extralenticular AQP5 trafficking.

In the ocular lens, calcium gradually increases from the lens periphery to the lens center[8,202,203], and AQP5 gradually inserts from the cytoplasmic vesicles to the plasma membrane in maturing fiber cells. Additionally, known AQP5 interacting proteins which regulate extralenticular AQP5 trafficking such as ezrin and TRPV1 are expressed in the lens and, in the case of TRPV1, regulate AQP5 trafficking to the plasma membrane[116]. In lens fiber cells, AQP5 T259 phosphorylation is observed[450], and AQP5 is present in both lipid raft and non-lipid raft plasma membrane domains[208]. Detailed mechanisms of lenticular AQP5 regulation – particularly calcium-, AQP5 protein-protein-, and AQP5 T259 phosphorylation-regulated AQP5 trafficking and the molecular identity of AQP5 containing cytoplasmic vesicles – require investigation and will further inform the specific roles of AQP5 to normal lens physiology.

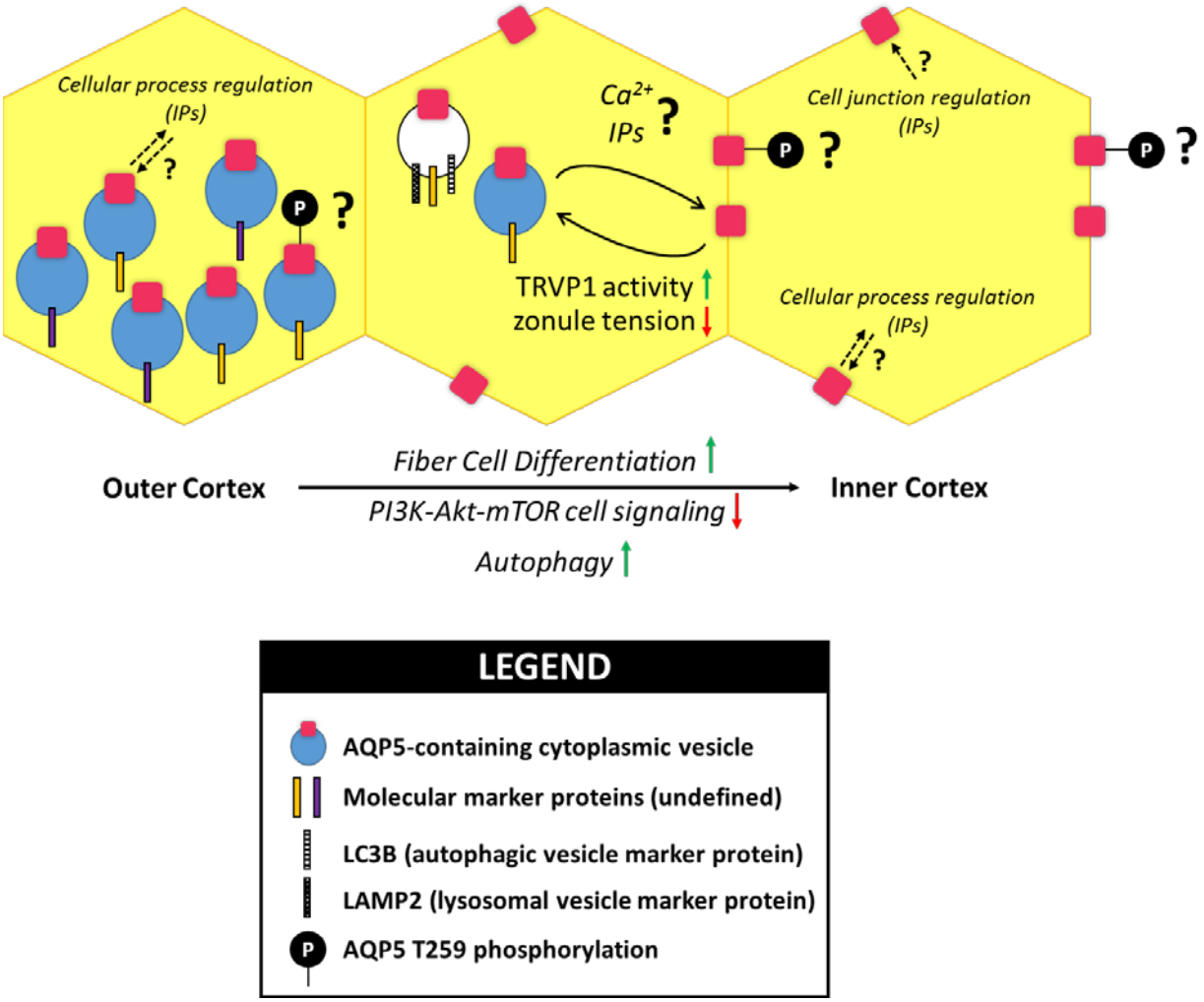

Figure 1.10. AQP5 trafficking and subcellular localization in the ocular lens.
AQP5-containing cytoplasmic vesicles gradually traffick to the plasma membrane during *fiber cell differentiation* from the **outer cortex** to the **inner cortex**. Lenticular AQP5 exhibits dynamic subcellular localization in response to TRPV1 activation or zonular tension reduction. Several forms of extralenticular AQP5 regulation are established which may play a role in the regulation of lenticular AQP5 trafficking and subcellular localization such as *PI3K-Akt-mTOR cell signaling* pathway activity, AQP5 interacting proteins (*IPs*), AQP5 C-terminal phosphorylation at threonine-259 (**AQP5 T259 phosphorylation**), and Ca^{2+}-mediated trafficking mechanisms. AQP5 regulation of cellular processes such as cell-cell junction protein expression (*Cell junction regulation*) and potential regulation by novel cellular processes such as *autophagy* (*Cellular process regulation*) remain unclear but viable in the ocular lens. Determination of AQP5 interacting proteins, AQP5 phospho-T259 spatial expression, and subcellular compartment molecular markers represent viable methods by which to elucidate forms of lenticular AQP5 regulation.

In this thesis, I use the bovine lens as a model to immunohistochemically define lenticular AQP5 subcellular localization and to identify putative trafficking mechanisms using organelle marker proteins for colocalization analysis. Additionally, I define putative AQP5 interacting proteins via

co-immunoprecipitation techniques combined with mass spectrometric analysis of fiber cell membranes. I define relative AQP5 pT259 protein expression levels and spatial expression across the bovine lens. Lastly, I define PI3K-Akt-mTOR pathway activation in bovine lenses using Western blot analysis including expression of ribosomal protein S6 phosphorylation (pRPS6), which is a positive marker of mTOR kinase activity.

CHAPTER II. SPECIFIC AIMS

The lens is a biconvex optical lens in the eye that adjustably refracts light onto the retina, the photoreceptor cell layer of the eye. Proper cellular water regulation is necessary for lens transparency and thereby proper lens function. Aquaporins (AQPs) are conserved transmembrane channels that enable osmotic diffusion of water across the plasma membrane. The lens expresses aquaporin-0 (AQP0), aquaporin-1 (AQP1), and aquaporin-5 (AQP5) which collectively regulate lens water content. AQP5 is the second AQP in addition to AQP0 expressed in lens fiber cells. While AQP0 is constitutively secreted to lens fiber cell plasma membranes, AQP5 undergoes regulated secretion to the plasma membrane in lens fiber cells. Detailed cellular mechanisms of the regulation of AQP5 secretion in the lens are unclear and an active area of lens research.

AQP5 is expressed in cytoplasmic vesicles in epithelial cells and the peripheral differentiating fiber cells in mouse, rat, and human lens cortex. AQP5 increasingly inserts to the plasma membrane with fiber cell differentiation, and cytoplasmic AQP5 expression dissipates as AQP5 is fully inserted into the plasma membrane prior to fiber cell maturation. AQP5-containing cytoplasmic vesicle secretion to fiber cell plasma membranes in the postnatal mouse lens coincides spatially with AQP0 C-terminal truncation, which corresponds to a closed water pore conformation in AQP0 isolated from sheep lenses. AQP5 subcellular localization in the differentiating fiber cells of the cortex in adult mouse and rat lenses is subject to mechanosensitive regulation as function of tension across the zonules of Zinn. Mechanosensitive AQP5 plasma membrane insertion increases lens fiber cell membrane water permeability. These data suggest that AQP5 functions as a regulated water channel whose expression and subcellular localization are important to normal lens water regulation.

The molecular composition of cytoplasmic vesicles directly relates to regulation of their trafficking. In the rat parotid gland, cytoplasmically localized AQP5 is present on Rab4-containing and Rab5-containing endosomes. Rab4 expression is associated with the temporal dynamics of internalized VEGFR2 trafficking to the endothelial cell plasma membrane from recycling endosomes. Newly synthesized plasma membrane proteins can be trafficked to the plasma membrane through the conventional secretory pathway or through unconventional protein secretion mechanisms such as autophagosome, endosome, or lysosome secretion. The molecular composition of lenticular AQP5-containing cytoplasmic vesicles and the nature of their secretion to the plasma membrane is unclear. To better understand AQP5 regulation in normal lens physiology, we propose to examine the conservation of AQP5 spatial expression in mammalian lenses and further investigate AQP5 secretion regulation mechanisms using the bovine lens as a model.

AQP5 C-terminal protein-protein interactions also directly affect AQP5 plasma membrane localization. AQP5 plasma membrane localization in the ICR mouse lacrimal gland requires expression of prolactin inducible protein (PIP), an AQP5 C-terminal interacting protein. In the Sjögren's syndrome model mouse lacrimal gland, murine urinary protein 4 (Mup4) interacts with the AQP5 C-terminus rather than PIP and AQP5 plasma membrane localization is undetectable by immunofluorescence. AQP5 also regulates cellular processes such as cell junction protein expression through C-terminal interactions. C-terminal phosphorylation of aquaporins in general typically negatively inhibits aquaporin protein-protein interactions. AQP5 is C-terminally phosphorylated at T259 in the ocular lens. The relative expression and spatial expression of lenticular AQP5 phospho-T259 have not been investigated. **We hypothesize that the molecular composition of AQP5-containing cytoplasmic vesicles and AQP5 interacting proteins will identify mechanisms which underpin regulated AQP5 trafficking to fiber cell plasma membranes in the bovine lens**. **We, therefore, propose to define the subcellular localization of AQP5-containing cytoplasmic vesicles, define AQP5**

interacting proteins, and spatially map AQP5 T259 phosphorylation in the bovine lens to better understand this regulation. To test our hypotheses, we propose the following aims:

Aim 1: Define AQP5 spatial expression and cytoplasmic subcellular localization in the bovine lens.

AQP5 immunofluorescence confocal microscopy analyses will be conducted in differentiating lens fiber cells of bovine lens cryosections. AQP5 plasma membrane insertion will be quantified using surface plot analysis. Colocalization analyses of AQP5 and organelle-specific markers including calnexin (endoplasmic reticulum protein), TOMM20 (mitochondrial protein), LC3B (autophagosome protein), LIMP-2 (lysosome protein), and DiI (lipid membrane marker dye) in bovine lens tissue sections will be conducted using confocal analysis as described in Aim 1. Transmission electron microscopy analyses of differentiating lens fiber cells will be conducted in bovine lens tissue sections.

Aim 2: Define potential mechanisms of AQP5 plasma membrane trafficking in the bovine lens.

Ex vivo cultured bovine lenses will be subjected to pharmacological treatment to alter secretion of AQP5-containing cytoplasmic vesicles to the plasma membrane. Pharmacological treatment will be tested based on the identity of AQP5-containing cytoplasmic vesicles. AQP5 immunofluorescence confocal microscopy analyses of bovine lens cryosections from cultured lenses will be conducted as described in Aim 1.

Aim 3: Identify AQP5 interacting proteins and the expression of AQP5 phospho-T259 (AQP5 pT259) in the bovine lens.

AQP5 coimmunoprecipitation (co-IP) assays will be conducted on bovine lens cortical and nuclear fiber cell membranes. Significantly enriched, putative AQP5 interactors will be identified in AQP5 co-immunoprecipitates via liquid chromatography-tandem mass spectrometry (LC-MS/MS). Enrichment of AQP5 and putative interactors from AQP5 co-IP assays will be confirmed via Western blot analysis. Relative AQP5 pT259 expression will be evaluated in the bovine fiber cells via Western blot analysis. AQP5 pT259 spatial expression will be evaluated via immunofluorescence confocal microscopy analyses in lens fiber cells of bovine lens cryosections as outlined in Aim 1.

The proposed studies will clarify the importance of AQP5 spatial expression conservation in mammalian lenses. Additionally, these studies will provide additional mechanistic information on regulated secretion of AQP5-containing cytoplasmic vesicles, clarify *putative* additional roles of AQP5 expression, and define the relevance of AQP5 T259 phosphorylation in the ocular lens. Collectively, the information from these studies will provide a more complete understanding of the role of AQP5 in normal lens physiology.

CHAPTER III. Aquaporin-5-Containing Autolysosome Secretion in the Bovine Lens

This chapter is adapted from "Lens aquaporin-5 inserts into bovine fiber cell plasma membranes via unconventional protein secretion" published in Investigative Ophthalmology & Visual Science and has been reproduced with the permission of the publisher and my co-authors Kevin L. Schey, Ph.D., Sujoy Bhattacharya, Ph.D., and Lee Cantrell[465].

3.1 Introduction

The ocular lens is a transparent, biconvex tissue in the eye that adjustably refracts visible light onto the retina enabling high acuity vision over a wide range of distances[1–3]. The optical properties of the lens are a function of its specialized cellular organization which is comprised of an anterior monolayer of epithelial cells that overlay and differentiate into lens fiber cells at the lens equator[466]. Fiber cells differentiate gradually through a process of protein synthesis, cell migration, cell elongation, and programmed organelle degradation forming a gradient of cellular differentiation and spatiotemporal protein expression from the lens periphery to the lens core.

Aquaporins (AQPs) are transmembrane water channels that represent one group of spatiotemporally expressed proteins in the lens. Mammalian lenses express AQP0[37–40], AQP1[40,41], and AQP5[40,43,44,46]. Collectively, lens AQPs regulate lens transparency and refractive index[36] by controlling lens osmotic balance. In lens epithelial cells, AQP1 is expressed on the apical plasma membrane[42,45] and AQP5 is expressed cytoplasmically [45,111,168]. In lens fiber cells, AQP0 is expressed on the apical and basolateral plasma membranes while AQP5 is cytoplasmically expressed in the newly differentiating fiber cells and is gradually inserted into the plasma membrane as fiber cells mature [45,46,111,168].

The important role of AQP5 in maintaining lens homeostasis is implied by its expression in all mammalian lenses studied to date including human[46,112,167,450], bovine[46], mouse[44,46,111,112,116,167,168], rat[46,111,116], rabbit[40], and dog[467] lenses. Functional studies demonstrate the relationship between AQP5 expression and lens osmotic homeostasis. For example, basal water content and volume are increased by ~22% and 12%, respectively, in AQP5 knockout ($AQP5^{-/-}$) mouse lenses relative to wild type ($AQP5^{+/+}$) lenses following osmotic perturbation in hyperglycemic media[49,110]. $AQP5^{-/-}$ mouse lenses develop cataract under the same conditions but remain transparent[42,110] following normoglycemic culture in contrast to $AQP5^{+/+}$ and $AQP0^{-/-}$ mice[58,66–69]. $AQP5^{-/-}$ mice also develop age-related cataract around six months at a higher frequency than $AQP5^{+/+}$ mice through upregulation of vimentin expression via miR-124–3p.1 expression[112]. The same effect is achieved in mice with a leucine to proline missense mutation at residue 51 in AQP5, $AQP5^{L51P}$, which corresponds to a homologous mutation in humans ($hAQP5^{L51P}$) associated with congenital cataract[112].

Functional studies also demonstrate the relationship between AQP5 subcellular localization and fiber cell plasma membrane water permeability (P_{H2O}) in the lens. Immunohistochemical studies show AQP5 primarily localized to the plasma membrane in the fiber cells of the mouse lens cortex and to cytoplasmic vesicles in the rat lens cortex and the extent of fiber cell permeability correlates to plasma membrane AQP5 abundance[111]. Cytoplasmic AQP5 in rat lenses is dynamically inserted into fiber cell plasma membranes in response to changes in zonular tension and thereby increases fiber cell plasma membrane water permeability (P_{H2O})[111,116].

While the expression and functional regulation of lenticular AQP5 is currently being investigated, the molecular identity of lens AQP5-containing cytoplasmic vesicles remains unclear. AQP5 has been shown to localize to autophagosomes for degradation in both mouse and rat submandibular glands[312,313]. In this study, we spatially map AQP5 in the bovine lens,

define the molecular identity of AQP5-containing cytoplasmic compartments, and investigate mechanisms of AQP5 plasma membrane insertion. In the bovine lens, we find that AQP5 is expressed cytoplasmically in the lens epithelial and outer cortical fiber cells then is gradually inserted into fiber cell plasma membranes in the inner cortex similar to other mammalian lenses. Based on our immunofluorescence analysis in the outer cortex, AQP5 appears to be associated with and possibly incorporated into mitochondria in the bovine lens. Thereafter, AQP5-containing cytoplasmic vesicles are identified as LC3B-positive, LIMP-2 positive vesicles in which TOMM20-containing mitochondria appear to degrade possibly as a specialized method of normal lens mitochondrial autophagic degradation. These AQP5-containing cytoplasmic vesicles appear to dock with the plasma membrane with subsequent AQP5 plasma membrane insertion. AQP5 plasma membrane insertion is partially inhibited by bafilomycin A1 suggesting a novel type of AQP5 trafficking through lysosome secretion, a form of type III unconventional protein secretion, in the mammalian cells.

3.2 Experimental Materials & Procedures

Tissue
Frozen bovine lenses (1-2 years old) used for lens microdissection were obtained from Pel-Freez Biologicals (Rogers, AK). Fresh bovine lenses (1-2 years old) used for immunofluorescence were obtained from Light Hill Meats (Lynnville, TN, USA) and Cedar Hill Meat Processing (Cedar Hill, TN).

Reagents
All chemicals, unless otherwise stated, were obtained from Sigma-Aldrich (St. Louis, MO). Bafilomycin A1 was purchased from Millipore Sigma (Burlington, MA).

Antibodies
Affinity-purified rabbit anti-AQP5 IgG antibody targeted towards amino acid residues 249-265 of rat AQP5 (AB15858) and normal goat IgG antibody (NI02-100UG) were obtained from Millipore Sigma. Rabbit anti-PI3K p110α IgG (4249), anti-Akt IgG (9272), anti-phospho-Akt (phospho-Ser473) IgG (4060), anti-mTOR IgG (2983), rabbit anti-phospho-mTOR (phospho-Ser2481) IgG (2974), rabbit anti-S6 ribosomal protein IgG (2217), rabbit anti-phospho S6 ribosomal protein (phospho-Ser240/phospho-Ser244) (5364), and normal rabbit IgG (2729) antibodies were obtained from Cell Signaling Technology (Danvers, MA). Goat anti-calnexin IgG was obtained from LifeSpan Biosciences (LS-B4403; Dallas, TX). Rabbit anti-LC3B IgG was obtained from MyBioSource, Inc. (MBS9435173; San Diego, CA). Rabbit anti-LIMP-2 IgG was obtained from Novus Biologicals, LLC (NB400-129; Centennial, CO). Mouse anti-TOMM20 IgG was obtained from Abcam (ab56783; Waltham, MA). Goat anti-connexin 50 IgG (sc-20746) and normal mouse IgG antibody were obtained from Santa Cruz Biotechnology (sc-2025; Dallas, TX). Secondary antibodies (goat anti-rabbit Alexa Fluor 488, goat anti-rabbit Alexa Fluor 647, donkey anti-rabbit Alexa Fluor 488, and donkey anti-goat Alexa Fluor 647) were obtained from Fisher Scientific. Secondary antibody used for Western blotting was obtained from Fisher Scientific (goat anti-rabbit DyLight 680, goat anti-mouse DyLight 800, and donkey anti-goat DyLight 800; Waltham, MA).

Other Biologics
Alexa Fluor 488- or Alexa Fluor 647-conjugated wheat germ agglutinin (WGA) was used to label fiber cell plasma membranes. Vybrant™ CM-DiI Cell-Labeling Solution (cat# V22888) was used to universally label lipid membranes in fiber cells.

Immunofluorescence

Fresh or cultured bovine lenses were fixed in 2% paraformaldehyde with or without 0.01% glutaraldehyde in phosphate buffered saline (PBS; 24 or 72 hours at room temperature), cryoprotected in 10% sucrose-PBS (2 days, 4°C), 20% sucrose-PBS (1 hour, room temperature), and 30% sucrose-PBS ($\geq$ 7 days, 4°C), snap frozen in liquid nitrogen, encased in Tissue-Tek® O.C.T. Compound (Sakura Finetek USA, Inc.; Torrance, CA), cryosectioned parallel (axially) to the optic axis at 20 µm thickness using a Leica CM3050 S cryostat (Leica Biosystems Inc; Buffalo Grove, IL), and finally were transferred onto plain microscope slides. Next, lens tissue cryosections (i.e. "sections") were triply washed in PBS, incubated in blocking solution (6% bovine serum albumin, 6% normal goat serum, in PBS) for 2-3 hours to reduce nonspecific labelling, and immunolabeled with rabbit anti-AQP5 (1:400), goat anti-calnexin (1:100), mouse anti-TOMM20 (1:200), rabbit anti-LC3B (1:400), rabbit anti-Sec22β (1:100), or rabbit anti-LIMP2 (1:250) primary antibody in blocking solution (16 hours, 4^{O}C) followed by Alexa488- or Alexa647-conjugated goat or donkey secondary antibodies in blocking solution (2 hours, room temperature). Normal rabbit IgG, normal goat IgG, and normal mouse IgG were used as host-specific negative controls for nonspecific IgG binding. In certain cases, 0.1% Triton X-100 was included in PBS washes or blocking solution prior to incubation with secondary antibodies. Following immunolabeling, sections underwent subsequent fluorescent labeling with DAPI-dilactate (1:100 in PBS) to label cellular nuclei singularly or DAPI-dilactate *in combination with* Alexa488- or Alexa647-conjugated wheat germ agglutinin (WGA; 1:100 in PBS, 1 hour, room temperature) to label fiber cell plasma membranes *or* Vybrant™ CM-DiI Cell-Labeling Solution Lipid (1:5000 in 50% ethanol-PBS) to label cellular lipid membranes. Following immunolabeling and labeling, sections were coverslipped in ProLong™Glass Antifade Mountant and imaged using a Zeiss LSM 880 confocal laser scanning microscope (Carl Zeiss Inc; White Plains, NY). Images were post-processed to improve resolution using Airyscan processing (Zeiss). Background fluorescence (i.e. fluorescence from normal IgG incubated, negative control tissue) was subtracted using Adobe Photoshop CS6 (Adobe; San Jose, CA).

***Ex Vivo* Whole Lens Culture & Image Segmentation Analysis**

Fresh bovine lenses were cultured in *complete medium* at 37 °C in 4% CO_2 as outlined previously[309] using a Forma™ Model 370 Series Steri-Cycle™ CO_2 Incubator (ThermoFisher Scientific; Waltham, MA). Briefly, complete M199 medium consisted of M199 medium (11-150-059, Fisher Scientific), 10% fetal bovine serum, 1% penicillin, and 1% streptomycin. After 2 hours of culture, lenses free of cataract were treated with 10 nM bafilomycin A1 or 0.1% DMSO, the vehicle (negative) control, for 24 hours. Cultured bovine lenses were cryosectioned for immunofluorescence analysis and imaged as outlined above. Nikon NIS Elements version 5.3.0 software was used to perform image segmentation to quantify relative AQP5 expression changes in the cortical fiber cell plasma membranes of cultured bovine lenses due to bafilomycin A1 treatment. Relative AQP5 expression was defined as the mean intensity of AQP5 immunofluorescence with bafilomycin A1 treatment normalized to vehicle control.

Transmission Electron Microscopy (TEM)

Fresh bovine lenses were placed in 1% glutaraldehyde in 0.1M cacodylate buffer (2 days, room temperature). Thereafter, tissue chunks were excised from these lenses near the lens equator and incubated in 2.5% glutaraldehyde-0.1 M cacodylate (2 days, room temperature) followed by post-fixation in 1% OsO_4 (1 hour, room temperature). The tissue was dehydrated using a graded ethanol series and infiltrated with Epon-812 (Electron Microscopy Sciences, cat# RT 13940; Hatfield, PA) using propylene oxide as the transition solvent. The Epon-812 was polymerized at 60^{O} C for 48 hours and the samples were sectioned at 70 nm for TEM using a Leica UC7 Ultramicrotome. TEM was performed on a Tecnai T12 electron microscope (ThermoFisher Scientific) at 100 kV using an AMT CCD camera (AMT; Woburn, MA).

Lens Microdissection

Bovine lenses were microdissected into four distinct regions by modifying microdissection techniques adapted for embryonic chick lenses previously described by Walker and Menko[468]. These regions are the central epithelium (EC), the equatorial epithelium (EE), the peripheral fiber cells (FP), and the central fiber cells (FC). The equatorial epithelium includes the nascent fiber cells of the lens modiolus in the bovine lens. Dissection of FP cells from FC cells was modified by isolating these two regions using a trephine with a 14.3 mm outer diameter following microdissection of the EC and EE cells. Lens tissue outside and inside the trephine were designated as FP cells and FC cells respectively. Microdissected fractions from frozen or cultured bovine lenses were homogenized in Extraction Buffer (EB; 2.5% sodium dodecyl sulfate, 44.4 mM *n*-octyl β-D glucopyranoside, 1% Triton X-100, 25 mM Tris, 100 mM NaCl, 1 mM $MgCl_2$, 5 mM EDTA, pH 7.4) containing 20 mM sodium orthovanadate, 20 mM NaF, and protease inhibitor cocktail (100 µL per gram of tissue; Sigma-Aldrich). Homogenates were centrifuged at 4696 g for 30 minutes. The supernatant or EB-soluble fraction (EBSF) for each lens region was isolated for Western blot analysis and the insoluble pellet was discarded.

Western Blot Analysis

4X Laemmli Sample Buffer (Bio-Rad; Hercules, CA) and 1M DTT were added to the EBSF for each lens region to a final concentration of 1X and 50mM, respectively. 50 µg EBSF was loaded onto 4–20% gradient Mini-PROTEAN Tris-Glycine gels (Bio-Rad) using Tris-Glycine-SDS running buffer (Bio-Rad), and the Mini-PROTEAN Tetra Cell system was used for protein separation. Thereafter, proteins from the gel were transferred to methanol-activated PVDF membranes in Towbin Buffer with SDS (25 mM Tris, 192 mM glycine, 20% methanol, 0.025% SDS) at 20V for 5-7 hours. Protein-laden PVDF membranes (immunoblots) were blocked for 1 hour at room temperature in Intercept Blocker Buffer (LI-COR Biotechnology, cat# 927-70001 or 927-60001; Lincoln, NE). Immunoblots were incubated in Intercept Blocking Buffer containing anti-PI3K p110α (1:1000), anti-Akt (1:1000), anti-phospho-Akt (phospho-Ser473; 1:1000), anti-mTOR (1:1000), anti-phospho-mTOR (phospho-Ser2481; 1:1000), anti-S6 ribosomal protein (RPS6; 1:1000), anti-phospho-RPS6 (phospho-Ser240/phospho-Ser244; 1:1000) primary antibody (16-18 hours, $4^{O}C$) then containing goat anti-rabbit DyLight680 antibody (1:12000; Fisher Scientific) or goat anti-mouse DyLight800 antibody (room temperature, 2 hours). Immunoblots were reprobed for β-Actin using anti-β-Actin primary antibody (1:1000, 18 hours, $4^{O}C$) then goat anti-rabbit DyLight680 antibody as outlined above. Immunoblots were scanned using an Odyssey CLx fluorescence imager (Li-COR Biotechnology). Total protein expression of mTOR, phospho-mTOR, RPS6, phospho-RPS6, and β-Actin for each lens region was calculated via densitometric analysis. β-Actin was used as a loading control.

LC-MS/MS for Identifying LIMP-2 Peptides

Frozen bovine lens anterior and posterior poles were shaved off to yield a center section approximately 3 mm thick. The cortex was removed by trephine center-punch at 7/16" and homogenized in homogenizing buffer 25 mM Tris, 5 mM EDTA, 1 mM DTT, 150 mM NaCl, and 1 mM PMSF pH 8.0 then centrifuged at 100,000g for 30 minutes to pellet the membrane fraction. The membrane fraction was subsequently washed in homogenizing buffer once, homogenizing buffer with 8M urea twice, then cold 0.1 M NaOH. Urea-insoluble/NaOH-insoluble membrane fraction proteins were taken up in 50 mM triethylammonium bicarbonate (TEAB) and 5% SDS and 75 µg protein was isolated. Protein isolate was reduced and alkylated with addition of 10 mM dithiothreitol and 20 mM iodoacetamide. Alkylated proteins were acidified with phosphoric acid to 2.5% and precipitated with 100 mM TEAB in methanol. Precipitate was loaded on an S-Trap micro (Protifi), washed four times with 100 mM TEAB in methanol, and digested in 0.25 µg/µL trypsin in 50 mM TEAB for 2 hours at $46^{O}C$. Peptides were eluted from

the S-Trap with 66 mM TEAB, 0.2% formic acid, and then 66 mM TEAB and 50% acetonitrile (ACN). Eluted peptides were dried by a Speed Vac vacuum concentrator and rehydrated in 0.1 % triethylamine (TEA). Peptides were basic reverse phase separated on an in-house fabricated STAGE tip. Briefly, two 1.0 mm Empore C18 filter plugs were added to a pipette tip and 2 mg 5µm C18 resin (Phenomenex) was added to the top of the C18 filter plug. Peptides were loaded to the stage tip after equilibration and washed twice in 0.1% TEA. Peptides were eluted from the STAGE tip in progressive fractions of ACN (5%, 7.5%, 10%, 12.5%, 15%, 20%, 30%, 50% ACN in 0.1% TEA). Dried fractions were reconstituted in 0.1% formic acid. Approximately 400 ng of each basic reverse phase fraction was separately loaded onto a trap column before separation along a 95-minute gradient from 5% - 37% ACN. Peptides were measured on a Thermo Scientific Velos Pro linear ion trap instrument operating in top15 data dependent acquisition mode. RAW files were searched with FragPipe version 17.0 and modified to accommodate the low-resolution mass analyzer used in this study. Briefly, each sample was selected as part of a single experiment and searched with MSFragger version 3.4 with precursor mass tolerance of $\pm$ 500 ppm and fragment mass tolerance of $\pm$ 0.7 Da. Peptides of length 7-50 in mass range 500-5000 with charge 1-4 were included in a database of reviewed and unreviewed proteins (downloaded 12/08/2016, length 32,167). Cysteine carbamidomethylation was included as a default modification. Up to two variable modifications of methionine oxidation and N-terminal excision were allowed per peptide. Protein level results were filtered at 5% false discovery rate (FDR) while peptides, PSMs, and ions were filtered at 1% FDR. FragPipe outputs were used for protein level data interpretation in R.

Statistical Analysis

All assays were conducted in at least triplicate and experimental results are represented as the data *mean* $\pm$ *standard error of the mean* (*SEM*). Statistical significance of experimental results was determined with the Student's t-test. *P*-values $\leq$ 0.05 were considered statistically significant.

3.3 Results

AQP5 has been spatially mapped in human[46], mouse[45,46,168], rat[46,116], and rabbit lenses[40]. AQP5 spatial expression is broadly consistent across these species: AQP5 is cytoplasmic in lens epithelial cells and in young, differentiating fiber cells of the lens cortex and, as fiber cells mature, is gradually inserted into fiber cell plasma membranes. AQP5 expression remains localized to the plasma membrane in mature fiber cells to the lens core.

AQP5 Localization and Membrane Insertion

Based on these findings, we hypothesized that this general AQP5 spatial expression pattern is characteristic of mammalian lenses and would also be observed in bovine lenses. Confocal microscopy analysis of bovine lens cryosections immunolabeled for AQP5 shows that AQP5 is expressed throughout the bovine lens in both lens epithelial cells and lens fiber cells (Figures 1A -1B). AQP5 expression is cytoplasmic in bovine lens epithelial cells and in the incipient fiber cells of the lens modiolus (Figures 1C-1D). Interestingly, nuclear AQP5 expression consistently becomes detectable in the peripheral outer cortex immediately after fiber cells exit the lens modiolus and undergo substantial elongation (Figure 3.1C-1D, closed arrows). AQP5 plasma membrane insertion, defined as colocalization between AQP5 immunolabeling and WGA labeling, is detectable alongside cytoplasmic AQP5 expression as differentiating cortical fiber cells mature (Figures 1E and 1F, arrowheads). AQP5 expression is completely localized to the plasma membrane in the inner cortex and remains integral to the membrane through to the lens core. AQP5 nuclear expression disappears as AQP5 is inserted into the plasma membrane in

the inner cortex (Figure 3.1E and 1F, open arrows). AQP5 nuclear expression in the bovine lens appears to coincide with a reduction in cortical fiber cell nuclear size and change in morphology from smooth and elliptical in the outer cortex to irregular and elliptical in the inner cortex (Figures 1C-1F).

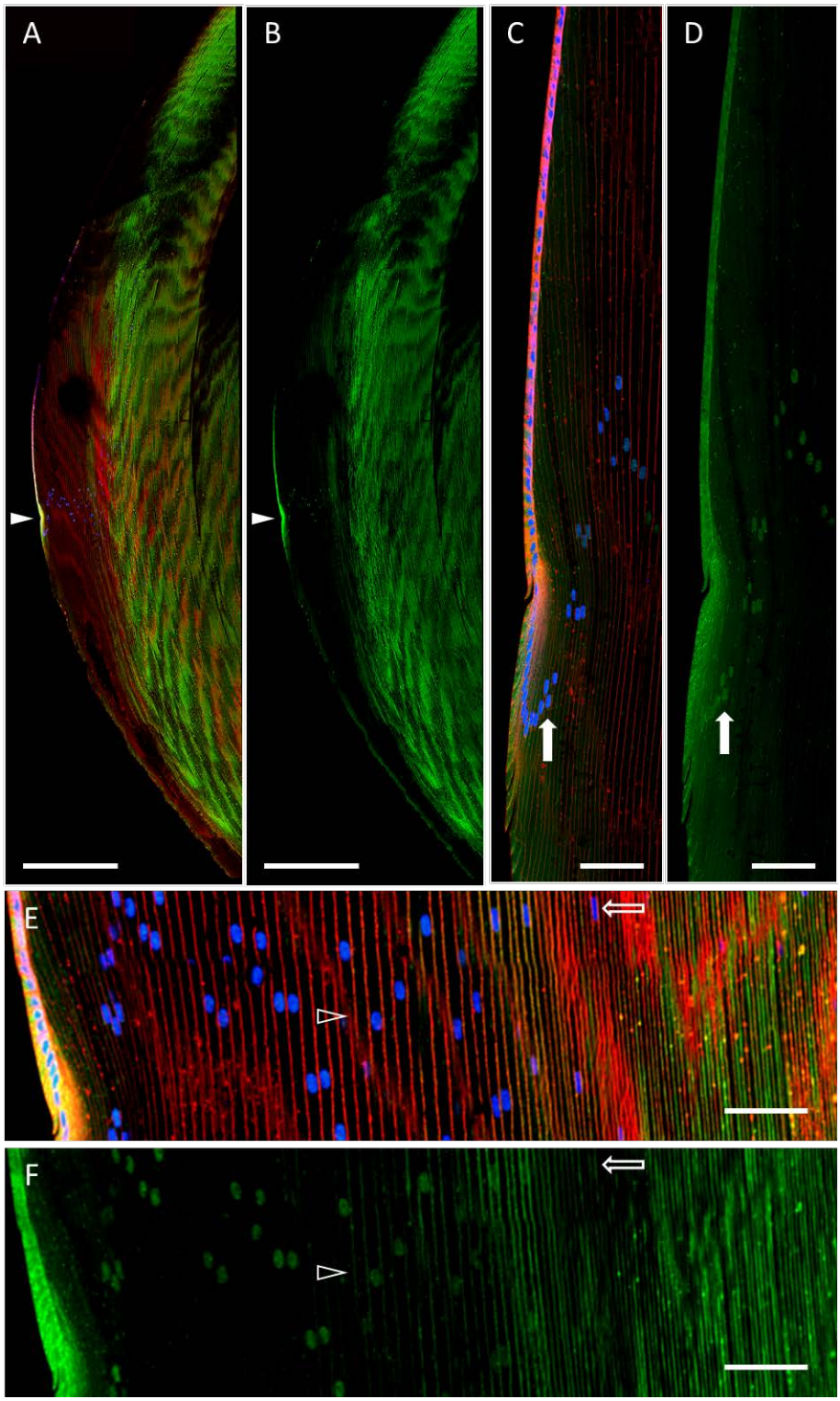

Figure 3.1. AQP5 spatial expression in the bovine lens.

A. A low-magnification, high-resolution image of AQP5 immunolabeling (***green***) in the bovine lens with WGA labeling of plasma membranes (***red***) and DAPI labeling of cell nuclei (***blue***). The *closed arrowhead* denotes the lens modiolus.

B. A replicate image of **A** with AQP5 immunolabeling only displayed.

C. A medium-magnification, high-resolution image of the lens modiolus and nearby outer cortical fiber cells. The *closed arrow* denotes the nucleus of an outer cortical fiber cell.

D. A replicate image of **C** with AQP5 immunolabeling only displayed. The *filled arrow* denotes AQP5 immunolabeling in the same cell nucleus demarcated in **B** and marks the appearance of AQP5 immunolabeling in outer cortical lens fiber cell nuclei.

E. A medium-magnification, high-resolution image of the lens cortex. The *open arrowhead* denotes the appearance of AQP5 plasma membrane insertion. The *open arrow* denotes the nucleus of a differentiating cortical fiber cell.

F. A replicate image of **E** with AQP5 immunolabeling only displayed. The scale bars denote 500 µm (**A**, **B**) and 100 µm (**C**-**F**). The *open arrow* denotes AQP5 immunolabeling in the same cell nucleus demarcated in **E** and marks the disappearance of AQP5 immunolabeling in inner cortical lens fiber cell nuclei.

AQP5 plasma membrane insertion was quantified based on the normalized radial distance *r/a*, where *r = the radial distance to the lens center*, and *a = lens radius*[8], as was done for previous mammalian lenses[46]. The fluorescence intensities of AQP5 and WGA in Figure 3.1 were converted to gray values (Figure 3.2A and 3.2B) and collinear surface plots of these gray values as a function of *r/a* quantitatively depict the spatial relationship between AQP5 expression and the plasma membrane across the lens bow region (Figure 3.2C-2E). AQP5 plasma membrane insertion is defined as *r/a* values with overlap between AQP5 and WGA gray values. AQP5 immunolabeling intensity peaks in the lens modiolus decreases significantly with *r/a* in the outer cortical fiber cells. The surface plot data for cytoplasmic AQP5 immunolabeling is nonuniform which reflects cytoplasmic AQP5 expression. Decreased AQP5 immunofluorescence intensity in the medial outer cortex may be a result of: 1) reduced AQP5 local concentration due to fiber cell volumetric expansion during cellular elongation, 2) AQP5 C-terminal epitope masking, or 3) reduced AQP5 expression in this region, though this observation remains to be further studied. Initial AQP5 plasma membrane insertion is detectable from *r/a* 0.979 (Figures 3.2C and 3.2D, black star) to *r/a* 0.958 (Figures 3.2C and 3.2E, blue star). Cytoplasmic AQP5 immunolabeling is detected between these *r/a* values as well. Full AQP5 membrane insertion occurs at *r/a* 0.958 (blue star), which is in the outer cortex-inner cortex transitional region. AQP5 remains localized to the plasma membrane from $0.958 \geq r/a \geq 0.000$ (data not shown).

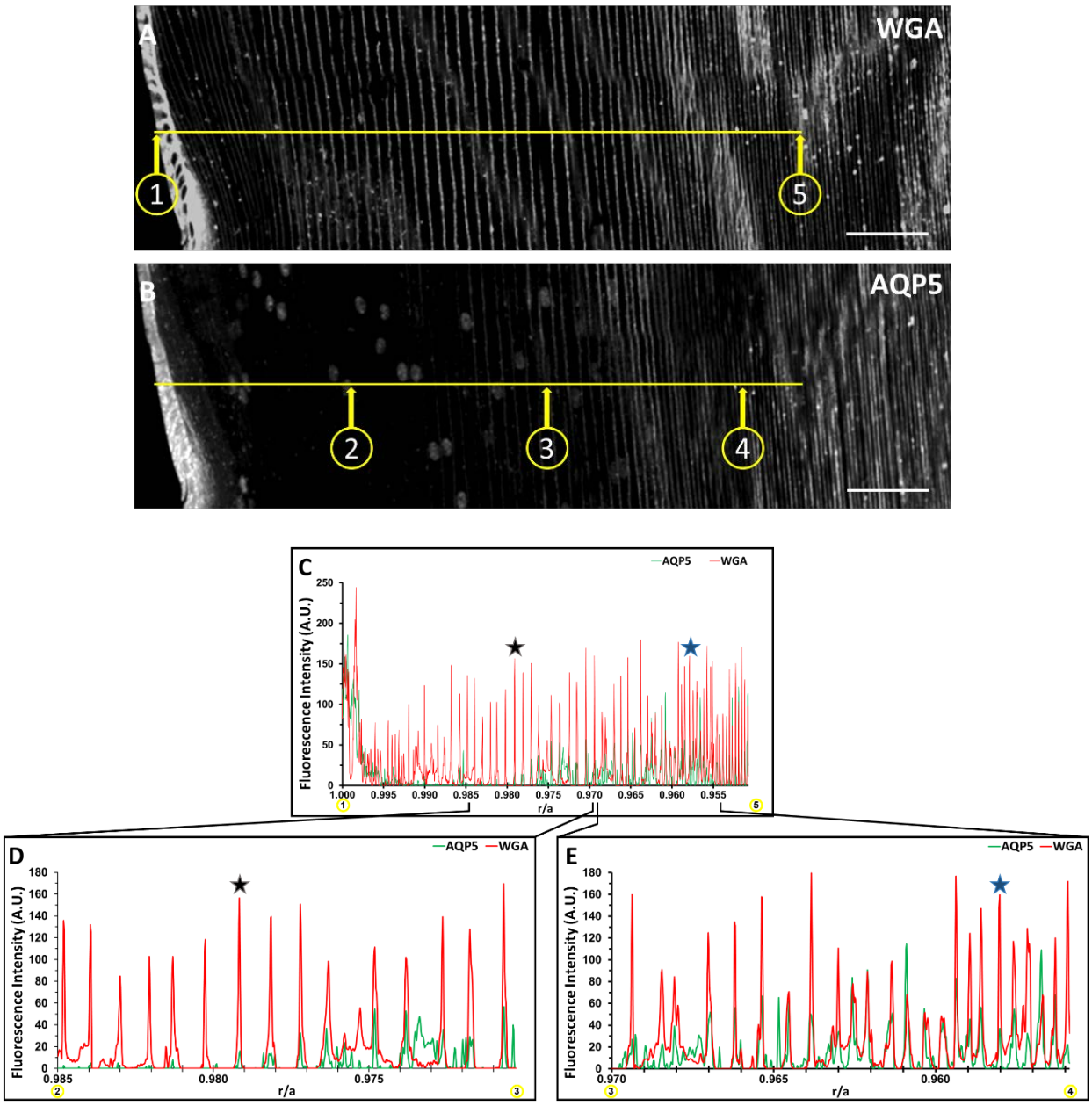

Figure 3.2. Cytoplasmic AQP5 is progressively inserted into cortical fiber plasma membranes during fiber cell differentiation in the bovine lens.

A. A grayscale image of **Figure 3.1E** with WGA labeling only displayed. Distinct points in space on a lens cryosection (n = 1) are represented by the quotient r/a, where r = distance from any point to the center of the lens perpendicular to the optical axis, and a = *radius of the lens*, which is 8000 µm for this section. Point ① in **C** corresponds to r/a = 1.000 and point ⑤ corresponds to r/a = 0.950. The horizontal, *yellow line* in **C** connects points ① and ⑤.

B. A replicate, grayscale image of **Figure 3.1E** with AQP5 immunolabeling only displayed. The horizontal, *yellow line* displayed is collinear to the line in **B** and connects points ②, ③, and ④ which correspond to *r/a* = 0.985, *r/a* = 0.970, and *r/a* = 0.955, respectively.

C. Two-dimensional surface plots of the fluorescence intensity gray values of WGA in **B** (*red line*) and AQP5 in **D** (*green line*) across the *yellow line* from points ① to ⑤.

D. Two-dimensional surface plots of the fluorescence intensity gray values of WGA in **B** (*red line*) and AQP5 in **D** (*green line*) across the *yellow line* from points ② to ③.

E. Two-dimensional surface plots of the fluorescence intensity gray values of WGA in **B** (*red line*) and AQP5 in **D** (*green line*) across the *yellow line* from points ③ to ④. AQP5 fluorescence intensity maximizes at *r/a* = 0.998 then decreases rapidly to near undetectable levels at *r/a* = 0.989. AQP5 fluorescence intensity increases inversely with *r/a* and is partially overlapped in space by the fluorescence intensity of WGA from 0.979 (*black star*) $\geq$ *r/a* $\geq$ 0.958 (*blue star***)** (**D-E**). AQP5 fluorescence intensity is entirely overlapped by that of WGA in space at 0.958 (*blue star*) (**D**). This trend continues to the lens center (0.958 $\geq$ *r/a* $\geq$ 0.000, *data not shown*). The scale bars denote 100 µm (**A**-**C**).

Identification of AQP5 Cytoplasmic Structures

Previous studies revealed variability in the morphology of AQP5-containing cytoplasmic vesicles in mouse[46,168], rat[46], and human[46] lens cortical fiber cells. To more accurately characterize AQP5-containing cytoplasmic vesicles in the bovine lens, we conducted high resolution confocal microscopy imaging of AQP5 expression in bovine lens cortical fiber cells (Figure 3.3). Cytoplasmic AQP5 expression in bovine lens fiber cells is localized to tubular and spheroidal cytoplasmic vesicles in the outer cortex (Figure 3.3, *arrowheads*). As fiber cells begin to differentiate at the lens equator, AQP5-containing cytoplasmic vesicles are less than 1 µm in diameter, up to 20 µm in length, and predominately tubular in morphology (Figure 3.3B, *open arrowheads*). As fiber cells mature and exit the lens modiolus, AQP5-containing cytoplasmic vesicles become predominately spheroidal and spheroidal, tubular (Figure 3.3, *closed arrowheads*) with spheroid regions varying up 3 µm in diameter (Figures 3.3C and 3.3D). Small puncta (< 0.45 µm) are visible that correspond to nonspecific immunofluorescence based on their appearance in negative control normal IgG immunolabeling controls (Figure 3.3C-3 and 3.3C-4).

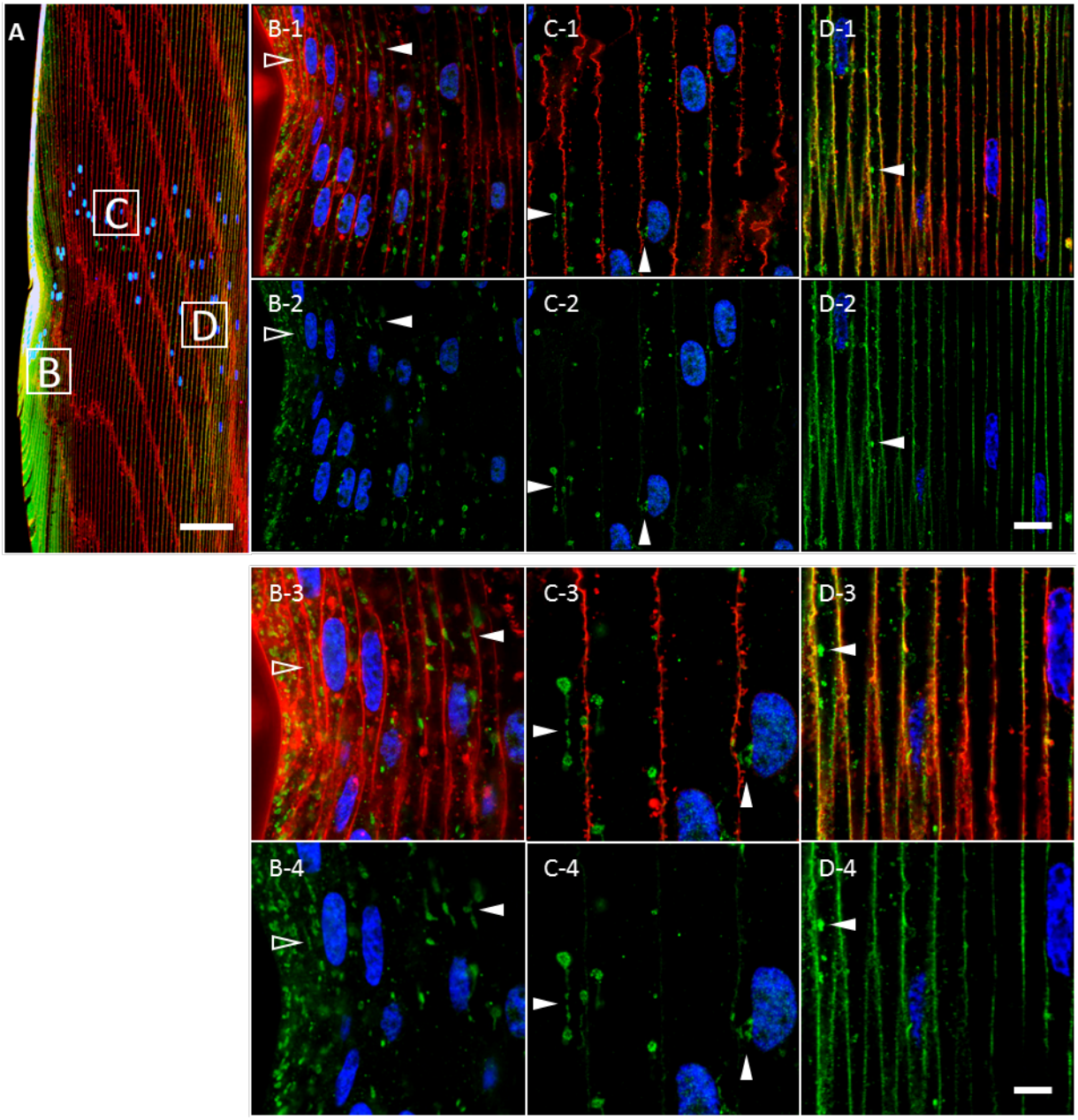

Figure 3.3. Cytoplasmic AQP5 immunolabeling in cortical fiber cells is localized to spheroidal, tubular structures in the bovine lens bow region.

A*.** A low-magnification representative image of AQP5 immunolabeling (green***) in the bovine lens bow region. Plasma membranes (***red***) and cellular nuclei (***blue***) are labeled by WGA and DAPI, respectively. The *peripheral outer cortex* (i.e. includes *lens modiolus*), *medial outer cortex*, and *outer cortex-inner cortex transitional region* are demarcated by ***B***, ***C***, and ***D***, respectively, and correspond spatially with the images in ***B*-*D***.

B-1 – ***D-1*.** High-magnification images of AQP5 immunolabeling (***green***) in the cortical fiber cell regions demarcated in **A**. AQP5-containing cytoplasmic vesicles were primarily

tubular in morphology in the incipient fiber cells of the lens modiolus (*open arrowheads*) and spheroidal, tubular in the cells outside of the lens modiolus (*closed arrowheads*). AQP5-containing cytoplasmic vesicles became slightly irregular in the outer cortex-inner cortex transitional region.

B-2 – ***D-2*****.** Replicate images of ***B-1*** – ***D-1*** depicting AQP5 immunolabeling and DAPI labeling only.

B-3 – ***D-3*****.** Enlarged images of AQP5-containing cytoplasmic vesicles denoted by the *arrowheads* in ***B-1*** – ***D-1***. The spheroidal and tubular domains within AQP5-containing cytoplasmic vesicles vary in size up to a maximum width and length of approximately 3 µm and 20 µm, respectively.

B-4 – ***D-4*****.** Replicate images of ***B-3*** – ***D-3*** depicting AQP5 immunolabeling and DAPI labeling only.

Scale bars represent 100 µm (**A**), 10 µm (***B-1***, ***B-2***, ***C-1***, ***C-2***, ***D-1***, and ***D-2***) and 5 µm (***B-3***, ***B-4***, ***C-3***, ***C-4***, ***D-3***, and ***D-4***.

To test whether AQP5-containing cytoplasmic vesicles were morphologically distinct structures amongst cytoplasmic vesicles in bovine lens cortical fiber cells, we analyzed DiI-labeled, AQP5 immunolabeled bovine lens cryosections (Figure 3.4). DiI is a lipophilic dye that labels all cytoplasmic cellular lipid membranes and the plasma membrane. In the lens modiolus, tubular DiI-labeled cytoplasmic compartments overlap entirely with tubular, AQP5-containing cytoplasmic vesicles indicating these structures as morphologically unique (Figure 3.4A, open arrowheads). In this region, DiI-labeled spheroidal, tubular cytoplasmic compartments and AQP5-containing, cytoplasmic vesicles typically overlap, but such compartments lacking AQP5 expression are readily observable in this region (Figure 3.4A, striped arrowheads). In outer cortical fiber cells, with the exception of the lens modiolus, spheroidal, tubular DiI-labeled cytoplasmic compartments are identical to AQP5-containing, cytoplasmic vesicles with rare exceptions indicating that large, spheroidal, tubular cytoplasmic structures in the outer cortex are uniquely AQP5-containing cytoplasmic vesicles (Figure 3.4, closed white arrowheads).

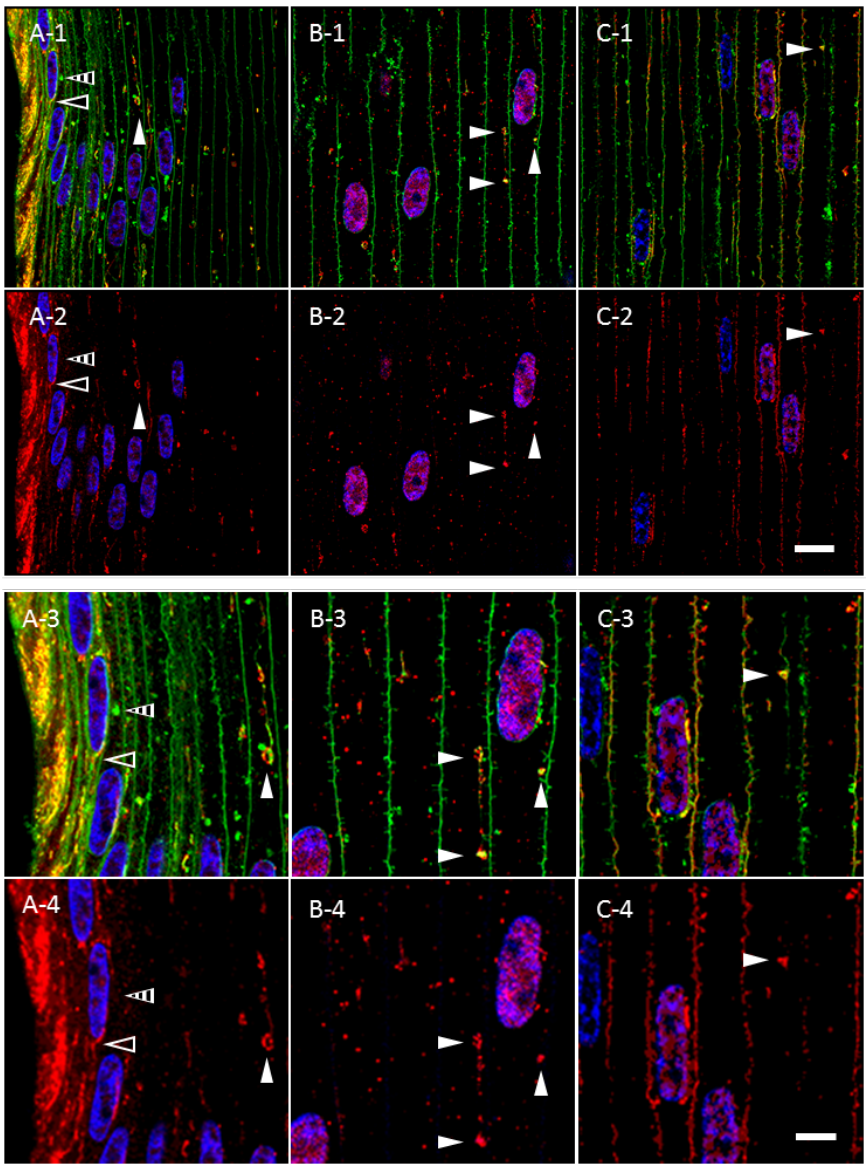

Figure 3.4. AQP5-containing, cytoplasmic vesicles represent a morphologically, distinct cluster of cytoplasmic vesicles in bovine lens cortical fiber cells outside the lens modiolus.

A-1 – ***C-1*****.** High-magnification confocal images of AQP5 immunolabeling (***red***) and DiI fluorescent labeling (***green***) in the *peripheral outer cortex* (***A***), *medial outer cortex* (***B***), and *outer cortex-inner cortex transitional region* (***C***) of the bovine lens as demarcated in ***Figure 3.3A***.

In the lens modiolus (***A***), tubular DiI-labeled cytoplasmic compartments (*open arrowheads*) overlap with tubular, AQP5-containing cytoplasmic vesicles. In these cells, both AQP5-negative (*striped arrowheads*) and AQP5-containing (*closed white arrowheads*) DiI-labeled cytoplasmic structures are readily observable (*striped arrowheads*). In the peripheral outer cortical fiber cells outside the lens modiolus,

medial outer cortex (***B***), and *outer cortex-inner cortex transitional region* (***C***), spheroidal, tubular DiI-labeled cytoplasmic compartments (*closed white arrowheads*) overlap with AQP5-containing, cytoplasmic vesicles with rare exceptions.

A-2 – ***C-2*****.** Replicate images of ***A-1*** – ***C-1*** with AQP5 immunolabeling and DAPI labeling only displayed.

A-3 – ***C-3*****.** Enlarged images of DiI-labeled cytoplasmic structures demarcated by arrowheads in ***A-1***, ***B-1***, and ***C-1***. Red puncta that do not colocalize with DiI represent nonspecific immunofluorescence based on normal IgG immunolabeling negative controls.

A-4 – ***C-4*****.** Replicate images of ***A-3***, ***B-3***, and ***C-3*** with AQP5 immunolabeling and DAPI labeling only displayed.

Scale bars represent 10 µm (***A-1***, ***A-2***, ***B-1***, ***B-2***, ***C-1***, and ***C-2***) and 5 µm (***A-3***, ***A-4***, ***B-3***, ***B-4***, ***C-3***, and ***C-4***).

Immunohistochemical studies of mitochondria[469] in chick lens fiber cells revealed structures similar in morphology to AQP5-containing cytoplasmic vesicles. To determine the molecular composition of bovine lens fiber cell AQP5-containing cytoplasmic vesicles, we tested AQP5-containing cytoplasmic vesicles for the presence of mitochondrial import receptor subunit TOM20 homolog (TOMM20) (Figure 3.5). TOMM20 is ubiquitously expressed in all tubular (Figure 3.5, *open arrowheads*) and spheroidal, tubular (Figure 3.5, *closed arrowheads*) AQP5-containing cytoplasmic vesicles observed. Colocalization between AQP5 and TOMM20 expression in these vesicles is high but nonuniform throughout the entirety of structures. TOMM20 expression dissipates during full AQP5 plasma membrane insertion in the bovine lens fiber cells of the outer cortex-inner cortex transition zone (Figure 3.5C). TOMM20 expression is not detected on the plasma membrane. The co-expression of AQP5 and TOMM20 in bovine lens cortical fiber cells indicates that TOMM20 is a molecular marker of AQP5-containing cytoplasmic vesicles.

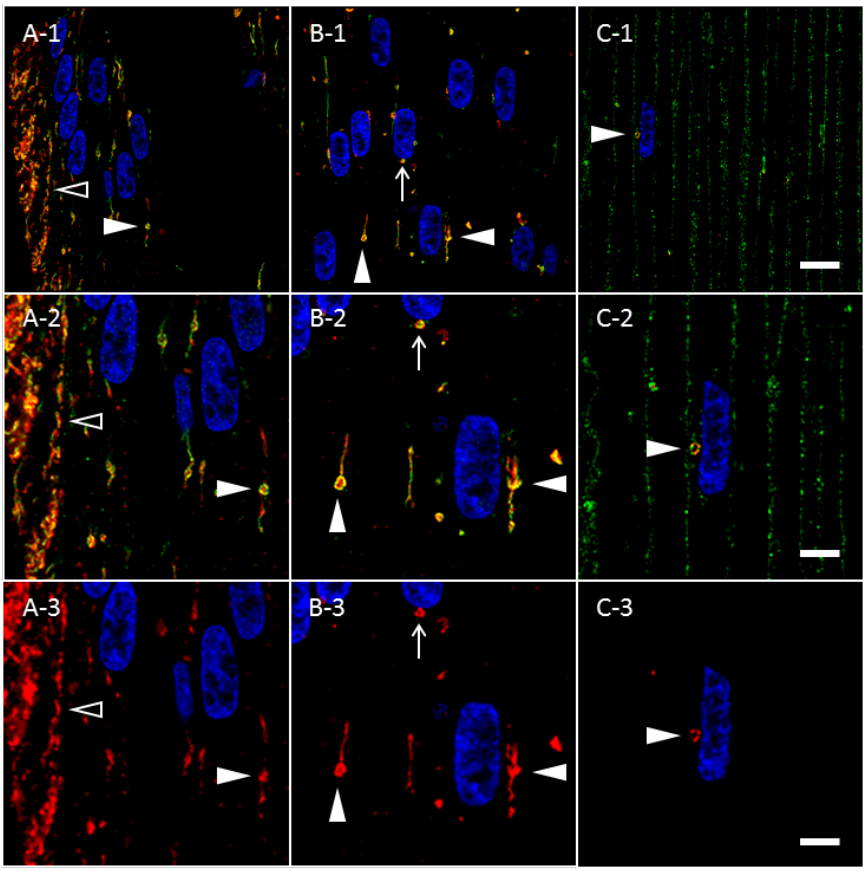

Figure 3.5. TOMM20 and AQP5 are *co-expressed* molecular markers for the same cluster of cytoplasmic vesicles in the bovine lens cortex.

A-1 – ***C-1*.** High-magnification confocal images of *AQP5* immunolabeling (***green***) and *TOMM20* immunolabeling (***red***) in the *peripheral outer cortex* (**A**), *medial outer cortex* (**B**), and *outer cortex-inner cortex transitional region* (**C**) of the bovine lens as demarcated in **Figure 3.3A**.

Tubular (***A***, *open arrowheads*) and spheroidal, tubular (**B** and **C**; *closed arrowheads*) AQP5-containing cytoplasmic vesicles and TOMM20-containing cytoplasmic vesicles colocalize in the outer cortex of bovine lenses. TOMM20-containing, AQP5-containing cytoplasmic vesicles are frequently apposed to fiber cell nuclei (***5B***, *arrow*; **5C**, *closed arrowhead*).

A-2 – ***C-2*.** Enlarged images of AQP5-containing cytoplasmic vesicles demarcated by arrowheads in ***A-1***, ***B-1***, and ***C-1***.

A-3 – ***C-3*.** Replicate images of ***A-2***, ***B-2***, and ***C-2*** with TOMM20 immunolabeling and DAPI labeling only displayed.

Scale bars represent 10 µm (***A-1***, ***A-2***, ***B-1***, ***B-2***, ***C-1***, and ***C-2***) and 5 µm (***A-3***, ***B-3***, and ***C-3***).

To corroborate mitochondrial protein expression in AQP5-containing cytoplasmic vesicles, we tested AQP5-containing cytoplasmic vesicles for expression of cytochrome c oxidase subunit IV (COX IV; Figure 3.6), an inner mitochondrial membrane protein. Similar to TOMM20, COX IV is expressed in tubular (Figure 3.6A, *open arrowheads*) and spheroidal, tubular (Figures 3.6A - 3.6C, *closed arrowheads*) AQP5-containing cytoplasmic vesicles. COX IV expression also dissipates as AQP5 is fully inserted into bovine lens fiber cell plasma membranes of the outer cortex-inner cortex transition zone (Figure 3.6C). The co-expression of AQP5 and COX IV in bovine lens cortical fiber cells indicates that COX IV is also a molecular marker of AQP5-containing cytoplasmic vesicles.

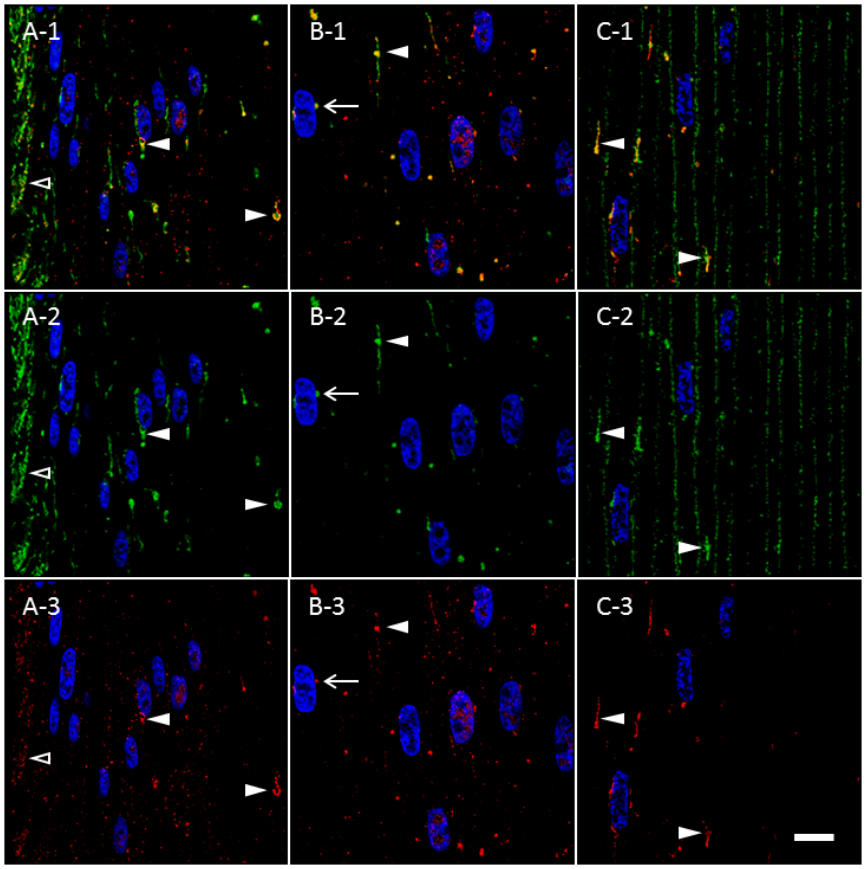

Figure 3.6. Cytochrome c oxidase subunit IV (COX IV) and AQP5 are *co-expressed* molecular markers for the same cluster of cytoplasmic vesicles in the bovine lens cortex.

A-1 – ***C-1*.** High-magnification confocal images of *AQP5* immunolabeling (***green***) and *COX IV* immunolabeling (***red***) in the *peripheral outer cortex* (**A**), *medial outer cortex* (**B**), and *outer cortex-inner cortex transitional region* (**C**) of the bovine lens as demarcated in ***Figure 3.3A***.

Tubular (***A***, *open arrowheads*) and spheroidal, tubular (**B** and **C**; *closed arrowheads*) AQP5-containing cytoplasmic vesicles and COX IV-containing cytoplasmic vesicles colocalize in the outer cortex of bovine lenses. COX IV-

containing, AQP5-containing cytoplasmic vesicles are frequently apposed to fiber cell nuclei (***3.6B***, *arrow*).

A-2 – ***C-2*****.** Replicate images of ***A-1***, ***B-1***, and ***C-1*** with AQP5 immunolabeling and DAPI labeling only displayed.

A-3 – ***C-3*****.** Replicate images of ***A-1***, ***B-1***, and ***C-1*** with COX IV immunolabeling and DAPI labeling only displayed.

Scale bar represents 10 µm.

We next tested AQP5-containing cytoplasmic vesicles for expression of calnexin (Figure 3.7), a resident endoplasmic reticulum (ER) integral membrane protein that functions as chaperone[470]. Calnexin is cytoplasmically expressed in irregular, punctate vesicles or tubular, plaque-like ER compartments apposed to fiber cell plasma membranes in the peripheral outer cortex and medial outer cortex. Calnexin expression increasingly localizes to the perinuclear ER and tubular ER apposed to fiber cell plasma membranes with fiber cell differentiation (Figures 3.7B and 3.7C, arrows). Nevertheless, we observed minimal calnexin expression in AQP5-containing cytoplasmic vesicles. However, calnexin-containing ER vesicles form frequent appositions (Figure 3.7, striped arrowheads) with AQP5-containing cytoplasmic vesicles.

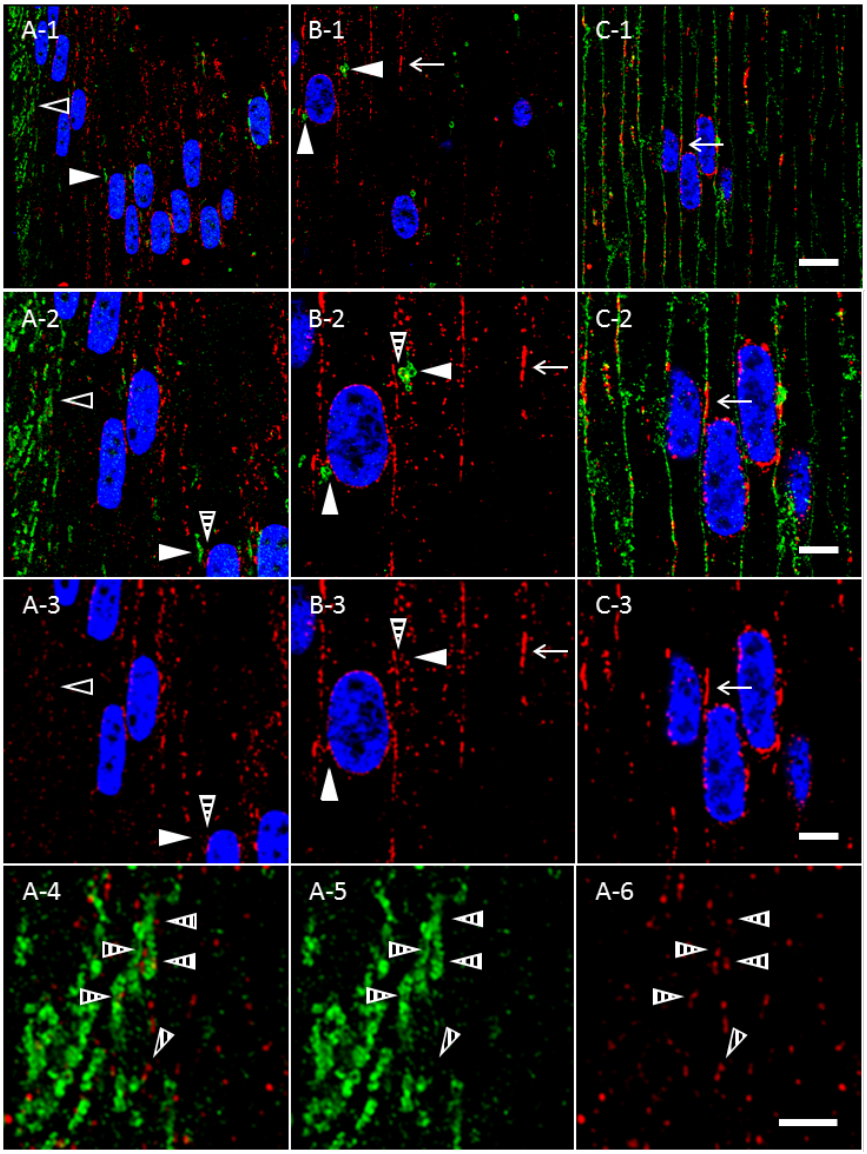

Figure 3.7. AQP5-containing cytoplasmic vesicles and calnexin-containing endoplasmic reticula fail to overlap in the bovine lens cortex.

A-1 – ***C-1*****.** High-magnification confocal images of *AQP5* immunolabeling (***green***) and *calnexin* labeling (***red***) in the *peripheral outer cortex* (***A-1***), *medial outer cortex* (***B-1***), and *outer cortex-inner cortex transitional region* (***C-1***) of the bovine lens (demarcated in **Figure 3.3A**). Calnexin is an integral membrane protein in the endoplasmic reticulum (ER). In the *peripheral outer cortex* and *medial outer cortex*, calnexin is cytoplasmically expressed in irregular, punctate vesicles or tubular, plaque-like ER compartments apposed to fiber cell plasma membranes. Calnexin is also expressed in the perinuclear ER (***B-1***, ***B-2***, ***C-1***, and ***C-2***). By the outer cortex-inner cortex transitional region, calnexin expression is primarily localized to the perinuclear ER and tubular ER apposed to fiber cell plasma membranes (***B*** and ***C***, arrows).

AQP5-containing cytoplasmic vesicles lack significant calnexin expression. However, calnexin-containing ER form multiple appositions (***A-3***, ***A-4***, ***A-5***, ***A-6***, ***B-3***, and ***B-4,*** *striped arrowheads*) with tubular (***A***, *open arrowheads*) and spheroidal, tubular (***A*** and ***B***; *closed arrowheads*) AQP5-containing cytoplasmic vesicles.

A-2 – ***C-2*****.** Enlarged images of the AQP5-containing cytoplasmic vesicles demarcated by the *arrowheads* in ***A-1*** and ***B-1*** and of the calnexin-containing tubular ER compartment demarcated by the *arrows* in ***B-1*** and ***C-1***.

A-3 – ***C-3*****.** Replicate images of ***A-2***, ***B-2***, and ***C-2*** with calnexin immunolabeling and DAPI labeling only displayed.

A-4**.** Enlarged image of tubular AQP5-containing cytoplasmic vesicles demarcated by the *open arrowhead* in ***A-2***. These vesicles typically form several appositions with calnexin-containing ER (*striped arrowheads*)

A-5**.** A replicate image of ***A-4*** with AQP5 immunolabeling only displayed.

A-6**.** A replicate image of ***A-4*** with calnexin immunolabeling only displayed.

Scale bars represent 10 µm (***A-1***, ***B-1***, and ***C-1***) and 5 µm (***A-2***, ***A-3***, ***B-2***, ***B-3***, ***C-2***, and ***C-3***).

Despite AQP5 plasma membrane insertion in the bovine lens cortex, mitochondrial degradation occurs universally within the vertebrate ocular lens[307–309,363,364] and occurs through mitophagy in the mouse lens as BNIP3L/NIX expression, a mitophagy protein, is required for mitochondrial elimination to create the organelle-free zone[310]. In the mouse lens, autophagosomes are TOMM20-positive and LC3B-positive[308]. Thus, we hypothesized that AQP5- and TOMM20-containing cytoplasmic vesicles in bovine lens fiber cells might become autophagic vesicles and also express microtubule-associated protein light chain 3B (LC3B), an autophagy-specific molecular marker and peripheral membrane protein within autophagosomes, amphisomes, and autolysosomes. We analyzed TOMM20-containing cytoplasmic vesicles in the bovine lens for LC3B expression in bovine lens fiber cells (Figure 3.8). In the lens modiolus, tubular TOMM20-containing cytoplasmic vesicles are readily observable as in Figure 3.5 (Figure 3.8A, *open arrowheads*), but LC3B expression in these structures is virtually undetectable. In peripheral outer cortical fiber cells outside of the lens modiolus, LC3B expression (Figure 3.8A, *striped arrowheads*) is sparse and sporadically localized to spheroidal, tubular TOMM20-containing cytoplasmic vesicles (Figure 3.8A, *closed arrowheads*). LC3B expression and colocalization within TOMM20-containing cytoplasmic vesicles increase as a function of fiber cell differentiation suggesting that mitochondria, and thereby AQP5-containing cytoplasmic vesicles, are incorporated into autophagosomes and potentially into amphisomes and autolysosomes as well. By the outer cortex-inner cortex transitional region, TOMM20-containing cytoplasmic vesicles ubiquitously express LC3B (Figures 3.8B and 3.8C). The linear morphology of LC3B-positive structures in the bovine lens outer cortex is interesting to note as autophagosomes are typically globular. Nevertheless, there are examples of linear autophagosomes in the literature[471,472].

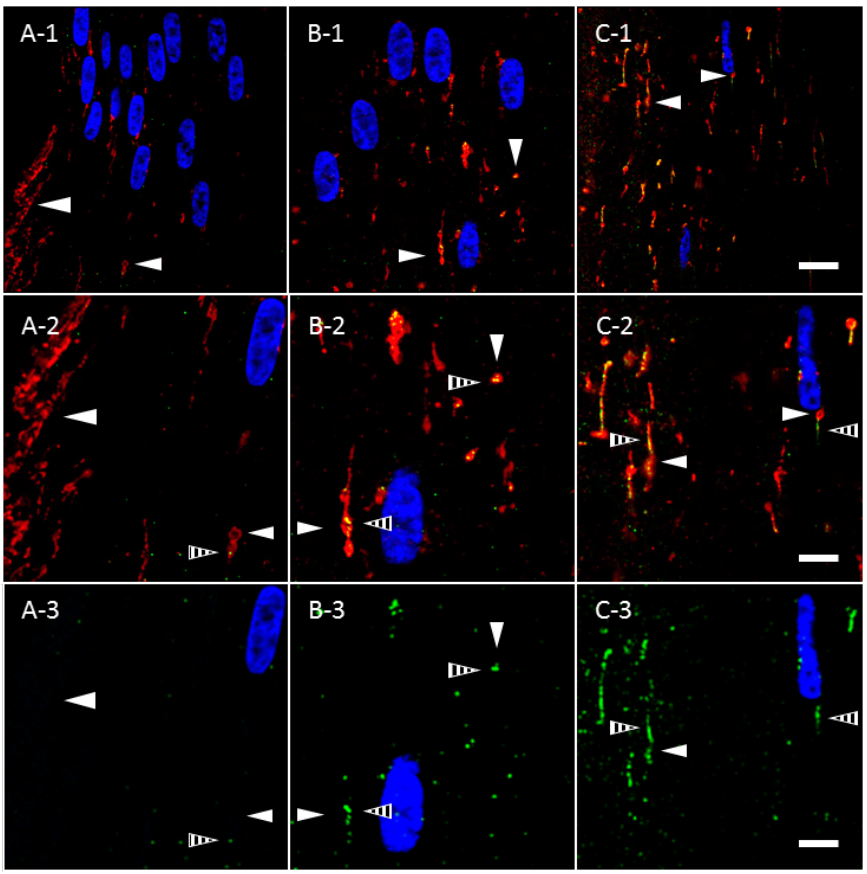

Figure 3.8. TOMM20-containing cytoplasmic vesicles express LC3B prior to complete AQP5 plasma membrane insertion in bovine lens cortical fiber cells.

A-1 – ***C-1*.** High-magnification confocal images of *TOMM20* immunolabeling (***red***) and *LC3B* immunolabeling (***green***) in the *peripheral outer cortex* (***A***), *medial outer cortex* (***B***), and *outer cortex-inner cortex transitional region* (***C***) of the bovine lens (***Figure 3.3A***).

In the peripheral outer cortex, LC3B is faintly expressed (***A***) in punctate, cytoplasmic vesicles (***A***, ***B***, and ***C***; *striped arrowheads*). TOMM20-containing cytoplasmic vesicles (*closed arrowheads*) in the peripheral outer cortex colocalize minimally with LC3B. As outer cortical fiber cells mature, LC3B expression is upregulated. Thus, LC3B-containing cytoplasmic vesicles are significantly larger and more abundant in the *medial outer cortex* (***B***) and *outer cortex-inner cortex transitional region (**C**)* relative to the *peripheral outer cortex*. LC3B colocalizes with the TOMM20-containing cytoplasmic vesicles in the *medial outer cortex* and the *outer cortex-inner cortex transitional region* (***B*** and ***C***).

A-2 – ***C-2*.** Enlarged images of the TOMM20-containing cytoplasmic vesicles demarcated by the *arrowheads* in ***A-1***, ***B-1***, and ***C-1***.

A-3 – ***C-3*.** Replicate images of ***A-2***, ***B-2***, and ***C-2*** with LC3B immunolabeling and DAPI labeling only displayed.

Scale bars represent 10 µm (***A-1***, ***B-1***, and ***C-1***) and 5 µm (***A-2***, ***A-3***, ***B-2***, ***B-3***, ***C-2***, and ***C-3***).

Gheyas et al 2022 demonstrated that inhibition of phosphoinositide-3-kinase (PI3K) signaling induced a significant increase in LAMP1-positive lysosomes and complete organelle degradation in cultured embryonic lenses[311]. As mentioned above mitochondria in the mouse are degraded via mitophagy. To identify potential mechanisms of autophagic induction and test for a potential association with PI3K signaling in the bovine lens, we conducted regional Western blot expression analysis of the PI3K catalytic subunit p110α in microdissected bovine lens tissue as outlined in Walker et al 1999[468] (Figure 3.9A, arrow). We also analyzed expression of the PI3K substrate and kinase Akt (Figure 3.9B, arrow) and Akt Ser473 phosphorylation (Akt pS473; Figure 3.9C, arrow). Mammalian target of rapamycin complex 2 (mTORC2) phosphorylates Akt at S473 which is required for Akt activation[473]. PI3K p110α is represented by bands at 110 kDa, and Akt and Akt pS473 are represented by bands at approximately 58 kDa. PI3K p110α, Akt, and Akt pS473 are expressed in the central epithelium and the equatorial epithelial and cortical fiber cells. Of these, PI3K p110α singularly is detected in the posterior fiber cells, and none is detected in the central fiber cells. PI3K expression in the central epithelium and the equatorial epithelial and cortical fiber cells is comparable but decreases significantly in posterior fiber cells. Both Akt and Akt pS473 expression decrease from the central epithelium to the equatorial epithelial and cortical fiber cells.

A.

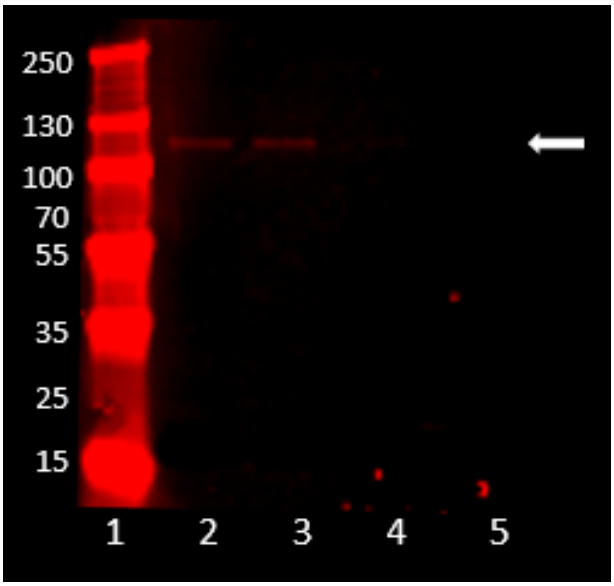

B.

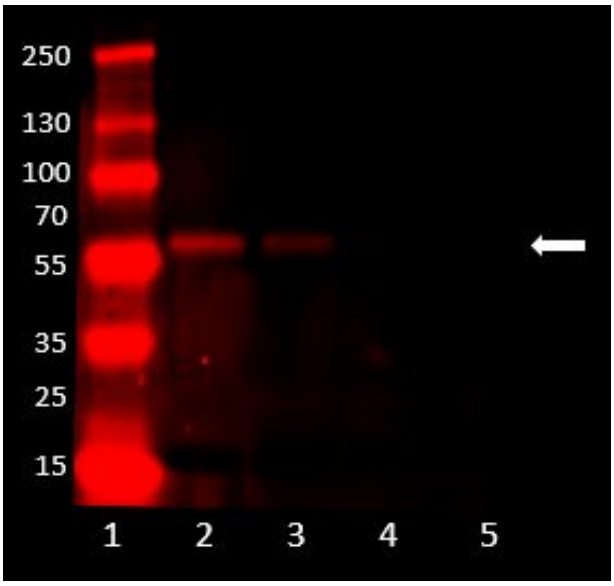

C.

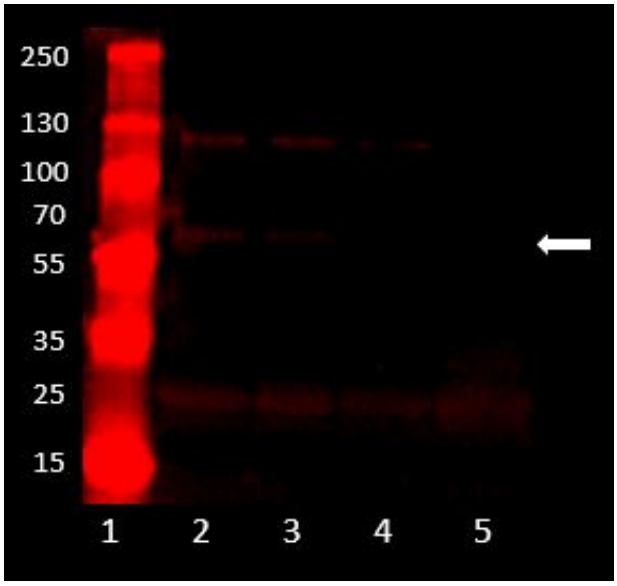

Figure 3.9. Regional phosphoinositide 3-kinase (PI3K) expression and activity in bovine ocular lenses.

Western blots of whole tissue lysate from a microdissected bovine lens with tissue from the *central epithelium* is represented by Lane 2, the *equatorial epithelium and equatorial cortical fiber cells* by Lane 3, the *posterior lens fiber cells* are represented by Lane 4, and the *central lens fiber cells* are represented by Lane 5. Protein ladder is Lane 1. Blots were incubated with primary IgG and goat anti-rabbit-DyLight680.

A. PI3K p110α expression (*arrow*) is represented by the band at approximately 110 kDa.

B. Akt (p-Akt) expression (*arrow*) is represented by the band at approximately 58 kDa. Akt is phosphorylated at S473 by active PI3K.

C. Phosphorylated S473 Akt (p-Akt) expression (*arrow*) is represented by the band at approximately 58 kDa. Akt S473 phosphorylation is a positive marker of PI3K catalytic activity.

Basu et al 2014 discovered that organelle degradation in the embryonic chick lens is directly regulated by mTOR kinase activity[309]. Pharmacological inhibition of mTOR induces organelle degradation in treated lenses on a faster timescale than control lenses. mTOR inhibition also induces autophagy and upregulates markers of autophagic induction such as increased organelle LC3B expression and LC3B lipidation to LC3-II[314,324] which were observed in the embryonic chick lens. To test for a potential association with mTOR signaling in the bovine lens, we again conducted regional Western blot analysis in microdissected bovine lens tissue for mTOR expression (Figure 3.10A, closed arrow), mTOR S2481 phosphorylation (mTOR p2481; Figure 3.10B, closed arrow), and 40S ribosomal protein S6 Ser240/Ser244 phosphorylation (pRPS6; Figure 3.10C, closed arrow) with β-actin serving as a loading control. mTOR is activated by phosphorylation at S2481[474], and RPS6 is a substrate of active mTOR which is phosphorylated to yield pRPS6[326]. mTOR and mTOR p2481 are represented by bands at 289 kDa, and pRPS6 is represented by bands at approximately 29 kDa. mTOR and pRPS6 are expressed in the bovine lens central epithelium, equatorial epithelial and cortical fiber cells, and the posterior fiber cells. The expression of both decreases in bovine lens posterior fiber cells and is undetectable in the central fiber cells. mTOR pS2481 is faintly expressed in the bovine lens central epithelium and the equatorial epithelial and cortical fiber cells but undetectable in the posterior and central fiber cells.

A.

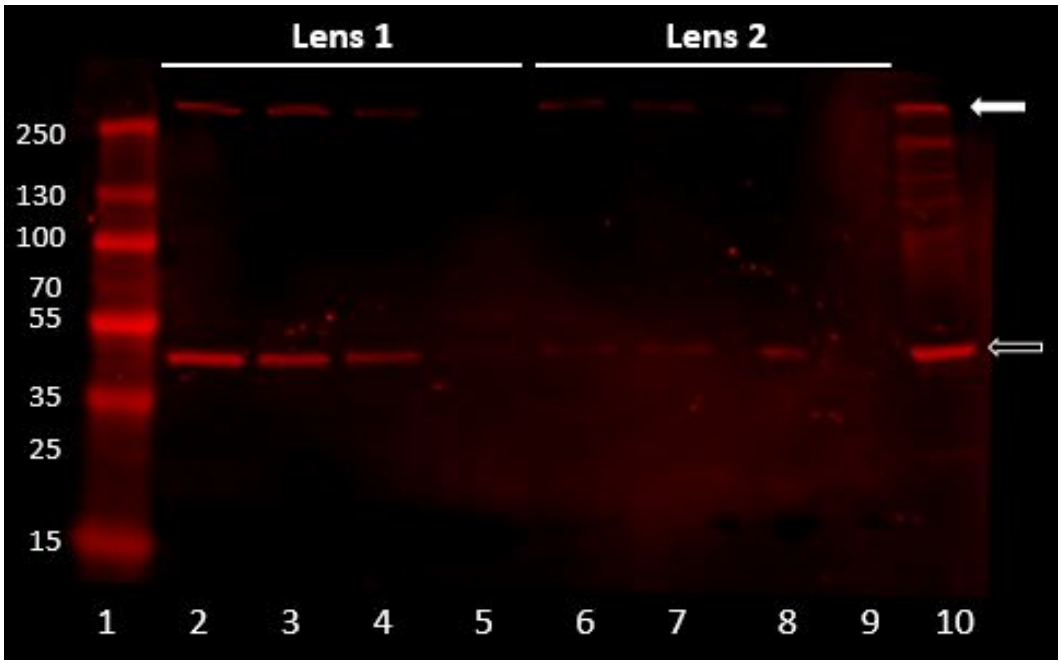

B.

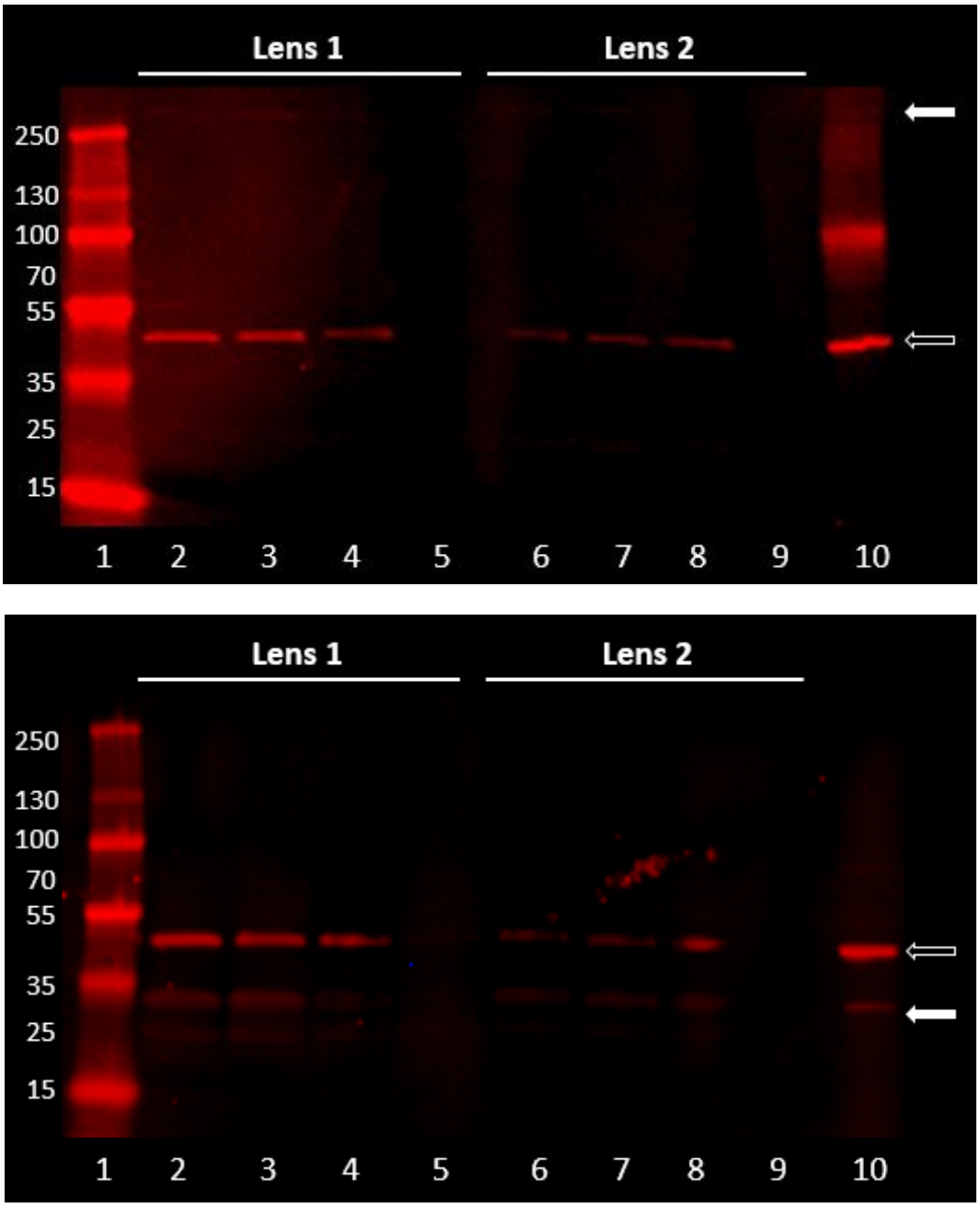

Figure 3.10. Regional mammalian target of rapamycin (mTOR) expression and activity in bovine ocular lenses.

Western blots of whole tissue lysate from two microdissected bovine lenses with tissue from Lens 1 in Lanes 2-5 and from Lens 2 in Lanes 6-9. Protein ladder is Lane 1. The *central* epithelium is represented by Lanes 2 and 6. The *equatorial epithelium and equatorial cortical fiber cells* are represented by Lanes 3 and 7. The *posterior lens fiber cells* are represented by Lanes 4 and 8. The *central lens fiber cells* are represented by Lanes 5 and 9. Blots were incubated with primary IgG and goat anti-rabbit-DyLight680. Blots were reprobed for β-actin protein expression (*open arrow*) represented by the band at approximately 42 kDa.

A. mTOR expression (*closed arrow*) is represented by the band at approximately 289 kDa. The positive control, HEK293 cell lysate, is represented by Lane 10.

B. Phosphorylated S2481 mTOR (p-mTOR) expression (*closed arrow*) is represented by the band at approximately 289 kDa. The positive control, HEK293 cell lysate, is represented by Lane 10. mTOR S2481 phosphorylation is a positive marker of mTOR catalytic activity.

C. Phosphorylated 40S ribosomal protein S6 (phospho-RPS6) expression (*closed arrow*) is represented by the band at approximately 29 kDa. Active mTOR phosphorylates RPS6 at S240 and S244. Therefore, RPS6 S240/S244 phosphorylation is a positive marker of mTOR catalytic activity. The positive control, NIH/3T3 cell lysate, is represented by Lane 10.

Autolysosomes containing mitochondria and in the process of mitophagy have been previously reported in the lens[308,363,364]. Given our observation of LC3B expression in AQP5- and TOMM20-containing cytoplasmic vesicles in bovine lens fiber cells, we hypothesized that a portion of these mitochondria would also express specific autolysosomal and lysosomal molecular markers such as lysosomal integral membrane protein 2 (LIMP-2). LIMP-2, also known as scavenger receptor class B member 2 (SCARB2), delivers β-glucocerebrosidase[475] to the lysosome and also transports cholesterol in lysosomes[476]. We analyzed TOMM20-containing cytoplasmic vesicles in bovine cortical lens fiber cells for LIMP-2 expression (Figure 3.11). In the lens modiolus, LIMP-2 expression in TOMM20-containing cytoplasmic vesicles is similar to that observed for LC3B. In peripheral outer cortical fiber cells outside of the lens modiolus, LIMP-2 expression (Figure 3.11, *striped arrows*) is also sparse and rarely overlaps TOMM20-containing cytoplasmic vesicles (Figure 3.11A, *closed arrowheads*). LIMP-2 expression in TOMM20-containing cytoplasmic vesicles also increases as a function of fiber cell differentiation. By the outer cortex-inner cortex transitional region, TOMM20-containing cytoplasmic vesicles express LIMP-2 with near ubiquity (Figures 3.11B and 3.11C). LIMP-2 expression in the lens was confirmed via tandem mass spectrometry (Figures 3.11D and 3.11E). These findings suggest that LC3B-positive autophagosomes or amphisomes merge with LIMP-2-positive lysosomes to become autolysosomes after incorporation of AQP5-containing cytoplasmic vesicles.

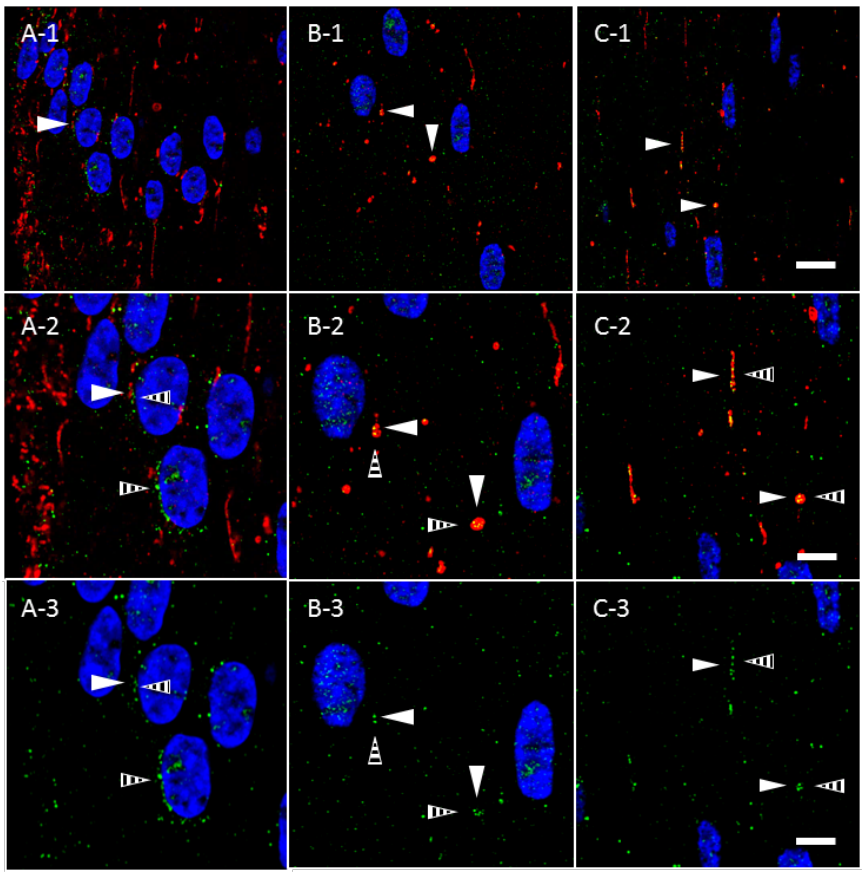
A-1
B-1
C-1
A-2
B-2
C-2
A-3
B-3
C-3

D.

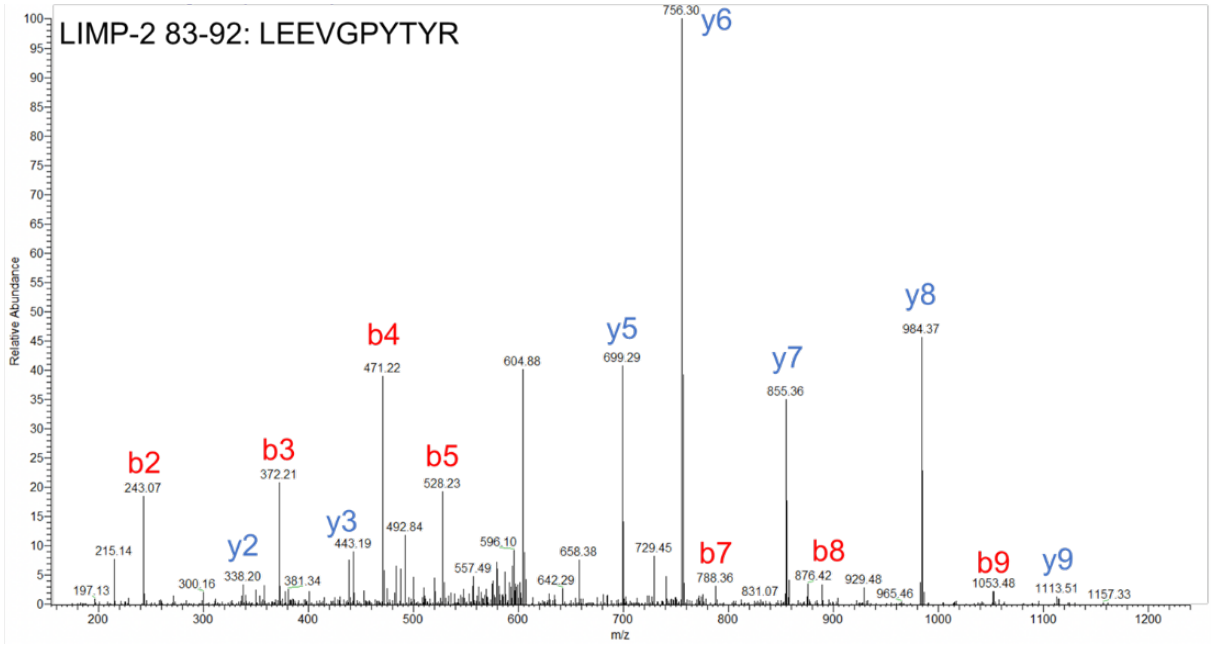
LIMP-2 83-92: LEEVGPYTYR
Relative Abundance
m/z
y6
756.30
y8
984.37
y5
699.29
b4
471.22
y7
855.36
604.88
b2
243.07
b3
372.21
b5
528.23
y3
443.19
492.84
y2
338.20
596.10
658.38
729.45
b7
788.36
b8
876.42
b9
1053.48
y9
1113.51
215.14
197.13
300.16
381.34
557.49
642.29
831.07
929.48
965.46
1157.33

E.

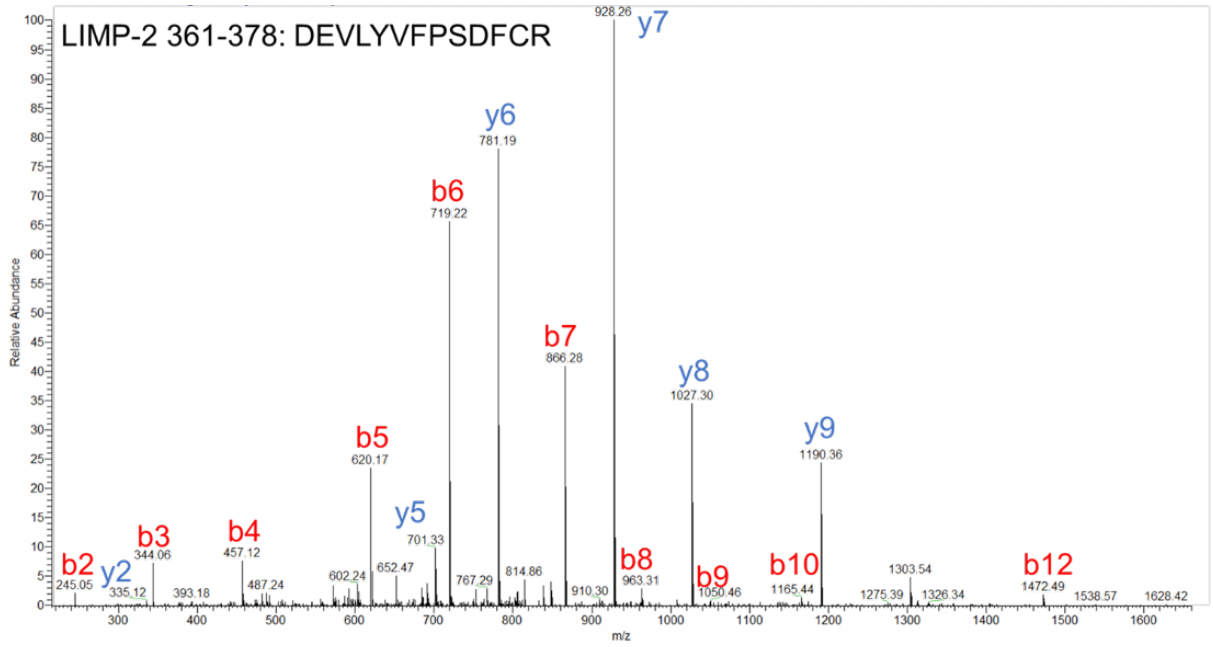

Figure 3.11. TOMM20-containing cytoplasmic vesicles express LIMP-2 prior to full AQP5 plasma membrane insertion in bovine lens cortical fiber cells.

A-1 – ***C-1*.** High-magnification confocal images of *TOMM20* immunolabeling (***red***) and *LIMP-2* immunolabeling (***green***) in the *peripheral outer cortex* (***A***), *medial outer cortex* (***B***), and *outer cortex-inner cortex transitional region* (***C***) of the bovine lens (***Figure 3.3A***).

In the peripheral outer cortex, LIMP-2 is faintly expressed (***A***) in cytoplasmic vesicles (***A***, ***B***, and ***C***; *striped arrowheads*). TOMM20-containing cytoplasmic vesicles (*closed arrowheads*) in the peripheral outer cortex partially colocalize with LIMP-2. LIMP-2 expression is upregulated with fiber cell differentiation and simultaneously increased in TOMM20-containing cytoplasmic vesicles. LIMP-2 colocalizes with the TOMM20-containing cytoplasmic vesicles in the *medial outer cortex* and the *outer cortex-inner cortex transitional region* (***B*** and ***C***).

A-2 – ***C-2*.** Enlarged images of the TOMM20-containing cytoplasmic vesicles demarcated by the *arrowheads* in ***A-1***, ***B-1***, and ***C-1***.

A-3 – ***C-3*.** Replicate images of ***A-2***, ***B-2***, and ***C-2*** with LIMP-2 immunolabeling and DAPI labeling only displayed.

Scale bars represent 10 µm (***A-1***, ***B-1***, and ***C-1***) and 5 µm (***A-2***, ***A-3***, ***B-2***, ***B-3***, ***C-2***, and ***C-3***).

***D*.** High mass resolution CID spectrum of doubly-charged LIMP-2 peptide 82-93, m/z 824.16, acquired on a Thermo Fisher Velos Pro linear ion trap. The observed mass corresponds to one carbamidomethylated cysteine residue on the peptide (b12, y2). The peptide amino acid sequence is included above.

E. High mass resolution CID spectrum of doubly-charged LIMP-2 peptide 361-378, m/z 824.16, acquired on a Thermo Fisher Velos Pro linear ion trap. The observed mass corresponds to one carbamidomethylated cysteine residue on the peptide (b12, y2). The peptide amino acid sequence is included above.

Given these results, we hypothesized that transmission electron microscopy (TEM) of bovine lens cortical fiber cells would reveal vesicular structures with similar morphology and subcellular localization to AQP5-containing cytoplasmic vesicles. Immunofluorescence analysis of bovine lens cryosections revealed spheroidal, tubular AQP5-containing cytoplasmic vesicles are often in close proximity or apposed to cortical fiber cell plasma membranes (Figure 3.12A-1, *arrowheads*) or cellular nuclei (Figure 3.12A-2, *arrowheads*) in the bovine lens. TEM analysis revealed vesicular structures in close proximity and apposed to bovine cortical fiber cell plasma membranes (Figures 3.12B-1 and 3.12B-4, *arrows*) and cellular nuclei (Figures 3.12B-2, 3.12B-3, 3.12B-5, and 3.12B-6, *arrows*). These structures appear to have spheroidal morphology similar to AQP5-containing cytoplasmic vesicles. In the TEM images, vesicular structures are often observed proximal to cytoplasmic structures with *apparent* tubular morphology (Figures 3.12B-4 and 3.12B-5, *arrowheads*). In some cases, vesicular structures of interest *appear* to be comprised of mitochondria (Figure 3.12B-6; *arrowhead*). The vesicular structures of interest in our TEM images typically contain multiple complex membrane patterns which are characteristic of autophagic vesicles such as autophagosomes, amphisomes, and autolysosomes. However, the morphology of these vesicular organelles does not unequivocally identify potential autophagic vesicles and proximal tubular vesicles. Our results suggest that these vesicular structures detected in our TEM analysis are likely synonymous with AQP5-containing cytoplasmic vesicles detected in our immunofluorescence analysis based on subcellular localization and apparent morphology in the bovine lens cortex.

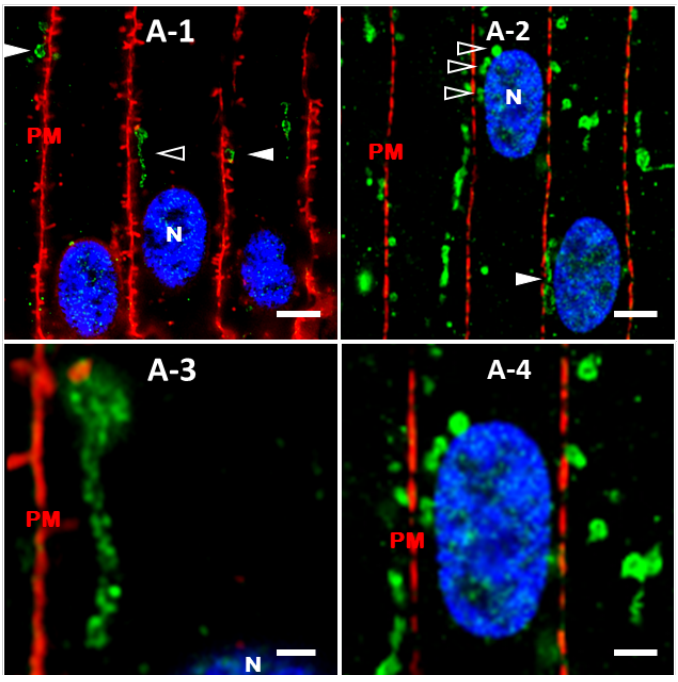

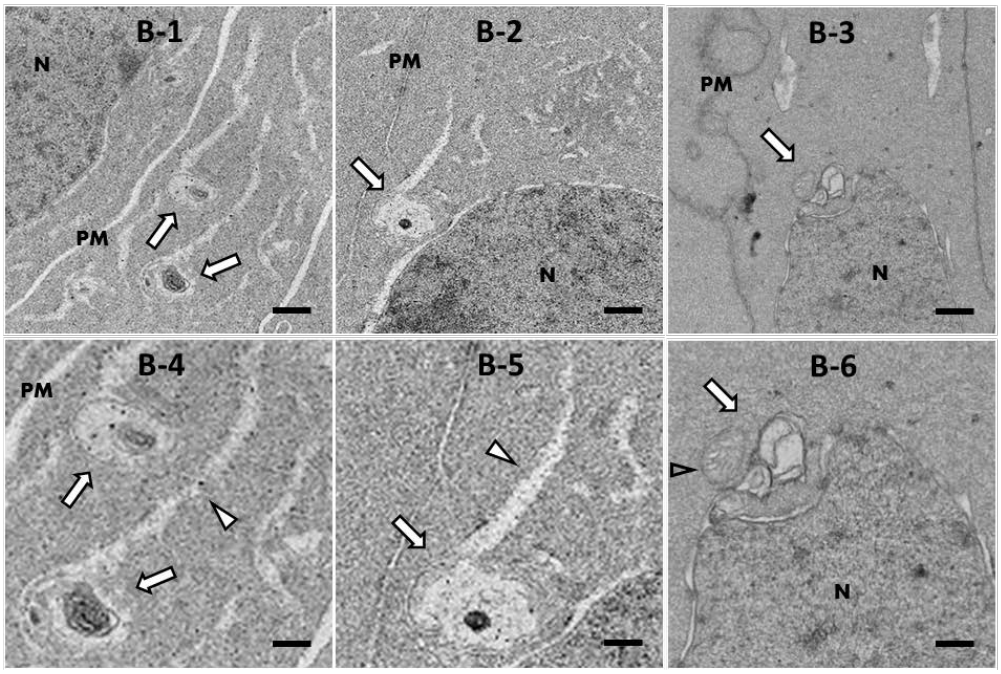

Figure 3.12. AQP5-containing cytoplasmic vesicles are congruent in subcellular localization with vesicular structures identified via TEM analysis in bovine lens cortical fiber cells.

A*.** High resolution, confocal images of AQP5 immunofluorescence (green***) in the medial outer cortex of the bovine lens. *Plasma membranes* (**PM**) are labeled with WGA (red) (***A-1***) or connexin-50 (red) (***A-2***). *Cellular nuclei* (**N**) are labeled with DAPI staining (***blue***), respectively. AQP5-containing cytoplasmic vesicles (*arrowheads*) are distinctive amongst fiber cell cytoplasmic vesicles in the bovine lens outer cortex (***Figure 3.4***). AQP5-containing cytoplasmic vesicles are frequently in close proximity or apposed to fiber cell plasma membranes (***A-1***) and cellular nuclei (***A-2***). The structures demarcated with *open arrowheads* in ***A-1*** and ***A-2*** are enlarged and shown in ***A-3*** and ***A-4***, respectively. The scale bars represent 5 µm (**A-1** and **A-2**) and 2.5 µm (**A-3** and **A-4**).

B*.** Transmission electron microscopy (TEM) images of a vesicular structures of interest (*arrows*) in outer cortical fiber cells of the bovine lens in close proximity or apposed to the plasma membrane (B-1*** and ***B-4***) or cellular nuclei (***B-2***, ***B-3***, ***B-5***, and ***B-6***). These vesicular structures were roughly spheroidal in morphology, similar to AQP5-containing cytoplasmic vesicles and often in close proximity to cytoplasmic structures which *appear* tubular in morphology (***B-4*** and ***B-5***, *arrowheads*). At times, vesicular structures of interest appear to be comprised of mitochondria (***B-6***, *arrowhead*). The structures demarcated with *arrows* in ***B-1***, ***B-2***, and ***B-3*** are enlarged and shown in ***B-4***, ***B-5***, and ***B-6***, respectively. The scale bars represent 500 nm (***B-1***, ***B-2***, and ***B-3***) and 250 nm (***B-4***, ***B-5***, and ***B-6***).

AQP5 Vesicle-Plasma Membrane Localization

Further analysis of TEM images in the outer cortex shows vesicular structures with complex membrane morphology in very close proximity to the plasma membrane (Figure 3.13). We regularly observed AQP5-containing cytoplasmic vesicles which appear to be docked with the plasma membrane in the medial outer cortex prior to AQP5 plasma membrane insertion

(Figures 3.13A-1, 3.13A-2, and 3.13A-3; *arrowheads*). In the outer cortex-inner cortex transitional region, similar AQP5-containing cytoplasmic vesicles appear to be docked to the plasma membrane (Figures 3.13A-4, 3.13A-5, and 3.13A-6; *arrowheads*) where AQP5 insertion occurs. AQP5 signal occurs in the plasma membrane between strong Cx50 signals with some colocalization observed (Figures 3.13A-5 and 3.13A-6; *arrows*). In turn, we observed vesicular structures in close contact with the plasma membrane in bovine lens cortical fiber cells from the same regions (Figure 3.13B-1, *striped arrow*). The overlap of the AQP5 immunofluorescence with the Cx50 along with the close proximity of the vesicles to the plasma membrane in TEM suggests that these vesicles are docked or are even in the process of fusing with plasma membrane. Higher resolution studies are required to conclusively show docking and fusion processes.

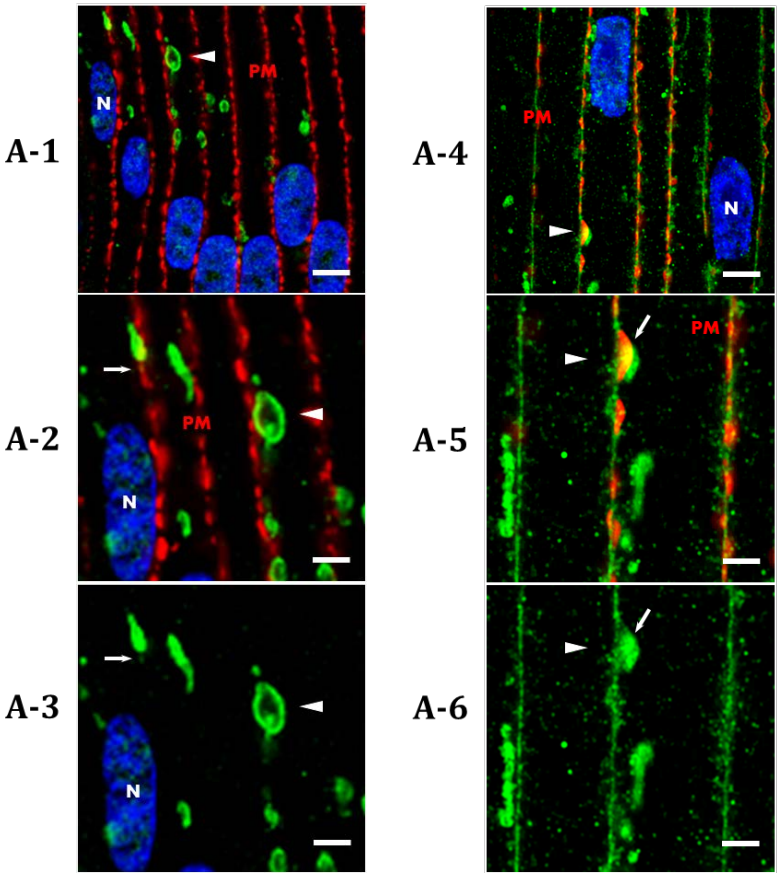

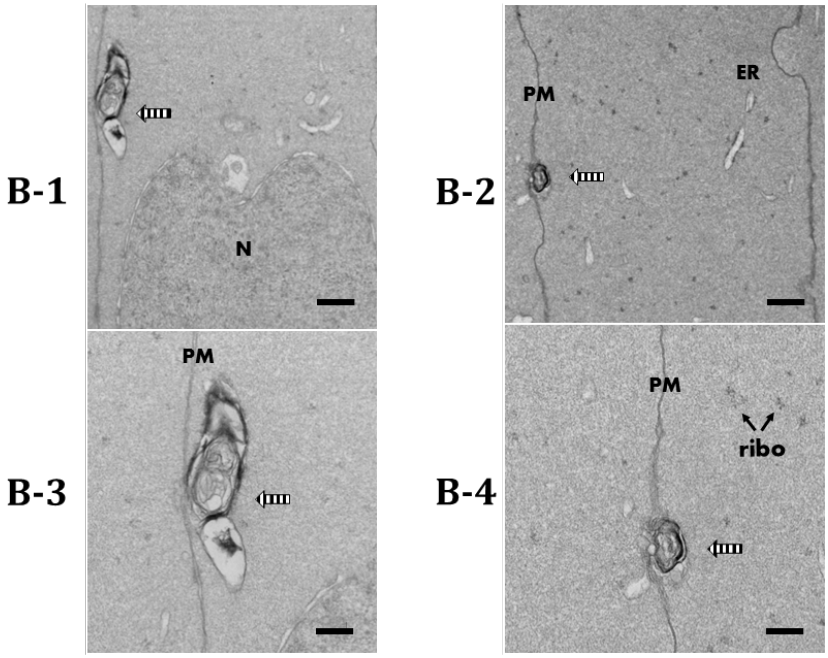

Figure 3.13. AQP5-containing cytoplasmic vesicles and vesicular structures identified via TEM analysis exhibit *potential* docking behavior in bovine lens cortical fiber cells.

A. High resolution, confocal images of AQP5 immunofluorescence (***green***) in the *medial outer cortex* (***A-1***, ***A-2***, ***A-3***) and *outer cortex-inner cortex transitional region* (***A-4***, ***A-5***, ***A-6***) of the bovine lens. *Plasma membranes* (**PM**) are labeled with connexin-50. *Cellular nuclei* (**N**) are labeled with DAPI staining (***blue***), respectively. AQP5-containing cytoplasmic vesicles (*arrowheads*) appear in close apposition to and exhibit *potential* docking with fiber cell plasma membranes in the *medial outer cortex* (***A-1***). Docking of AQP5-containing cytoplasmic vesicles in the *outer cortex-inner cortex transitional region* (***A-4***) is expected to result in vesicular fusion since full AQP5 plasma membrane insertion occurs prior to the *inner cortex* (**Figure 3.2**). AQP5-containing cytoplasmic vesicles demarcated with *arrowheads* in ***A-1*** and ***A-4*** are enlarged and shown in ***A-2*** and ***A-3*** and in ***A-5*** and ***A-6***, respectively. AQP5 plasma membrane insertion is denoted by the *arrows* in ***A-2***, ***A-3***, ***A-5***, and ***A-6***. The scale bars represent 5 µm (***A-1*** and ***A-4***) and 2.5 µm (***A-2***, ***A-3***, ***A-5***, ***A-6***).

B. Transmission electron microscopy (TEM) images of vesicular structures of interest (*striped arrows*) in the bovine lens outer cortex exhibit *potential* docking (***B-1***, ***B-2***, ***B-3***, and ***B-4***) to the fiber cell plasma membrane. The vesicular structures in ***B-1*** and ***B-3*** are enlarged and shown in ***B-2*** and ***B-4***, respectively. These structures are congruent with AQP5-containing cytoplasmic vesicle in subcellular localization. The *endoplasmic reticulum* (**ER**) and *ribosomes* (**ribo**) are also visible. The scale bars represent 500 nm (***B-1*** and ***B-2***) and 250 nm (***B-3*** and ***B-4***).

Together, these data support a mechanism of AQP5 plasma membrane insertion through unconventional protein secretion (UPS)[378,379] in bovine lens cortical fiber cells – via protein targeting to autophagosomes, amphisomes, or lysosomes predestined for fusion with the

plasma membrane. These processes, "autophagosome secretion"[380,477,478], "amphisome secretion"[391,445], and "lysosome secretion"[381,391,479] respectively, are discrete mechanisms of secretion with unique molecular machineries. Secretory autophagosomes, but not degradative autophagosomes, specifically express the SNARE protein vesicle-trafficking protein SEC22β (Sec22β)[377,391]. We found TOMM20-containing mitochondria, the signals of which overlap almost entirely with AQP5-containing cytoplasmic vesicles (Figure 3.5), lacked apparent Sec22β expression (Figure 3.14).

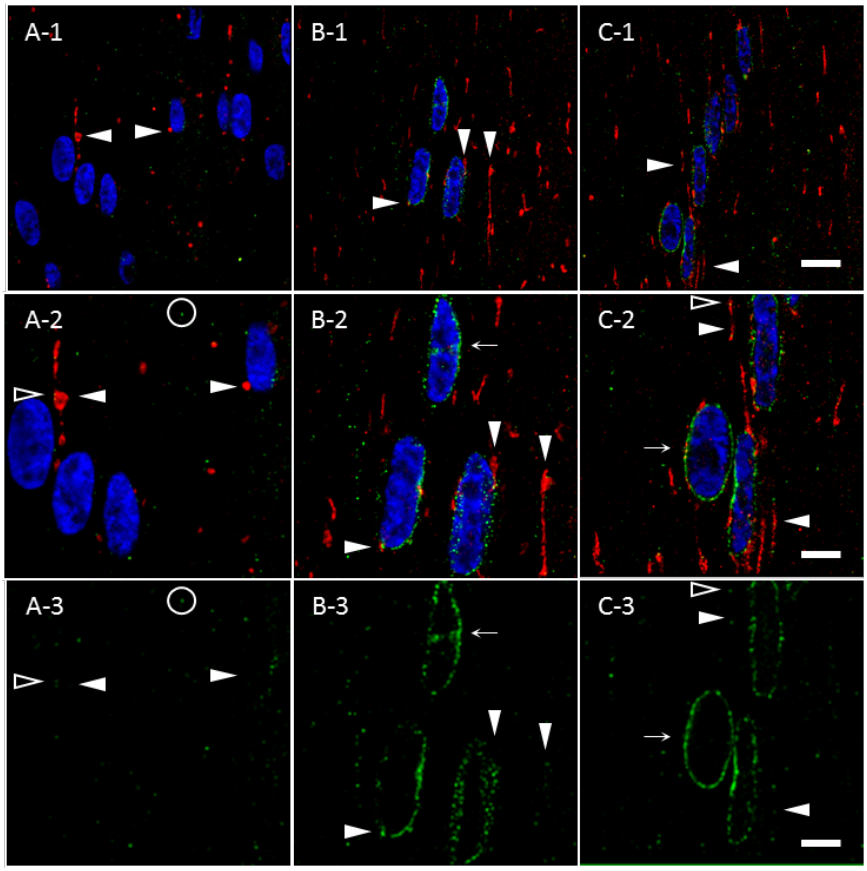

Figure 3.14. TOMM20-containing cytoplasmic vesicles lack significant Sec22β expression in bovine lens cortical fiber cells.

A-1 – ***C-1*.** High-magnification images of *Sec22β* immunolabeling (***green***) and *TOMM20* immunolabeling (***red***) in the *peripheral outer cortex* (**A**), *medial outer cortex* (**B**), and *outer cortex-inner cortex transitional region* (**C**) as demarcated in **Figure 3A**.

TOMM20-containing cytoplasmic vesicles (**closed arrowheads**) are expressed throughout the outer cortex. Initial *Sec22β* expression in the *peripheral outer cortex* (**A**) is weak but strengthens within the *medial outer cortex* (**B**) and remains consistent within the rest of the outer cortex in **C**. Throughout the outer cortex, *Sec22β* is initially expressed within diffuse, punctate cytoplasmic vesicles (**A**, *hollow circle*) that tangibly but insignificantly colocalize with TOMM20-containing cytoplasmic vesicles (***A-2***, ***A-3***, ***C-2***, and ***C-3***; *open arrowheads*). Excluding the

lens modiolus, *Sec22β* is also ubiquitously expressed within the cellular nucleus-contiguous rough endoplasmic reticulum (***B-2***, ***B-3***, ***C-2***, and ***C-3***; *closed arrows*).

A-2 – ***C-2*****.** Enlarged images of the TOMM20-containing cytoplasmic vesicles demarcated by arrowheads in ***A-1***, ***B-2,*** and ***C-1***.

A-3 – ***C-3*****.** Replicate images of ***A-2*** – ***C-2*** depicting *Sec22β* immunolabeling and DAPI labeling only.

Scale bars denote 10 µm (***A-1*** – ***C-1***) and 5 µm (***A-2 – C-2*** and ***A-3 – C-3***).

The absence of Sec22β co-labeling with TOMM20-containing mitochondria in combination with our TEM analyses suggests that AQP5-containing cytoplasmic vesicles become LC3B-containing autophagosomes or amphisomes that fuse with lysosomes that then undergo lysosome secretion in the outer cortex-inner cortex transitional region. To test this hypothesis, we examined AQP5 plasma membrane expression in *ex vivo* cultured bovine lenses treated with 10 nM bafilomycin A1 for 24 hours to inhibit autophagosome-lysosome fusion and thereby reduce lysosome secretion (Figure 3.15). Following *ex vivo* lens culture, AQP5 expression is still detected in the bovine lens cortex (Figures 3.15A-C). Relative AQP5 expression, that is mean fluorescence intensity of AQP5 with bafilomycin A1 treatment relative to vehicle control, was quantified in fiber cell plasma membranes in the bovine lens *medial outer cortex* and *outer cortex-inner cortex transitional region* (Figure 3.15D). Confocal microscopy imaging parameters used to acquire *ex vivo* cultured bovine lens data were kept consistent for quantitative comparison. Despite sample variation, there was no significant difference in relative AQP5 expression in fiber cell plasma membranes of the *medial outer cortex*. In contrast, relative AQP5 fiber cell plasma membrane expression in the *outer cortex-inner cortex transitional region*, where full insertion of AQP5-containing cytoplasmic vesicles with fiber cell plasma membrane occurs, was decreased by approximately 27%. These results are consistent with our hypothesis of AQP5 lysosome secretion in the bovine lens.

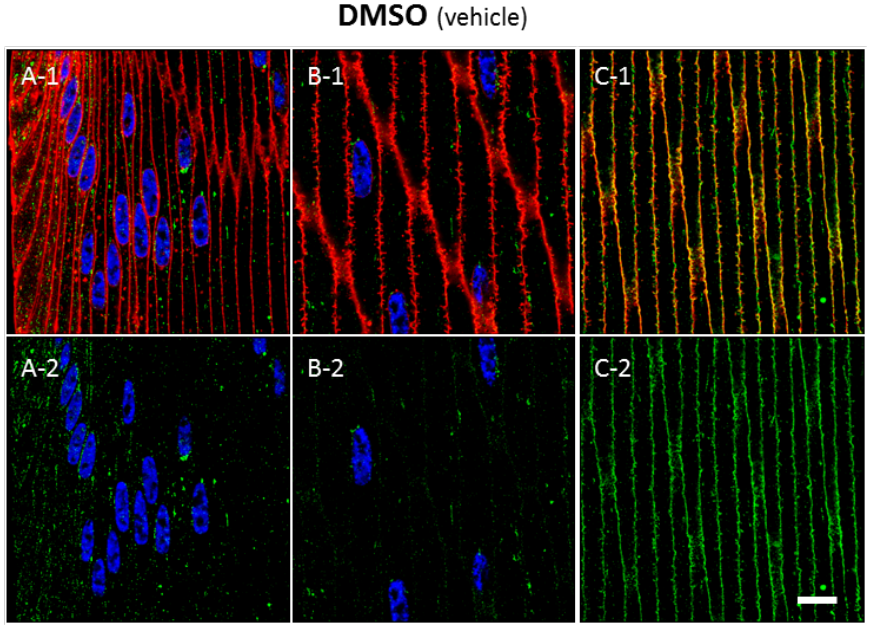

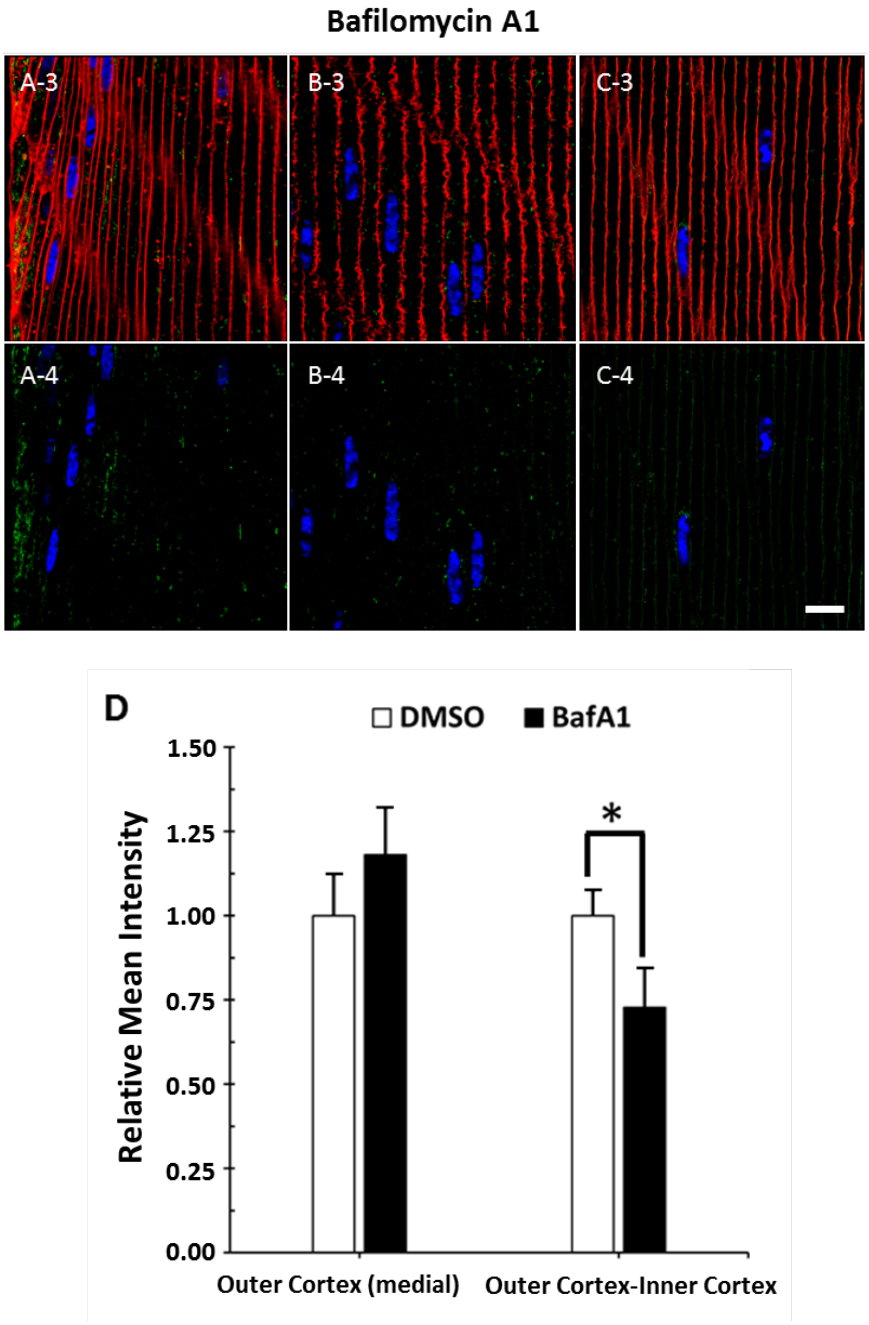

Figure 3.15. Autophagosome-lysosome fusion inhibition via bafilomycin A1 treatment decreases AQP5 plasma membrane expression in the bovine lens cortex.

A-1 – ***C-1*****.** High-magnification confocal images of *AQP5* immunolabeling (***green***) and *WGA* labeling (***red***) in the *peripheral outer cortex* (***A***), *medial outer cortex* (***B***), and *outer cortex-inner cortex transitional region* (***C***) of the bovine lens following 24 hours *ex vivo* culture in complete M199 medium with vehicle (0.1% DMSO) (***Figure 3.3A***).

A-2 – ***C-2*****.** Replicate images of ***A-1***, ***B-1***, and ***C-1*** with AQP5 immunolabeling and DAPI labeling only displayed.

A-3 – ***C-3*****.** High-magnification confocal images of *AQP5* immunolabeling (***green***) and *WGA* labeling (***red***) in the *peripheral outer cortex* (***A***), *medial outer cortex* (***B***), and *outer cortex-inner cortex transitional region* (***C***) of the bovine lens following 24 hours *ex vivo* culture with 10 nM bafilomycin A1 (***Figure 3.3A***).

A-4 – ***C-4*****.** Replicate images of ***A-3***, ***B-3***, and ***C-3*** with AQP5 immunolabeling and DAPI labeling only displayed.

Scale bars represent 10 µm (***A***, ***B***, and ***C***)

D**.** Quantification and statistical analysis of the relative AQP5 expression, defined as relative mean intensity, in fiber cells of the *medial outer cortex* and *outer cortex-inner cortex transitional region* of bovine lens cryosections following 24 hours *ex vivo* culture with vehicle control 0.1% DMSO (DMSO, n = 7) or with 10 nM bafilomycin A1 (BafA1, n = 8). Two-tailed Student's t-test was significant (*) a *p*-value of 0.032.

3.4 Discussion

The goals of this study were to determine how bovine lenticular AQP5 expression patterns compare to other mammalian lenses, to determine the subcellular localization of AQP5-containing cytoplasmic vesicles, and to identify potential trafficking mechanisms of AQP5-containing cytoplasmic vesicles to the plasma membrane. In this study, we reveal that bovine lens AQP5 expression patterns are similar to that of other mammalian lenses, being cytoplasmic in lens epithelial cells and young, differentiating lens fiber then shifting to lens fiber cell plasma membranes with cellular maturation. We have also for the first time defined AQP5 subcellular localization in ocular lens cortical fiber cells in detail and discovered that cytoplasmic AQP5 trafficks to the plasma membrane in these cells via lysosome secretion, a novel mechanism of aquaporin trafficking.

AQP5 spatial expression has previously been investigated in mouse[45,46,111,168], rat[46,111], rabbit[40], and human[46] lenses. While Grey et al., 2013 validated AQP5 expression in bovine lenses via Western blot analysis[46], this study represents the first histological study of AQP5 spatial expression in the bovine lens. AQP5 is ubiquitously expressed throughout the bovine lens; being cytoplasmic in epithelial and fiber cells and gradually trafficking to plasma membrane during fiber cell differentiation (Figure 1). This spatial expression pattern is consistent with previously studied lenses and further suggests that this general expression pattern is characteristic of AQP5 expression in all mammalian lenses. In bovine lenses we measured AQP5 plasma membrane insertion to occur at a normalized r/a value of 0.958 (Figure 3.2). Grey et al 2013 defined this value in mouse and rat lenses as *r/a* 0.95 and *r/a*~ 0.75 to ~0.65, respectively[46]. This equivalence suggests similarity in regulation of AQP5 plasma membrane insertion in mouse and bovine lenses relative to rat lenses, but the implications of these values remain to be investigated. AQP5 expression in differentiating bovine outer cortical fiber cell nuclei becomes apparent as fiber cells exit the lens modiolus (Figures 1C-1D) and disappears as AQP5 trafficks to the plasma membrane (Figures 1E-1F). Cho et al., in 2015, demonstrated that AQP5 trafficks to the nucleus in rat parotid gland cells following treatment with the muscarinic acetylcholine receptor agonist cevimeline resulting in reduction in the size of cellular nuclei and a change in the morphology of cellular nuclei from smooth and circular to rough and irregular[426]. We speculate that nuclear localization of AQP5 in the bovine lens outer

cortex may play a role in shrinkage of fiber cell nuclei and change in their morphology from smooth to irregular during cellular differentiation as occurs in the inner cortex (Figures 3.1E-1F). We seek to test this hypothesis in future studies.

This is also the first study to characterize AQP5-containing cytoplasmic vesicles in a mammalian lens for intrinsic properties such as morphology or molecular composition. The presence of micrometer-scale tubular and spheroidal, tubular AQP5-containing cytoplasmic compartments (Figure 3.3) is a novel finding in cortical lens fiber cells. Within bovine cortical lens fiber cells, AQP5-containing cytoplasmic vesicles are also morphologically distinct (Figures 3.4A-3 and 3.4A-4) which enables their identification via downstream TEM analysis.

Molecular analysis revealed that AQP5-containing cytoplasmic vesicles and mitochondria are nearly indistinguishable cytoplasmic compartments in bovine lens cortical fiber cells. TOMM20 (Figure 3.5), a protein subunit within the translocase of the outer mitochondrial membrane, and cytochrome c oxidase IV (COX IV) (Figure 3.6), a mitochondrial marker protein in the electron transport chain, both colocalize to AQP5-containing cytoplasmic vesicles in bovine lens cortical fiber cells, indicating that AQP5 is either incorporated into mitochondria or into mitochondria-containing cytoplasmic vesicles. TEM analysis in bovine lens cortical fiber cells revealed vesicular structures with complex membranes potentially indicative of autophagic vesicles. These vesicular structures exhibited similar subcellular localization to AQP5-containing cytoplasmic vesicles (Figure 3.12), which is congruent with incorporation of AQP5-containing cytoplasmic vesicles into autophagosomes and possibly amphisomes and then finally into autolysosomes. These data are consistent with TEM analysis of fiber cells in human and embryonic chick lenses conducted by Costello et al., 2013 in which mitochondria are incorporated into autolysosomes[308]. Calnexin immunofluorescence analysis suggested that AQP5-containing cytoplasmic vesicles are not endoplasmic reticular compartments (Figure 3.7).

Mitochondria undergo autophagic degradation to generate an organelle-free zone (OFZ) in the lens to prevent light scatter[308]. TOMM20 colocalizes with LC3B, a specific protein marker of autophagosomes and amphisomes, in the embryonic chick lens prior to mitochondrial degradation. Immunofluorescence analysis revealed LC3B colocalization with TOMM20 in bovine lens cortical fiber cells (Figure 3.8) that peaks within the outer cortex-inner cortex transitional region. LIMP-2 is a β-glucocerebrosidase receptor and specific protein marker of lysosomes[475] and colocalization of LIMP-2 with TOMM20 (Figure 3.11), similar to LC3B, indicates lysosomal involvement in mitochondrial degradation. This finding is in agreement with previous data that show LC3B expression peaks and autolysosomes are abundant in the outer cortex-inner cortex transitional region in mice just prior to mitochondrial elimination to form the OFZ[363,364,480].TOMM20 and LC3B immunolabeling fade to become undetectable in mature fiber cells. AQP5 also is fully inserted into bovine lens fiber cell plasma membranes the outer cortex-inner cortex transitional region. The disappearance of TOMM20 and LC3B immunolabeling indicates that mitochondria are incorporated into autophagosomes that merge with lysosomes via an amphisome intermediate to become autolysosomes and degrade mitochondria, consistent with the conservation of mitochondrial autophagy in the lens across species. Genetic deletion studies suggest that lenticular mitochondrial autophagy is specific and technically mitophagy in the mouse lens[310]. This possibility remains to be tested in the bovine lens. Nevertheless, our data suggest that AQP5 undergoes unconventional protein secretion via autolysosomes in manner similar to the thrombopoietin receptor (Mpl)[401]. The amphisome intermediate required for autolysosome formation remains to be identified histologically, and direct amphisome secretion via this amphisome intermediate in a manner similar to glycophorin A[481] remains a potential additional mechanism of AQP5-containing cytoplasmic vesicle secretion.

mTOR activity is inversely correlated with autophagic induction[314], and the PI3K/Akt/mTOR pathway is implicated in autophagic organelle degradation in the embryonic chick lens[309,311,482]. Pharmacological inhibition of *ex vivo* cultured lenses with either PI3K or

mTOR antagonists induces organelle degradation on a faster timescale than in vehicle-treated control lenses. Western blot analysis of the PI3K/Akt/mTOR signaling pathway in the bovine lens demonstrates expression of each protein in the epithelial cells and the fiber cell mass excluding the central fiber cells (Figures 3.9 and 3.10). The relative expression of each and phosphorylation of Akt S473, mTOR S2481, and RPS6 S240 and S244, which are markers of PI3K/Akt/mTOR signaling pathway activation, decrease with fiber cell maturation. While additional work is needed to confirm direct association between PI3K/Akt/mTOR pathway signaling with AQP5-containing, TOMM20-containing cytoplasmic vesicles, our results are consistent with previous studies and suggest this signaling pathway in the regulation of AQP5 subcellular localization in the bovine lens.

The persistence of AQP5 immunolabeling despite mitochondrial degradation and AQP5 plasma membrane insertion implies that AQP5-containing cytoplasmic vesicles are trafficked to the plasma membrane through the unconventional protein secretion pathway of lysosome secretion[381]. Immunofluorescence and TEM analysis respectively show that AQP5-containing cytoplasmic structures and vesicular structures with complex membrane morphologies exhibit potential docking behavior with fiber cell plasma membranes in the medial outer and cortex-inner cortex transitional region where AQP5 plasma membrane insertion primarily occurs (Figure 3.13). Thus, our results are consistent with unconventional protein secretion of autolysosomes, although electron tomography is needed to unequivocally identify fusion processes and potential mitochondria and autophagic vesicles (i.e. autophagosomes, amphisomes, and autolysosomes) in our TEM data. Nevertheless, this is the first study to report autolysosome secretion as potential trafficking mechanism of plasma membrane insertion for AQP5, for aquaporins as a protein family in any tissue, and for any protein in lens fiber cells. The absence of Sec22β colocalization with TOMM20 (Figure 3.14) indicates that mitochondria, and therefore AQP5, are not incorporated into secretory autophagosomes and that AQP5-containing cytoplasmic vesicles undergo autolysosome secretion and potentially amphisome secretion as well. Autophagosome secretion, amphisome secretion, and lysosome secretion are classified as Type III unconventional protein secretion mechanisms[378,391]. Thus, while mitochondrial degradation through autophagy in bovine lens cortical fiber cells is consistent with other mammalian lenses, our data suggest that AQP5 is uniquely trafficked in bovine lenses through secretory autolysosomes via LC3B-containing autophagosomes. Results from bafilomycin A1 treatment of *ex vivo* lens cultured bovine lenses support this hypothesis (Figure 3.15). Upon treatment, relative AQP5 fiber cell plasma membrane expression in bovine lenses decreases by approximately 27% in the *outer cortex-inner cortex transitional region*, where AQP5 plasma membrane insertion primarily occurs (Figure 3.15D). This is consistent with bafilomycin A1 inhibition of autophagosome-lysosome fusion and suggests an accumulation of AQP5-containing autophagosomes unable to mature into autolysosomes for secretion.

Results from bafilomycin A1 treatment also provide further evidence that AQP5 functions as a regulatory water channel whose trafficking is inducible in the mammalian lens. Petrova et al has previously demonstrated dynamic AQP5 subcellular localization changes in response to changes in zonular tension via mechanosensitive TRPV1 channel agonism[111,116]. Since AQP5 plasma membrane insertion significantly increases fiber cell water permeability in both mouse and rat lenses[111], regulation of AQP5 subcellular localization can alter lens water homeostasis. Whether regulation of AQP5 subcellular localization via TRPV1 channels involves lysosome secretion remains to be investigated.

In non-lenticular tissues, cytoplasmic AQP5 undergoes regulated secretion to the plasma membrane in the salivary glands and in model cell systems upon M_3 muscarinic acetylcholine receptor (AChR) activation[423,424], β-adrenergic receptor activation[45,402,483], TRPV4 activation[186,430], and osmotic perturbation[186,430]. Downstream signal transduction effectors of these activators such as nitric oxide, protein kinase G, protein kinase A (PKA) activity, and calcium have all been implicated in the alteration of AQP5 plasma membrane trafficking. To our

knowledge, this is the first study to characterize the subcellular localization of cytoplasmic AQP5 vesicles targeted to the plasma membrane for regulated secretion. Our results demonstrate a novel mechanism of cytoplasmic AQP5 trafficking to the plasma membrane. The effects of nonlenticular effector proteins such as the β-adrenergic receptors or corresponding downstream effectors such as PKA on AQP5 plasma membrane trafficking in the lens remain to be investigated.

In addition to the novel trafficking mechanism elucidated in this study, our results demonstrate possible AQP5 expression in viable mitochondria, which, if confirmed, along with aquaporin-8 (AQP8)[119] and aquaporin-9 (AQP9)[484] would represent the third aquaporin discovered in mitochondria. These results raise a variety of questions about the conservation of this AQP5 unconventional protein secretion across mammalian lenses and the implications of AQP5 in active mitochondria. Mitochondrial AQP8 and AQP9 function as peroxiporins and thereby resist accumulation of the reactive oxygen species (ROS) H_2O_2, a byproduct of aerobic respiration which is detrimental to proper mitochondrial function[485–488]. AQP8 is expressed in the lens epithelial cells and exhibits peroxiporin function *in vitro* in cultured human lens epithelial cells (HLEs)[48,49]. AQP5 also functions as a peroxiporin facilitating H_2O_2 transport in transfected cells[49,489] and in the lens with wild type mouse lenses containing significantly more H_2O_2 content relative to AQP5 knockout mouse lenses[49]. Of note is the reported crosstalk between autophagy and oxidative stress[490] in which H_2O_2 blocks the progression of autophagy via reversibly inhibition of ATG4[491]. Thus, AQP5 peroxiporin function is a plausible role for AQP5 incorporation into mitochondria and autophagic vesicles in the bovine lens fiber cells, and it is reasonable to conjecture potential roles for AQP5 in regulating mitochondrial viability and autophagic induction in the bovine lens. Future studies should address these and other relevant exciting questions both in the mammalian lens and in other tissues expressing AQP5.

3.5 Conclusions

In summary, bovine lenticular AQP5 expression patterns are similar to AQP5 expression patterns in other mammalian lenses being cytoplasmic in the epithelial cells and young fiber cells then gradually trafficking to the plasma the plasma membrane during fiber cell differentiation. In outer cortical bovine lens fiber cells, cytoplasmically expressed AQP5 is first associated with TOMM20-positive mitochondria and thereafter localized to LC3B-positive autophagosomes that merge with lysosomes to become LIMP-2-positive autolysosomes. PI3K/Akt/mTOR signaling pathway protein expression and activity decrease with fiber cell maturation consistent with a potential role of this signaling pathway in regulation of autophagic induction and AQP5 subcellular localization in the bovine lens. Based on the loss of TOMM20 and COX IV immunofluorescence and incorporation of AQP5 into the plasma membrane, these autolysosomes likely degrade mitochondria in differentiating lens fiber cells and appear to undergo plasma membrane fusion through a process of autolysosome secretion and potentially amphisome secretion. AQP5 trafficking to the plasma membrane is bafilomycin A1-sensitive indicating the importance of autophagosome-lysosome fusion for AQP5 plasma membrane insertion in the bovine lens.

CHAPTER IV. Aquaporin-5 Interacting Proteins and T259 Phosphorylation in the Bovine Lens

4.1 Introduction

Aquaporins (AQPs) are a family of transmembrane channels that enable diffusion of water down cellular osmotic gradients and thereby regulate osmotic homeostasis in a wide variety of tissues such as the ocular lens[56,492]. The lens is comprised of a monolayer of epithelial cells which differentiate into postmitotic lens fiber cells comprise 99% of the lens bulk. Nascent cortical fiber cells differentiate from epithelial cells into mature nuclear fiber cells through a process of broad changes in protein expression and cellular morphology.

Osmotic homeostasis is the lens is critical for lenticular transparency and lens fiber cells, which comprise the bulk of lens tissue, express aquaporin-0 (AQP0) and aquaporin-5 (AQP5), to regulate lens water content[58,110]. In addition to its water transport role in the lens, AQP0 also functions as an important structural protein via its interactions with filensin[493], phakinin[493], and ezrin[494] and as a cell junctional protein via AQP0-AQP0 tetramer-tetramer interactions[59] in the lens. The role of AQP0 as a structural and junctional protein is distinct from its role as a water channel as fiber cell morphology abnormalities and cataractogenesis cannot be fully rescued with transgenic expression of AQP1 in AQP0-null mice[64,65].

The C-terminus is the primary binding site of AQP interacting proteins[149] and the binding site for AQP0 protein-protein interactions (REFS). Similarly, AQP5 interacts *in vitro* with cell junctional proteins: tight junction protein ZO-1, plakoglobin, β-catenin, and desmoglein-2[154] via its C-terminus in Madin-Darby canine kidney (MDCK) cells. AQP5 interaction with these proteins reduces their expression which attributes structural protein function to AQP5 and a specific role in cell junction formation. Additionally, AQP5 interacts via its C-terminus, in human minor salivary glands (MSGs), with another structural protein ezrin[435], a member of the ezrin/radixin/moesin (ERM) protein family which links actin filaments to the plasma membranes[433,434]. AQP5 protein-protein interactions are also implicated in its subcellular localization which affects its role in water transport. In MSGs of Sjögren's syndrome patients, AQP5 subcellular localization is altered and AQP5 fails to properly traffick to the plasma membrane[411,414]. Interaction with ezrin may affect subcellular localization as AQP5–ezrin complexes in human MSGs were absent in apical regions or mislocalized to the basolateral acini[435]. AQP5 interacts via its C-terminus with prolactin-inducible protein (PIP) in lacrimal and salivary glands which appears to affect its subcellular localization within the plasma membrane[422,436]. In mouse lacrimal glands, AQP5 interaction with major urinary protein (Mup4) instead of PIP in the NOD mouse, a model of Sjögren's syndrome, results in retention of AQP5 within the cytoplasm rather than plasma membrane subcellular localization[422].

The AQP C-terminus is also a common target site of cellular kinases for phosphorylation, which is often inhibitory towards AQP protein-protein interactions. For example, aquaporin-2 (AQP2) phosphorylation at Ser256 (S256) reduces its C-terminal interaction with lysosomal trafficking regulator (LYST)-interacting protein 5 (LIP5)[152], G-actin, annexin-2, protein phosphatase 1C, clathrin heavy chain, dynamin, heat shock cognate 71 kDa protein (Hsc70) and heat shock protein 70 (Hsp70)[153]. In the lens, AQP0 C-terminal phosphorylation at Ser235 (S235) reduces its C-terminal interaction with calmodulin (CaM)[150,151]. AQP5 undergoes C-terminal phosphorylation at Thr259 (T259) upon PKA activation via cyclic adenosine monophosphate (cAMP) treatment of the submandibular and parotid salivary glands[156]. AQP5 phospho-T259 (pT259) was spatially localized to plasma membrane and to vacuole-like formations within the plasma membrane formed sequentially after cAMP treatment. Additionally, AQP5 T259 phosphorylation was shown to affect AQP5 plasma membrane diffusion in transfected MDCK cells[438].

To our knowledge, AQP5 interacting partners in the lens have not been identified. Furthermore, Wang et al. 2013[450] detected AQP5 T259 phosphorylation via a phosphoproteomics screen in the ocular lens, but the spatial expression of AQP5 pT259 and the effects of AQP5 T259 phosphorylation upon AQP5 protein-protein interactions in the lens remain unclear. In this study, we couple regional co-immunoprecipitation assays and LC-MS/MS analysis to define potential lenticular AQP5 interacting partners in the bovine lens. Additionally, we define the relative AQP5 T259 phosphorylation and AQP5 pT259 spatial expression in the bovine lens. Our analyses revealed cytoplasmic serine-tRNA ligase (seryl-tRNA synthetase), serine/threonine-protein kinase 24 (STK24; also known as mammalian STE20-like protein kinase 3 or MST3), sorting nexin 8 (SNX8), dolichyl-diphosphooligosaccharide-protein glycosyltransferase subunit 2 (RPN2; also known as ribophorin-II), and dolichyl-diphosphooligosaccharide-protein glycosyltransferase 48 kDa subunit (DDOST) as potential AQP5 interacting partners in bovine lens cortical fiber cells while RPN2 was the only AQP5 interacting partner identified in bovine lens nuclear lens fiber cells. AQP5 pT259 expression was cytoplasmic in bovine lens cortical fiber cells and peripheral, adult nuclear fiber cells but localized to the plasma membrane in the central, embryonic nuclear fiber cells. Lenticular AQP5 interacting proteins broadly regulate autophagy which represents a potential novel cellular process associated with AQP5 function in the ocular lens.

4.2 Experimental Materials & Procedures

Tissue
Frozen bovine lenses (1-2 years old) used for AQP5 phospho-T259 (AQP5 pT259) expression analysis and co-immunoprecipitation were obtained from Pel-Freez Biologicals (Rogers, AK). Fresh bovine lenses (1-2 years old) used for immunofluorescence were obtained from Auckland Meat Processors (Otahuhu, New Zealand).

Reagents
Mass spectrometry-grade modified trypsin and dimethyl pimelimidate (DMP) were obtained from Thermo Fisher Scientific (Waltham, MA). Protein A coupled magnetic beads were obtained from Millipore Sigma (Burlington, MA). Odyssey Blocker Buffer was purchased from Li-COR Biotechnology (Lincoln, NE) Triton X-100 and all other chemicals were obtained from Sigma-Aldrich (Saint Louis, MO). All solvents were high performance liquid chromatography (HPLC) grade and obtained from Thermo Fisher Scientific.

Antibodies
Affinity-purified rabbit anti-AQP5 IgG targeted towards amino acid residues 249-265 of rat AQP5 was obtained from Millipore Sigma. Affinity-purified rabbit anti-AQP5 phospho-T259 IgG targeted towards amino acid residues 249-265 of rat AQP5 with phosphorylated T259 was kindly provided by Takahiro Hasegawa, Ph.D. of the University of Tokushima (Tokushima, Japan). Mouse anti-dolichyl-diphosphooligosaccharide-protein glycosyltransferase subunit 2 (ribophorin II; RPN2) IgG (sc-166241) was obtained from Santa Cruz Biotechnology (Dallas, TX). Affinity-purified normal rabbit IgG antibody was obtained from Cell Signaling Technology (Danvers, MA). Secondary antibody (goat anti-rabbit Alexa Fluor 488) used for immunofluorescence was obtained from Fisher Scientific. Secondary antibodies used for Western blotting were obtained from Fisher Scientific (goat anti-rabbit DyLight 680 and goat anti-mouse DyLight 800) (Waltham, MA).

Immunofluorescence

Fresh bovine lenses were fixed in 2% paraformaldehyde-0.01% glutaraldehyde in phosphate buffered saline (PBS; 72 hours at room temperature), cryoprotected in 10% sucrose-PBS (2 days, 4°C), 20% sucrose-PBS (1 hour, room temperature), and 30% sucrose-PBS ($\geq$ 7 days, 4°C), snap frozen in liquid nitrogen, encased in Tissue-Tek® O.C.T. Compound (Sakura Finetek USA, Inc.; Torrance, CA), cryosectioned perpendicularly (equatorially) to the optic axis at 30 µm thickness using a Leica CM3050 S cryostat (Leica Biosystems Inc; Buffalo Grove, IL), and finally were transferred onto plain microscope slides. Next, lens tissue cryosections (i.e. "sections") were triply washed in PBS, incubated in blocking solution (3% bovine serum albumin, 3% normal goat serum, in PBS) for 2-3 hours to reduce nonspecific labelling, and immunolabeled with rabbit anti-AQP5 (1:200) or rabbit AQP5 anti-phospho-T259 (1:200) primary antibody in blocking solution (16 hours, 4^{O}C) followed by Alexa488- or Alexa647-conjugated goat secondary antibodies in blocking solution (2 hours, room temperature). Following immunolabeling, sections underwent subsequent fluorescent labeling with DAPI-dilactate (1:100 in PBS) to label cellular nuclei in combination with Alexa647-conjugated wheat germ agglutinin (WGA; 1:100 in PBS, 1 hour, room temperature) to label fiber cell plasma membranes. Following fluorescent labeling, sections were coverslipped in VECTASHIELD® Antifade Mounting Medium and imaged using a Zeiss LSM 710 confocal laser scanning microscope (Carl Zeiss Inc; White Plains, NY). Background fluorescence was subtracted using Adobe Photoshop CS6 (Adobe; San Jose, CA).

AQP5 pT259 Expression Analysis

Preparation of Fiber Cell Membranes

Tissue from a decapsulated frozen bovine lens was dissected from at a distance of 3 mm from the equatorial edge of the lens surface. Tissue peripheral and medial to the dissection point was defined as the lens cortex and nucleus, respectively. Tissue was homogenized in homogenizing buffer (HB) comprised of 25 mM Tris, 5 mM EDTA, 10 mM NaF, 1 mM Na_3VO_4, 1 mM PMSF, pH 7.4. The homogenate was centrifuged at 200,000g for 90 minutes, and the supernatant was removed. The remaining pellets, the cortical and nuclear membrane fractions, were resuspended and centrifuged sequentially as outlined above in HB, 8M urea twice, and deionized and filtered water twice. Washed cortical and nuclear membrane fractions were then solubilized in 50 mM Tris-5% sodium dodecyl sulfate (SDS).

Preparation of Samples for Western Blotting

4X Laemmli Sample Buffer (final concentration 1X) and 1M DTT (final concentration of 50mM) were added to 28 µL of solubilized cortical and nuclear membrane fractions to yield a final volume of 40 µL.

Co-immunoprecipitation

Preparation of Detergent-Soluble Membranes

Tissue from five frozen bovine lenses was dissected 1 mm from the equatorial edge of the lens surface. Tissue peripheral to the dissection point was comprised of equatorial epithelial cells and cortical fiber cells, and tissue medial to this point was comprised of nuclear fiber cells. Tissue was homogenized in homogenizing buffer (HB) comprised of 25 mM Tris, 5 mM EDTA, 20 mM NaF, 2 mM Na_3VO_4, 1 mM PMSF, and 0.1% mammalian protease inhibitor cocktail, pH 7.4. The homogenate was centrifuged at 88,000g for 20 minutes, and the supernatant was removed. The remaining pellets, referred to as the cortical and nuclear membrane fractions, were superficially rinsed with HB without resuspension to remove excess supernatant. Fiber cell membranes were resuspended and separately solubilized for two hours at 4^{O}C in solubilization buffer (SB) consisting of 25 mM Tris, 1% Triton X-100, 20 mM NaF, 2 mM Na_3VO_4, 1 mM PMSF, and 0.1% mammalian protease inhibitor cocktail, pH 7.4. Membranes were centrifuged

at 4696 g for 12-20 minutes, and the pellets (i.e. detergent-insoluble fraction) were discarded. The detergent-soluble membrane fractions (DSF) were isolated for further analysis and the detergent-insoluble fractions were discarded.

Antibody Crosslinking to Magnetic Beads
Anti-AQP5 IgG antibody and normal rabbit IgG antibody were incubated with Protein A coupled magnetic beads for 3 hours at 4^{O}C then crosslinked to the beads via DMP. Antibody-crosslinked magnetic beads (IgG-mag beads) were incubated with 1M glycine, pH 3.0 for 20 minutes. IgG-mag beads were rinsed with phosphate-buffered saline (PBS) with 0.1% Tween 20, pH 7.4 once then several times with SB. The DSF was each split into two fractions. One DSF fraction was incubated with anti-AQP5 IgG mag beads while the other fraction was incubated with normal rabbit IgG-mag beads (negative control) for 2 hours at 4^{O}C. Following removal of the unbound fraction, IgG-mag beads from each fraction were washed four times with 1000 µL of SB. Precipitates were eluted by incubation with shaking in 20 µL 10% sodium dodecyl sulfate (SDS) at 70^{O}C for 35 minutes. The eluted precipitates, the eluate, from the two fractions are referred to as the anti-AQP5 IgG coIP (AQP5 coIP) eluate and the normal rabbit IgG coIP (NR coIP) eluate.

Preparation of Samples for Mass Spectrometric Analysis
20 µL 100 mM TEAB, pH 7.55 was added to AQP5 and NR coIP eluates. 10 µL of each diluted coIP eluate was used to for Western blot analysis. The remaining 30 µL of diluted eluate were reduced with dithiothreitol (DTT; final concentration of 10 mM) at 55^{O}C for 25 minutes and alkylated with iodoacetamide (final concentration 55 mM) at room temperature for 25 minutes. Iodoacetylated eluate proteins were precipitated with 3.44 µL 12% phosphoric acid then combined with 227 µL of S-Trap binding buffer (90% MeOH, 100 mM final TEAB). The entire volume from each fraction was overlaid on individual S-trap Micro spin columns and subjected to ultrafiltration by centrifugation at room temperature. Bound proteins, the retentate, were isolated from the filtrate and were washed three times with 150 µL S-Trap binding buffer by filling and centrifuging the spin columns. The bound proteins were digested for 1 hour at 47^{O}C in the spin column by addition of 50 mM TEAB pH 8.5, 1 mM $CaCl_2$, and 0.01 µg/µL trypsin. The resulting peptides were eluted by addition of 40 µL 50 mM TEAB, 40 µL 0.2% aqueous formic acid, and finally 35 µL 50% ACN-0.2% formic acid, respectively, to the S-Trap Micro spin column. Following addition of each volume, the spin columns were centrifuged at 4,000g as before. After elution, the peptides were dried by a speedvac concentrator and reconstituted in 2% ACN-0.1% formic acid.

Preparation of Samples for Western Blotting
4X Laemmli Sample Buffer (final concentration 1X), 1M DTT (final concentration of 50mM), and MilliQ H_2O were added to 10 µL of DSF (input), diluted coIP eluate, and immunodepleted fraction (IDP) from each fraction (in 5% SDS-50 mM TEAB) to yield a final volume of 25 µL.

nanoLC-ESI-MS/MS
Reconstituted peptides were loaded onto and separated by a one-dimensional fused silica capillary column (200 mm × 100 µm) packed with Phenomenex Jupiter resin with 3 µm particle size and 300 Å pore size. HPLC separation was performed using the following gradient at a flow rate of 350 µL per minute: ACN (0.1% formic acid) under the following gradient: 1-3min, 2% ACN (0.1% formic acid); 3-73 min, 2-40% ACN (0.1% formic acid); 73-78 min, 40-98% ACN (0.1% formic acid); 78-79 min, 98% ACN (0.1% formic acid); 79-80 min, 99-2% ACN (0.1% formic acid); 80-90 min (column re-equilibration), 2% ACN (0.1% formic acid). The eluate was directly infused into a Q Exactive HF mass spectrometer (Thermo Fisher Scientific) with a nanoelectrospray ionization source. The instrument was operated in data dependent mode with

one precursor scan event per MS/MS scan to identify the top fifteen most abundant ions in each MS scan for fragmentation.

nanoLC-ESI-MS/MS Data Analysis

AQP5 coIP and NR coIP eluates were generated per each coIP experiment with a total of three experiments (n = 3) for a total of twelve samples. The twelve raw data files were processed downstream with Sequest against a Uniprot bovine proteome database (https://www.uniprot.org/proteomes/UP000009136). The searching parameters include trypsin specificity with cleavage after proline, a maximum of two missed cleavage sites, a static modification of cysteine carbamidomethylation, variable modifications of methionine oxidation and asparagine deamination, precursor mass tolerance of < 1.25 Da, and fragment ion mass tolerance < 0.5 Da. Putative AQP5 interacting partners were defined as proteins with a spectral count fold change $\geq$ 2, that are statistically significant by the Fisher's Exact test, and whose spectral counts positively correlate with AQP5 spectral counts.

Western blotting

Samples were loaded onto 4–20% gradient Mini-PROTEAN Tris-glycine gels using Tris-glycine-SDS running buffer, and the Mini-PROTEAN Tetra Cell system (Bio-Rad; Hercules, CA) was used for protein separation. The samples were allowed to run into the gel until the loading dye ran off the gel. Proteins from the gel were transferred to methanol-activated polyvinylidene fluoride (PVDF) membranes in Towbin Buffer with SDS (25 mM Tris, 192 mM glycine, 20% methanol, 0.05% SDS) at 25V for 8-9 hours. Protein-laden PVDF membranes (blots) were blocked for 1 hour at room temperature in Odyssey Blocker Buffer, and then incubated with rabbit anti-AQP5 (1:1000), rabbit anti-AQP5 phospho-T259 (AQP5 pT259) (1:1000), or mouse anti-RPN2 (1:1000) IgG antibody at 4^{O}C for 16-23 hours. The blots were washed with 0.1% Tween20-PBS four to six times for five minutes then incubated with a goat anti-rabbit DyLight680 (1:10000) or goat anti-mouse DyLight800 (1:10000) antibody for 2 hours at room temperature. For AQP5 pT259 analysis, blocked blots were first incubated in anti-AQP5 pT259 and conjugate secondary antibodies, stripped with 2% SDS, 62.5 mM Tris, 0.8% β-mercaptoethanol pH 6.8 at 50°C for 45 min, and were reprobed with anti-AQP5 and conjugate secondary antibodies. Blot bands were visualized using fluorescence detection via an Odyssey CLx Imaging System (LI-COR Biotechnology).

4.3 Results

AQP5 interacting partners in the bovine lens

AQP5 interactions with cell junctional proteins[154], the cell structural protein ezrin[435], and potential trafficking regulatory proteins PIP[422,436] and Mup4[422] has previously been documented. Interestingly, AQP5 also interacts with autophagy regulator CDGSH iron-sulfur domain-containing protein 2 (also known as nutrient-deprivation autophagy factor-1 or NAF-1) in MDCK cells[154,495] which is in accordance with our histological data (Chapter 3) which shows AQP5 colocalized to autophagosomal and autolysosomal compartments in the bovine lens cortex. Thus, we expected AQP5 to interact with proteins with congruent cellular functions in the bovine lens and were particularly interested in cellular processes that linked AQP5 interacting proteins to our histological data.

To test this expectation, we co-immunoprecipitated AQP5 from bovine lens cortical and nuclear fiber cell membranes (Figure 4.1). We excluded the membrane-depleted soluble fraction from our analyses due to significant interference from lens crystallins and discarded the Triton X-100 insoluble fraction. Western blot analysis of anti-AQP5 IgG co-immunoprecipitation eluates demonstrated enrichment of AQP5 from the detergent-soluble fraction (DSF) of cortical and

nuclear fiber cell membranes and relative to normal IgG negative control eluates. As expected, normal IgG failed to demonstrate statistically significant AQP5 immunodepletion or enrichment relative to DSF. AQP5 expression is represented by the protein bands at approximately 25 kDa (Figures 4.1A and 4.1C, *blue arrows*). AQP5 expression remained detectable in the "immunodepleted fraction" (IDP) following separation from the co-immunoprecipitate despite attempts to immunodeplete residual AQP5 with additional anti-AQP5 IgG antibody in our control experiments (data not shown). This may be a result of AQP5 posttranslational modifications or protein-protein interactions masking the anti-AQP5 IgG antibody epitope though this remains to be determined. As expected, AQP5 expression remains detectable in the IDP of negative control IgG treated samples. Densitometric analysis revealed that we specifically enriched AQP5 via co-immunoprecipitation in the bovine lens cortex and nucleus approximately 403% and 571%, respectively, relative to nonspecific background from normal IgG control (Figures 4.1B and 4.1D), respectively). Relative to detergent soluble fraction (DSF) input from the cortex and nucleus, AQP5 enrichment from AQP5 co-immunoprecipitation was 282% and 217%, respectively (Figures 4.1B and 4.1D), respectively).

A.

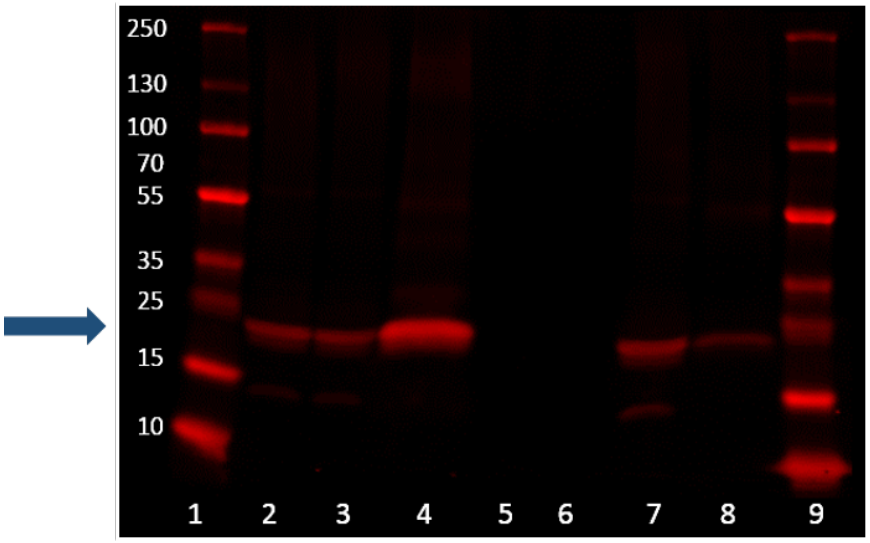

B.

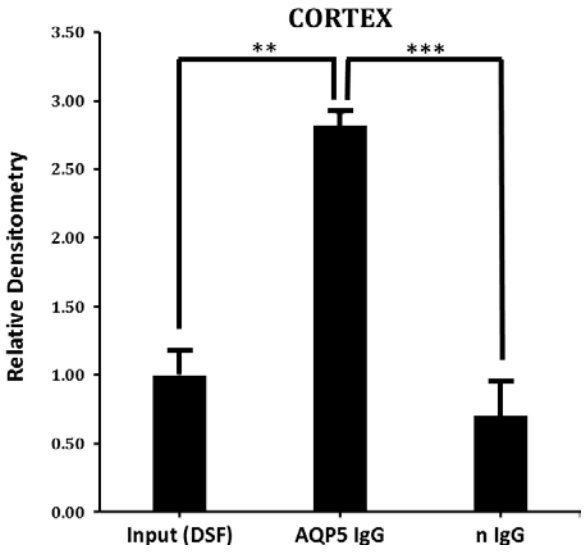
CORTEX
**
***
Relative Densitometry
3.50
3.00
2.50
2.00
1.50
1.00
0.50
0.00
Input (DSF)
AQP5 IgG
n IgG

C.

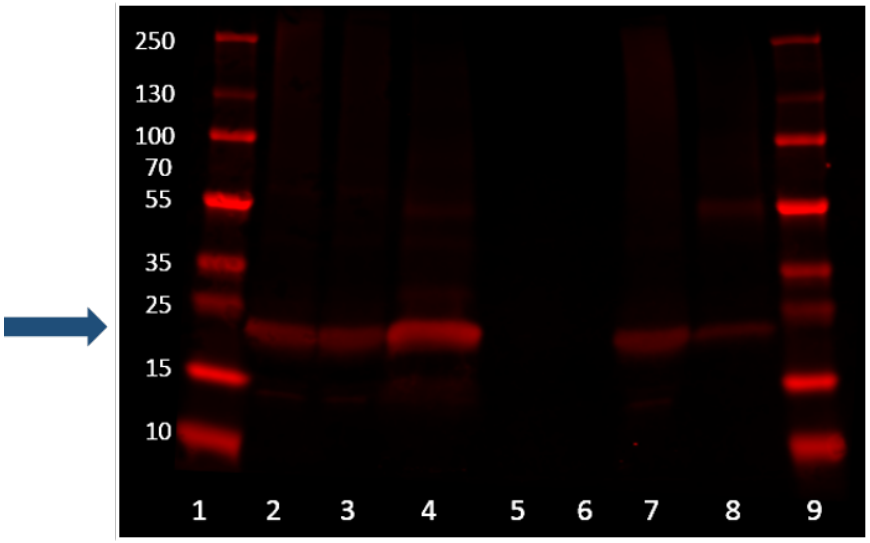
250
130
100
70
55
35
25
15
10
1
2
3
4
5
6
7
8
9

D.

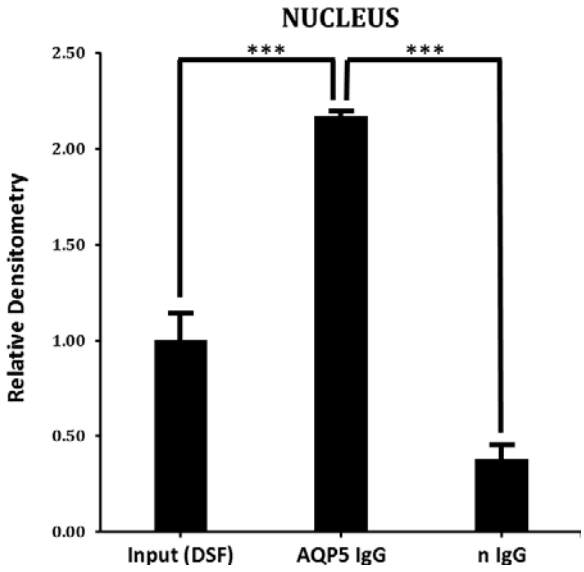

Figure 4.1. Potential AQP5 interacting partners in bovine lens cortical fiber cell membranes enriched by AQP5 co-immunoprecipitation.

A. A representative Western blot of AQP5 protein expression (***red***) from AQP5 co-immunoprecipitation of cortical fiber cell membranes from bovine lens tissue. The detergent soluble fraction, immunodepleted fractions (IDP), and eluates were evaluated for AQP5 expression. Lane assignments are as follows: Ladder (Lanes 1 and 9), detergent soluble fraction (Lane 2), IDP – anti-AQP5 IgG (Lane 3), Eluate – anti-AQP5 IgG (Lane 4), IDP – normal rabbit IgG (Lane 7), Eluate – normal rabbit IgG (Lane 8), and Triton buffer (Lanes 5 and 6). AQP5 is represented by the band at approximately 25 kDa (*blue arrow*).

B. Normalized densitometric analysis of Western blot bands from the cortex detergent soluble fraction (Input (DSF)), eluate from anti-AQP5 IgG, and the normal IgG control from AQP5 co-immunoprecipitation analysis (n =3). AQP5 is enriched in the eluate from anti-AQP5 IgG by 282% relative to the DSF and by 403% relative to the normal IgG control. Student t-Test statistical significance levels below P-values of 0.05 and 0.01 are represent by two (******) and three asterisks (*******), respectively.

C. A representative Western blot of AQP5 protein expression (***red***) from AQP5 co-immunoprecipitation of cortical fiber cell membranes from bovine lens tissue. The detergent soluble fraction, immunodepleted fractions (IDP), and eluates were evaluated for AQP5 expression. Lane assignments are as follows: Ladder (Lanes 1 and 9), detergent soluble fraction (Lane 2), IDP – anti-AQP5 IgG (Lane 3), Eluate – anti-AQP5 IgG (Lane 4), IDP – normal rabbit IgG (Lane 7), Eluate – normal rabbit IgG (Lane 8), and Triton buffer (Lanes 5 and 6). AQP5 is represented by the band at approximately 25 kDa (*blue arrow*).

D. Normalized densitometric analysis of Western blot bands from the nucleus detergent soluble fraction (Input (DSF)), eluate from anti-AQP5 IgG, and the normal IgG control from AQP5 co-immunoprecipitation analysis (n =3). AQP5 is enriched in the eluate from anti-AQP5 IgG by 217% relative to the DSF and by 571% relative to the normal IgG control. Student t-Test statistical significance levels below P-values of 0.05 and 0.01 are represent by two (******) and three asterisks (*******), respectively.

To define potential AQP5 interacting proteins, we digested protein in co-immunoprecipitation eluates with trypsin followed by nanoLC-ESI-MS/MS analysis. Protein identifications were made with a minimum of two unique peptides in triplicate co-immunoprecipitation assays. Proteins in anti-AQP5 IgG eluates statistically enriched (i.e. Fisher's Exact testing) by spectral counts relative to normal IgG control eluates were considered potential AQP5 interacting partners (Figure 4.2). We identified serine-tRNA ligase, cytoplasmic (seryl-tRNA synthetase), serine/threonine-protein kinase 24 (STK24; also known as mammalian STE20-like protein kinase 3 or MST3), sorting nexin 8 (SNX8), dolichyl-diphosphooligosaccharide-protein glycosyltransferase subunit 2 (RPN2; also known as ribophorin-II), and dolichyl-diphosphooligosaccharide-protein glycosyltransferase 48 kDa subunit (DDOST) as potential AQP5 interacting partners in bovine lens cortical fiber cells (Figure 4.2A) while RPN2 was the only AQP5 interacting partner identified in bovine lens nuclear lens fiber cells (Figure 4.2B). Of potential AQP5 interacting proteins in bovine lens cortical fiber cell membranes, seryl-tRNA synthetase was surprisingly the most highly enriched by spectral count fold change followed by STK24. Co-immunoprecipitated RPN2 spectral counts are drastically reduced in bovine lens nuclear fiber cell membranes relative to cortical fiber cell membranes which may be a reflection of lenticular endoplasmic reticular organelle degradation as RPN2 is part of the oligosaccharyl transferase (OST) complex which localizes to rough endoplasmic reticulum membranes[496,497]. DDOST is also a protein subunit within the OST, so it is unclear why DDOST is not also detected in AQP5 co-immunoprecipitation eluates from bovine lens nuclear fiber cell membranes.

A.

PROTEIN	Spectral Counts AQP5 IgG coIP *n=3*	Spectral Counts IgG coIP *n=3*	Fisher's Exact Test *p-value* *(*p < 0.00096)*	Fold Change
Aquaporin-5 (AQP5)	29 | 36 | 39	5 | 5 | 10	< 0.00010	5.2
Serine-tRNA ligase, cytoplasmic	8 | 11 | 18	0 | 0 | 1	< 0.00010	37
Serine/threonine-protein kinase 24	13 | 18 | 20	2 | 4 | 0	< 0.00010	8.8
Sorting nexin-8	8 | 24 | 15	3 | 6 | 1	< 0.00010	4.7
Dolichyl-diphosphooligosaccharide protein glycosyltransferase 48 kDa subunit (DDOST)	56 | 59 | 59	21 | 16 | 23	< 0.00010	2.9
Dolichyl-diphosphooligosaccharide-protein glycosyltransferase subunit 2 (RPN2)	128 | 121 | 122	50 | 40 | 47	< 0.00010	2.7

B.

PROTEIN	Spectral Counts AQP5 IgG coIP *n=3*	Spectral Counts IgG coIP *n=3*	Fisher's Exact Test *p-value* *(*p < 0.00252)*	Fold Change
Aquaporin-5 (AQP5)	11 | 25 | 24	0 | 2 | 1	< 0.00010	20
Dolichyl-diphosphooligosaccharide-protein glycosyltransferase subunit 2 (RPN2)	10 | 19 | 15	1 | 6 | 10	< 0.00010	2.6

Figure 4.2. Potential AQP5 interacting partners in bovine lens cortical fiber cell membranes enriched by AQP5 co-immunoprecipitation.

A. AQP5 co-immunoprecipitation eluate protein spectral counts from cortical fiber cell membranes (*n* = 3) were reported via *Scaffold* v.*4*. Anti-AQP5 IgG eluate (*Spectral Counts AQP5 IgG coIP*) and normal rabbit IgG eluate (*Spectral Counts IgG coIP*, negative control) spectral counts for the same proteins are displayed. Fisher's exact test (FET) was applied to determine statistically significant dependence between AQP5 co-immunoprecipitation and the spectral counts of putative interacting partners. A *P-value* < 0.00096 indicates statistically significant dependence. The "Fold Change" is the quotient of *Spectral Counts AQP5 IgG coIP* divided by *Spectral Counts IgG coIP*.

B. AQP5 co-immunoprecipitation eluate protein spectral counts from nuclear fiber cell membranes (*n* = 3) were reported via *Scaffold* v.*4*. Anti-AQP5 IgG eluate (*Spectral Counts AQP5 IgG coIP*) and normal rabbit IgG eluate (*Spectral Counts IgG coIP*, negative control) spectral counts for the same proteins are displayed. Fisher's exact test (FET) was applied to determine statistically significant dependence between AQP5 co-immunoprecipitation and the spectral counts of putative interacting partners. A *P-value* < 0.00252 indicates statistically significant dependence. The "Fold Change" is the quotient of *Spectral Counts AQP5 IgG coIP* divided by *Spectral Counts IgG coIP*.

To corroborate *potential* bovine lens fiber cells AQP5 interacting partners identified in our studies, we reprobed Western blots from our AQP5 co-immunoprecipitation assays to test for specific enrichment of RPN2 as a general indicator of the probable validity of identified proteins as AQP5 interacting partners (Figure 4.3). Reprobed Western blots demonstrate clear enrichment of RPN2 in anti-AQP5 IgG eluates relative to the normal IgG negative control eluates from bovine lens cortical and nuclear fiber cell membranes (Figures 4.3A and 4.3B, respectively). RPN2 expression is represented by protein bands between 60-65 kDa (Figure 4.3, *blue arrows*). This is consistent a previous study which listed the apparent molecular weight of purified canine RPN2 as 63kDa based on Western blot analysis[497]. Thus, our reprobe results are consistent our co-immunoprecipitation assay proteomics results and with RPN2 being a *potential* AQP5 interacting protein in bovine lens cortical and nuclear fiber cells.

A.

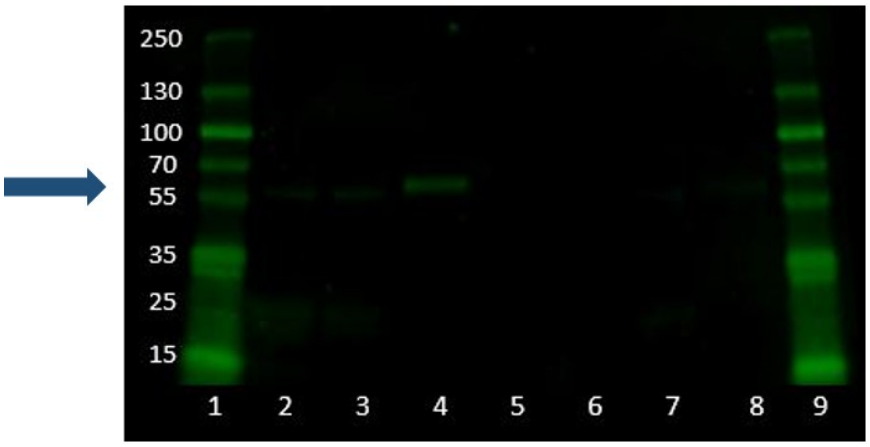

B.

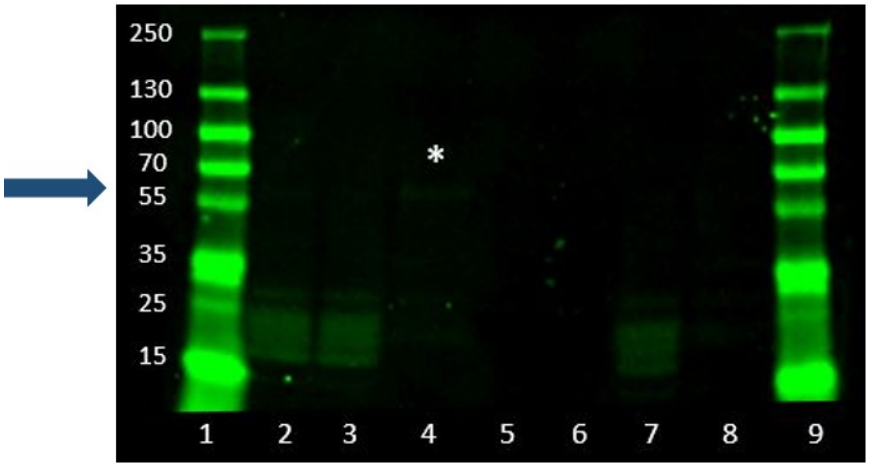

Figure 4.3. Reprobe of AQP5 co-immunoprecipitation assay fractions from bovine lens cortical and nuclear fiber cell membranes for specific enrichment of RPN2.

A. A representative reprobe of Western blots from AQP5 co-immunoprecipitation assays in cortical fiber cell membranes (***Figure 4.1***) for RPN2. Lane assignments are as follows: Ladder (Lanes 1 and 9), detergent soluble fraction (Lane 2), immunodepleted fraction (IDP) – anti-AQP5 IgG (Lane 3), eluate – anti-AQP5 IgG (Lane 4), IDP – normal IgG (Lane 7), eluate – normal IgG (Lane 8), and Triton buffer (Lanes 5 and 6). RPN2 is represented by bands approximately 60-65 kDa (*blue arrow*).

B. A representative reprobe of Western blots from AQP5 co-immunoprecipitation assays in cortical fiber cell membranes (***Figure 4.1***) for RPN2. Lane assignments are as follows: Ladder (Lanes 1 and 9), detergent soluble fraction (Lane 2), immunodepleted fraction (IDP) – anti-AQP5 IgG (Lane 3), eluate – anti-AQP5 IgG (Lane 4), IDP – normal IgG (Lane 7), eluate – normal IgG (Lane 8), and Triton buffer (Lanes 5 and 6). RPN2 is represented by bands approximately 60-65 kDa (*blue arrow*). The asterisk (*) denotes a band that is representative of RPN2 expression in Lane 4.

AQP5 T259 phosphorylation in the bovine lens

AQP5 expression levels and spatial mapping have previously been defined in human[46], mouse[45,46,168], rat[46,116], and rabbit lenses[40]. Additionally, Grey et al. 2013 defined AQP5 expression levels in bovine lenses[46], and we confirm that AQP5 spatial expression patterns in bovine lenses are consistent with other mammalian lenses (Chapter 3). Although AQP5 T259 phosphorylation has been confirmed in the lens[450], AQP5 pT259 expression levels and spatial expression are unclear and necessary to define to better understand regulation of AQP5 protein-protein interactions in the lens. To define relative AQP5 pT259 expression levels, we analyzed AQP5 pT259 expression in bovine lens cortical and nuclear fiber cells via Western blot analysis (Figure 4.4A) reprobing for unphosphorylated AQP5 as a loading and normalization control (Figure 4.4B). Preliminary densitometric analysis (n = 1) revealed relative AQP5 pT259 expression in cortical fiber cell membranes is approximately four times higher than nuclear fiber cell membranes using unphosphorylated AQP5 as a loading control (Figure 4.4).

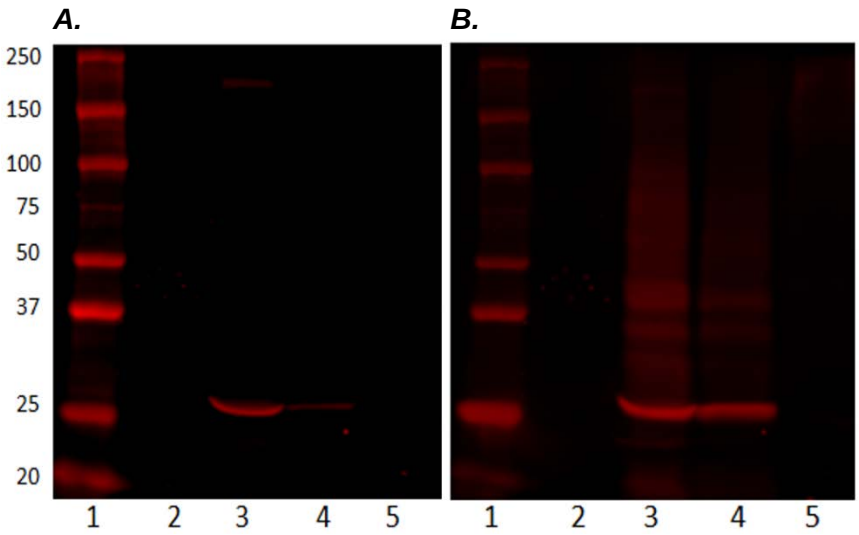

Figure 4.4. AQP5 and AQP5 phospho-T259 (pT259) exhibit differential immunolabeling in fiber cells of the bovine lens.

A. A representative Western blot of AQP5 pT259 protein expression (***red***) in cortical (Lane 3) and nuclear membranes (Lane 4) fractions from bovine lens tissue. Lane assignments are as follows: Ladder (Lane 1), buffer (Lane 2), and HeLa cell lysate (Lane 5). HeLa cell lysate represents a mammalian cell negative control for AQP5 protein expression. AQP5 pT259 is represented by the bands at approximately 25 kDa.

B. Reprobe of the Western blot in ***A*** for AQP5 protein expression (***red***) in cortical (Lane 3) and nuclear membranes (Lane 4) fractions from bovine lens tissue. Lane assignments are the same as in ***A***.

To define lenticular AQP5 pT259 spatial expression and differences in spatial expression patterns with AQP5, we conducted AQP5 and AQP5 pT259 immunofluorescence analysis in bovine lens tissue sections (Figure 4.5). In the bovine lens, unphosphorylated AQP5 is primarily cytoplasmic in cortical fiber cells and localized to the plasma membrane in nuclear fiber cells. AQP5 pT259 expression is also cytoplasmic in bovine lens cortical fiber cells but remains cytoplasmic in adult nuclear fiber cells localizing to vesicular structures apparently apposed to fiber cell membranes (Figures 4.5C-3 and 4.5C-4). In the embryonic nuclear fiber cells of the bovine lens core, AQP5 pT259 expression is localized to the plasma membrane (Figures 4.5D-3 and 4.5D-4) similar to unphosphorylated AQP5.

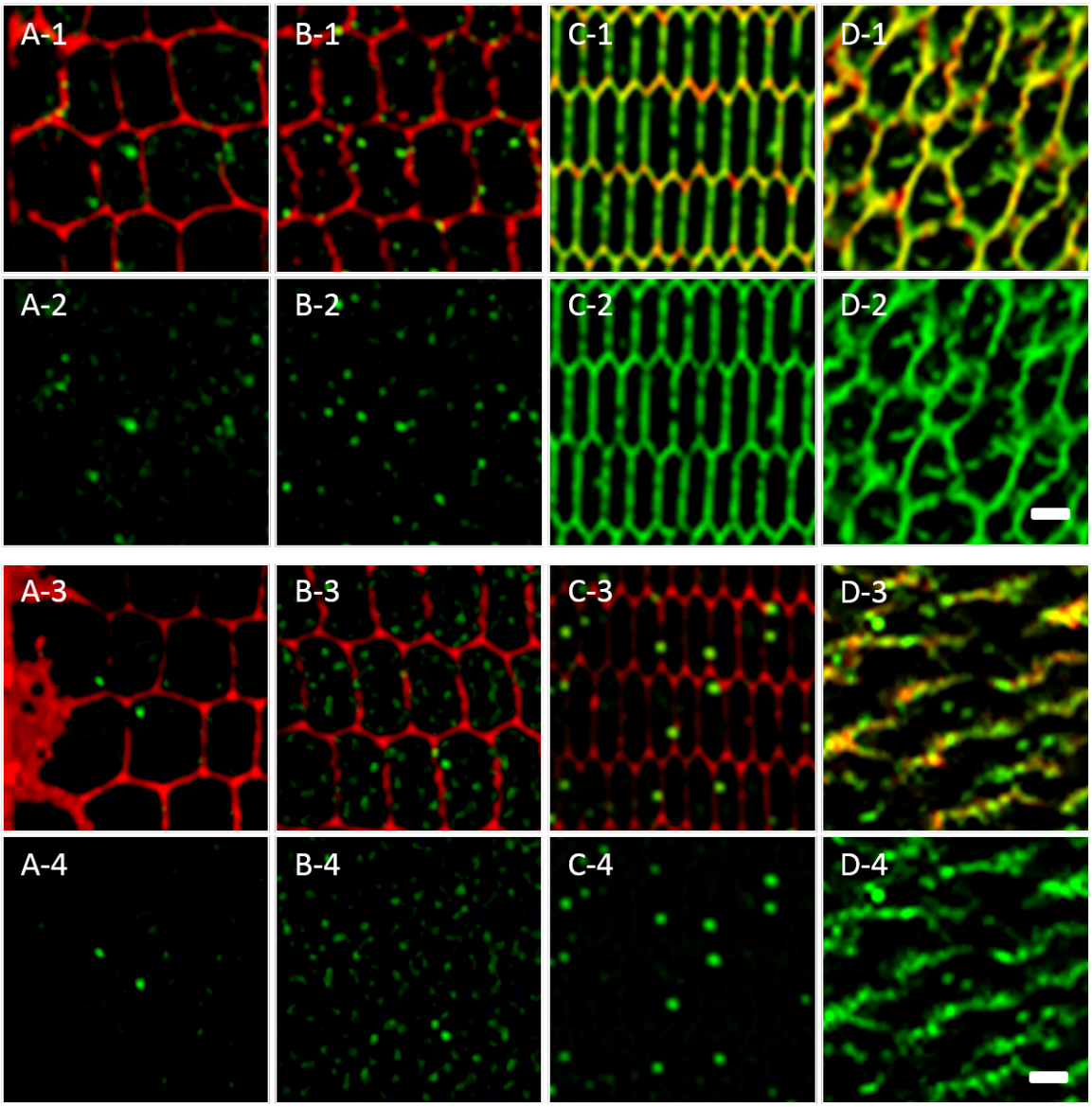

Figure 4.5. AQP5 and AQP5 phospho-T259 (pT259) exhibit differential AQP5 spatial expression patterns in fiber cells of the bovine lens.

A-1 – ***D-1*.** Medium-magnification confocal images of AQP5 immunolabeling (***green***) and WGA fluorescent labeling (***red***) in the *peripheral outer cortex* (***A***), *medial outer cortex* (***B***), *adult nucleus* (***C***), and *embryonic nucleus* (***D***) of the bovine lens.

In the *peripheral outer cortex* (***A***) and *medial outer cortex* (***B***), AQP5 is localized to cytoplasmic vesicles then is localized to the plasma membrane in the *adult nucleus* (***C***), and *embryonic nucleus* (***D***).

A-2 – ***D-2*.** Replicate images of ***A-1*** – ***D-1*** with AQP5 immunolabeling only displayed.

A-3 – ***D-3*****.** Medium-magnification confocal images of AQP5 phosphorylated at T259 (AQP5 pT259) immunolabeling (***green***) and WGA fluorescent labeling (***red***) in the *peripheral outer cortex* (***A***), *medial outer cortex* (***B***), *adult nucleus* (***C***), and *embryonic nucleus* (***D***) of the bovine lens.

In the *peripheral outer cortex* (***A***), *medial outer cortex* (***B***), and *adult nucleus* (***C***) AQP5 pT259 is localized to cytoplasmic vesicles then is localized to the plasma membrane in the *embryonic nucleus* (***D***).

A-4 – ***C-4*****.** Replicate images of ***A-3***, ***B-3***, and ***C-3*** with AQP5 pT259 immunolabeling only displayed.

Scale bars represent 10 µm.

4.4 Discussion

The goals of this study were to define AQP5 threonine-259 phosphorylation (AQP5 pT259) expression and AQP5 interacting partners in the bovine lens to better understand AQP5 roles and regulation in the ocular lens. In this study, we reveal that AQP5 pT259 is expressed throughout bovine lens fiber cells but differs from unphosphorylated AQP5 in regional fiber cell plasma membrane expression and that AQP5 appears to interact with multiple proteins that indirectly regulate the process of autophagy in the bovine lens cortex.

In published work of non-lenticular cells, AQP5 was discovered to interact via its C-terminus with ZO1, plakoglobin, β-catenin, and desmoglein-2 at the plasma membrane and thereby regulate the expression of these interacting proteins and cell junctional formation[154]. Therefore, we expected lenticular AQP5 interacting partners that co-immunoprecipitated with AQP5 to reveal cellular processes regulated by AQP5 in ocular lens. Densitometric analysis suggested that we enriched AQP5 relative to the detergent soluble membrane fractions from bovine lens cortex and nucleus via co-immunoprecipitation (Figure 4.1). Statistical analysis of densitometry results revealed that AQP5 enrichment was specific compared to nonspecific background from normal IgG control, which prompted us to examine anti-AQP5 IgG eluates for potential AQP5 interacting partners. Despite titration of anti-AQP5 antibody to maximize total amount of co-immunoprecipitated AQP5 (*data not shown*), we were unable to fully immunodeplete from cortical or nuclear bovine detergent soluble membrane fractions via co-immunoprecipitation (Figures 4.1A and 4.1C; Lane 3). Since commercially available AQP5 antibodies target its C-terminus which is the site of the vast majority of AQP protein-protein interactions[149], this result suggests epitope masking via interacting proteins or potential C-terminal modifications inhibitory to AQP5-antibody interaction. Thus, the inability to immunodeplete AQP5 via C-terminal antibody co-immunoprecipitation also suggests additional potential AQP5 interacting partners remain to be discovered outside those identified in this study possibly via modification of our co-immunoprecipitation methods or alternative methods of identifying protein-protein interactions.

Nevertheless, LC-MS/MS analysis of AQP5 co-immunoprecipitation eluates revealed several statistically enriched, potential AQP5 interacting proteins in cortical detergent soluble membranes (Figure 4.2A) including seryl-tRNA synthetase, serine/threonine-protein kinase 24 (STK24; also known as mammalian STE20-like protein kinase 3 or MST3), sorting nexin 8 (SNX8), dolichyl-diphosphooligosaccharide-protein glycosyltransferase 48 kDa subunit (DDOST), and dolichyl-diphosphooligosaccharide-protein glycosyltransferase subunit 2 (RPN2). Interestingly, we did not identify cell junction AQP5 interacting proteins as did Login et al. 2020[154], but this difference may be a result of methods differences as the authors in that study

employed glutathione S-transferase (GST) fusion-tagged AQP5 transfected into Madin-Darby canine kidney (MDCK) cells and glutathione-conjugated beads to enrich AQP5 interacting proteins. Nevertheless, it is probable that AQP5 interacts with at least some of the same cell junction AQP5 interacting proteins identified in Login et al. 2020 and ezrin, an AQP5 interacting protein identified by Chivasso et al. 2021 which also interacts with AQP0 in the ocular lens[494]. Cantrell et al. 2021 confirmed expression of prolactin-inducible protein (PIP) in the ocular lens[451], and thus lenticular AQP5 may interact with PIP as it does in the lacrimal[422] and salivary glands[436], but this remains to be determined. It is unlikely that AQP5 interacts with major urinary protein 4 (Mup4) as this protein has not been detected in the ocular lens.

Of the potential AQP5 interacting partners revealed in this study, one common cellular process that links them in the ocular lens and to our histological data (Chapter 3) is the process of autophagy. Serine/threonine-protein kinase 24 (STK24), identified in the coIP study, modulates the PI3K/Akt/mTOR pathway[498]. STK24 knockdown increases Akt activity via phosphorylation at S473 and T308 in HepG2 cells, which in turn increases mTOR activation. This increase in Akt phosphorylation is inhibited by PI3K inhibition, which in turn inhibits mTOR activity. mTOR inhibition induces autophagy[314] which is constitutively active in the lens[307]. Proteomic analysis suggests that STK24 is expressed throughout adult lens outer cortical fiber cells[291] which implies a potential role in autophagic induction in the same lenticular region in which autophagy is constitutive and in which AQP5 in the bovine lens increasingly localizes to autophagosomes and lysosomes (Chapter 3). The potential interaction between AQP5 and seryl-tRNA synthetase may be also be related to mTOR activity. Amino acid availability regulates mTOR activation with leucyl-tRNA synthetase, for example, serving as an amino acid sensor. Unc-51-like kinase 1 (ULK1) phosphorylates leucyl-tRNA synthetase inducing its detachment from the lysosomal membrane and reducing its binding to leucine which results in mTOR complex 1 (mTORC1) inhibition[324,499,500]. It is unclear whether seryl-tRNA synthetase functions as an amino acid sensor, but loss-of-function mutation of the seryl-tRNA synthetase *CG17259* upregulates autophagy in *Drosophila melanogaster*. Thus, as a potential AQP5 interacting protein in the bovine lens, seryl-tRNA synthetase represents a possibly novel mechanism of autophagy control by a tRNA synthetase in the bovine lens.

SNX8 is an endosomal protein comprised of a phosphoinositide-binding Phox homology (PX) domain[501] and a BAR domain, which senses membrane curvature and targets proteins to phosphoinositide-enriched, tubular membranes in the endolysosomal network[502]. SNX8 negatively regulates endosome to Golgi trafficking[503] and innate immune response to RNA viruses relocating to mitochondria upon viral infection[504]. Interestingly, sorting nexin-9 (SNX9) also localizes to mitochondria and is essential to formation of mitochondria-derived vesicles (MDVs)[505], which function in mitochondrial quality control by delivering damaged mitochondrial components such as oxidized proteins to lysosomes for degradation[506–508]. Mitochondria undergo autophagic degradation in the lens via incorporation into autolysosomes[308,310,311], and it is thought that autophagosome-lysosome fusion is preceded by autophagosome-late endosome fusion forming an amphisome intermediate which fuses with lysosomes to form autolysosomes[445]. Our histological data suggest that lenticular AQP5 may be a mitochondrial aquaporin as AQP5-containing cytoplasmic vesicles colocalize with mitochondrial marker proteins in lens fiber cells prior to colocalization of these mitochondrial markers with the autophagosomal marker protein LC3B (Figure 3.8). Subsequently, our data suggest that mitochondrial marker-positive, AQP5-containing cytoplasmic vesicles undergo unconventional protein secretion through autolysosomes and possibly amphisome-intermediates (Figure 3.11). Collectively, these data are suggestive of a potential role for SNX8 in localization of lenticular AQP5 to mitochondria and for AQP5 and SNX8 in mitochondrial regulation in the ocular lens. Interaction between AQP5 and a resident endosomal sorting nexin are supportive of the formation of an amphisome-intermediate in unconventional protein secretion of AQP5 in the bovine lens.

RPN2 and DDOST are protein subunits of the mammalian oligosaccharyltransferase (OST) complex, a resident endoplasmic reticular, multiprotein complex which N-glycosylates proteins by transferring $Glc_3Man_9GlcNAc_2$ (Glc = Glucose, Man = Mannose, and GlcNAc = N-acetylglucosamine) to asparagine residues of target proteins within the consensus sequence Asn-X-Ser or Asn-X-Thr where X is any amino acid except proline[497]. AQP5 is weakly glycosylated in the cochlea[509], cornea[510], and parotid gland[511], and it is possible that AQP5 glycosylation occurs in the bovine lens as faint AQP5 immunoreactive bands are present at the apparent molecular weight corresponding to glycosylated AQP5 in the Western blot analysis of rat and bovine lens fiber cell membranes conducted by Grey et al. 2013[46]. Interestingly, putative AQP5 glycosylation in the bovine lens fiber cells appears to be very weak relative to unglycosylated AQP5 except for in inner cortical fiber cells[46]. This may be indicative of a role for the OST in glycosylation related trafficking of AQP5 as glycosylation is known to play a role in cellular trafficking[512], but this remains to be determined. Recently, Login et al. demonstrated that AQP5 interacts with dolichyl-diphosphooligosaccharide-protein glycosyltransferase subunit 1 (RPN1; also known as ribophorin-I), another protein subunit of the OST. RPN2 is also commonly expressed at the limiting membranes of autophagic vesicles[496]. Furthermore, RPN2 expression decreases from the outer cortex to the inner cortex[291], and decreased RPN2 expression strongly upregulates autophagic induction in HepG2 cells[513]. Genetic mutation of OST component proteins including DDOST, whose expression decreases from the outer cortex to the inner cortex similar to RPN2[291], also upregulates autophagy in *Drosophila*[514]. Thus, RPN2 and DDOST are additional potential AQP5 interacting proteins in the ocular lens directly related to the cellular process of autophagy. It is interesting to note that RPN2 was the only statistically enriched potential AQP5 interacting protein detected in nuclear detergent soluble membranes (Figure 4.2B). This may be representative of a rearrangement of AQP5 interacting proteins in the bovine lens upon insertion into fiber cell plasma membrane or a function of cessation of autophagy in the lens which occurs concomitantly with the completion of organelle degradation. These possibilities remain to be examined, and additional potential AQP5-interacting proteins in the ocular lens nucleus remain to be defined.

The aquaporin C-terminus is the primary binding site for interacting proteins[149] and a target for AQP0, AQP2, and AQP5 phosphorylation by PKA[150,156,515]. AQP0 and AQP2 protein-protein interactions are a regulated by C-terminal phosphorylation with C-terminal phosphorylation reducing the AQP0-calmodulin interaction[150,151] and reducing the AQP2 protein-protein interactions with lysosomal trafficking regulator (LYST)-interacting protein 5 (LIP5)[152] and G-actin, annexin-2, protein phosphatase 1C, clathrin heavy chain, dynamin, heat shock cognate 71 kDa protein (Hsc70), and heat shock protein 70 (Hsp70)[153]. We expected similar inhibition of AQP5 protein-protein interactions in the bovine lens but were unsuccessful at testing this hypothesis directly with peptide affinity chromatography. Nevertheless, we were kindly provided enough anti-AQP5 phospho-T259 (AQP5 pT259) antibody by Takahiro Hasegawa, Ph.D. of the University of Tokushima (Tokushima, Japan) to conduct Western blot and immunofluorescence analysis to determine relative AQP5 and AQP5 pT259 expression differences in the bovine lens (Figures 4.4 and 4.5). Relative AQP5 pT259 expression *appears* to be roughly four times higher in the cortex than the nucleus in the bovine lens though more experimentation is needed to accurately statistically confirm region-specific differences in total AQP5 T259 phosphorylation levels. Furthermore, AQP5 pT259 has a different spatial expression pattern compared to unphosphorylated AQP5 being cytoplasmically localized in the mature fiber cells of the adult nucleus after unphosphorylated AQP5 is inserted into fiber cell plasma membranes (Figure 4.5). Our results suggest that commercial anti-AQP5 may not co-immunoprecipitate AQP5 and that AQP5 pT259 may play a significant role in AQP5 protein-protein interactions particularly in the lens cortex. Furthermore, further histological analysis of AQP5 may be required to extend our current histological data (Chapter 3) to more thoroughly understand AQP5 trafficking in the bovine lens.

4.5 Conclusions

Seryl-tRNA synthetase, serine/threonine-protein kinase 24 (STK24 or MST3), sorting nexin 8 (SNX8), dolichyl-diphosphooligosaccharide-protein glycosyltransferase subunit 2 (RPN2; ribophorin-II), and dolichyl-diphosphooligosaccharide-protein glycosyltransferase 48 kDa subunit (DDOST) represent potential AQP5 interacting partners in the bovine lens cortex, and RPN2 represents a potential AQP5 interacting partner in the bovine lens nucleus. These putative lenticular AQP5 interacting proteins have disparate functions but are linked as regulators of autophagic induction. AQP5 pT259 exhibits similar cytoplasmic spatial expression to unphosphorylated AQP5 expression in the bovine lens cortex. In the bovine lens nucleus, AQP5 pT259 exhibits divergent spatial expression to unphosphorylated AQP5 in the bovine lens nucleus and remains cytoplasmic in the periphery of the nucleus then localizes to the plasma membrane in the nucleus core. Collectively, the potential association of lenticular AQP5 with interacting proteins which broadly regulate autophagy suggests a novel, potential role for AQP5 in regulation of autophagy in the ocular lens, specifically in differentiating cortical lens fiber cells. Since AQP C-terminal phosphorylation is generally inhibitory towards AQP protein-protein interactions, AQP5 T259 phosphorylation is poised to modulate such a role through regulation of lenticular AQP5 protein-protein interactions particularly in the cortex, where autophagic organelle degradation occurs and AQP5 pT259 expression is significant relative to unphosphorylated AQP5.

CHAPTER V. SUMMARY AND FUTURE DIRECTIONS

The research presented in this dissertation began in 2015. Since that time, progress in aquaporin and lens research has been substantial. In particular, much progress has been made in understanding the role of AQP5 in the lens especially in the context of other lens aquaporins. We have learned how spatial expression of lenticular AQP0 and AQP5 in lens fiber cells changes during development and that AQP5 remains cytoplasmically localized until AQP0 is C-terminally truncated in the mouse lens[168]. We have learned that AQP5 can dynamically traffick to fiber cell plasma membranes in peripheral lens fiber cells and in the fiber cell tips of the anterior lens suture in response to zonular tension perturbation[111,116]. We have also learned that AQP5 plasma membrane insertion in the ocular lens increases fiber cell plasma membrane water transport and that genetic deletion of AQP5 increases total water content upon osmotic perturbation[110]. We have learned more about the regulation of AQP5 in general in that AQP5 T259 phosphorylation affects AQP5 plasma membrane diffusivity[438]. Plasma membrane diffusivity affects plasma membrane protein incorporation into lipid raft domains and protein-protein interactions, and therefore AQP5 T259 phosphorylation may regulate both in the ocular lens as AQP5 T259 phosphorylation was previously confirmed in human lens fiber cells[450]. Interestingly, we have learned that AQP5 serves additional roles outside of water transport, cellular differentiation, cellular migration, and cellular elongation. AQP5 peroxiporin function has been demonstrated in nonlenticular tissues and in the ocular lens[49,489,516]. AQP5 has also emerged as a regulator of cellular structure through its regulation of cell junction protein expression upon localization to the plasma membrane via C-terminal protein-protein interactions[154]. Furthermore, we have learned that AQP5 interacts with CDGSH iron-sulfur domain-containing protein 2, a protein which regulates Beclin 1-mediated autophagic induction at the endoplasmic reticulum, which opens the possibility of AQP5 regulating additional cellular processes such as autophagy[154]. Ultimately, the past seven years has given us a greater understanding of the unique role of AQP5 in lens osmotic balance, in the lens microcirculation system, and in other potential lenticular processes canonically unassociated with cellular water transport such as autophagy.

The long-term goals of lenticular AQP5 research are to better understand the unique role of AQP5 in ocular lens fiber cells, which comprise the bulk of lens cellular mass[5]. The unique role of AQP5 is of particular importance in the lens as the second aquaporin known to be expressed in mammalian lens fiber cells alongside AQP0[38,46]. One of the specific goals of this study was to better understand the regulation of lenticular AQP5 trafficking by examining bovine cortical lens fiber cells to determine the subcellular localization of cytoplasmic AQP5-containing vesicles prior to plasma membrane insertion. A combination of immunofluorescence and transmission electron microscopic analysis indicated that AQP5 trafficks to bovine lens cortical fiber membranes through autolysosome-mediated and possibly amphisome-mediated unconventional protein secretion. AQP5-containing cytoplasmic vesicles overlap with bovine lens fiber cell mitochondria which *appear* to be eliminated during this process without apparent degradation of cytoplasmic AQP5. Furthermore, AQP5 may represent a mitochondrial aquaporin in the incipient differentiating fiber cells of the lens modiolus, and AQP5 and lens mitochondrial proteins are co-expressed in the same cytoplasmic compartments in bovine lens fiber cells. Lastly, our histological analysis revealed that AQP5 localizes to fiber cell nuclei prior to nuclear elimination. Additional Western blot analysis revealed the PI3K/Akt/mTOR signaling pathway as a possible mechanism by which bovine lenticular autophagic induction is regulated. **Based on our preliminary data demonstrating nearly ubiquitous AQP5 and TOMM20 colocalization in cytoplasmic compartments in the bovine lens, we hypothesized that AQP5-containing cytoplasmic vesicles may represent autophagic structures and undergo regulated unconventional protein secretion into fiber cell plasma membranes in**

the bovine lens. Recent studies have shown that mitochondrial, Golgi apparatus, and ER elimination in the lens requires expression of the mitophagy receptor BNIP3L/NIX[310,375]. Moreover, PI3K[311] and mTOR[309] signaling inhibition were recently shown to induce autophagic clearance of lens subcellular organelles in the ocular lens with the PI3K/Akt signaling pathway directly implicated in mitochondrial and ER elimination and pan-PI3K inhibition implicated in complete fiber cell organelle degradation including cellular nuclei[311]. Despite the mounting evidence demonstrating autophagic clearance of lenticular mitochondria and our data showing unconventional protein secretion of AQP5 in the bovine lens, the specifics of AQP5 unconventional protein secretion in the bovine lens remain unclear including the possibility of AQP5 expression in active lenticular mitochondria and mechanistic details about the regulation of this process.

An additional specific goal of this study was to identify AQP5 interacting proteins and quantify relative AQP5 T259 phosphorylation in the bovine lens cortex and nucleus. In non-lenticular cells, AQP5 interacts via its C-terminus with cell junctional proteins ZO-1, plakoglobin, β-catenin, and desmoglein-2 at the plasma membrane[154] and putative subcellular localization regulatory proteins PIP and Mup4 in exocrine glands[422,436]. Thereby AQP5 regulates cell junctional protein expression at the plasma membrane in MDCK cells and appears to be regulated by PIP and Mup4 and localize to the plasma membrane and cytoplasmic respectively based on C-terminal binding with these interacting proteins. We conducted co-immunoprecipitation analysis to enrich AQP5 and proteomics analysis of co-immunoprecipitates to identify several *putative* AQP5 interactors in the bovine lens cortex and nucleus. In the bovine lens, cytoplasmic serine-tRNA ligase (seryl-tRNA synthetase), serine/threonine-protein kinase 24 (STK24; also known as mammalian STE20-like protein kinase 3 or MST3), sorting nexin 8 (SNX8), dolichyl-diphosphooligosaccharide-protein glycosyltransferase subunit 2 (RPN2; also known as ribophorin-II), and dolichyl-diphosphooligosaccharide-protein glycosyltransferase 48 kDa subunit (DDOST) were identified as putative AQP5 interactors in the cortex and RPN2 was identified as putative AQP5 interactor in the nucleus. **We hypothesized that AQP5 would interact with proteins which are associated with the process of autophagy in the bovine lens particularly in cortical fiber cells.** There are several lines of evidence that connect putative lenticular AQP5 interacting proteins to the cellular process of autophagy including knockdown experiments which implicate the involvement of proteins such as STK24 or immunolocalization experiments which implicate the involvement of proteins such as SNX8 and RPN2. Direct interaction between AQP5 and putative interactors in the bovine lens requires confirmation (i.e. reciprocal co-immunoprecipitation analysis). Furthermore, the direct involvement of lenticular AQP5 and the relationship between its putative interactors in the bovine lens and in the process of autophagy remains to be elucidated. Lastly, the role that C-terminal phosphorylation in the modulation of AQP5 protein-protein interactions in the bovine lens also requires investigation.

In conclusion, the results of the work presented in this dissertation provide a mechanism of AQP5 trafficking to the plasma membrane in bovine lens cortical fiber cells and evidence of a potential role for AQP5 in the constitutive lenticular process of autophagy via protein-protein interactions which may be modulated through AQP5 C-terminal phosphorylation. I have provided evidence of AQP5 as a potential mitochondrial aquaporin in the bovine lens and the first example of an aquaporin or lens protein inserted into the plasma membrane via unconventional protein secretion via autolysosomes. Lastly, I have provided evidence of additional phenomenon which we did not directly test but consistently observed such as nuclear expression of AQP5 and coincidental degradation of bovine lens mitochondria prior to AQP5 plasma membrane insertion. Further experimentation to address important remaining questions outlined below would provide additional information about the molecular and functional details of our results.

1. *Is AQP5 a mitochondrial aquaporin in the bovine lens?*

Our data demonstrate co-expression of AQP5 and mitochondrial markers TOMM20 and COX IV to the same cytoplasmic vesicles (Figures 3.5 and 3.6) in bovine lens cortical fiber cells. In the lens modiolus, several TOMM20-positive cytoplasmic structures exhibit no or minimal LC3B expression (Figure 3.7A). Our observations raise the possibility that AQP5 represents a mitochondrial aquaporin in the incipient, differentiating lens fiber cells of the bovine lens cortex. This possibility is strengthened by the observation by Varadaraj and Kumari 2020 that AQP5 exhibits peroxiporin function in the lens based on AQP5 genetic deletion experiments[49]. AQP8 and AQP9, the only two known mitochondrial aquaporins, function as peroxiporins and thereby resist accumulation of the reactive oxygen species (ROS) such as H_2O_2, a byproduct of aerobic respiration which is detrimental to proper mitochondrial function[119,484,486,487]. AQP8 is expressed in the lens epithelial cells and exhibits peroxiporin function in vitro in cultured human lens epithelial cells (HLEs)[48,49]. AQP5 also functions as a peroxiporin facilitating H_2O_2 transport in transfected cells[49,489] and in the lens with wild type mouse lenses containing significantly more H_2O_2 content relative to AQP5 knockout mouse lenses[49]. Thus, there are experimental data to support a role for AQP5 as a mitochondrial aquaporin through its peroxiporin function.

To answer this question, a combination of immunofluorescence analysis and *ex vivo* bovine lens culture could be applied to concurrently label AQP5-containing cytoplasmic vesicles and active mitochondria. Active mitochondria can be fluorescently labeled via an aldehyde-fixable MitoTracker probe, which accumulate and label active mitochondria based on mitochondrial membrane potential[517], in bovine lenses following *ex vivo* culture. Thereafter, these bovine lenses can be cryosectioned and analyzed for AQP5 expression in active mitochondria via existing immunofluorescence analysis methods outlined in Chapter 3 of this thesis dissertation. Image segmentation can be done to quantify the relative AQP5 expression levels in active bovine lenticular mitochondria and hypothetical regional changes in this expression including in bovine lens epithelial cells. Mitoprobe fluorescence specificity can be tested via control experiments which incorporate treatment with carbonyl cyanide m-chlorophenylhydrazone (CCCP) or carbonyl cyanide p-trifluoromethoxylphenyl-hydrazone (FCCP), which are a chemical uncouplers of electron transport chain that eliminate mitochondrial membrane potential and therefore MitoTracker staining[518–520].

Additionally, mitochondrial isolation and subsequent proteomics analysis could be conducted to define proteins which are present in bovine lens mitochondria. Such analysis could unambiguously identify the presence of AQP5 in these mitochondria. ImmunoTEM analysis could also be conducted to confirm proteomics findings.

2. *Do AQP5-containing vesicles simultaneously function as degradative autolysosomes in lenticular mitochondrial elimination and as secretory autolysosomes in unconventional secretion of lenticular AQP5 in the bovine lens?*

Our histological data demonstrate that AQP5-containing, TOMM20-containing cytoplasmic structures increasingly acquire expression of autolysosomal markers LC3B and LIMP-2. Furthermore, our data demonstrate that TOMM20 immunofluorescence is drastically reduced and largely disappears during fiber cell maturation in the bovine lens. Mitochondrial elimination occurs via autophagic degradation canonically in the literature[18,308,310,366,469]. Direct proof of autolysosomal AQP5-containing cytoplasmic vesicles degrading mitochondria in the bovine lens is essential to more clearly understand the role of AQP5 in the bovine lens and the connection between AQP5 expression and lens autophagy and mitochondrial dynamics.

To test degradative function of AQP5-containing cytoplasmic vesicles in the bovine lens, bovine lenses could be subjected to *ex vivo* culture and treatment with cell-permeable lysosome probes such as LysoTracker Red DND 99, which fluoresce specifically in acidic cytoplasmic vesicles like lysosomes. Our routine histological analysis could be applied to section bovine lenses following *ex vivo* culture and mitochondria can be labeled with TOMM20

or COX IV as in Chapter 3. Immunogold TEM analysis could be applied to identify AQP5-containing cytoplasmic vesicles and TOMM20 or COX IV in degrading mitochondria within autolysosomal compartments of the bovine lens. The progression of mitochondrial degradation could be tracked morphologically by this immunogold TEM experiment.

3. *What mechanisms directly underpin AQP5 unconventional protein secretion in the bovine lens?*

Our observation of unconventional protein secretion of AQP5 in the bovine lens via autolysosomes requires raises several questions about the mechanisms which underpin this process. Canonically, unconventional protein secretion of lysosomes is triggered via local, approximately micromolar intracellular calcium concentrations[381]. Secretory lysosomes dock at the plasma membrane and fuse upon this local increase of calcium via lysosomal TRP channel transient receptor potential mucolipin 1 (TRPML1)[391,521]. Therefore, artificially increasing local calcium concentration in the bovine lens cortical fiber cells could theoretically be induced via a cell-permeable calcium ionophore such as A23187 to test the conservation of calcium-induced autolysosome secretion in the lens.

Furthermore, we observed apparent docking and fusion of AQP5-containing cytoplasmic vesicles via immunofluorescence analysis and autophagic structures via transmission electron microscopy (TEM) analysis in the bovine lens. Cytoplasmic vesicle docking and fusion could be confirmed experimentally via electron tomography (i.e. three-dimensional TEM) analysis[522]. Immunogold electron tomography can be used to analyze AQP5-containing cytoplasmic vesicles and unequivocally identify subcellular localization, docking and fusion behavior, and test potential mechanisms of secretion[523]. We attempted AQP5 immunogold TEM prior to the completion of this dissertation (Chapter 3) but not immunogold electron tomography. AQP5 antibody antigenicity was lost upon tissue processing (i.e. cold methanol substitution) for immunogold TEM analysis. Thus, we were unsuccessful in our efforts, but multiple improvements could be made to overcome this limitation including use of a more hydrophilic resin or optimization of the glutaraldehyde concentration used for fixation[524,525].

Once fixation conditions are optimized to improve antigenicity of AQP5 antibodies following TEM processing, confirmation of AQP5-containing cytoplasmic vesicle docking and fusion behavior also requires optimization of our current TEM analysis protocol to improve resolution of the organelle membranes. To our knowledge, our work (Chapter 3) represents the third study in which transmission electron microscopy was applied to investigate subcellular structures in intact bovine lens fiber cells along with Kuszak et al. 1996 and Rose et al. 2006[493,526]. There are technical limitations to our current TEM protocol which require optimization and may have contributed to insufficient resolution in our TEM analysis to unequivocally conclude vesicular docking and fusion. Rapid fixation is essential to preserve morphology of mitochondria and autophagic structures[527,528], and bovine lens dissections can be performed at the abattoir rather than in the laboratory to reduce interim time between eye extraction and subsequent immersion fixation. Additionally, fixative composition can be further optimized to yield better resolution of organelle membranes such as the inner and outer limiting membranes of autophagosomes and the membranes of mitochondria[529,530].

With these improvements, we could begin to investigate why mitochondria appear to be degraded based on loss of mitochondrial protein immunofluorescence while AQP5 immunofluorescence localizes to fiber cell plasm membranes. Immunogold electron tomography could be used to observe mitochondria throughout the cortex as fiber cells differentiate to better understand the dichotomy in AQP5 plasma membrane insertion and drastic reduction of mitochondrial proteins

4. *Does AQP5 traffick to the plasma membrane in bovine lens fiber cells via amphisome-mediated unconventional protein secretion?*

Using TOMM20 expression as a proxy for AQP5 expression, our histological analysis of AQP5-containing cytoplasmic vesicles in bovine lens cortical fiber cells (Chapter 3) revealed TOMM20-positive cytoplasmic structures which progressively acquire LC3B and LIMP-2 expression and are *apparently* negative for Sec22β expression during cellular maturation. Subsequently, AQP5 is inserted into the plasma membrane. Thus, our results are indicative of unconventional secretion of lenticular AQP5 via autolysosomes in the bovine lens cortex. Degradative autophagosomes fuse with lysosomes via an amphisome intermediate[445,531]. That is, mature autophagosomes fuse with late endosomes/multivesicular bodies (MVBs) to form amphisomes which then fuse with lysosomes to form autolysosomes whose cargo is subsequently degraded. Consequently, amphisomes are comprised of marker proteins indicative of autophagosomes and distinguishing the two from each other and autolysosomes requires the identifying the expression of autophagosome specific marker proteins such as LC3B *and* late endosome marker proteins such as Rab7[391,445,531]. Distinguishing amphisomes from autolysosomes requires the absence of lysosomal marker expression such as LIMP-2 or lysosome-associated membrane glycoprotein 1 (LAMP-1)[391,532].

Given the challenge of simultaneously and unambiguously distinguishing AQP5-containing cytoplasmic vesicles (i.e. TOMM20-containing cytoplasmic structures), autophagosomes, amphisomes, autolysosomes, and lysosomes via immunofluorescence, immunogold electron tomography represents a straightforward technique by which to identify amphisomes. Amphisomes can be identified morphologically via process of elimination. Two dimensional and three dimensional transmission electron microscopy are routinely applied to identify autophagic structures and vesicular fusion, respectively[345,533,534]. Two dimensional TEM was applied recently to identify both autophagosomes and autolysosomes in lenticular epithelial and fiber cells[308]. Thus, these structures should be more readily apparent in bovine lens tissue with improvement of our current immunologically and fusion of these structures. Evidence of autophagic structures which exhibit Rab7 immunogold labeling, lack lysosome marker protein immunolabeling (e.g. LIMP-2 or LAMP-1), and undergo fusion with the plasma membrane would be suggestive of unconventional protein secretion in the bovine lens via amphisome-intermediates. If such structures are empirically determined to be morphologically distinct, then AQP5 immunogold labeling could then be used to directly confirm this route of secretion as a mechanism of AQP5-containing cytoplasmic vesicular trafficking to fiber cell plasma membranes in the bovine lens cortex.

5. *Is unconventional protein secretion of AQP5 via autolysosomes a conserved process in other mammalian lenses?*

To our knowledge, our histological analysis of bovine lenticular AQP5-containing cytoplasmic vesicles (Chapter 3) represents the first to molecularly classify the identity (i.e. subcellular localization) of cytoplasmic AQP5-containing compartments in the ocular lens. The conservation of this process in the ocular lens is unclear. The morphological dimensions of lenticular AQP5-containing cytoplasmic vesicles in the bovine lens are noteworthy in comparison to those depicted in axial (i.e. horizontal/sagittal) lens tissue sections in the published literature[40,111,116]. There are no reported AQP5-containing cytoplasmic vesicles in the ocular lens comprised of micrometer-sized spheroid domains or tubular domains up to tens of microns in length. Our results are suggestive of unique AQP5 cytoplasmic subcellular localization in the bovine lens in comparison to mouse, rat, human, and rabbit lenses.

Though there is some debate regarding necessity of autophagic degradation broadly via canonical autophagy in lenticular organelle degradation[307,363,364], mitochondrial elimination via autophagy appears to be conserved in mammalian lenses[308–310,375,469]. Thus, conservation of unconventional AQP5 secretion to the plasma membrane in the ocular lens via autolysosomes

remains an open question. This question can be tackled by analysis of lenses from multiple species and conducting the same histological analyses that we have conducted in our current study. We have no concrete rationale to suggest why unconventional protein secretion of AQP5 might occur in the bovine lens or whether this is the primary mechanism by which AQP5 is trafficked to the plasma membrane in the bovine lens. One speculative reason might be the size of bovine lens fiber cells. Bovine lens fiber cells are up to 20 mm in length, which is significantly longer than mouse or rat lens fiber cells[535]. Elongation of cells such as bovine lens fiber cells require large amounts of plasma membrane which is overcome in cells with similar plasma membrane requirements for cellular elongation such as neurons through secretion of exosomes and lysosomes. For example, neurite outgrowth requires exocytosis of late endosomes and lysosomes for the elongation of the developing neuronal processes[536]. Perhaps, unconventional protein secretion of AQP5 via autolysosomes in the bovine lens occur for similar reasons. This can be tested by histological examination of AQP5-containing cytoplasmic vesicles in mammalian lenses of various lens fiber cell lengths to identify any correlation with unconventional protein secretion. If such a correlation exists, AQP5 secretion to fiber cell plasma membranes via autolysosomes would be more likely to occur in rabbit or ovine lenses but not in mouse or rat lenses.

6. *Does AQP5 C-terminal phosphorylation play a role in AQP5 secretion to the plasma membrane?*

Based on our histological analysis (Chapter 4), AQP5 pT259 expression remains localized to cytoplasmic compartments throughout fiber cell maturation. To our knowledge, cytoplasmic AQP5 expression in nuclear fiber cells has not been reported in the literature. This novel finding raises several questions and it is critical to understand the relationship between AQP5 C-terminal T259 phosphorylation and subcellular localization in bovine lens fiber cells. AQP5 T259 phosphorylation is not directly correlated to cellular secretion of AQP5 to the plasma membrane[156,438]. Nevertheless, AQP5 T259 is homologous to AQP2 S256, whose phosphorylation regulates its plasma membrane secretion and expression levels[153,515,537].

Total AQP5 pT259 expression can be directly upregulated pharmacologically through induction of protein kinase A activity (PKA) via agonism of β-adrenergic receptors with isoproterenol[156]. Lens fiber cells express PKA whose activity can be upregulated via isoproterenol-mediated agonism of lenticular adrenergic β-adrenergic receptors[538]. To test if AQP5 pT259 expression can be inducibly increased, bovine lenses can be *ex vivo* cultured and treated with isoproterenol. If there is an increase in AQP5 pT259 expression, general changes in AQP5 and AQP5 pT259 subcellular localization can be analyzed via our histological protocols. While it is difficult to test the effects of AQP5 T259 phosphorylation without the use of genetic engineering techniques, correlations can be drawn between changes in subcellular localization and phosphorylated AQP5

7. *Are the putative AQP5 interacting proteins true interactors? Do these interacting proteins directly interact with AQP5?*

In our co-immunoprecipitation analysis, we specifically enriched for AQP5 directly using anti-AQP5 IgG antibodies and conducted proteomics analysis to identify *putative* AQP5 interactors in the bovine lens. These *putative* interactors require confirmation via reciprocal co-immunoprecipitation analysis which result in the enrichment of AQP5 to confirm that they are true AQP5 interacting proteins. To test for direct AQP5 interaction, AQP5 and putative AQP5 interactors in the bovine lens could first be purified and reconstituted in liposomes. Thereafter, AQP5 and putative bovine lenticular interactors could be subjected to AQP5 co-immunoprecipitation and reciprocal co-immunoprecipitation for stoichiometric enrichment using Western blot analysis. AQP5 C-terminal peptide competition assays could be applied as an additional control to confirm direct interactions.

8. *Are there additional putative AQP5 interacting proteins which were undetected by our AQP5 co-immunoprecipitation analyses?*

We enriched for AQP5 in our co-immunoprecipitation analyses using an anti-AQP5 IgG antibody whose immunogen is the AQP5 C-terminus. As stated above, the AQP C-terminus is the primary binding site of AQP interacting proteins. This holds true for known AQP5 interacting proteins. Moreover, we were unable to fully immunodeplete AQP5 from cortical or nuclear bovine lens fiber cell membranes (Figure 4.1), and the amount of AQP5 which we could immunodeplete plateaued despite increasing amounts of anti-AQP5 IgG in optimization experiments (*data not shown*). These results suggest steric hindrance to a portion of AQP5 protein in the bovine lens, and it is therefore reasonable to propose that the "co-immunoprecipitation resistant" portion of bovine lens fiber cell AQP5 may interact with additional proteins which were not identified in our current co-immunoprecipitation analyses.

To address this experimental limitation and broaden identification of putative AQP5 interacting proteins in the bovine lens, we could repeat our current AQP5 co-immunoprecipitation analysis using a commercially developed antibody (e.g. from ThermoFisher) targeted towards whole, purified bovine AQP5 protein. We could roughly purify AQP5 from bovine lenses, salivary gland, lacrimal glands, or corneas using a combination of size exclusion and ion exchange chromatography. Roughly purified, AQP5-containing membrane fractions could then be further purified via affinity chromatography using currently available anti-AQP5 antibodies targeted towards the AQP5 C-terminus. Such affinity chromatography experiments could be designed to immunoprecipitate AQP5 (i.e. rather than co-immunoprecipitate AQP5) and thereby incorporate use of harsher buffers such as RIPA buffer to better access the AQP5 C-terminus antigen for enhanced AQP5 enrichment and purification. We have successfully purified AQP5 via immunoprecipitation using RIPA buffer (*data not shown*), so we could adapt the associated protocol for this purpose. AQP5 purification quality could be determined via a SDS PAGE of AQP5 immunoprecipitates combined with Coomassie blue, Western blot, and mass spectrometric analysis. Sufficiently pure AQP5 could be submitted to commercial vendors for antibody development.

Following antibody development, current AQP5 co-immunoprecipitation protocols combined with Western blot and mass spectrometric analyses would be repeated as outlined in Chapter 4 to identify additional putative AQP5 interacting proteins in the bovine lens. Additional, putative bovine lenticular AQP5 interacting proteins can be confirmed via reciprocal co-immunoprecipitation and liposome reconstitution assays (as outlined above) combined with protein competition assays to confirm direct AQP5 protein-protein interactions.

9. *Does AQP5 play a direct role in regulation of bovine lenticular mitochondrial autophagy?*

There is crosstalk between autophagy and oxidative stress in which H_2O_2 blocks the progression of autophagy via reversible inhibition of ATG4[490,491]. Thus, AQP5 peroxiporin function is a plausible role for *putative* AQP5 incorporation into mitochondria and incorporation into autophagic vesicles in the bovine lens fiber cells. To determine whether AQP5 has a direct role in the regulation of autophagic mitochondrial elimination in the bovine lens, expression plasmids encoding AQP5 siRNA or shRNA under a fiber cell specific promoter such as the AQP0 or βB1-crystallin promoter could be microinjected into *ex vivo* cultured bovine lenses as outlined in Shestopalov and Bassnett 1999[539]. Green fluorescent protein (GFP) or CD46 could be incorporated into such plasmids and transfected into control lenses as necessary to confirm proper plasmid encoded protein expression. Knockdown of AQP5 mRNA transcript expression could be confirmed via fluorescence *in situ* hybridization[540], and knockdown of AQP5 protein expression can be confirmed histologically via AQP5 immunofluorescence analysis. The power of the techniques applied by Shestopalov and Bassnett 1999 is that fiber cell knockdown of

AQP5 can be selectively performed so cellular layers within a specific lens region are targeted while other lens fiber cell regions would remain unperturbed.

Thus, AQP5 expression could be targeted at different stages of fiber cell differentiation. An experiment could be designed to knockdown AQP5 expression prior to fiber cell differentiation or following the process of mitochondrial incorporation into autophagic structures to determine if mitochondrial organelle degradation occurs as normal. Furthermore, bovine lenses with AQP5 expression knockdown could be tested for oxidative stress related changes in autophagic mitochondrial elimination in the lens. Quantitative H_2O_2 analysis can be done as outlined in Varadaraj and Kumari 2020 using the H_2O_2-specific probe AbGreen, which is cell-permeable and reacts with H_2O_2 to produce green fluorescence[49]. AQP5 knockout mouse lenses were analyzed following *ex vivo* culture with AbGreen probe and exposure to H_2O_2 revealing a specific role for AQP5 in reduction of whole lens H_2O_2. The same analysis could be conducted using bovine lenses with knocked down AQP5 expression.

REFERENCES

1. Cramer, A. *Het accommodatievermogen dere oogen physiologisch toegelicht*. (De erven Loosjes, 1853).
2. Den Tonkelaar, I., Henkes, H. E. & Van Leersum, G. K. Antonie Cramer's explanation of accommodation. *Doc. Ophthalmol.* **74**, 87–93 (1990).
3. Palanker, D. Optical Properties of the Eye. *American Academy of Ophthalmology* https://www.aao.org/munnerlyn-laser-surgery-center/optical-properties-of-eye (2013).
4. Schematic diagram of the human eye. *National Eye Institute Media Library* https://medialibrary.nei.nih.gov/search?keywords=&f[0]=category:6#/media/1821.
5. Cvekl, A. & Ashery-Padan, R. The cellular and molecular mechanisms of vertebrate lens development. *Development* **141**, 4432–4447 (2014).
6. Song, S. *et al.* Functions of the intermediate filament cytoskeleton in the eye lens. *J Clin Invest* **119**, 1837–1848 (2009).
7. Bhat, S. P. The ocular lens epithelium. *Biosci Rep* **21**, 537–563 (2001).
8. Mathias, R. T., Rae, J. L. & Baldo, G. J. Physiological Properties of the Normal Lens. *Physiol. Rev.* **77**, 21–50 (1997).
9. Andley, U. P. The lens epithelium: Focus on the expression and function of the α-crystallin chaperones. *Int. J. Biochem. Cell Biol.* **40**, 317–323 (2008).
10. Wiley, L. A., Shui, Y. B. & Beebe, D. C. Visualizing lens epithelial cell proliferation in whole lenses. *Mol. Vis.* **16**, 1253–1259 (2010).
11. Mochizuki, T. & Masai, I. The lens equator: A platform for molecular machinery that regulates the switch from cell proliferation to differentiation in the vertebrate lens. *Dev. Growth Differ.* **56**, 387–401 (2014).
12. DELAYE, M. & TARDIEU, A. Short-range order of crystallin proteins accounts for eye lens transparency. *Nature* **302**, 415–417 (1983).
13. Taylor, V. L. *et al.* Morphology of the normal human lens. *Investig. Ophthalmol. Vis. Sci.* **37**, 1396–1410 (1996).
14. Kuwabara, T. & Imaizumi, M. Denucleation process of the lens. *Invest. Ophthalmol.* **13**, 973–981 (1974).
15. Kuwabara, T. The maturation of the lens cell: a morphologic study. *Exp. Eye Res.* **20**, 427–443 (1975).
16. Vrensen, G. F. J. M., Graw, J. & De Wolf, A. Nuclear breakdown during terminal differentiation of primary lens fibres in mice: A transmission electron microscopic study. *Exp. Eye Res.* **52**, 647–659 (1991).
17. Wride, M. A. Lens fibre cell differentiation and organelle loss: many paths lead to clarity. *Philos. Trans. R. Soc. Lond. B. Biol. Sci.* **366**, 1219–1233 (2011).
18. Bassnett, S. The fate of the Golgi apparatus and the endoplasmic reticulum during lens fiber cell differentiation. *Investig. Ophthalmol. Vis. Sci.* **36**, 1793–1803 (1995).
19. Al-Ghoul, K. J., Taylor, V. L. & Costello, M. J. Light Microscopic Variation of Fiber Cell Size, Shape and Ordering in the Equatorial Plane of Bovine and Human Lenses. *Investig. Ophthalmol. Vis. Sci.* **37**, 0–4 (1996).
20. Schey, K. L., Petrova, R. S., Gletten, R. B. & Donaldson, P. J. The role of aquaporins in ocular lens homeostasis. *Int. J. Mol. Sci.* **18**, 1–17 (2017).
21. Artal, P. & Guirao, A. Contributions of the cornea and the lens to the aberrations of the human eye. *Opt. Lett.* **23**, 1713–1715 (1998).
22. Kato, K. *et al.* Immunoreactive αA crystallin in rat non-lenticular tissues detected with a sensitive immunoassay method. *Biochim. Biophys. Acta (BBA)/Protein Struct. Mol.* **1080**, 173–180 (1991).
23. Srinivasan, A. N., Nagineni, C. N. & Bhat, S. P. αA-crystallin is expressed in non-ocular

tissues. *J. Biol. Chem.* **267**, 23337–23341 (1992).
24. Bloemendal, H. *et al.* Ageing and vision: Structure, stability and function of lens crystallins. *Prog. Biophys. Mol. Biol.* **86**, 407–485 (2004).
25. Broide, M. L., Berland, C. R., Pande, J., Ogun, O. O. & Benedek, G. B. Binary-liquid phase separation of lens protein solutions. *Proc. Natl. Acad. Sci. U. S. A.* **88**, 5660–5664 (1991).
26. Slingsby, C., Wistow, G. J. & Clark, A. R. Evolution of crystallins for a role in the vertebrate eye lens. *Protein Sci.* **22**, 367–380 (2013).
27. Alberti, S. & Hyman, A. A. Are aberrant phase transitions a driver of cellular aging? *BioEssays* **38**, 959–968 (2016).
28. Hu, X. *et al.* Expression of neovascular associated factors PEDF and αB-crystallin in human lens epithelial cells. *Curr. Eye Res.* **45**, 1385–1389 (2020).
29. Jong, W. W. De, Caspers, G. & Leunissen, J. A. M. Genealogy of the alpha-crystallin--small heat-shock protein superfamily. *Int J Biol Macromol* **22**, 151–162 (1998).
30. Siezen, R. J., Fisch, M. R., Slingsby, C. & Benedek, G. B. Opacification of γ-crystallin solution from calf lens in relation to cold cataract formation. *Proc. Natl. Acad. Sci. U. S. A.* **82**, 1701–1705 (1985).
31. Horwitz, J. The function of alpha-crystallin in vision. *Semin. Cell Dev. Biol.* **11**, 53–60 (2000).
32. Horwitz, J. α-Crystallin can function as a molecular chaperone. *Proc. Natl. Acad. Sci. U. S. A.* **89**, 10449–10453 (1992).
33. Wistow, G. & Slingsby, C. *Structure and evolution of crystallins*. *Encyclopedia of the Eye* (Academic Press, 2010). doi:10.1016/B978-0-12-809324-5.01525-X.
34. de Jong, W. W. Evolution of lens and crystallins. in *Molecular and Cellular Biology of the Eye Lens* (ed. Bloemendal, H.) 221–278 (Wiley, 1981).
35. Pierscionek, B., Smith, G. & Augusteyn, R. C. The refractive increments of bovine alpha-, beta-, and gamma-crystallins. *Vis. Res* **27**, 1539–1541 (1987).
36. Agre, P., Sasaki, S. & Chrispeels, M. J. Aquaporins: a family of water channel proteins. *Am J Physiol* **265**, F461 (1993).
37. Broekhuyse, R. M., Kuhlmann, E. D. & Stols, A. L. H. Lens membranes II. Isolation and characterization of the main intrinsic polypeptide (MIP) of bovine lens fiber membranes. *Exp. Eye Res.* **23**, 365–371 (1976).
38. Bok, D., Dockstader, J. & Horwitz, J. Immunocytochemical localization of the lens main intrinsic polypeptide (MIP26) in communicating junctions. *J. Cell Biol.* **92**, 213–220 (1982).
39. Fitzgerald, P. G., Bok, D. & Horwitz, J. Immunocytochemical localization of the main intrinsic polypeptide (MIP) in ultrathin frozen sections of rat lens. *J. Cell Biol.* **97**, 1491–1499 (1983).
40. Bogner, B. *et al.* Aquaporin expression and localization in the rabbit eye. *Exp. Eye Res.* **147**, 20–30 (2016).
41. Hasegawa, H., Lian, S. C., Finkbeiner, W. E. & Verkman, A. S. Extrarenal tissue distribution of CHIP28 water channels by in situ hybridization and antibody staining. *Am. J. Physiol. - Cell Physiol.* **266**, C893–C903 (1994).
42. Ruiz-Ederra, J. & Verkman, A. S. Accelerated cataract formation and reduced lens epithelial water permeability in aquaporin-1-deficient mice. *Investig. Ophthalmol. Vis. Sci.* **47**, 3960–3967 (2006).
43. Wang, Z., Han, J. & Schey, K. L. Spatial differences in an integral membrane proteome detected in laser capture microdissected samples. *J Proteome Res* **7**, 2696–2702 (2008).
44. Bassnett, S., Wilmarth, P. A. & David, L. L. The membrane proteome of the mouse lens fiber cell. *Mol. Vis.* **15**, 2448–63 (2009).
45. Sindhu Kumari, S., Varadaraj, M., Yerramilli, V. S., Menon, A. G. & Varadaraj, K. Spatial

expression of aquaporin 5 in mammalian cornea and lens, and regulation of its localization by phosphokinase A. *Mol Vis* **18**, 957–967 (2012).
46. Grey, A. C. *et al.* Verification and spatial localization of aquaporin-5 in the ocular lens. *Exp. Eye Res.* **108**, 94–102 (2013).
47. Tran, T. L. *et al.* Aquaporins 6-12 in the human eye. *Acta Ophthalmol.* **91**, 557–563 (2013).
48. Hayashi, R., Hayashi, S., Fukuda, K., Sakai, M. & Machida, S. Immunolocation of Aquaporin 8 in Human Cataractous Lenticular Epithelial Cells. *Biomed. Hub* **2**, 1–5 (2017).
49. Varadaraj, K. & Kumari, S. S. Lens aquaporins function as peroxiporins to facilitate membrane transport of hydrogen peroxide. *Biochem. Biophys. Res. Commun.* **524**, 1025–1029 (2020).
50. Fushimi, K. *et al.* Cloning and expression of apical membrane water channel of rat kidney collecting tubule. *Nature* **361**, 549–552 (1993).
51. Ishibashi, K. *et al.* Molecular cloning and expression of a member of the aquaporin family with permeability to glycerol and urea in addition to water expressed at the basolateral membrane of kidney collecting duct cells. *Proc. Natl. Acad. Sci. U. S. A.* **91**, 6269–6273 (1994).
52. Ishibashi, K. *et al.* Molecular characterization of human Aquaporin-7 gene and its chromosomal mapping. *Biochim. Biophys. Acta - Gene Struct. Expr.* **1399**, 62–66 (1998).
53. Elkjær, M. L. *et al.* Immunolocalization of aquaporin-8 in rat kidney, gastrointestinal tract, testis, and airways. *Am. J. Physiol. - Ren. Physiol.* **281**, F1047-1057 (2001).
54. Hatakeyama, S. *et al.* Cloning of a new aquaporin (AQP10) abundantly expressed in duodenum and jejunum. *Biochem. Biophys. Res. Commun.* **287**, 814–819 (2001).
55. Ishibashi, K. *et al.* Molecular cloning of a new aquaporin superfamily in mammals: AQPX1 and AQPX2. in *Molecular Biology and Physiology of Water and Solute Transport* (eds. Hohmann, S. & Nielsen, S.) 123–126 (Kluwer Academic/Plenum Publishers, 2000). doi:DOI https://doi.org/10.1007/978-1-4615-1203-5_17.
56. Schey, K. L., Wang, Z., L. Wenke, J. & Qi, Y. Aquaporins in the eye: Expression, function, and roles in ocular disease. *Biochim. Biophys. Acta - Gen. Subj.* **1840**, 1513–1523 (2014).
57. Yang, B. & Verkman, A. S. Water and glycerol permeabilities of aquaporins 1-5 and MIP determined quantitatively by expression of epitope-tagged constructs in Xenopus oocytes. *J. Biol. Chem.* **272**, 16140–16146 (1997).
58. Shiels, A. *et al.* Optical dysfunction of the crystalline lens in aquaporin-0-deficient mice. *Physiol. Genomics* **7**, 179–186 (2001).
59. Gonen, T., Cheng, Y., Kistler, J. & Walz, T. Aquaporin-0 membrane junctions form upon proteolytic cleavage. *J. Mol. Biol.* **342**, 1337–1345 (2004).
60. Pao, G. M. *et al.* Evolution of the MIP family of integral membrane transport proteins. *Mol. Microbiol.* **5**, 33–37 (1991).
61. Al-Ghoul, K. J. *et al.* Lens structure in MIP-deficient mice. *Anat Rec A Discov Mol Cell Evol Biol* **273**, 714–730 (2003).
62. Kumari, S. S. & Varadaraj, K. Intact AQP0 performs cell-to-cell adhesion. *Biochem. Biophys. Res. Commun.* **390**, 1034–1039 (2009).
63. Liu, J., Xu, J., Gu, S., Nicholson, B. J. & Jiang, J. X. Aquaporin 0 enhances gap junction coupling via its cell adhesion function and interaction with connexin 50. *J. Cell Sci.* **124**, 198–206 (2011).
64. Varadaraj, K., Kumari, S. S. & Mathias, R. T. Transgenic expression of AQP1 in the fiber cells of AQP0 knockout mouse: Effects on lens transparency. *Exp. Eye Res.* **91**, 393–404 (2010).
65. Kumari, S. S., Eswaramoorthy, S., Mathias, R. T. & Varadaraj, K. Unique and analogous

functions of aquaporin 0 for fiber cell architecture and ocular lens transparency. *Biochim. Biophys. Acta - Mol. Basis Dis.* **1812**, 1089–1097 (2011).
66. Hu, S., Wang, B., Qi, Y. & Lin, H. The Arg233Lys AQP0 mutation disturbs aquaporin0-calmodulin interaction causing polymorphic congenital cataract. *PLoS One* **7**, e37637 (2012).
67. Senthil Kumar, G. *et al.* An MIP/AQP0 mutation with impaired trafficking and function underlies an autosomal dominant congenital lamellar cataract. *Exp. Eye Res.* **110**, 136–141 (2013).
68. Kumari, S. S., Gandhi, J., Mustehsan, M. H., Eren, S. & Varadaraj, K. Functional characterization of an AQP0 missense mutation, R33C, that causes dominant congenital lens cataract, reveals impaired cell-to-cell adhesion. *Exp. Eye Res.* **116**, 371–385 (2013).
69. Song, Z., Wang, L., Liu, Y. & Xiao, W. A novel nonsense mutation in the MIP gene linked to congenital posterior polar cataracts in a Chinese family. *PLoS One* **10**, e0119296 (2015).
70. Sindhu Kumari, S. *et al.* Role of Aquaporin 0 in lens biomechanics. *Biochem. Biophys. Res. Commun.* **462**, 339–345 (2015).
71. Nielsen, S., Smith, B. L., Christensen, E. I. & Agre, P. Distribution of the aquaporin CHIP in secretory and resorptive epithelia and capillary endothelia. *Proc. Natl. Acad. Sci. U. S. A.* **90**, 7275–7279 (1993).
72. Au, C. G. *et al.* Changes in skeletal muscle expression of AQP1 and AQP4 in dystrophinopathy and dysferlinopathy patients. *Acta Neuropathol.* **116**, 235–246 (2008).
73. Solenov, E. I., Vetrivel, L., Oshio, K., Manley, G. T. & Verkman, A. S. Optical measurement of swelling and water transport in spinal cord slices from aquaporin null mice. *J. Neurosci. Methods* **113**, 85–90 (2002).
74. Nielsen, S., Smith, B. L., Christensen, E. I., Knepper, M. A. & Agre, P. CHIP28 water channels are localized in constitutively water-permeable segments of the nephron. *J. Cell Biol.* **120**, 371–383 (1993).
75. Saadoun, S., Papadopoulos, M. C., Hara-Chikuma, M. & Verkman, A. S. Impairment of angiogenesis and cell migration by targeted aquaporin-1 gene disruption. *Nature* **434**, 786–792 (2005).
76. Ernst, S. A., Palacios, J. R. & Siegel, G. J. Immunocytochemical localization of Na+,K+-ATPase catalytic polypeptide in mouse choroid plexus. *J. Histochem. Cytochem.* **34**, 189–195 (1986).
77. Wu, Q., Delpire, E., Hebert, S. C. & Strange, K. Functional demonstration of Na+-K+-2Cl- cotransporter activity in isolated, polarized choroid plexus cells. *Am. J. Physiol. - Cell Physiol.* **275**, 1565–1572 (1998).
78. Ma, T. *et al.* Severely impaired urinary concentrating ability in transgenic mice lacking aquaporin-1 water channels. *J. Biol. Chem.* **273**, 4296–4299 (1998).
79. Stamer, W. D., Snyder, R. W., Smith, B. L., Agre, P. & Regan, J. W. Localization of aquaporin CHIP in the human eye: Implications in the pathogenesis of glaucoma and other disorders of ocular fluid balance. *Investig. Ophthalmol. Vis. Sci.* **35**, 3867–3872 (1994).
80. Funaki, H. *et al.* Localization and expression of AQP5 in cornea, serous salivary glands, and pulmonary epithelial cells. *Am J Physiol* **275**, C1151–C1157 (1998).
81. Hamann, S. *et al.* Aquaporins in complex tissues: distribution of aquaporins 1-5 in human and rat eye. *Am J Physiol* **274**, C1332-45 (1998).
82. Li, J., Kuang, K., Nielsen, S. & Fischbarg, J. Molecular identification and immunolocalization of the water channel protein aquaporin 1 in CBCECs. *Investig. Ophthalmol. Vis. Sci.* **40**, 1288–1292 (1999).
83. Yoshimichi, G., Yoshimatsu, H., Masaki, T. & Sakata, T. Immunocytochemical localization of aquaporin-1 in bovine corneal endothelial cells and keratocytes. *Exp. Biol. Med.* **226**,

463–467 (2001).
84. Macnamara, E. *et al.* Aquaporin-1 expression is decreased in human and mouse corneal endothelial dysfunction. *Mol. Vis.* **10**, 51–56 (2004).
85. Verkman, A. S., Ruiz-Ederra, J. & Levin, M. H. Functions of aquaporins in the eye. *Prog. Retin. Eye Res.* **27**, 420–433 (2008).
86. Thiagarajah, J. R. & Verkman, A. S. Aquaporin deletion in mice reduces corneal water permeability and delays restoration of transparency after swelling. *J. Biol. Chem.* **277**, 19139–19144 (2002).
87. Sasaki, S. *et al.* Cloning, characterization, and chromosomal mapping of human aquaporin of collecting duct. *J Clin Invest* **93**, 1250–1256 (1994).
88. Verkman, A. S., Anderson, M. O. & Papadopoulos, M. C. Aquaporins: Important but elusive drug targets. *Nat. Rev. Drug Discov.* **13**, 259–277 (2014).
89. Verkerk, A. O., Lodder, E. M. & Wilders, R. Aquaporin channels in the heart—physiology and pathophysiology. *Int. J. Mol. Sci.* **20**, 1–20 (2019).
90. Ikeda, M. & Matsuzaki, T. Regulation of aquaporins by vasopressin in the kidney. *Vitam Horm* **98**, 307–337 (2015).
91. Jung, H. J. & Kwon, T.-H. Molecular mechanisms regulating aquaporin-2 in kidney collecting duct. *Am. J. Physiol. - Ren. Physiol.* **311**, F1318–F1328 (2016).
92. Yang, B., Gillespie, A., Carlson, E. J., Epstein, C. J. & Verkman, A. S. Neonatal Mortality in an Aquaporin-2 Knock-in Mouse Model of Recessive Nephrogenic Diabetes Insipidus. *J. Biol. Chem.* **276**, 2775–2779 (2001).
93. Nakahigashi, K. *et al.* Upregulation of aquaporin-3 is involved in keratinocyte proliferation and epidermal hyperplasia. *J. Invest. Dermatol.* **131**, 865–873 (2011).
94. Ishibashi, K. *et al.* Immunolocalization and effect of dehydration on AQP3, a basolateral water channel of kidney collecting ducts. *Am. J. Physiol. - Ren. Physiol.* **272**, (1997).
95. Hara-Chikuma, M. *et al.* Chemokine-dependent T cell migration requires aquaporin-3-mediated hydrogen peroxide uptake. *J. Exp. Med.* **209**, 1743–1752 (2012).
96. Ma, T. *et al.* Nephrogenic diabetes insipidus in mice lacking aquaporin-3 water channels. *Proc Natl Acad Sci U S A* **97**, 4386–4391 (2000).
97. Hasegawa, H., Ma, T., Skach, W., Matthay, M. A. & Verkman, A. S. Molecular cloning of a mercurial-insensitive water channel expressed in selected water-transporting tissues. *J Biol Chem* **269**, 5497–5500 (1994).
98. Rash, J. E. & Ellisman, M. H. Studies of excitable membranes. I. Macromolecular specializations of the neuromuscular junction and the nonjunctional sarcolemma. *J. Cell Biol.* **63**, 567–586 (1974).
99. Wolburg, H., Wolburg-Buchholz, K., Fallier-Becker, P., Noell, S. & Mack, A. F. *Structure and Functions of Aquaporin-4-Based Orthogonal Arrays of Particles*. *International Review of Cell and Molecular Biology* vol. 287 (Elsevier Inc., 2011).
100. Dermietzel, R. Visualization by freeze-fracturing of regular structures in glial cell membranes. *Naturwissenschaften* **60**, 208 (1973).
101. Frigeri, A., Gropper, M. A., Turck, C. W. & Verkman, A. S. Immunolocalization of the mercurial-insensitive water channel and glycerol intrinsic protein in epithelial cell plasma membranes. *Proc Natl Acad Sci U S A .* **92**, 4328–4331 (1995).
102. Manley, G. T. *et al.* Aquaporin-4 deletion in mice reduces brain edema after acute water intoxication and ischemic stroke. *Nat. Med.* **6**, 159–163 (2000).
103. Yang, B., Zador, Z. & Verkman, A. S. Glial cell aquaporin-4 overexpression in transgenic mice accelerates cytotoxic brain swelling. *J. Biol. Chem.* **283**, 15280–15286 (2008).
104. Shibuya, S. & Wakayama, Y. Freeze-fracture studies of myofiber plasma membrane in X chromosome-linked muscular dystrophy (mdx) mice. *Acta Neuropathol.* **76**, 179–184 (1988).
105. Wakayama, Y. *et al.* Reduced aquaporin 4 expression in the muscle plasma membrane

of patients with Duchenne muscular dystrophy. *Arch. Neurol.* **59**, 431–437 (2002).
106. Raina, S., Preston, G. M., Guggino, W. B. & Agre, P. Molecular cloning and characterization of an aquaporin cDNA from salivary, lacrimal, and respiratory tissues. *J Biol Chem* **270**, 1908–1912 (1995).
107. Nejsum, L. N. *et al.* Functional requirement of aquaporin-5 in plasma membranes of sweat glands. *Proc. Natl. Acad. Sci. U. S. A.* **99**, 511–516 (2002).
108. Matsuzaki, T. *et al.* Immunolocalization of the water channel, aquaporin-5 (AQP5), in the rat digestive system. *Arch Histol Cytol* **66**, 307–315 (2003).
109. Ehlers, N. & Hjortdal, J. Corneal thickness: Measurement and implications. *Exp. Eye Res.* **78**, 543–548 (2004).
110. Sindhu Kumari, S. & Varadaraj, K. Aquaporin 5 knockout mouse lens develops hyperglycemic cataract. *Biochem. Biophys. Res. Commun.* **441**, 333–338 (2013).
111. Petrova, R. S. *et al.* Dynamic functional contribution of the water channel AQP5 to the water permeability of peripheral lens fiber cells. *Am. J. Physiol. - Cell Physiol.* **314**, C191–C201 (2018).
112. Tang, S. *et al.* AQP5 regulates vimentin expression via miR-124–3p.1 to protect lens transparency. *Exp. Eye Res.* **205**, 108485 (2021).
113. Gao, J., Sun, X., White, T. W., Delamere, N. A. & Mathias, R. T. Feedback Regulation of Intracellular Hydrostatic Pressure in Surface Cells of the Lens. *Biophys J* **109**, 1830–1839 (2015).
114. Chen, Y. *et al.* The ciliary muscle and zonules of Zinn modulate lens intracellular hydrostatic pressure through transient receptor potential vanilloid channels. *Investig. Ophthalmol. Vis. Sci.* **60**, 4416–4424 (2019).
115. Shahidullah, M. *et al.* TRPV1 activation stimulates NKCC1 and increases hydrostatic pressure in the mouse lens. *Am. J. Physiol. - Cell Physiol.* **318**, C969–C980 (2020).
116. Petrova, R. S., Bavana, N., Zhao, R., Schey, K. L. & Donaldson, P. J. Changes to zonular tension alters the subcellular distribution of AQP5 in regions of influx and efflux of water in the rat lens. *Investig. Ophthalmol. Vis. Sci.* **61**, 36 (2020).
117. Yasui, M., Kwon, T. H., Knepper, M. A., Nielsen, S. & Agre, P. Aquaporin-6: An intracellular vesicle water channel protein in renal epithelia. *Proc. Natl. Acad. Sci. U. S. A.* **96**, 5808–5813 (1999).
118. Skowronski, M. T. *et al.* AQP7 is localized in capillaries of adipose tissue, cardiac and striated muscle: implications in glycerol metabolism. *Am J Physiol Ren. Physiol* **292**, F956-965 (2007).
119. Calamita, G. *et al.* The inner mitochondrial membrane has aquaporin-8 water channels and is highly permeable to water. *J. Biol. Chem.* **280**, 17149–17153 (2005).
120. Zhu, S., Ran, J. & Yang, B. Aquaporins in Digestive System. 123–130 (2017) doi:10.1007/978-94-024-1057-0.
121. Elkjar, M. L. *et al.* Immunolocalization of AQP9 in liver, epididymis, testis, spleen, and brain. *Biochem. Biophys. Res. Commun.* **276**, 1118–1128 (2000).
122. Ishibashi, K., Morinaga, T., Kuwahara, M., Sasaki, S. & Imai, M. Cloning and identification of a new member of water channel (AQP10) as an aquaglyceroporin. *Biochim. Biophys. Acta - Gene Struct. Expr.* **1576**, 335–340 (2002).
123. Laforenza, U., Scaffino, M. F. & Gastaldi, G. Aquaporin-10 represents an alternative pathway for glycerol efflux from human adipocytes. *PLoS One* **8**, e54474 (2013).
124. Laforenza, U., Scaffino, M. F. & Gastaldi, G. Aquaporin-10 represents an alternative pathway for glycerol efflux from human adipocytes. *PLoS One* **8**, e54474 (2013).
125. Gotfryd, K. *et al.* Human adipose glycerol flux is regulated by a pH gate in AQP10. *Nat Commun* **9**, 4749 (2018).
126. Morinaga, T., Nakakoshi, M., Hirao, A., Imai, M. & Ishibashi, K. Mouse aquaporin 10 gene (AQP10) is a pseudogene. *Biochem. Biophys. Res. Commun.* **294**, 630–634 (2002).

127. Tanaka, Y., Morishita, Y. & Ishibashi, K. Aquaporin10 is a pseudogene in cattle and their relatives. *Biochem Biophys Rep* **1**, 16–21 (2015).
128. Ishibashi, K., Tanaka, Y. & Morishita, Y. The role of mammalian superaquaporins inside the cell. *Biochim Biophys Acta* **1840**, 1507–1512 (2014).
129. Yakata, K. *et al.* Aquaporin-11 containing a divergent NPA motif has normal water channel activity. *Biochim. Biophys. Acta - Biomembr.* **1768**, 688–693 (2007).
130. Morishita, Y. *et al.* Disruption of Aquaporin-11 Produces Polycystic Kidneys following Vacuolization of the Proximal Tubule. *Mol. Cell. Biol.* **25**, 7770–7779 (2005).
131. Itoh, T. *et al.* Identification of a novel aquaporin, AQP12, expressed in pancreatic acinar cells. *Biochem. Biophys. Res. Commun.* **330**, 832–838 (2005).
132. Omasits, U., Ahrens, C. H., Müller, S. & Wollscheid, B. Protter: Interactive protein feature visualization and integration with experimental proteomic data. *Bioinformatics* **30**, 884–886 (2014).
133. Murata, K. *et al.* Structural determinants of water permeation through aquaporin-1. *Nature* **407**, 599–605 (2000).
134. Törnroth-Horsefield, S., Hedfalk, K., Fischer, G., Lindkvist-Petersson, K. & Neutze, R. Structural insights into eukaryotic aquaporin regulation. *FEBS Lett.* **584**, 2580–2588 (2010).
135. Kreida, S. & Törnroth-Horsefield, S. Structural insights into aquaporin selectivity and regulation. *Curr Opin Struct Biol* **33**, 126–134 (2015).
136. Kaldenhoff, R., Kai, L. & Uehlein, N. Aquaporins and membrane diffusion of CO2 in living organisms. *Biochim. Biophys. Acta - Gen. Subj.* **1840**, 1592–1595 (2014).
137. Sui, H., Han, B. G., Lee, J. K., Walian, P. & Jap, B. K. Structural basis of water-specific transport through the AQP1 water channel. *Nature* **414**, 872–878 (2001).
138. Beitz, E., Wu, B., Holm, L. M., Schultz, J. E. & Zeuthen, T. Point mutations in the aromatic/arginine region in aquaporin 1 allow passage of urea, glycerol, ammonia, and protons. *Proc Natl Acad Sci U S A* **103**, 269–274 (2006).
139. Wree, D., Wu, B., Zeuthen, T. & Beitz, E. Requirement for asparagine in the aquaporin NPA sequence signature motifs for cation exclusion. *FEBS J.* **278**, 740–748 (2011).
140. Guan, X. G. *et al.* NPA motifs play a key role in plasma membrane targeting of aquaporin-4. *IUBMB Life* **62**, 222–226 (2010).
141. Woo, J. *et al.* Membrane trafficking of AQP5 and cAMP dependent phosphorylation in bronchial epithelium. *Biochem. Biophys. Res. Commun.* (2008) doi:10.1016/j.bbrc.2007.11.078.
142. Ishibashi, K. Aquaporin subfamily with unusual NPA boxes. *Biochim. Biophys. Acta - Biomembr.* **1758**, 989–993 (2006).
143. Wu, B., Steinbronn, C., Alsterfjord, M., Zeuthen, T. & Beitz, E. Concerted action of two cation filters in the aquaporin water channel. *EMBO J* **28**, 2188–2194 (2009).
144. Eriksson, U. K. *et al.* Subangstrom resolution X-ray structure details aquaporin-water interactions. *Science (80-.).* **340**, 1346–1349 (2013).
145. Harries, W. E. C., Akhavan, D., Miercke, L. J. W., Khademi, S. & Stroud, R. M. The channel architecture of aquaporin 0 at a 2.2-Å resolution. *Proc Natl Acad Sci U S A* **101**, 14045–14050 (2004).
146. Gonen, T., Silz, P., Kistler, J., Cheng, Y. & Walz, T. Aquaporin-0 membrane junctions reveal the structure of a closed water pore. *Nature* **429**, 193–197 (2004).
147. Fellert, M. *et al.* High-resolution x-ray structure of human aquaporin 5. **105**, (2008).
148. Frick, A. *et al.* X-ray structure of human aquaporin 2 and its implications for nephrogenic diabetes insipidus and trafficking. *Proc Natl Acad Sci U S A* **111**, 6305–6310 (2014).
149. Sjöhamn, J. & Hedfalk, K. Unraveling aquaporin interaction partners. *Biochim Biophys Acta* **1840**, 1614–1623 (2014).
150. Kalman, K., Németh-Cahalan, K. L., Froger, A. & Hall, J. E. Phosphorylation determines

the calmodulin-mediated Ca2+ response and water permeability of AQP0. *J Biol Chem* **283**, 21278–21283 (2008).
151. Lindsey Rose, K. M. *et al.* Aquaporin 0-calmodulin interaction and the effect of aquaporin 0 phosphorylation. *Biochemistry* **47**, 339–347 (2008).
152. Roche, J. V. *et al.* Phosphorylation of human aquaporin 2 (AQP2) allosterically controls its interaction with the lysosomal trafficking protein LIP5. *J Biol Chem* **292**, 14636–14648 (2017).
153. Moeller, H. B., Praetorius, J., Rützler, M. R. & Fenton, R. A. Phosphorylation of aquaporin-2 regulates its endocytosis and protein-protein interactions. *Proc Natl Acad Sci U S A* **107**, 424–429 (2010).
154. Login, F. H., Palmfeldt, J., Cheah, J., Yamada, S. & Nejsum, L. N. Aquaporin-5 regulation of cell-cell adhesion proteins: an elusive 'tail' story. *Am J Physiol Cell Physiol* **320**, C282–C292 (2020).
155. Reichow, S. L. *et al.* Allosteric mechanism of water-channel gating by Ca2+-calmodulin. *Nat Struct Mol Biol* **20**, 1085–1092 (2013).
156. Hasegawa, T. *et al.* Novel phosphorylation of aquaporin-5 at its threonine 259 through cAMP signaling in salivary gland cells. *Am J Physiol Cell Physiol* **301**, C667–C678 (2011).
157. Jensen, H. H., Login, F. H., Koffman, J. S., Kwon, T. H. & Nejsum, L. N. The role of aquaporin-5 in cancer cell migration: A potential active participant. *Int. J. Biochem. Cell Biol.* **79**, 271–276 (2016).
158. *Aquaporins*. (Springer Netherlands, 2017). doi:10.1007/978-94-024-1057-0.
159. Preston, G. M., Jin Sup Jung, Guggino, W. B. & Agre, P. The mercury-sensitive residue at cysteine 189 in the CHIP28 water channel. *J. Biol. Chem.* **268**, 17–20 (1993).
160. Parvin, M. N. *et al.* Subcellular redistribution of AQP5 by vasoactive intestinal polypeptide in the Brunner's gland of the rat duodenum. *Am. J. Physiol. - Gastrointest. Liver Physiol.* **288**, 1283–1291 (2005).
161. Sandoval, P. C. *et al.* Proteome-wide measurement of protein half-lives and translation rates in vasopressin-sensitive collecting duct cells. *J. Am. Soc. Nephrol.* **24**, 1793–1805 (2013).
162. Buck, T. M., Eledge, J. & Skach, W. R. Evidence for stabilization of aquaporin-2 folding mutants by N-linked glycosylation in endoplasmic reticulum. *Am. J. Physiol. - Cell Physiol.* **287**, 1292–1299 (2004).
163. Hendriks, G. *et al.* Glycosylation is important for cell surface expression of the water channel aquaporin-2 but is not essential for tetramerization in the endoplasmic reticulum. *J. Biol. Chem.* **279**, 2975–2983 (2004).
164. Baumgarten, R., Van De Pol, M. H. J., Wetzels, J. F. M., Van Os, C. H. & Deen, P. M. T. Glycosylation is not essential for vasopressin-dependent routing of aquaporin-2 in transfected Madin-Darby canine kidney cells. *J. Am. Soc. Nephrol.* **9**, 1553–1559 (1998).
165. Sato, K., Kobayashi, K., Aida, S. & Tamai, S. Bronchiolar expression of aquaporin-3 (AQP3) in rat lung and its dynamics in pulmonary oedema. *Pflugers Arch. Eur. J. Physiol.* **449**, 106–114 (2004).
166. Calamita, G. *et al.* Expression and immunolocalization of the aquaporin-8 water channel in rat gastrointestinal tract. *Eur. J. Cell Biol.* **80**, 711–719 (2001).
167. Barandika, O. *et al.* Increased aquaporin 1 and 5 membrane expression in the lens epithelium of cataract patients. *Biochim. Biophys. Acta - Mol. Basis Dis.* **1862**, 2015–2021 (2016).
168. Petrova, R. S., Schey, K. L., Donaldson, P. J. & Grey, A. C. Spatial distributions of AQP5 and AQP0 in embryonic and postnatal mouse lens development. *Exp. Eye Res.* **132**, 124–135 (2015).
169. DiGiovanni, S. R., Nielsen, S., Christensen, E. I. & Knepper, M. A. Regulation of

collecting duct water channel expression by vasopressin in Brattleboro rat. *Proc. Natl. Acad. Sci. U. S. A.* **91**, 8984–8988 (1994).
170. Kim, S., Jo, C. H. & Kim, G. H. Psychotropic drugs upregulate aquaporin-2 via vasopressin-2 receptor/cAMP/ protein kinase A signaling in inner medullary collecting duct cells. *Am. J. Physiol. - Ren. Physiol.* **320**, F963–F971 (2021).
171. Skowronska, A., Mlotkowska, P., Majewski, M., Nielsen, S. & Skowronski, M. T. Expression of aquaporin 1 and 5 and their regulation by ovarian hormones, arachidonic acid, forskolin and cAMP during implantation in pigs. *Physiol Res* **4**, (65AD).
172. Sidhaye, V., Hoffert, J. D. & King, L. S. cAMP has distinct acute and chronic effects on aquaporin-5 in lung epithelial cells. *J. Biol. Chem.* **280**, 3590–3596 (2005).
173. Boone, M., Kortenoeven, M. L. A., Robben, J. H., Tamma, G. & Deen, P. M. T. Counteracting vasopressin-mediated water reabsorption by ATP, dopamine, and phorbol esters: Mechanisms of action. *Am. J. Physiol. - Ren. Physiol.* **300**, 761–771 (2011).
174. Kuriyama, H. *et al.* Coordinated regulation of fat-specific and liver-specific glycerol channels, aquaporin adipose and aquaporin 9. *Diabetes* **51**, 2915–2921 (2002).
175. Towne, J. E., Krane, C. M., Bachurski, C. J. & Menon, A. G. Tumor Necrosis Factor-α Inhibits Aquaporin 5 Expression in Mouse Lung Epithelial Cells. *J Biol Chem* **276**, 18657–18664 (2001).
176. Jiang, X. X. *et al.* Aquaporin 5 plays a role in estrogen-induced ectopic implantation of endometrial stromal cells in endometriosis. *PLoS One* **10**, 1–15 (2015).
177. King, L. S., Nielsen, S. & Agre, P. Aquaporins in complex tissues. I. Developmental patterns in respiratory and glandular tissues of rat. *Am. J. Physiol. - Cell Physiol.* **273**, C1541–C1548 (1997).
178. González-Dávalos, L. *et al.* Glucocorticoid gene regulation of aquaporin-7. *Vitam Horm* **112**, 179–207 (2020).
179. Li, X. *et al.* Molecular characterization, chromosomal and expression patterns of three aquaglyceroporins (AQP3, 7, 9) from pig. *Comp. Biochem. Physiol. - B Biochem. Mol. Biol.* **149**, 468–476 (2008).
180. Pastor-Soler, N. M. *et al.* Aquaporin 9 expression in the developing rat epididymis is modulated by steroid hormones. *Reproduction* **139**, 613–621 (2010).
181. Umenishi, F. & Schrier, R. W. Identification and characterization of a novel hypertonicity-responsive element in the human aquaporin-1 gene. *Biochem. Biophys. Res. Commun.* **292**, 771–775 (2002).
182. Umenishi, F. & Schrier, R. W. Hypertonicity-induced aquaporin-1 (AQP1) expression is mediated by the activation of MAPK pathways and hypertonicity-responsive element in the AQP1 gene. *J. Biol. Chem.* **278**, 15765–15770 (2003).
183. Umenishi, F., Yoshihara, S., Narikiyo, T. & Schrier, R. W. Modulation of hypertonicity-induced aquaporin-1 by sodium chloride, urea, betaine, and heat shock in murine renal medullary cells. *J. Am. Soc. Nephrol.* **16**, 600–607 (2005).
184. Lanaspa, M. A. *et al.* The expression of aquaporin-1 in the medulla of the kidney is dependent on the transcription factor associated with hypertonicity, TonEBP. *J. Biol. Chem.* **285**, 31694–31703 (2010).
185. Hoffert, J. D., Leitch, V., Agre, P. & King, L. S. Hypertonic induction of aquaporin-5 expression through an ERK-dependent pathway. *J. Biol. Chem.* **275**, 9070–9077 (2000).
186. Sidhaye, V. K. *et al.* Transient receptor potential vanilloid 4 regulates aquaporin-5 abundance under hypotonic conditions. *Proc. Natl. Acad. Sci. U. S. A.* **103**, 4747–4752 (2006).
187. Qi, H., Li, L., Zong, W., Hyer, B. J. & Huang, J. Expression of aquaporin 8 is diversely regulated by osmotic stress in amnion epithelial cells. *J. Obstet. Gynaecol. Res.* **35**, 1019–1025 (2009).
188. Moon, Y., Hong, S. J., Shin, D. & Jung, Y. Increased aquaporin-1 expression in choroid

plexus epithelium after systemic hyponatremia. *Neurosci. Lett.* **395**, 1–6 (2006).
189. Han, M. *et al.* Activation of TGR5 restores AQP2 expression via the HIF pathway in renal ischemia-reperfusion injury. *Am J Physiol Ren. Physiol* **320**, F308–F321 (2021).
190. Kawedia, J. D. *et al.* Hypoxia and Hypoxia Mimetics Decrease Aquaporin 5 (AQP5) Expression Through Both Hypoxia Inducible factor-1α and Proteasome-Mediated Pathways. *PLoS One* **8**, e57541 (2013).
191. Sachdeva, R. & Singh, B. Insights into structural mechanisms of gating induced regulation of aquaporins. *Prog Biophys Mol Biol* **114**, 69–79 (2014).
192. Ball, L. E., Garland, D. L., Crouch, R. K. & Schey, K. L. Post-translational modifications of Aquaporin 0 (AQP0) in the normal human lens: Spatial and temporal occurrence. *Biochemistry* **43**, 9856–9865 (2004).
193. Wenke, J. L., Rose, K. L., Spraggins, J. M. & Schey, K. L. MALDI Imaging Mass Spectrometry Spatially Maps Age-Related Deamidation and Truncation of Human Lens Aquaporin-0. *Invest Ophthalmol Vis Sci* **56**, 7398–7405 (2015).
194. Tong, J., Canty, J. T., Briggs, M. M. & McIntosh, T. J. The water permeability of lens aquaporin-0 depends on its lipid bilayer environment. *Exp. Eye Res.* **113**, 32–40 (2013).
195. Németh-Cahalan, K. L., Kalman, K. & Hall, J. E. Molecular Basis of pH and Ca2+ Regulation of Aquaporin Water Permeability. *J. Gen. Physiol.* **123**, 573–580 (2004).
196. Reichow, S. L. & Gonen, T. Noncanonical Binding of Calmodulin to Aquaporin-0: Implications for Channel Regulation. *Structure* **16**, 1389–1398 (2008).
197. Gutierrez, D. B., Garland, D. & Schey, K. L. Spatial analysis of human lens aquaporin-0 post-translational modifications by MALDI mass spectrometry tissue profiling. *Exp. Eye Res.* **93**, 912–920 (2011).
198. Bassnett, S., Croghan, P. C. & Duncan, G. Diffusion of lactate and its role in determining intracellular pH in the lens of the eye. *Exp. Eye Res.* **44**, 143–147 (1987).
199. Pasquale, L. R., Mathias, R. T., Austin, L. R., Brink, P. R. & Ciunga, M. Electrostatic properties of fiber cell membranes from the frog lens. *Biophys. J.* **58**, 939–945 (1990).
200. Mathias, R. T., Riquelme, G. & Rae, J. L. Cell to cell communication and pH in the frog lens. *J. Gen. Physiol.* **98**, 1085–1103 (1991).
201. Jacob, T. J. Raised intracellular free calcium within the lens causes opacification and cellular uncoupling in the frog. *J. Physiol.* **341**, 595–601 (1983).
202. Baldo, G. J., Gao, J. & Mathias, R. T. Intracellular Ca2+-Concentration Gradient Within the Lens. in *Association for Research in Vision and Ophthalmology Annual Meeting* 3539 (Investigative Ophthalmology & Visual Science, 2002).
203. Rhodes, J. D. & Sanderson, J. The mechanisms of calcium homeostasis and signalling in the lens. *Exp. Eye Res.* **88**, 226–234 (2009).
204. Robinson, N. E. & Robinson, A. B. Deamidation of human proteins. *Proc Natl Acad Sci U S A* **98**, 12409–12413 (2001).
205. Gonen, T., Cheng, Y., Sliz, P. & Hiroaki, Y. Lipid-protein interactions in double-layered two-dimensional AQP0 crystals. *Nature* **438**, 633–8 (2005).
206. Schey, K. L., Gutierrez, D. B., Wang, Z., Wei, J. & Grey, A. C. Novel Fatty Acid Acylation of Lens Integral Membrane Protein Aquaporin-0. *Biochemistry* **49**, 9858–9865 (2010).
207. Tong, J., Briggs, M. M., Mlaver, D., Vidal, A. & McIntosh, T. J. Sorting of lens aquaporins and connexins into raft and nonraft bilayers: Role of protein homo-oligomerization. *Biophys J* **97**, 2493–2502 (2009).
208. Wang, Z. & Schey, K. L. Proteomic analysis of lipid raft-like detergent-resistant membranes of lens fiber cells. *Invest Ophthalmol Vis Sci* **56**, 8349–8360 (2015).
209. Ouweneel, A. B., Thomas, M. J. & Sorci-Thomas, M. G. The ins and outs of lipid rafts: Functions in intracellular cholesterol homeostasis, microparticles, and cell membranes. *J. Lipid Res.* **61**, 676–686 (2020).
210. Li, L., So, L. & Spector, A. Membrane cholesterol and phospholipid in consecutive

concentric sections of human lenses. *J Lipid Res* **26**, 600–609 (1985).
211. Li, L. K., So, L. & Spector, A. Age-dependent changes in the distribution and concentration of human lens cholesterol and phospholipids. *Biochim Biophys Acta* **917**, 112–120 (1987).
212. Li, L. K. & So, L. Age dependent lipid and protein changes in individual bovine lenses. *Curr Eye Res* **6**, 599–605 (1987).
213. Zeuthen, T. & Klaerke, D. A. Transport of water and glycerol in aquaporin 3 is gated by H+. *J. Biol. Chem.* **274**, 21631–21636 (1999).
214. De Almeida, A. *et al.* Exploring the gating mechanisms of aquaporin-3: New clues for the design of inhibitors? *Mol. Biosyst.* **12**, 1564–1573 (2016).
215. Gunnarson, E. *et al.* Identification of a molecular target for glutamate regulation of astrocyte water permeability. *Glia* **56**, 587–596 (2008).
216. Gunnarson, E. *et al.* Lead induces increased water permeability in astrocytes expressing aquaporin 4. *Neuroscience* **136**, 105–114 (2005).
217. Han, Z., Wax, M. B. & Patil, R. V. Regulation of aquaporin-4 water channels by phorbol ester-dependent protein phosphorylation. *J. Biol. Chem.* **273**, 6001–6004 (1998).
218. Zelenina, M., Zelenin, S., Bondar, A. A., Brismar, H. & Aperia, A. Water permeability of aquaporin-4 is decreased by protein kinase C and dopamine. *Am. J. Physiol. - Ren. Physiol.* **283**, (2002).
219. Yasui, M. *et al.* Rapid gating and anion permeability of an intracellular aquaporin. *Nature* **402**, 184–187 (1999).
220. Nielsen, S., DiGiovanni, S. R., Christensen, E. I., Knepper, M. A. & Harris, H. W. Cellular and subcellular immunolocalization of vasopressin-regulated water channel in rat kidney. *Proc Natl Acad Sci U S A* **90**, 11663–11667 (1993).
221. Nielsen, S. *et al.* Vasopressin increases water permeability of kidney collecting duct by inducing translocation of aquaporin-CD water channels to plasma membrane. *Proc Natl Acad Sci U S A* **92**, 1013–1017 (1995).
222. Hoffert, J. D. *et al.* Vasopressin-stimulated increase in phosphorylation at Ser269 potentiates plasma membrane retention of aquaporin-2. *J Biol Chem* **283**, 24617–24627 (2008).
223. Cheung, P. W., Terlouw, A., Janssen, S. A., Brown, D. & Bouley, R. Inhibition of non-receptor tyrosine kinase Src induces phosphoserine 256-independent aquaporin-2 membrane accumulation. *J. Physiol.* **597**, 1627–1642 (2019).
224. Balkom, B. W. M. Van *et al.* LIP5 interacts with aquaporin 2 and facilitates its lysosomal degradation. *J Am Soc Nephrol* **20**, 990–1001 (2009).
225. Kamsteeg, E. J. *et al.* Short-chain ubiquitination mediates the regulated endocytosis of the aquaporin-2 water channel. *Proc. Natl. Acad. Sci. U. S. A.* **103**, 18344–18349 (2006).
226. Moeller, H. B., Fenton, R. A., Zeuthen, T. & MacAulay, N. Vasopressin-dependent short-term regulation of aquaporin 4 expressed in Xenopus oocytes. *Neuroscience* **164**, 1674–1684 (2009).
227. Carmosino, M. *et al.* Trafficking and phosphorylation dynamics of AQP4 in histamine-treated human gastric cells. *Biol. Cell* **99**, 25–36 (2007).
228. Beitz, E. *et al.* Determinants of AQP6 trafficking to intracellular sites versus the plasma membrane in transfected mammalian cells. *Biol Cell* **98**, 101–109 (2006).
229. Rabaud, N. E. *et al.* Aquaporin 6 binds calmodulin in a calcium-dependent manner. *Biochem Biophys Res Commun* **383**, 54–57 (2009).
230. Bassnett, S. & Costello, M. J. The cause and consequence of fiber cell compaction in the vertebrate lens. *Exp Eye Res* **156**, 50–57 (2017).
231. Birkenfeld, J., de Castro, A., Ortiz, S., Pascual, D. & Marcos, S. Contribution of the gradient refractive index and shape to the crystalline lens spherical aberration and astigmatism. *Vision Res.* **86**, 27–34 (2013).

232. Vaghefi, E., Kim, A. & Donaldson, P. J. Active maintenance of the gradient of refractive index is required to sustain the optical properties of the lens. *Investig. Ophthalmol. Vis. Sci.* **56**, 7195–7208 (2015).
233. Sindhu Kumari, S. & Varadaraj, K. Intact and N- or C-terminal end truncated AQP0 function as open water channels and cell-to-cell adhesion proteins: End truncation could be a prelude for adjusting the refractive index of the lens to prevent spherical aberration. *Biochim. Biophys. Acta - Gen. Subj.* **1840**, 2862–2877 (2014).
234. Varadaraj, K. & Kumari, S. Deletion of seventeen amino acids at the C-terminal end of aquaporin 0 causes distortion aberration and cataract in the lenses of AQP0 ΔC/ΔC mice. *Investig. Ophthalmol. Vis. Sci.* **60**, 858–867 (2019).
235. Varadaraj, K., FitzGerald, P. G. & Kumari, S. S. Deletion of beaded filament proteins or the C-terminal end of Aquaporin 0 causes analogous abnormal distortion aberrations in mouse lens. *Exp. Eye Res.* **209**, 108645 (2021).
236. Armstrong, C. M. The Na/K pump, Cl ion, and osmotic stabilization of cells. *Proc. Natl. Acad. Sci. U. S. A.* **100**, 6257–6262 (2003).
237. Mathias, R. T. & Rae, J. L. Transport properties of the lens. *Am. J. Physiol. - Cell Physiol.* **249**, C181–C190 (1985).
238. Mathias, R. T., Kistler, J. & Donaldson, P. The lens circulation. *J. Membr. Biol.* **216**, 1–16 (2007).
239. Delamere, N. A. & Dean, W. L. Distribution of lens sodium-potassium-adenosine triphosphatase. *Investig. Ophthalmol. Vis. Sci.* **34**, 2159–2163 (1993).
240. Kobatashi, S., Roy, D. & Spector, A. Sodium/potassium ATPase in normal and cataractous human lenses. *Curr. Eye Res.* **2**, 327–334 (1982).
241. Giannone, A. A., Li, L., Sellitto, C. & White, T. W. Physiological Mechanisms Regulating Lens Transport. *Front. Physiol.* **12**, 1–7 (2021).
242. Schey, K. L. *et al.* Lens Aquaporins in Health and Disease: Location is Everything! *Front. Physiol.* **13**, 1–14 (2022).
243. Alvarez, L. J., Candia, O. A., Turner, H. C. & Polikoff, L. A. Localization of a Na(+)-K(+)-2Cl(-) cotransporter in the rabbit lens. *Exp. Eye Res.* **73**, 669–680 (2001).
244. Chee, K. N., Vorontsova, I., Lim, J. C., Kistler, J. & Donaldson, P. J. Expression of the sodium potassium chloride cotransporter (NKCC1) and sodium chloride cotransporter (NCC) and their effects on rat lens transparency. *Mol. Vis.* **16**, 800–812 (2010).
245. Frederikse, P. H. & Kasinathan, C. KCC2 expression supersedes NKCC1 in mature fiber cells in mouse and rabbit lenses. *Mol Vis* **21**, 1142–1150 (2015).
246. Haas, M. & Forbush 3rd, B. The Na-K-Cl cotransporters. *J Bioenerg Biomembr* **30**, 161–172 (1998).
247. Chee, K. S. N., Kistler, J. & Donaldson, P. J. Roles for KCC transporters in the maintenance of lens transparency. *Investig. Ophthalmol. Vis. Sci.* **47**, 673–682 (2006).
248. Damann, N., Voets, T. & Nilius, B. TRPs in Our Senses. *Curr Biol* **18**, 880–889 (2008).
249. Kadowaki, T. Evolutionary dynamics of metazoan TRP channels. *Pflugers Arch* **467**, 2043–2053 (2015).
250. Nilius, B. & Owsianik, G. The transient receptor potential family of ion channels. *Genome Biol* **12**, 218 (2011).
251. Caterina, M. J. *et al.* The capsaicin receptor: A heat-activated ion channel in the pain pathway. *Nature* **389**, 816–824 (1997).
252. Jordt, S. E., Tominaga, M. & Julius, D. Acid potentiation of the capsaicin receptor determined by a key extracellular site. *Proc Natl Acad Sci U S A* **97**, 8134–8139 (2000).
253. Tominaga, M. & Tominaga, T. Structure and function of TRPV1. *Pflugers Arch. Eur. J. Physiol.* **451**, 143–150 (2005).
254. Oh, U., Hwang, S. W. & Kim, D. Capsaicin activates a nonselective cation channel in cultured neonatal rat dorsal root ganglion neurons. *J Neurosci* **16**, 1659–1667 (1996).

255. Rosenbaum, T., Gordon-Shaag, A., Munari, M. & Gordon, S. E. Ca2+/calmodulin modulates TRPV1 activation by capsaicin. *J Gen Physiol* **123**, 53–62 (2004).
256. Cholewinski, A., Burgess, G. M. & Bevan, S. The role of calcium in capsaicin-induced desensitization in rat cultured dorsal root ganglion neurons. *Neuroscience* **55**, 1015–1023 (1993).
257. Koplas, P. A., Rosenberg, R. L. & Oxford, G. S. The role of calcium in the desensitization of capsaicin responses in rat dorsal root ganglion neurons. *J Neurosci* **17**, 3525–3537 (1997).
258. Nilius, B., Watanabe, H. & Vriens, J. The TRPV4 channel: Structure-function relationship and promiscuous gating behaviour. *Pflugers Arch* **446**, 298–303 (2003).
259. Garcia-Elias, A., Lorenzo, I. M., Vicente, R. & Valverde, M. A. IP3 receptor binds to and sensitizes TRPV4 channel to osmotic stimuli via a calmodulin-binding site. *J Biol Chem* **283**, 31284–31288 (2008).
260. Toft-Bertelsen, T. L. & Macaulay, N. TRPing to the Point of Clarity: Understanding the Function of the Complex TRPV4 Ion Channel. *Cells* **10**, 1–16 (2021).
261. Martínez-García, M. C. *et al.* Differential expression and localization of transient receptor potential vanilloid 1 in rabbit and human eyes. *Histol Histopathol* **28**, 1507–1516 (2013).
262. Nakazawa, Y., Donaldson, P. J. & Petrova, R. S. Verification and spatial mapping of TRPV1 and TRPV4 expression in the embryonic and adult mouse lens. *Exp. Eye Res.* **186**, 107707 (2019).
263. Shahidullah, M., Mandal, A. & Delamere, N. A. Damage to lens fiber cells causes TRPV4-dependent Src family kinase activation in the epithelium. *Exp. Eye Res.* **140**, 85–93 (2015).
264. Shahidullah, M., Mandal, A. & Delamere, N. A. Activation of TRPV1 channels leads to stimulation of NKCC1 cotransport in the lens. *Am. J. Physiol. - Cell Physiol.* **315**, C793–C802 (2018).
265. Shahidullah, M., Mandal, A. & Delamere, N. A. TRPV4 in porcine lens epithelium regulates hemichannel-mediated ATP release and Na-K-ATPase activity. *Am J Physiol Cell Physiol* **302**, C1751–C1761 (2012).
266. Yeager, M. & Nicholson, B. J. Structure of gap junction intercellular channels. *Curr. Opin. Struct. Biol.* **6**, 183–192 (1996).
267. Unger, V. M., Kumar, N. M., Gilula, N. B. & Yeager, M. Three-dimensional structure of a recombinant gap junction membrane channel. *Science (80-.).* **283**, 1176–1180 (1999).
268. Beyer, E. C., Paul, D. L. & Goodenough, D. A. Connexin43: A protein from rat heart homologous to a gap junction protein from liver. *J Cell Biol* **105**, 2621–2629 (1987).
269. Beyer, E. C., Kistler, J., Paul, D. L. & Goodenough, D. A. Antisera directed against connexin43 peptides react with a 43-kD protein localized to gap junctions in myocardium and other tissues. *J. Cell Biol.* **108**, 595–605 (1989).
270. Musil, L. S., Beyer, E. C. & Goodenough, D. A. Expression of the gap junction protein connexin43 in embryonic chick lens: molecular cloning, ultrastructural localization, and post-translational phosphorylation. *J. Membr. Biol.* **116**, 163–175 (1990).
271. Paul, D. L., Ebihara, L., Takemoto, L. J., Swenson, K. I. & Goodenough, D. A. Connexin46, a novel lens gap junction protein, induces voltage-gated currents in nonjunctional plasma membrane of Xenopus oocytes. *J Cell Biol* **115**, 1077–1089 (1991).
272. Rong, P. *et al.* Disruption of Gja8 (alpha8 connexin) in mice leads to microphthalmia associated with retardation of lens growth and lens fiber maturation. *Development* **129**, 167–174 (2002).
273. Kistler, J., Kirkland, B. & Bullivant, S. Identification of a 70,000-D Protein in lens membrane junctional domains. *J Cell Biol* **101**, 28–35 (1985).
274. Gruijters, W. T. M., Kistler, J., Bullivant, S. & Goodenough, D. A. Immunolocalization of MP70 in lens fiber 16-17-nm intercellular junctions. *J. Cell Biol.* **104**, 565–572 (1987).

275. White, T. W., Bruzzone, R., Goodenough, D. A. & Paul, D. L. Mouse Cx50, a functional member of the connexin family of gap junction proteins, is the lens fiber protein MP70. *Mol. Biol. Cell* **3**, 711–720 (1992).
276. Gong, X., Cheng, C. & Xia, C. H. Connexins in lens development and cataractogenesis. *J. Membr. Biol.* **218**, 9–12 (2007).
277. White, T. W., Goodenough, D. A. & Paul, D. L. Targeted ablation of connexin50 in mice results in microphthalmia and zonular pulverulent cataracts. *J. Cell Biol.* **143**, 815–825 (1998).
278. Gong, X. *et al.* Disruption of α3 connexin gene leads to proteolysis and cataractogenesis in mice. *Cell* **91**, 833–843 (1997).
279. Baruch, A. *et al.* Defining a link between gap junction communication, proteolysis, and cataract formation. *J. Biol. Chem.* **276**, 28999–29006 (2001).
280. Gao, J. *et al.* Connections between connexins, calcium, and cataracts in the lens. *J. Gen. Physiol.* **124**, 289–300 (2004).
281. Donaldson, P., Kistler, J. & Mathias, R. T. Molecular solutions to mammalian lens transparency. *News Physiol Sci* **16**, 118–123 (2001).
282. Bukauskas, F. F. & Verselis, V. K. Gap junction channel gating. *Biochim Biophys Acta* **1662**, 42–60 (2004).
283. Peracchia, C. Chemical gating of gap junction channels: Roles of calcium, pH and calmodulin. *Biochim. Biophys. Acta - Biomembr.* **1662**, 61–80 (2004).
284. Liu, J. *et al.* Phosphorylation of connexin 50 by protein kinase A enhances gap junction and hemichannel function. *J. Biol. Chem.* **286**, 16914–16928 (2011).
285. Wang, K. *et al.* Developmental truncations of connexin 50 by caspases adaptively regulate gap junctions/hemichannels and protect lens cells against ultraviolet radiation. *J. Biol. Chem.* **287**, 15786–15797 (2012).
286. Mathias, R. T., White, T. W. & Gong, X. Lens gap junctions in growth, differentiation, and homeostasis. *Physiol. Rev.* **90**, 179–206 (2010).
287. Jacob, T. J. C. The relationship between cataract, cell swelling and volume regulation. *Prog. Retin. Eye Res.* (1999) doi:10.1016/S1350-9462(98)00019-6.
288. Donaldson, P. J., Chee, K. S. N., Lim, J. C. & Webb, K. F. Regulation of lens volume: Implications for lens transparency. *Experimental Eye Research* (2009) doi:10.1016/j.exer.2008.05.011.
289. Paterson, C. A. Extracellular space of the crystalline lens. *Am J Physiol* **218**, 797–802 (1970).
290. Vaghefi, E., Walker, K., Pontre, B. P., Jacobs, M. D. & Donaldson, P. J. Magnetic resonance and confocal imaging of solute penetration into the lens reveals a zone of restricted extracellular space diffusion. *Am J Physiol Regul Integr Comp Physiol* **302**, 1250–1259 (2012).
291. Wang, Z., Cantrell, L. S. & Schey, K. L. Spatially Resolved Proteomic Analysis of the Lens Extracellular Diffusion Barrier. *Invest Ophthalmol Vis Sci* **62**, 25 (2021).
292. Grey, A. C., Jacobs, M. D., Gonen, T., Kistler, J. & Donaldson, P. J. Insertion of MP20 into lens fibre cell plasma membranes correlates with the formation of an extracellular diffusion barrier. *Exp. Eye Res.* **77**, 567–574 (2003).
293. Lim, J. C., Walker, K. L., Sherwin, T., Schey, K. L. & Donaldson, P. J. Confocal microscopy reveals zones of membrane remodeling in the outer cortex of the human lens. *Investig. Ophthalmol. Vis. Sci.* **50**, 4304–4310 (2009).
294. Gutierrez, D. B., Garland, D. L., Schwacke, J. H., Hachey, D. L. & Schey, K. L. Spatial distributions of phosphorylated membrane proteins aquaporin 0 and MP20 across young and aged human lenses. *Exp Eye Res* **149**, 59–65 (2016).
295. Lo, W. K. Adherens junctions in the ocular lens of various species: ultrastructural analysis with an improved fixation. *Cell Tissue Res.* **254**, 31–40 (1988).

296. Vaghefi, E., Pontre, B. P., Jacobs, M. D. & Donaldson, P. J. Visualizing ocular lens fluid dynamics using MRI: Manipulation of steady state water content and water fluxes. *Am. J. Physiol. - Regul. Integr. Comp. Physiol.* **301**, R335–R342 (2011).
297. Candia, O. A., Mathias, R. & Gerometta, R. Fluid circulation determined in the isolated bovine lens. *Investig. Ophthalmol. Vis. Sci.* **53**, 7087–7096 (2012).
298. Donaldson, P. J., Grey, A. C., Maceo Heilman, B., Lim, J. C. & Vaghefi, E. The physiological optics of the lens. *Prog Retin Eye Res* **56**, e1–e24 (2017).
299. Ebihara, L., Korzyukov, Y., Kothari, S. & Tong, J. J. Cx46 hemichannels contribute to the sodium leak conductance in lens fiber cells. *Am. J. Physiol. - Cell Physiol.* **306**, 506–513 (2014).
300. Donaldson, P. J. & Lim, J. C. Membrane Transporters: New Roles in Lens Cataract. in *Ophthalmology Research: Ocular Transporters in Ophthalmic Diseases and Drug Delivery* (eds. Tombran-Tink, J. & Barnstable, C. J.) 89–110 (Humana Press, Inc., 2008).
301. Gao, J. *et al.* Lens intracellular hydrostatic pressure is generated by the circulation of sodium and modulated by gap junction coupling. *J. Gen. Physiol.* **137**, 507–520 (2011).
302. Gao, J. *et al.* The effect of size and species on lens intracellular hydrostatic pressure. *Investig. Ophthalmol. Vis. Sci.* **54**, 183–192 (2013).
303. Vaghefi, E. & Donaldson, P. J. The lens internal microcirculation system delivers solutes to the lens core faster than would be predicted by passive diffusion. *Am. J. Physiol. - Regul. Integr. Comp. Physiol.* **315**, R994–R1002 (2018).
304. Varadaraj, K. *et al.* The role of MIP in lens fiber cell membrane transport. *J. Membr. Biol.* **170**, 191–203 (1999).
305. Yu, L., Chen, Y. & Tooze, S. A. Autophagy pathway: Cellular and molecular mechanisms. *Autophagy* **14**, 207–215 (2018).
306. Urbańska, K. & Orzechowski, A. The secrets of alternative autophagy. *Cells* **10**, 1–15 (2021).
307. Morishita, H. & Mizushima, N. Autophagy in the lens. *Exp Eye Res* **144**, 22–28 (2016).
308. Costello, M. J. *et al.* Autophagy and mitophagy participate in ocular lens organelle degradation. *Exp. Eye Res.* **116**, 141–150 (2013).
309. Basu, S., Rajakaruna, S., Reyes, B., Van Bockstaele, E. & Menko, A. S. Suppression of MAPK/JNK-MTORC1 signaling leads to premature loss of organelles and nuclei by autophagy during terminal differentiation of lens fiber cells. *Autophagy* **10**, 1193–1211 (2014).
310. Brennan, L. A. *et al.* BNIP3L/NIX is required for elimination of mitochondria, endoplasmic reticulum and Golgi apparatus during eye lens organelle-free zone formation. *Exp. Eye Res.* **174**, 173–184 (2018).
311. Gheyas, R., Ortega-Alvarez, R., Chauss, D., Kantorow, M. & Menko, A. S. Suppression of PI3K signaling is linked to autophagy activation and the spatiotemporal induction of the lens organelle free zone. *Exp. Cell Res.* **412**, 113043 (2022).
312. Azlina, A. *et al.* Roles of lysosomal proteolytic systems in AQP5 degradation in the submandibular gland of rats following chorda tympani parasympathetic denervation. *Am. J. Physiol. - Gastrointest. Liver Physiol.* **299**, 1106–1117 (2010).
313. Huang, Y. *et al.* Aquaporin 5 is degraded by autophagy in diabetic submandibular gland. *Sci. China Life Sci.* **61**, 1049–1059 (2018).
314. Laplante, M. & Sabatini, D. M. mTOR signaling at a glance. *J. Cell Sci.* **122**, 3589–3594 (2009).
315. Ersahin, T., Tuncbag, N. & Cetin-Atalay, R. The PI3K/AKT/mTOR interactive pathway. *Mol Biosyst* **11**, 1946–1954 (2015).
316. Manning, B. D. & Cantley, L. C. AKT/PKB Signaling: Navigating Downstream. *Cell* **129**, 1261–1274 (2007).
317. Carpenter, C. L. *et al.* Phosphoinositide 3-kinase is activated by phosphopeptides that

bind to the SH2 domains of the 85-kDa subunit. *J. Biol. Chem.* **268**, 9478–9483 (1993).
318. Liu, P., Cheng, H., Roberts, T. M. & Zhao, J. J. Targeting the phosphoinositide 3-kinase pathway in cancer. *Nat Rev Drug Discov* **8**, 627–644 (2009).
319. Maehama, T. & Dixon, J. E. PTEN: A tumour suppressor that functions as a phospholipid phosphatase. *Trends Cell Biol.* **9**, 125–128 (1999).
320. Vazquez, F. & Devreotes, P. Regulation of PTEN function as a PIP3 gatekeeper through membrane interaction. *Cell Cycle* **5**, 1523–1527 (2006).
321. Franke, T. F. *et al.* The protein kinase encoded by the Akt proto-oncogene is a target of the PDGF-activated phosphatidylinositol 3-kinase. *Cell* **81**, 727–736 (1995).
322. Alessi, D. R. *et al.* Characterization of a 3-phosphoinositide-dependent protein kinase which phosphorylates and activates protein kinase Bα. *Curr. Biol.* **7**, 261–269 (1997).
323. Sarbassov, D. D., Guertin, D. A., Ali, S. M. & Sabatini, D. M. Phosphorylation and regulation of Akt/PKB by the rictor-mTOR complex. *Science (80-.).* **5712**, (307AD).
324. Beugnet, A., Tee, A. R., Taylor, P. M. & Proud, C. G. Regulation of targets of mTOR (mammalian target of rapamycin) signalling by intracellular amino acid availability. *Biochem. J.* **372**, 555–566 (2003).
325. Richter, J. D. & Sonenberg, N. Regulation of cap-dependent translation by eIF4E inhibitory proteins. *Nature* **433**, 477–480 (2005).
326. Chauvin, C. *et al.* Ribosomal protein S6 kinase activity controls the ribosome biogenesis transcriptional program. *Oncogene* **33**, 474–483 (2014).
327. Ganley, I. G. *et al.* ULK1·ATG13·FIP200 complex mediates mTOR signaling and is essential for autophagy. *J Biol Chem* **284**, 12297–12305 (2009).
328. Hosokawa, N. *et al.* Nutrient-dependent mTORC1 association with the ULK1-Atg13-FIP200 complex required for autophagy. *Mol Biol Cell* **20**, 1981–1991 (2009).
329. Jung, C. H. *et al.* ULK-Atg13-FIP200 complexes mediate mTOR signaling to the autophagy machinery. *Mol Biol Cell* **20**, 1992–2003 (2009).
330. Wong, P. M., Puente, C., Ganley, I. G. & Jiang, X. The ULK1 complex sensing nutrient signals for autophagy activation. *Autophagy* **9**, 124–137 (2013).
331. Lin, M. G. & Hurley, J. H. Structure and function of the ULK1 complex in autophagy. *Curr. Opin. Cell Biol.* **39**, 61–68 (2016).
332. Gwinn, D. M. *et al.* AMPK phosphorylation of raptor mediates a metabolic checkpoint. *Mol Cell* **30**, 214–226 (2008).
333. Condon, K. J. & Sabatini, D. M. Nutrient regulation of mTORC1 at a glance. *J. Cell Sci.* **132**, 0–2 (2019).
334. Egan, D. F. *et al.* Phosphorylation of ULK1 (hATG1) by AMP-activated protein kinase connects energy sensing to mitophagy. *Science (80-.).* **331**, 456–461 (2011).
335. Tamargo-Gómez, I. & Mariño, G. AMPK: Regulation of metabolic dynamics in the context of autophagy. *Int. J. Mol. Sci.* **19**, (2018).
336. Feng, Y., He, D., Yao, Z. & Klionsky, D. J. The machinery of macroautophagy. *Cell Res* **24**, 24–41 (2014).
337. Cuervo, A. M. & Wong, E. Chaperone-mediated autophagy: Roles in disease and aging. *Cell Res.* **24**, 92–104 (2014).
338. Csizmadia, T. & Juhász, G. Crinophagy mechanisms and its potential role in human health and disease. *Prog Mol Biol Transl Sci* **172**, 239–255 (2020).
339. Weckman, A. *et al.* Autophagy in the endocrine glands. *J Mol Endocrinol* **52**, R151–R163 (2013).
340. Mijaljica, D., Prescott, M. & Devenish, R. J. Microautophagy in mammalian cells: Revisiting a 40-year-old conundrum. *Autophagy* **7**, 673–682 (2011).
341. Jin, M., Liu, X. & Klionsky, D. J. SnapShot: Selective autophagy. *Cell* **152**, 368-368.e2 (2013).
342. Papandreou, M. E. & Tavernarakis, N. Nucleophagy mediators and mechanisms. *Prog*

Mol Biol Transl Sci **172**, 1–14 (2020).
343. Klionsky, D. J. *et al.* A unified nomenclature for yeast autophagy-related genes. *Dev. Cell* **5**, 539–545 (2003).
344. Nakatogawa, H., Suzuki, K., Kamada, Y. & Ohsumi, Y. Dynamics and diversity in autophagy mechanisms: Lessons from yeast. *Nat. Rev. Mol. Cell Biol.* **10**, 458–467 (2009).
345. Ohsumi, Y. Historical landmarks of autophagy research. *Cell Res.* **24**, 9–23 (2014).
346. Juenemann, K. & Reits, E. A. Alternative macroautophagic pathways. *Int J Cell Biol* **2012**, 189794 (2012).
347. Russell, R. C. *et al.* ULK1 induces autophagy by phosphorylating Beclin-1 and activating VPS34 lipid kinase. *Nat. Cell Biol.* **15**, 741–750 (2013).
348. Karanasios, E. *et al.* Autophagy initiation by ULK complex assembly on ER tubulovesicular regions marked by ATG9 vesicles. *Nat. Commun.* **7**, 1–17 (2016).
349. Walker, S., Chandra, P., Manifava, M., Axe, E. & Ktistakis, N. T. Making autophagosomes: Localized synthesis of phosphatidylinositol 3-phosphate holds the clue. *Autophagy* **4**, 1093–1096 (2008).
350. Dooley, H. C. *et al.* WIPI2 Links LC3 Conjugation with PI3P, Autophagosome Formation, and Pathogen Clearance by Recruiting Atg12-5-16L1. *Mol. Cell* **55**, 238–252 (2014).
351. Lystad, A. H., Carlsson, S. R. & Simonsen, A. Toward the function of mammalian ATG12–ATG5-ATG16L1 complex in autophagy and related processes. *Autophagy* **15**, 1485–1486 (2019).
352. Nakatogawa, H. Mechanisms governing autophagosome biogenesis. *Nat. Rev. Mol. Cell Biol.* **21**, 439–458 (2020).
353. Weidberg, H. *et al.* LC3 and GATE-16/GABARAP subfamilies are both essential yet act differently in autophagosome biogenesis. *EMBO J.* **29**, 1792–1802 (2010).
354. Kim, P. K., Hailey, D. W., Mullen, R. T. & Lippincott-Schwartz, J. Ubiquitin signals autophagic degradation of cytosolic proteins and peroxisomes. *Proc. Natl. Acad. Sci. U. S. A.* **105**, 20567–20574 (2008).
355. Gatica, D., Lahiri, V. & Klionsky, D. J. Cargo recognition and degradation by selective autophagy. *Nat. Cell Biol.* **20**, 233–242 (2018).
356. Itakura, E., Kishi-Itakura, C. & Mizushima, N. The hairpin-type tail-anchored SNARE syntaxin 17 targets to autophagosomes for fusion with endosomes/lysosomes. *Cell* **151**, 1256–1269 (2012).
357. Lőrincz, P. & Juhász, G. Autophagosome-Lysosome Fusion. *J. Mol. Biol.* **432**, 2462–2482 (2020).
358. Jiang, P. *et al.* The HOPS complex mediates autophagosome-lysosome fusion through interaction with syntaxin 17. *Mol. Biol. Cell* **25**, 1327–1337 (2014).
359. Chen, Y. & Yu, L. Autophagic lysosome reformation. *Exp. Cell Res.* **319**, 142–146 (2013).
360. Mizushima, N., Yamamoto, A., Matsui, M., Yoshimori, T. & Ohsumi, Y. In vivo analysis of autophagy in response to nutrient starvation using transgenic mice expressing a fluorescent autophagosome marker. *Mol. Biol. Cell* **15**, 1101–1111 (2004).
361. Matsui, M., Yamamoto, A., Kuma, A., Ohsumi, Y. & Mizushima, N. Organelle degradation during the lens and erythroid differentiation is independent of autophagy. *Biochem. Biophys. Res. Commun.* **339**, 485–489 (2006).
362. Wignes, J. A., Goldman, J. W., Weihl, C. C., Bartley, M. G. & Andley, U. P. P62 expression and autophagy in αB-crystallin R120G mutant knock-in mouse model of hereditary cataract. *Exp. Eye Res.* **115**, 263–273 (2013).
363. Morishita, H. *et al.* Deletion of autophagy-related 5 (Atg5) and Pik3c3 genes in the lens causes cataract independent of programmed organelle degradation. *J Biol Chem* **288**, 11436–11447 (2013).
364. McWilliams, T. G. *et al.* A comparative map of macroautophagy and mitophagy in the

vertebrate eye. *Autophagy* **15**, 1296–1308 (2019).
365. Nakahara, M. *et al.* Degradation of nuclear DNA by DNase II-like acid DNase in cortical fiber cells of mouse eye lens. *FEBS J.* **274**, 3055–3064 (2007).
366. Brennan, L., Disatham, J. & Kantorow, M. Hypoxia regulates the degradation of non-nuclear organelles during lens differentiation through activation of HIF1a. *Exp. Eye Res.* **198**, 108129 (2020).
367. Mancias, J. D. & Kimmelman, A. C. Mechanisms of Selective Autophagy in Normal Physiology and Cancer. *J. Mol. Biol.* **428**, 1659–1680 (2016).
368. Marinković, M. & Novak, I. A brief overview of BNIP3L/NIX receptor-mediated mitophagy. *FEBS Open Bio* **11**, 3230–3236 (2021).
369. Marinković, M., Šprung, M. & Novak, I. Dimerization of mitophagy receptor BNIP3L/NIX is essential for recruitment of autophagic machinery. *Autophagy* **17**, 1232–1243 (2021).
370. Schweers, R. L. *et al.* NIX is required for programmed mitochondrial clearance during reticulocyte maturation. *Proc. Natl. Acad. Sci. U. S. A.* **104**, 19500–19505 (2007).
371. Sandoval, H. *et al.* Essential role for Nix in autophagic maturation of erythroid cells. *Nature* **454**, 232–235 (2008).
372. Zhang, J. & Ney, P. A. NIX induces mitochondrial autophagy in reticulocytes. *Autophagy* **4**, 354–356 (2008).
373. Houwen, B. Reticulocyte maturation. *Blood Cells* **18**, 167–186 (1992).
374. Ney, P. A. Normal and disordered reticulocyte maturation. *Curr Opin Hematol* **18**, 152–157 (2011).
375. Chauss, D. *et al.* Differentiation state-specific mitochondrial dynamic regulatory networks are revealed by global transcriptional analysis of the developing chicken lens. *G3 Genes, Genomes, Genet.* **4**, 1515–1527 (2014).
376. Viotti, C. ER to Golgi-Dependent Protein Secretion: The Conventional Pathway. in *Unconventional Protein Secretion: Methods and Protocols* (eds. Pompa, A. & Walker, J. M.) vol. 1459 175–190 (Humana Press, Inc., 2016).
377. New, J. & Thomas, S. M. Autophagy-dependent secretion: mechanism, factors secreted, and disease implications. *Autophagy* **15**, 1682–1693 (2019).
378. Gee, H. Y., Kim, J. & Lee, M. G. Unconventional secretion of transmembrane proteins. *Semin. Cell Dev. Biol.* **83**, 59–66 (2018).
379. Rabouille, C. Pathways of Unconventional Protein Secretion. *Trends Cell Biol.* **27**, 230–240 (2017).
380. Ponpuak, M. *et al.* Secretory autophagy. *Curr. Opin. Cell Biol.* **35**, 106–116 (2015).
381. Andrews, N. W. Regulated secretion of conventional lysosomes. *Trends Cell Biol.* **10**, 316–321 (2000).
382. Giuliani, F., Grieve, A. & Rabouille, C. Unconventional secretion: A stress on GRASP. *Curr. Opin. Cell Biol.* **23**, 498–504 (2011).
383. Cruz-Garcia, D., Malhotra, V. & Curwin, A. J. Unconventional protein secretion triggered by nutrient starvation. *Semin. Cell Dev. Biol.* **83**, 22–28 (2018).
384. Gerstenmaier, L. *et al.* The autophagic machinery ensures nonlytic transmission of mycobacteria. *Proc Natl Acad Sci U S A* **112**, E687–E692 (2015).
385. Munding, C. *et al.* The estrogen-responsive B box protein: A novel enhancer of interleukin-1β secretion. *Cell Death Differ.* **13**, 1938–1949 (2006).
386. Bell, J. L. *et al.* TRIM16 acts as an E3 ubiquitin ligase and can heterodimerize with other TRIM family members. *PLoS One* **7**, e37470 (2012).
387. Jena, K. K. *et al.* TRIM16 controls assembly and degradation of protein aggregates by modulating the p62-NRF2 axis and autophagy. *EMBO J* **37**, e98358 (2018).
388. Kimura, T. *et al.* Dedicated SNARE s and specialized TRIM cargo receptors mediate secretory autophagy. *EMBO J* **36**, 42–60 (2017).
389. Nakajima, K. I. *et al.* Involvement of BNIP1 in apoptosis and endoplasmic reticulum

membrane fusion. *EMBO J* **23**, 3216–3226 (2004).
390. Kinseth, M. A. *et al.* The Golgi-associated protein GRASP is required for unconventional protein secretion during development. *Cell* **130**, 524–534 (2007).
391. Buratta, S. *et al.* Lysosomal Exocytosis, Exosome Release and Secretory Autophagy: The Autophagic- and Endo-Lysosomal Systems Go Extracellular. *Int J Mol Sci* **21**, 2576 (2020).
392. Sun, W., Tian, B. X., Wang, S. H., Liu, P. J. & Wang, Y. C. The function of SEC22B and its role in human diseases. *Cytoskeleton* **77**, 303–312 (2020).
393. Noh, S. H. *et al.* Specific autophagy and ESCRT components participate in the unconventional secretion of CFTR. *Autophagy* **14**, 1761–1778 (2018).
394. Blott, E. J. & Griffiths, G. M. Secretory lysosomes. *Nat Rev Mol Cell Biol* **3**, 122–131 (2002).
395. Bandyopadhyay, D., Cyphersmith, A., Zapata, J. A., Kim, Y. J. & Payne, C. K. Lysosome transport as a function of lysosome diameter. *PLoS One* **9**, e86847 (2014).
396. Corrotte, M. & Castro-Gomes, T. *Lysosomes and plasma membrane repair*. *Current Topics in Membranes* vol. 84 (Elsevier Inc., 2019).
397. Rao, S. K., Huynh, C., Proux-Gillardeaux, V., Galli, T. & Andrews, N. W. Identification of SNAREs involved in synaptotagmin VII-regulated lysosomal exocytosis. *J Biol Chem* **279**, 20471–20479 (2004).
398. Andrews, N. W. Membrane resealing: synaptotagmin VII keeps running the show. *Sci STKE* **2005**, pe19 (2005).
399. Medina, D. L. *et al.* Transcriptional activation of lysosomal exocytosis promotes cellular clearance. *Dev. Cell* **21**, 421–430 (2011).
400. Sbano, L. *et al.* TFEB-mediated increase in peripheral lysosomes regulates store-operated calcium entry. *Sci. Rep.* **7**, 1–13 (2017).
401. Cleyrat, C. *et al.* Mpl traffics to the cell surface through conventional and unconventional routes. *Traffic* **15**, 961–982 (2014).
402. Kitchen, P. *et al.* Plasma membrane abundance of human aquaporin 5 is dynamically regulated by multiple pathways. *PLoS One* (2015) doi:10.1371/journal.pone.0143027.
403. Kessler, A. T. & Bhatt, A. A. Review of the Major and Minor Salivary Glands, Part 1: Anatomy, Infectious, and Inflammatory Processes. *J Clin Imaging Sci* **8**, (2018).
404. Humphrey, S. P. & Williamson, R. T. A review of saliva: normal composition, flow, and function. *J Prosthet Dent* **85**, 162–169 (2001).
405. Ma, T. *et al.* Defective secretion of saliva in transgenic mice lacking aquaporin-5 water channels. *J. Biol. Chem.* **274**, 20071–20074 (1999).
406. Thaysen, J. H., Thorn, N. A. & Schwartz, I. L. Excretion of sodium, potassium, chloride and carbon dioxide in human parotid saliva. *Am J Physiol* **178**, 155–159 (1954).
407. Turner, R. J. *et al.* Ion and water transport mechanisms in salivary glands. *Crit Rev Oral Biol Med* **4**, 385–391 (1993).
408. He, X. *et al.* Polarized distribution of key membrane transport proteins in the rat submandibular gland. *Pflugers Arch* **433**, 260–268 (1997).
409. Melvin, J. E., Yule, D., Shuttleworth, T. & Begenisich, T. Regulation of fluid and electrolyte secretion in salivary gland acinar cells. *Annu Rev Physiol* **67**, 445–469 (2005).
410. Krane, C. M. *et al.* Salivary acinar cells from aquaporin 5-deficient mice have decreased membrane water permeability and altered cell volume regulation. *J Biol Chem* **276**, 23413–23420 (2001).
411. Steinfeld, S. *et al.* Abnormal distribution of aquaporin-5 water channel protein in salivary glands from Sjögren's syndrome patients. *Lab. Investig.* **81**, 143–148 (2001).
412. Tsubota, K., Hirai, S., King, L. S., Agre, P. & Ishida, N. Defective cellular trafficking of lacrimal gland aquaporin-5 in Sjogren's syndrome. *Lancet* **357**, 688–689 (2001).
413. Lee, B. H. *et al.* Autoantibodies against muscarinic type 3 receptor in Sjögren's syndrome

inhibit aquaporin 5 trafficking. *PLoS One* **8**, e53113 (2013).
414. Yoshimura, S. *et al.* Abnormal distribution of AQP5 in labial salivary glands is associated with poor saliva secretion in patients with Sjögren's syndrome including neuromyelitis optica complicated patients. *Mod. Rheumatol.* **26**, 384–390 (2016).
415. Ohashi, Y., Dogru, M. & Tsubota, K. Laboratory findings in tear fluid analysis. *Clin. Chim. Acta* **369**, 17–28 (2006).
416. Liu, Y. *et al.* Expression Profiles of CircRNA and mRNA in Lacrimal Glands of AQP5–/– Mice With Primary Dry Eye. *Front. Physiol.* **11**, 1010 (2020).
417. Hu, S. *et al.* Lacrimal gland homeostasis is maintained by the AQP5 pathway by attenuating endoplasmic reticulum stress inflammation in the lacrimal gland of AQP5 knockout mice. *Mol. Vis.* **27**, 679–690 (2021).
418. Mircheff, A. K. Lacrimal fluid and electrolyte secretion: A review. *Curr. Eye Res.* **8**, 607–617 (1989).
419. Selvam, S. *et al.* Transepithelial bioelectrical properties of rabbit acinar cell monolayers on polyester membrane scaffolds. *Am. J. Physiol. - Cell Physiol.* **293**, 1412–1419 (2007).
420. Ohashi, Y. *et al.* Abnormal protein profiles in tears with dry eye syndrome. *Am. J. Ophthalmol.* **136**, 291–299 (2003).
421. Sasaki, Y., Tsubota, K., Kawedia, J. D., Menon, A. G. & Yasui, M. The Difference of Aquaporin 5 Distribution in Acinar and Ductal Cells in Lacrimal and Parotid Glands. *Curr. Eye Res.* **32**, 923–929 (2007).
422. Ohashi, Y., Tsuzaka, K., Takeuchi, T. & Sasaki, Y. Altered distribution of aquaporin 5 and its C-terminal binding protein in the lacrimal glands of a mouse model for Sjögren's syndrome. *Curr. Eye Res.* **33**, 621–629 (2008).
423. Ishikawa, Y., Iida, H. & Ishida, H. The muscarinic acetylcholine receptor-stimulated increase in aquaporin-5 levels in the apical plasma membrane in rat parotid acinar cells is coupled with activation of nitric oxide/cGMP signal transduction. *Mol. Pharmacol.* **61**, 1423–1434 (2002).
424. Ishikawa, Y. *et al.* Identification of AQP5 in lipid rafts and its translocation to apical membranes by activation of M3 mAChRs in interlobular ducts of rat parotid gland. *Am J Physiol Cell Physiol* **289**, C1303-1311 (2005).
425. Ishikawa, Y., Cho, G., Yuan, Z., Inoue, N. & Nakae, Y. Aquaporin-5 water channel in lipid rafts of rat parotid glands. *Biochim. Biophys. Acta* **1758**, 1053–1060 (2006).
426. Cho, G. *et al.* Activation of muscarinic receptors in rat parotid acinar cells induces AQP5 trafficking to nuclei and apical plasma membrane. *Biochim. Biophys. Acta - Gen. Subj.* **1850**, 784–793 (2015).
427. Bragiel, A. M., Wang, D., Pieczonka, T. D., Shono, M. & Ishikawa, Y. Mechanisms Underlying Activation of α1-Adrenergic Receptor-Induced Trafficking of AQP5 in Rat Parotid Acinar Cells under Isotonic or Hypotonic Conditions. *Int J Mol Sci* **17**, E1022 (2016).
428. Ishikawa, Y., Eguchi, T., Skowronski, M. T. & Ishida, H. Acetylcholine acts on M3 muscarinic receptors and induces the translocation of Aquaporin5 water channel via cytosolic Ca2+ elevation in rat parotid glands. *Biochem. Biophys. Res. Commun.* **245**, 835–840 (1998).
429. Ishikawa, Y., Skowronski, M. T. & Ishida, H. Persistent increase in the amount of aquaporin-5 in the apical plasma membrane of rat parotid acinar cells induced by a muscarinic agonist SNI-2011. *FEBS Lett.* **477**, 253–257 (2000).
430. Liu, X. *et al.* A role for AQP5 in activation of TRPV4 by hypotonicity: Concerted involvement of AQP5 and TRPV4 in regulation of cell volume recovery. *J. Biol. Chem.* **281**, 15485–15495 (2006).
431. Zhang, Y. *et al.* Activation of transient receptor potential vanilloid subtype 1 increases secretion of the hypofunctional, transplanted submandibular gland. *Am. J. Physiol. -*

Gastrointest. Liver Physiol. **299**, G54–G62 (2010).
432. Muroi, S. I. & Isohama, Y. Ezrin regulates ca2+ ionophore-induced plasma membrane translocation of aquaporin-5. *Int. J. Mol. Sci.* **22**, (2021).
433. Bretscher, A., Reczek, D. & Berryman, M. Ezrin: A protein requiring conformational activation to link microfilaments to the plasma membrane in the assembly of cell surface structures. *J. Cell Sci.* **110**, 3011–3018 (1997).
434. Tsukita, S., Yonemura, S. & Tsukita, S. ERM proteins: Head-to-tail regulation of actin-plasma membrane interaction. *Trends Biochem. Sci.* **22**, 53–58 (1997).
435. Chivasso, C. *et al.* Ezrin is a novel protein partner of aquaporin-5 in human salivary glands and shows altered expression and cellular localization in sjögren's syndrome. *Int. J. Mol. Sci.* **22**, 1–15 (2021).
436. Chivasso, C. *et al.* Unraveling Human AQP5-PIP Molecular Interaction and Effect on AQP5 Salivary Glands Localization in SS Patients. *Cells* **10**, (2021).
437. Ablimit, T. *et al.* Changes of aquaporin 5-distribution during release and reaccumulation of secretory granules in isoproterenol-treated mouse parotid gland. *J Electron Microsc* **55**, 183–189 (2006).
438. Koffman, J. S., Arnspang, E. C., Marlar, S. & Nejsum, L. N. Opposing effects of cAMP and T259 phosphorylation on plasma membrane diffusion of the water channel aquaporin-5 in madin-darby canine kidney cells. *PLoS One* (2015) doi:10.1371/journal.pone.0133324.
439. Bacia, K., Scherfeld, D., Kahya, N. & Schwille, P. Fluorescence correlation spectroscopy relates rafts in model and native membranes. *Biophys. J.* **87**, 1034–1043 (2004).
440. Pan, Y. *et al.* Identification of aquaporin-5 and lipid rafts in human resting saliva and their release into cevimeline-stimulated saliva. *Biochim. Biophys. Acta - Gen. Subj.* **1790**, 49–56 (2009).
441. Wandinger-Ness, A. & Zerial, M. Rab Proteins and the Compatmentalization of the Endosomal System. *Cold Spring Harb. Perspect. Biol.* **6**, a022616 (2014).
442. Nashida, T., Yoshie, S., Imai, A. & Shimomura, H. Co-localization of rab4 with endocytosis-related proteins in the rat parotid glands. *Arch Histol Cytol* **66**, 45–52 (2003).
443. Stenmark, H. Rab GTPases as coordinators of vesicle traffic. *Nat. Rev. Mol. Cell Biol.* **10**, 513–525 (2009).
444. Zhao, Y. G. & Zhang, H. Autophagosome maturation: An epic journey from the ER to lysosomes. *J. Cell Biol.* **218**, 757–770 (2019).
445. Ganesan, D. & Cai, Q. Understanding amphisomes. *Biochem. J.* **478**, 1959–1976 (2021).
446. Moss, F. J. *et al.* Aquaporin-7: A Dynamic Aquaglyceroporin With Greater Water and Glycerol Permeability Than Its Bacterial Homolog GlpF. *Front. Physiol.* **11**, 1–16 (2020).
447. Ishibashi, K. *et al.* Cloning and functional expression of a second new aquaporin abundantly expressed in testis. *Biochem. Biophys. Res. Commun.* **237**, 714–718 (1997).
448. Oppitz, M., Mack, A. & Drews, U. Ca2+-Mobilization and Cell Contraction after Muscarinic Cholinergic Stimulation of the Chick Embryo Lens. *Investig. Ophthalmol. Vis. Sci.* **44**, 4813–4819 (2003).
449. Mitchell, C. A., Risau, W. & Drexler, H. C. A. Regression of vessels in the tunica vasculosa lentis is initiated by coordinated endothelial apoptosis: A role for vascular endothelial growth factor as a survival factor for endothelium. *Dev. Dyn.* **213**, 322–333 (1998).
450. Wang, Z., Han, J., David, L. L. & Schey, K. L. Proteomics and phosphoproteomics analysis of human lens fiber cell membranes. *Investig. Ophthalmol. Vis. Sci.* (2013) doi:10.1167/iovs.12-11168.
451. Cantrell, L. S. & Schey, K. L. Data-Independent Acquisition Mass Spectrometry of the Human Lens Enhances Spatiotemporal Measurement of Fiber Cell Aging. *J. Am. Soc. Mass Spectrom.* **32**, 2755–2765 (2021).

452. Nadolski, M. J. & Linder, M. E. Protein lipidation. *FEBS J* **274**, 5202–5210 (2007).
453. Fujiwara, Y. *et al.* Structural basis for the membrane association of ankyrinG via palmitoylation. *Sci. Rep.* **6**, 1–11 (2016).
454. Valdez-Taubas, J. & Pelham, H. Swf1-dependent palmitoylation of the SNARE Tlg1 prevents its ubiquitination and degradation. *EMBO J.* **24**, 2524–2532 (2005).
455. Lam, K. K. Y. *et al.* Palmitoylation by the DHHC protein Pfa4 regulates the ER exit of Chs3. *J. Cell Biol.* **174**, 19–25 (2006).
456. Yanai, A. *et al.* Palmitoylation of huntingtin by HIP14is essential for its trafficking and function. *Nat. Neurosci.* **9**, 824–831 (2006).
457. Yang, H., Qu, L., Ni, J., Wang, M. & Huang, Y. Palmitoylation participates in G protein coupled signal transduction by affecting its oligomerization. *Mol. Membr. Biol.* **25**, 58–71 (2008).
458. Gahbauer, S. & Böckmann, R. A. Membrane-mediated oligomerization of G protein coupled receptors and its implications for GPCR function. *Front. Physiol.* **7**, 494 (2016).
459. Aicart-Ramos, C., Valero, R. A. & Rodriguez-Crespo, I. Protein palmitoylation and subcellular trafficking. *Biochim. Biophys. Acta* **1808**, 2981–2994 (2011).
460. Vetrivel, K. S. *et al.* Alzheimer disease Aβ production in the absence of S-palmitoylation-dependent targeting of BACE1 to lipid rafts. *J. Biol. Chem.* **284**, 3793–3803 (2009).
461. Levental, I., Lingwood, D., Grzybek, M., Coskun, Ü. & Simons, K. Palmitoylation regulates raft affinity for the majority of integral raft proteins. *Proc. Natl. Acad. Sci. U. S. A.* **107**, 22050–22054 (2010).
462. Dai, G. Neuronal KCNQ2/3 channels are recruited to lipid raft microdomains by palmitoylation of BACE1. *J. Gen. Physiol.* **154**, (2022).
463. Wang, Z. & Schey, K. L. Proteomic analysis of S-palmitoylated proteins in ocular lens reveals palmitoylation of AQP5 and MP20. *Investig. Opthalmology Vis. Sci.* **59**, 5648–5658 (2018).
464. Suzuki, H., Nishikawa, K., Hiroaki, Y. & Fujiyoshi, Y. Formation of aquaporin-4 arrays is inhibited by palmitoylation of N-terminal cysteine residues. *Biochim Biophys Acta* **1778**, 1181–1189 (2008).
465. Gletten, R. B., Cantrell, L. S., Bhattacharya, S. & Schey, K. L. Lens Aquaporin-5 Inserts Into Bovine Fiber Cell Plasma Membranes Via Unconventional Protein Secretion. *Invest Ophthalmol Vis Sci* **63**, 5 (2022).
466. Shi, Y. *et al.* The stratified syncytium of the vertebrate lens. *J. Cell Sci.* **122**, 1607–1615 (2009).
467. Karasawa, K. *et al.* Patterns of aquaporin expression in the canine eye. *Vet. J.* **190**, e72–e77 (2011).
468. Walker, J. L. & Menko, A. S. α6 Integrin is regulated with lens cell differentiation by linkage to the cytoskeleton and isoform switching. *Dev. Biol.* **210**, 497–511 (1999).
469. Bassnett, S. & Beebe, D. C. Coincident loss of mitochondria and nuclei during lens fiber cell differentiation. *Dev. Dyn.* **194**, 85–93 (1992).
470. Ou, W., Cameron, P. H., Thomas, D. Y. & Bergeron, J. J. M. Association of folding intermediates of glycoproteins with calnexin during protein maturation. *Nature* **364**, 771–776 (1993).
471. Uemura, T. *et al.* A cluster of thin tubular structures mediates transformation of the endoplasmic reticulum to autophagic isolation membrane. *Mol Cell Biol* **34**, 1695–1706 (2014).
472. Zhuang, X. *et al.* ATG9 regulates autophagosome progression from the endoplasmic reticulum in Arabidopsis. *Proc Natl Acad Sci U S A* **114**, E426–E435 (2017).
473. Dan, H. C., Antonia, R. J. & Baldwin, A. S. PI3K/Akt promotes feedforward mTORC2 activation through IKKα. *Oncotarget* **7**, 21064–21075 (2016).
474. Soliman, G. A. *et al.* mTOR Ser-2481 autophosphorylation monitors mTORC-specific

catalytic activity and clarifies rapamycin mechanism of action. *J. Biol. Chem.* **285**, 7866–7879 (2010).
475. Reczek, D. *et al.* LIMP-2 Is a Receptor for Lysosomal Mannose-6-Phosphate-Independent Targeting of β-Glucocerebrosidase. *Cell* **131**, 770–783 (2007).
476. Heybrock, S. *et al.* Lysosomal integral membrane protein-2 (LIMP-2/SCARB2) is involved in lysosomal cholesterol export. *Nat. Commun.* **10**, (2019).
477. Dupont, N. *et al.* Autophagy-based unconventional secretory pathway for extracellular delivery of IL-1β. *EMBO J.* **30**, 4701–4711 (2011).
478. Gonzalez, C. D., Resnik, R. & Vaccaro, M. I. Secretory Autophagy and Its Relevance in Metabolic and Degenerative Disease. *Front. Endocrinol. (Lausanne).* **11**, 1–12 (2020).
479. Jaiswal, J. K., Andrews, N. W. & Simon, S. M. Membrane proximal lysosomes are the major vesicles responsible for calcium-dependent exocytosis in nonsecretory cells. *J. Cell Biol.* **159**, 625–635 (2002).
480. Brennan, L. A. *et al.* Spatial expression patterns of autophagy genes in the eye lens and induction of autophagy in lens cells. *Mol. Vis.* **18**, 1773–1786 (2012).
481. Griffiths, R. E. *et al.* Maturing reticulocytes internalize plasma membrane in glycophorin A-containing vesicles that fuse with autophagosomes before exocytosis. *Blood* **119**, 6296–6306 (2012).
482. Weber, G. F. & Menko, A. S. Phosphatidylinositol 3-kinase is necessary for lens fiber cell differentiation and survival. *Investig. Ophthalmol. Vis. Sci.* **47**, 4490–4499 (2006).
483. Kosugi-Tanaka, C. *et al.* Protein kinase A-regulated membrane trafficking of a green fluorescent protein-aquaporin 5 chimera in MDCK cells. *Biochim. Biophys. Acta - Mol. Cell Res.* **1763**, 337–344 (2006).
484. Amiryl-Moghaddam, M. *et al.* Brain mitochondria contain aquaporin water channels: evidence for the expression of a short AQP9 isoform in the inner mitochondrial membrane. *FASEB J.* **19**, 1459–1467 (2005).
485. Liu, Y., Fiskum, G. & Schubert, D. Generation of reactive oxygen species by the mitochondrial electron transport chain. *J. Neurochem.* **80**, 780–787 (2002).
486. Marchissio, M. J., Francés, D. E. A., Carnovale, C. E. & Marinelli, R. A. Mitochondrial aquaporin-8 knockdown in human hepatoma HepG2 cells causes ROS-induced mitochondrial depolarization and loss of viability. *Toxicol. Appl. Pharmacol.* **264**, 246–254 (2012).
487. Watanabe, S., Moniaga, C. S., Nielsen, S. & Hara-Chikuma, M. Aquaporin-9 facilitates membrane transport of hydrogen peroxide in mammalian cells. *Biochem. Biophys. Res. Commun.* **471**, 191–197 (2016).
488. Krüger, C. *et al.* The importance of aquaporin-8 for cytokine-mediated toxicity in rat insulin-producing cells. *Free Radic. Biol. Med.* **174**, 135–143 (2021).
489. Rodrigues, C. *et al.* Human Aquaporin-5 Facilitates Hydrogen Peroxide and Cancer Cell Migration. *Cancers (Basel).* **11**, 932 (2019).
490. Lee, J., Giordano, S. & Zhang, J. Autophagy, mitochondria and oxidative stress: Cross-talk and redox signalling. *Biochem. J.* **441**, 523–540 (2012).
491. Scherz-Shouval, R. *et al.* Reactive oxygen species are essential for autophagy and specifically regulate the activity of Atg4. *EMBO J.* **26**, 1749–1760 (2007).
492. Day, R. E. *et al.* Human aquaporins: Regulators of transcellular water flow. *Biochim. Biophys. Acta - Gen. Subj.* **1840**, 1492–1506 (2014).
493. Rose, K. M. L. *et al.* The C Terminus of Lens Aquaporin 0 Interacts With the Cytoskeletal Proteins Filensin and CP49. *Investig. Ophthalmol. Vis. Sci.* **47**, 1562–1570 (2006).
494. Wang, Z. & Schey, K. L. Aquaporin-0 interacts with the FERM domain of ezrin/radixin/moesin proteins in the ocular lens. *Investig. Ophthalmol. Vis. Sci.* **52**, 5079–5087 (2011).
495. Chang, N. C., Nguyen, M., Germain, M. & Shore, G. C. Antagonism of Beclin 1-

dependent autophagy by BCL-2 at the endoplasmic reticulum requires NAF-1. *EMBO J.* **29**, 606–618 (2010).
496. Dunn, W. A. J. Studies on the mechanisms of autophagy: Formation of the autophagic vacuole. *J. Cell Biol.* **110**, 1923–1933 (1990).
497. Silberstein, S., Kelleher, D. J. & Gilmore, R. The 48-kDa subunit of the mammalian oligosaccharyltransferase complex is homologous to the essential yeast protein WBP1. *J. Biol. Chem.* **267**, 23658–23663 (1992).
498. Iglesias, C. *et al.* The MST3/STK24 kinase mediates impaired fasting blood glucose after a high-fat diet. *Diabetologia* **60**, 2453–2462 (2017).
499. Beugnet, A., Tee, A. R., Taylor, P. M. & Proud, C. G. ERRATUM: Regulation of targets of mTOR (mammalian target of rapamycin) signalling by intracellular amino acid availability. *Biochem. J.* **372**, 555–566 (2003).
500. Han, J. M. *et al.* Leucyl-tRNA synthetase is an intracellular leucine sensor for the mTORC1-signaling pathway. *Cell* **149**, 410–424 (2012).
501. Teasdale, R. D., Loci, D., Houghton, F., Karlsson, L. & Gleeson, P. A. A large family of endosome-localized proteins related to sorting nexin 1. *Biochem. J.* **358**, 7–16 (2001).
502. Pylypenko, O., Lundmark, R., Rasmuson, E., Carlsson, S. R. & Rak, A. The PX-BAR membrane-remodeling unit of sorting nexin 9. *EMBO J.* **26**, 4788–4800 (2007).
503. Dyve, A. B., Bergan, J., Utskarpen, A. & Sandvig, K. Sorting nexin 8 regulates endosome-to-Golgi transport. *Biochem. Biophys. Res. Commun.* **390**, 109–114 (2009).
504. Guo, W. *et al.* SNX8 modulates the innate immune response to RNA viruses by regulating the aggregation of VISA. *Cell. Mol. Immunol.* **17**, 1126–1135 (2020).
505. Neuspiel, M. *et al.* Cargo-Selected Transport from the Mitochondria to Peroxisomes Is Mediated by Vesicular Carriers. *Curr. Biol.* **18**, 102–108 (2008).
506. Soubannier, V. *et al.* A vesicular transport pathway shuttles cargo from mitochondria to lysosomes. *Curr. Biol.* **22**, 135–141 (2012).
507. Soubannier, V., Rippstein, P., Kaufman, B. A., Shoubridge, E. A. & McBride, H. M. Reconstitution of Mitochondria Derived Vesicle Formation Demonstrates Selective Enrichment of Oxidized Cargo. *PLoS One* **7**, (2012).
508. McLelland, G. L., Soubannier, V., Chen, C. X., McBride, H. M. & Fon, E. A. Parkin and PINK1 function in a vesicular trafficking pathway regulating mitochondrial quality control. *EMBO J.* **33**, 282–295 (2014).
509. Mhatre, A. N., Steinbach, S., Hribar, K., Hoque, A. T. M. S. & Lalwani, A. K. Identification of aquaporin 5 (AQP5) within the cochlea: cDNA cloning and in situ localization. *Biochem. Biophys. Res. Commun.* **264**, 157–162 (1999).
510. Yu, D., Thelin, W. R., Randell, S. H. & Boucher, R. C. Expression profiles of aquaporins in rat conjunctiva, cornea, lacrimal gland and Meibomian gland. *Exp. Eye Res.* **103**, 22–32 (2012).
511. Matsuzaki, T., Suzuki, T., Koyama, H., Tanaka, S. & Takata, K. Aquaporin-5 (AQP5), a water channel protein, in the rat salivary and lacrimal glands: Immunolocalization and effect of secretory stimulation. *Cell Tissue Res.* **295**, 513–521 (1999).
512. Vagin, O., Kraut, J. A. & Sachs, G. Role of N-glycosylation in trafficking of apical membrane proteins in epithelia. *Am. J. Physiol. - Ren. Physiol.* **296**, F459-469 (2009).
513. Huang, L. *et al.* RPN2 promotes metastasis of hepatocellular carcinoma cell and inhibits autophagy via STAT3 and NF-κB pathways. *Aging (Albany. NY).* **11**, 6674–6690 (2019).
514. Arsham, A. M. & Neufeld, T. P. A genetic screen in Drosophila reveals novel cytoprotective functions of the autophagy-lysosome pathway. *PLoS One* **4**, (2009).
515. Fushimi, K., Sasaki, S. & Marumo, F. Phosphorylation of serine 256 is required for cAMP-dependent regulatory exocytosis of the aquaporin-2 water channel. *J Biol Chem* **272**, 14800–14804 (1997).
516. Rodrigues, C. *et al.* Rat Aquaporin-5 Is pH-Gated Induced by Phosphorylation and Is

Implicated in Oxidative Stress. *Int J Mol Sci* **17**, E2090 (2016).
517. Chazotte, B. Labeling mitochondria with mitotracker dyes. *Cold Spring Harb. Protoc.* **6**, 990–992 (2011).
518. Bantseev, V., Cullen, A. P., Trevithick, J. R. & Sivak, J. G. Optical function and mitochondrial metabolic properties in damage and recovery of bovine lens after in vitro carbonyl cyanide m-chlorophenylhydrazone treatment. *Mitochondrion* **3**, 1–11 (2003).
519. Pendergrass, W., Wolf, N. & Pool, M. Efficacy of MitoTracker Green™ and CMXRosamine to measure changes in mitochondrial membrane potentials in living cells and tissues. *Cytom. Part A* **61**, 162–169 (2004).
520. Bantseev, V. & Sivak, J. G. Confocal laser scanning microscopy imaging of dynamic TMRE movement in the mitochondria of epithelial and superficial cortical fiber cells of bovine lenses. *Mol. Vis.* **11**, 518–523 (2005).
521. Xu, J. *et al.* Mechanism of polarized lysosome exocytosis in epithelial cells. *J. Cell Sci.* **126**, 5086 (2013).
522. Zampighi, G. A. *et al.* Conical electron tomography of a chemical synapse: Vesicles docked to the active zone are hemi-fused. *Biophys. J.* **91**, 2910–2918 (2006).
523. Flechsler, J. *et al.* 2D and 3D immunogold localization on (epoxy) ultrathin sections with and without osmium tetroxide. *Microsc. Res. Tech.* **83**, 691–705 (2020).
524. Winey, M., Meehl, J. B., O'Toole, E. T. & Giddings, T. H. Conventional transmission electron microscopy. *Mol. Biol. Cell* **25**, 319–323 (2014).
525. Petralia, R. S. & Wang, Y. X. Review of Post-embedding Immunogold Methods for the Study of Neuronal Structures. *Front. Neuroanat.* **15**, 1–8 (2021).
526. Kuszak, J. R., Peterson, K. L. & Brown, H. G. Electron microscopic observations of the crystalline lens. *Microsc. Res. Tech.* **33**, 441–479 (1996).
527. Graham, L. & Orenstein, J. M. Processing tissue and cells for transmission electron microscopy in diagnostic pathology and research. *Nat. Protoc.* **2**, 2439–2450 (2007).
528. Yoshii, S. R. & Mizushima, N. Monitoring and measuring autophagy. *Int. J. Mol. Sci.* **18**, 1–13 (2017).
529. Ylä-Anttila, P., Vihinen, H., Jokitalo, E. & Eskelinen, E. L. *Monitoring autophagy by electron microscopy in Mammalian cells*. *Methods in Enzymology* vol. 452 (Elsevier Inc., 2009).
530. Qin, Y. *et al.* The combination of paraformaldehyde and glutaraldehyde is a potential fixative for mitochondria. *Biomolecules* **11**, 1–14 (2021).
531. Zhao, Y. G., Codogno, P. & Zhang, H. Machinery, regulation and pathophysiological implications of autophagosome maturation. *Nat. Rev. Mol. Cell Biol.* **22**, 733–750 (2021).
532. Humphries, W. H., Szymanski, C. J. & Payne, C. K. Endo-lysosomal vesicles positive for rab7 and lamp1 are terminal vesicles for the transport of dextran. *PLoS One* **6**, (2011).
533. Hurley, J. H. & Nogales, E. Next-generation electron microscopy in autophagy research. *Curr. Opin. Struct. Biol.* **41**, 211–216 (2016).
534. Jung, M., Choi, H. & Mun, J. Y. The autophagy research in electron microscopy. *Appl. Microsc.* **49**, 1–7 (2019).
535. Kuszak, J. R., Zoltoski, R. K. & Sivertson, C. Fibre cell organization in crystalline lenses. *Exp. Eye Res.* **78**, 673–687 (2004).
536. Arantes, R. M. E. & Andrews, N. W. A role for synaptotagmin VII-regulated exocytosis of lysosomes in neurite outgrowth from primary sympathetic neurons. *J. Neurosci.* **26**, 4630–4637 (2006).
537. Kamsteeg, E. J., Heijnen, I., Van Os, C. H. & Deen, P. M. T. The subcellular localization of an aquaporin-2 tetramer depends on the stoichiometry of phosphorylated and nonphosphorylated monomers. *J. Cell Biol.* **151**, 919–929 (2000).
538. Ireland, M. E. & Shanbom, S. Lens Beta-Adrenergic Receptors Functional Coupling to Adenylare Cyclase and Phoroaffiniry Labeling. *Invest. Ophthalmol. Vis. Sci.* **32**, 541–548

(1991).
539. Shestopalov, V. I. & Bassnett, S. Exogenous gene expression and protein targeting in lens fiber cells. *Investig. Ophthalmol. Vis. Sci.* (1999).
540. Lovicu, F. J., Steven, P., Saika, S. & McAvoy, J. W. Aberrant lens fiber differentiation in anterior subcapsular cataract formation: A process dependent on reduced levels of Pax6. *Investig. Ophthalmol. Vis. Sci.* **45**, 1946–1953 (2004).